Alma Mater Studiorum – Università di Bologna

DOTTORATO DI RICERCA IN

Scienze Biomediche e Neuromotorie

Ciclo XXXIV

Settore Concorsuale: 05/D1 - FISIOLOGIA

Settore Scientifico Disciplinare: BIO/09 – FISIOLOGIA

Central and peripheral manipulation of the sympathetic nervous system to study immune, thermoregulatory and sleep-related neural functions

Presentata da: Alessandra Occhinegro

Coordinatore Dottorato

Prof. Matilde Yung Follo

Supervisore

Dr. Davide Martelli

Co-Supervisore

Prof. Elisabetta Ciani

Esame finale anno 2021

“…non più per immaginazione,
ma per sensata esperienza
e necessaria dimostrazione.”

Galileo Galilei, Lettera a Gallanzone Gallanzoni, 1611

ABSTRACT

The Sympathetic Nervous System (SNS) regulates basic bodily functions, and its action is essential for the preservation of both the homeostasis of the organism and its adaptation to environmental challenges. The primary aim of this research project has been to investigate the effects of central and peripheral SNS manipulation on immune responses and on hypothermia and sleep-related brain neural plasticity.

This research project can be subdivided in three different sub-projects: 1) Study of the sympathetic reflex control of inflammation in mice subjected to different immune challenges; 2) Study of the mechanism driving the induction and resolution of brain Tau protein phosphorylation during and after synthetic torpor (ST); and 3) Study of the role of sleep in the dephosphorylation process of Tau during the recovery from ST.

The first set of experiments was aimed at studying the role of the endogenous inflammatory reflex in mice. The inflammatory reflex is activated in response to immune challenges and its efferent pathway, the splanchnic anti-inflammatory pathway (SAIP), inhibits the inflammatory response to immune challenges. The SAIP has been characterized almost exclusively when mobilized by challenges with TLR-4 agonists in rats and sheep, never in mice. It was also unknown whether the SAIP applies to other types of immune challenges. Hence, the effects of prior bilateral section of the greater sympathetic splanchnic nerves on cytokine responses to three different systemic immune challenges were investigated: (i) LPS, agonist of TLR4, (ii) Poly I:C, agonist of TLR3, and (iii) Pam2cys, agonist of TLR2 and TLR6. The results showed that the SAIP is also active in mice challenged with LPS, since it enhances systemic levels of the anti-inflammatory cytokine IL-10 while inhibiting those of pro-inflammatory cytokines TNF and MCP-1. Furthermore, the SAIP is also active against acute inflammation triggered by TLR3, TLR2, TLR6.

The second set of experiments was aimed at investigating the effects of ST and of the following recovery period on cortical and hippocampal Tau protein expression and phosphorylation, and the mechanism underlying these processes. ST is a peculiar hypometabolic/hypothermic condition resembling natural torpor, which can be induced in non-hibernators by the pharmacological inhibition of sympathetic premotor neurons in the Raphe Pallidus area. Interestingly, a strong sympathetic activation characterizes the period of rewarming leading to normothermia after the exit from ST. Tau is a microtubule-associated protein that, through its phosphorylation/dephosphorylation processes, plays a central role in neural plasticity. Animals entering torpor accumulate the hyperphosphorylated form of the Tau protein, resembling a similar pattern observed in several neurodegenerative diseases, called tauopathies. However,

contrary to what happens in neurodegenerative diseases, the accumulation of the hyperphosphorylated Tau observed in torpid animals is reversible: when animals recover from torpor, Tau is dephosphorylated to normal conditions. Recently, the same reversible phenomenon was described by immunohistochemistry also in rats entering ST, but the mechanism driving this process is unknown. Therefore, in this study, the levels of the Tau protein and its degree of phosphorylation, the expression of key enzymes involved in phosphorylation/dephosphorylation processes, the plasma levels of melatonin and other hormones and transmitters were determined in rats subjected to and recovering from ST. The results confirmed the reversibility of the Tau phosphorylation after the arousal from ST. It was also shown that, during ST and the recovery to euthermia, plasma melatonin concentration increased, suggesting a possible role for this hormone in Tau dephosphorylation process.

The third set of experiments was aimed at investigating the role of sleep in the dephosphorylation process of Tau protein in parietal cortex and hippocampus of rats recovering from ST. In particular, the levels of the Tau protein and its degree of phosphorylation, the expression of key enzymes involved in phosphorylation/dephosphorylation processes, the plasma levels of melatonin and other hormones and transmitters were studied 3 and 6 hours after the exit from ST. A peculiar feature of both natural and ST is the great sleep pressure that animals exhibit soon after the arousal from torpor. Since Slow Wave Activity in NREM sleep is considered to play a key role in neural plasticity, we investigated its possible role in Tau dephosphorylation by sleep depriving two groups of animals by gentle handling for either 3 or 6 hours after their exit from ST. The results showed that sleep deprivation does not impair Tau dephosphorylation process, but apparently accelerates it through a finely biochemically regulated process and does not affect melatonin levels.

ABBREVIATIONS

5-HT, serotonin
A, adrenaline
ACh, acetylcholine
aCSF, artificial cerebrospinal fluid
ANOVA, one-way analysis of variance
ANS, Autonomic Nervous System
ARs, adrenergic receptors
BAT, brown adipose tissue
C, control
CREB, cAMP response element-binding protein
CX, cortex
CAN, central autonomic networks
CNS, central nervous system
COMT, catechol *O*-methyltransferase
DAMPs, damage-associated molecular patterns
DMH, dorsomedial hypothalamus
DOMA, 3,4-dihydroxymandelic acid
DOPEG, 3,4-dihydroxyphenyl glycol
DOPGAL, 3,4-dihydroxyphenylglycoaldehyde
DTT, dithiothreitol
EEG, electroencephalogram
ENS, enteric nervous system
ER, early recovery
GABA, γ-aminobutyric acid
GRP78, Glucose regulating protein 78
Gsk3-β, Glycogen synthase kinase 3β
Hip, hippocampus
HPA axis, hypothalamic–pituitary–adrenal axis
IL, interleukin
INF-γ, interferon-γ
LBP, LPS-binding protein
LDS, lithium dodecyl sulfate
LPS, lipopolysaccharide

LTA, lipoteichoic acid

LPB, lateral parabrachial nucleus

MAO, monoamine oxidase

MAPK, Mitogen-activated protein kinase

MCP-1, monocyte chemoattractant protein-1

MHC, major histocompatibility complex

MCP-1, monocyte chemoattractant protein 1

MnPO, median preoptic nucleus

MOPEG, 4-hydroxyphenylglycol

MPA, Medial preoptic area

N, nadir

NA, noradrenaline

NFT, neurofibrillary tangles

NK, natural killer

NLRs, NOD-like receptors

NPY, neuropeptide Y

NS, normal sleep

NF-kB, nuclear factor kappa-light-chain-enhancer of activated B cells

Pam2Cys, S-[2,3-bis(palmitoyloxy)propyl] cysteine

PAMPs, pathogen-associated molecular patterns

PHF, paired helical filaments

PLC, phospholipase C

PMSF, phenylmethylsulfonyl fluoride

PNMT, phenylethanolamine-N-methyl-transferase

PNS, parasympathetic nervous system

POA, preoptic area

Poly I:C, polyinosinedeoxycytidylic acid

PP2A, Protein phosphatase 2

PRRs, Pattern recognition receptors

PVN, paraventricular nucleus

R3, 3h recovery

R6, 6h recovery

R3SD, 3h recovery sleep deprived

R6SD, 6h recovery sleep deprived

REM, rapid-eye-movement sleep

RPa, raphe pallidus area

RVLM, rostral ventrolateral medulla

RVMM, rostral ventromedial medulla

SAIP, splanchnic anti-inflammatory pathway

SCN, suprachiasmatic nucleus

SD, sleep deprived

SLC18A1, Solute Carrier Family 18 Member A1

SLC18A2, Solute Carrier Family 18 Member A2

SNS, sympathetic nervous system

SPNs, sympathetic preganglionic neurons

Src, Proto-oncogene tyrosine-protein kinase

ST, synthetic torpor

SWA, slow wave activity

Syk, Tyrosine-protein kinase

Ta, ambient temperature

Tb, body temperature

TH, Tyrosine-hydroxylase

Thy, Hypothalamic temperature

TLRs, Toll-like receptors

TNF, tumor necrosis factor

TRP, transient receptor potential family

UCP1, Uncoupling protein 1

VGLUT3, vesicular glutamate transporter 3

VIP, vasoactive intestinal polypeptide

VMA, vanillylmandelic acid

VMAT, vesicular monoamine transporter

WB, Western Blot

WSN, warm sensitive neurons

Xiap, X chromosome-linked inhibitor of apoptosis

1. INTRODUCTION

1.1 THE AUTONOMIC NERVOUS SYSTEM

The autonomic nervous system (ANS), a motor system also known as visceral or involuntary, is the branch of the nervous system that controls unconscious bodily functions. Its activity persists even in the absence of control by the somatic and voluntary components of the nervous system. The ANS is identifiable already in invertebrates as a simple visceral innervation but assumes a defined structural and functional organization in birds and mammals.

The principal function of the ANS is to control visceral organs, including those that belong to the cardiovascular system, and effectors in the skin, affecting therefore, among the different physiological functions also body temperature (Tb) and energy expenditure (Nakamura et al., 2005; Furness, 2006). It also controls pupillary response, urination and sexual arousal. The ANS targets include visceral organs of the thoracic, abdominal, and pelvic cavities: cardiac muscle, smooth muscle, endocrine and exocrine glands, lungs, digestive organs, kidneys, bladder, adipocytes, but also blood vessels and pupils. Taking into consideration the target organs, among main roles of ANS we can count regulation of blood pressure, thermoregulation, contraction of smooth muscles, gastrointestinal response to food, regulation of secretory activity of glands. All ANS functions are involved in the preservation of homeostasis of the organism and in the adaptation of physiological parameters to functional requirements dictated by behavior conditioned by environment (Furness, 2006; McCorry, 2007).

From the anatomical and functional point of view, the ANS is composed by three divisions: parasympathetic nervous system (PNS), sympathetic nervous system (SNS), and enteric nervous system (ENS). This thesis will only focus on the function and eventual manipulation of the SNS and PNS, but not of the ENS.

In particular, PSN and SNS operate in a coordinated way, acting reciprocally and synergically on target organs, in order to regulate metabolic and visceral functions. Both systems are tonically activated, and this allows to regulate bidirectionally neuronal frequency of discharge, increasing or decreasing it, determining an accurate modulation of organs functions (McCorry, 2007).

Typically, it refers to PSN and SNS, respectively, as “rest and digest” and “fight or flight” system. These appellations help in recognizing general activity and function of the two systems. The parasympathetic division predominates during quiet, resting conditions. The overall effect of the PNS under these conditions is to store energy and to regulate basic body functions such as digestion. On the other hand, the sympathetic division supports a general stimulation of metabolism with the aim of responding to stress and emergency, increasing the flow of blood

that is well-oxygenated and rich in nutrients to the tissues that need it, in particular, the working skeletal muscles. Moreover, heart rate and arterial pressure raise, pupils dilate, and cutaneous vasoconstriction occurs.

Although the apparent opposite functions, the two system work synergically and in a coordinated manner, together or independently, in order to regulate visceral functions and metabolism (Ondicova & Mravec, 2010).

The efferent nervous activity of ANS is mostly regulated by autonomic unconscious motor reflexes. Autonomic reflexes are mediated by neural pathways in the brainstem and spinal cord and generally regulate organ and system performance very rapidly (McDougall et al., 2014). The spinal reflexes are the simplest behaviors produced by central nervous system (CNS), but the variation of environmental and/or internal conditions could be also detected by sensory neurons and transmitted to the CNS and then to particular nuclei, the "central autonomic networks" (CAN; Roy & Green, 2019), that control the activity of peripheral autonomic nerves. The CAN is an integral element of an internal regulation system through which the brain controls visceromotor, neuroendocrine, pain, and behavioral responses essential for survival. It includes the insular cortex, amygdala, hypothalamus, periaqueductal gray, parabrachial complex, nucleus of the tractus solitarius, ventrolateral medulla, nucleus ambiguous and dorsal motor nucleus. These areas are pivotal for the autonomic outflow, both sympathetic and parasympathetic (Roy & Green, 2019). In the viscera, visceral receptors are predisposed to detect information about the physiological conditions of our inner environment. For example, arterial chemoreceptors, tension receptors in the carotid sinus and aortic arch (Furness, 2006), detect, respectively, hypoxemia and hypercapnia (Schultz et al., 2007), and pressure changes in the arterial blood pressure (Donald & Shepherd, 1979). The detected information reaches the CNS and is then relayed to autonomic premotor neurons, that are neurons in areas that constitute the CAN. The importance of autonomic premotor neurons is pivotal for their role in integration of peripheral sensory inputs and central command signals. The term "central command" was coined by Goodwin (Goodwin et al., 1972), and it was referred to a feedforward signal whereby activation of brain regions responsible for skeletal muscle motor unit recruitment results in the parallel activation of medullary neuronal circuits, causing autonomic activation (Basnayake et al., 2012).

The premotor autonomic neurons directly project to those neurons belonging to the parasympathetic and sympathetic division of the ANS. The SNS and PNS are both motor systems consisting of two neurons: the preganglionic and the postganglionic neuron. Preganglionic neurons with the body located in the CNS, synapse with postganglionic neurons

located in peripheral autonomic ganglia. The preganglionic fiber, often myelinated, releases acetylcholine (ACh), which binds to nicotinic receptors on postganglionic neurons. ACh stimulates fast excitation of autonomic ganglia through nicotinic receptors (α_3/β_4 type; Benarroch, 2020). From autonomic ganglia originate postganglionic fibers, that are unmyelinated fibers that reach the target cell. The main neurotransmitter released from postganglionic fibers differ for parasympathetic and sympathetic division, being respectively, ACh and noradrenaline (NA; Brunton et al., 2011). These autonomic peripheral nerves can also co-release other neurotransmitters, like neuropeptide Y (NPY) and ATP, for sympathetic fibers, or vasoactive intestinal polypeptide (VIP; McCorry, 2007), for parasympathetic nerves.

1.1.1 Central Control of the Autonomic Nervous System

The autonomic nervous system operates to maintain the internal homeostasis, therefore controlling all different systems (gastrointestinal system, cardiovascular system, thermoregulatory function, metabolism, immune system; Coote & Spyer, 2018). This requires a peculiar interaction between peripheral and central structures. In particular, in CNS many areas are considered homeostatic control centers, which regulate the stability within a physiological range of the variables of extracellular fluid compartment (and as a consequence also of the intracellular compartment), such as temperature, water volume, osmolality, pH, PO2, PCO2, nutrients, as the result of the continuous adjustment of "instrumental", such as heart rate, stroke volume, cardiac output, blood pressure, ventilation, muscle force.

The vast majority of premotor autonomic neurons is located in the forebrain and brainstem (Coote & Spyer, 2018). In the forebrain, the areas involved in autonomic function control are insular cortex, anterior and midcingulate cortex, amygdala, and hypothalamus.

Hypothalamus, especially but not only with its paraventricular nucleus (PVN), is considered the "autonomic master controller" due to its specialized innervation to all autonomic relay centers (Benarroch, 1993). It is crucial in the regulation of specific pattern of autonomic, endocrine, and arousal response to stressors (Benarroch, 2020). Arterial baroreceptors, chemoreceptors, atrial volume receptors, and osmoreceptors in circumventricular organs transmit to the PVN information about internal environmental status. The transfer of these information from PVN to functionally distinct neuronal circuits is exploited by topographically distributed innervations, that compose paraventriculospinal pathway. These fibers are characterized by specific neurotransmitters and are distributed in specific spinal segments, and within a segment, in some clusters of preganglionic neurons. The specificity of innervation

allows the PVN to influence precise peripheral effectors, such as adrenal glands (Benarroch, 1993; Benarroch, 2020).

Jointly with the forebrain, also the brainstem includes areas implicated in the integrated autonomic control. Among these, periaqueductal grey has a role in the reaction to stress and pain. The parabrachial nucleus controls cardiovascular, respiratory, and gastrointestinal reflexes, thermoregulation, and food intake. Due to its efferences to basal forebrain, parabrachial nucleus is involved in arousal system (Benarroch, 1993; Benarroch, 2020). Another important brainstem area is the nucleus of solitary tract: it is the first station of integration for visceral afferents, baroreceptor, cardiac, pulmonary, chemoreceptor, and other vagal and glossopharyngeal afferents, as relay to medullary neurons to reflexly controls cardiovascular, respiratory, and gastrointestinal functions.

Neurons of the rostral and caudal ventrolateral medulla are fundamental stations for various sympathoexcitatory and sympathoinhibitory effects, and they mediate the baroreflex, somatosympathetic reflex, vestibulosympathetic reflex, and cardiovascular responses. Moreover, pacemaker neurons in the rostral ventrolateral medulla (RVLM) may increase their activity in response to local hypoxia.

The reticular formation of the RVLM comprehends premotor sympathoexcitatory neurons that, projecting to the intermediolateral column, are fundamental for the sympathetic regulation of baroreceptors reflexes, essential for blood pressure control.

Instead, the rostral ventromedial medulla (RVMM), including the medullary raphe, containing premotor sympathetic neurons with thermoregulatory function, coordinates the sympathetic response to cold (Benarroch, 1993; Benarroch, 2020).

1.2 SYMPATHETIC NERVOUS SYSTEM

1.2.1 General Organization of Sympathetic Nervous System

The sympathetic preganglionic neurons (SPNs) cell bodies are located in the intermediolateral cell column of the grey matter in the spinal cord, between the first thoracic segment down to the second lumbar segment (T_1-L_2). The SPNs axons traverse the ventral horn to exit the spinal cord via the ventral roots and synapse with postganglionic neurons in peripheral sympathetic ganglia.

The sympathetic ganglia are divided in paravertebral and prevertebral ganglia (or collateral ganglia, or preaortic ganglia; ***Figure 1***).

The paravertebral ganglia are classified in four types:

- Cervical; comprises of superior, middle, and inferior ganglia that supply head, neck, and thorax. The inferior cervical ganglion is fused with the first thoracic ganglion to form the stellate ganglion.
- Thoracic; consists of a chain of ganglia, one for each thoracic segment. T_1-T_5 ganglia supply the aortic, cardiac, and pulmonary plexus.
- Lumbar; placed in front of lumbar tract.
- Pelvic; situated in front of the sacrum, form the sacral ganglia (Bankenahally & Krovvidi, 2016).

Each SPNs sends its projection to the respective segmental paravertebral ganglion where it synapses with a postganglionic sympathetic neuron. It also sends ascending or descending projections to other paravertebral ganglia located more rostrally or caudally. Therefore, the paravertebral ganglia are connected and form the so-called sympathetic chain.

The prevertebral ganglia, instead, are placed in the abdominal cavity between the paravertebral ganglia and the target organs, anteriorly and laterally to descending aorta. Among these ganglia there are the suprarenal (or splanchnic), the celiac, the superior and inferior mesenteric, and the hypogastric ganglia. Postganglionic fibers that originate from prevertebral suprarenal and celiac ganglia innervate stomach, duodenum, liver, gallbladder, pancreas, and spleen. Superior mesenteric ganglia are localized near the origin of superior mesenteric artery. Their postganglionic fibers innervate small intestine and the first section of large intestine. Inferior mesenteric ganglia are near the origin of inferior mesenteric artery and their postganglionic fibers innervate the final part of large intestine, kidneys, urinary bladder, and genital organs (Benarroch, 2014).

Sympathetic preganglionic fibers may travel for significant distance (they are often short) and can cross several ganglia, before losing their myelin sheaths, splitting in numerous end fibers and synapsing with postganglionic neurons, mostly with axodendritic synapses. Therefore, terminals of preganglionic fibers may synapse with numerous postganglionic neurons, in some ganglia this ratio is 1:20. In the same way, one postganglionic neuron may be supplied by several preganglionic fibers (Brunton et al., 2011).

Postganglionic neurons usually send long fibers which directly innervate target organs and release as neurotransmitter NA, that is the neurotransmitter of election for the sympathetic division (except for eccrine sweat glands that release ACh). Together with NA postganglionic neurons can also release somatostatin, neuropeptide Y and ATP (Brunton et al., 2011).

Among sympathetic ganglia, we could include the adrenal medulla, that is an endocrine gland also considered a sympathetic modified ganglion. This is largely because the adrenal gland origins from the neuroectoderm, as the rest of the nervous system, but mostly because some preganglionic fibers that originate between T_5 and T_8 pass through paravertebral and prevertebral ganglia and synapse with specialized neurons, also termed chromaffin cells, that function as modified postganglionic neurons in adrenal gland. These neuroendocrine cells do not have axons and release catecholamines, 80% adrenaline (A) and the remainder NA, directly in the bloodstream. The ability of adrenal gland to release A, together with NA, is caused by the presence in chromaffin neurons of the phenylethanolamine-N-methyl-transferase (PNMT) enzyme, that convert NA in A. Its presence makes adrenal gland a peculiar sympathetic ganglion, the only one able to release A. Thus, the organs can be stimulated in two ways: directly by the sympathetic nerves, and indirectly by the adrenal medulla that release catecholamines in the bloodstream (De Diego et al., 2008).

1.2.2 Catecholamines and Adrenergic Receptors

An important traditional classification of autonomic nerves is based on the primary transmitter molecule released from their terminals and varicosities.

The principal neurotransmitters of sympathetic nervous system are NA and A. The synthesis of NA starts in the sympathetic nerve ending: the enzymes involved in the production of NA are synthetized in soma of neurons and then transported along the axons to terminals (Brunton et al., 2011).

The first step in NA synthesis is the transformation of amino acid tyrosine in levodopa through the action of enzyme tyrosine-hydroxylase (TH), that is the limiting-enzyme in the pathway of NA biosynthesis (Zigmond et al., 1989). This enzyme, that is a substrate for protein kinase A (PKA), protein kinase C (PKC), and Ca^{2+}/calmodulin-dependent protein kinase II, is activated by the stimulation of sympathetic nerves and adrenal medulla. The phosphorylation of TH leads to increased hydroxylase activity: this represents a strategy to increase catecholamines production when nerves are stimulated. Moreover, also the TH gene expression is regulated depending on nerve stimulation, in fact there is a delayed increased gene expression that allows to keep stable the amount of catecholamines despite increased transmitter release. Finally, one more method of catecholamines content regulation is a feedback inhibition that catechol compounds exert on TH (Brunton et al., 2011).

Levodopa, the product of TH, is converted to dopamine by a decarboxylase.

Subsequently, dopamineβ-hydroxylase catalyzes dopamine transformation in NA. NA, in turn, is converted in A by PNMT (Brunton et al., 2011; Scanzano & Cosentino, 2015).

The transmitters are stored in membrane-bound vesicles by means of high-affinity antiporter specific for catecholamines: the vesicular monoamine transporters (VMATs) 1 and 2 or Solute Carrier Family 18 Member A1 (SLC18A1) and Solute Carrier Family 18 Member A1 (SLC18A2; Katzung, 2018; Yaffe et al., 2018).

The release of transmitter takes place when an action potential opens voltage-sensitive Ca^{2+} channels with consequently increase of intracellular Ca^{2+}. The vesicles fuse with surface of membrane and transmitters are released in the synaptic cleft. The release of catecholamines can be blocked by drugs such as guanethidine and bretylium (Katzung, 2018).

At this point, released catecholamines diffuse out of the cleft or are removed by reuptake into the nerve terminals or into perisynaptic glia cells by Na^{+}-dependent transporter. An example of this mechanism is the reuptake of NA by norepinephrine transporter (NET, or reuptake 1). NET can be inhibited by cocaine and certain antidepressant drugs, resulting in an increase of transmitter activity in the synaptic cleft (Katzung, 2018; Brunton et al., 2011).

Subsequently to reuptake of NA and A, catecholamines can be re-stored in vesicles or metabolized. The two major enzymes involved in the catabolism of catecholamines are monoamine oxidase (MAO) and COMT (catechol *O*-methyltransferase). These enzymes are widely diffuse in many districts, but the highest concentration of each is in liver and kidney. Moreover, both neurons and glia contain MAO and COMT (Purves et al., 2001). In particular, MAO is associated with outer membrane of mitochondria, also within the sympathetic nerve terminals, while COMT is mostly cytoplasmatic, except in the adrenal medulla where is localized in membrane bound form in chromaffin cells (Brunton et al., 2011).

The first step of metabolism of catecholamines is catalyzed by MAO and is the conversion of NA and A in the oxidatively deaminated to a short-lived intermediate (3,4-dihydroxyphenylglycoaldehyde, DOPGAL). Aldehyde dehydrogenase metabolizes DOPGAL to 3,4-dihydroxymandelic acid (DOMA), while aldehyde reductase metabolized DOPGAL to 3,4-dihydroxyphenyl glycol (DOPEG). The latter is the most common metabolite produce in sympathetic neurons and in adrenal chromaffin cells, where aldose reductase can also convert a catecholamine in its corresponding alcohol. At his point, DOPEG is converted to 3-methyl, 4-hydroxyphenylglycol (MOPEG) by COMT. Then MOPEG is converted to vanillylmandelic acid (VMA) by alcohol and aldehyde dehydrogenase. Alternatively, NA and A can be converted by COMT in normetanephrine and metanephrine, leading anyway to the formation of VMA.

This alternative pathway is common mostly in adrenal medulla. Regardless, VMA represents the main final products of catecholamines metabolism (Brunton et al., 2011).

Amongst the physiological functions of sympathetic nerves, we recognize: smooth muscle contraction in blood vessels supplying skin, kidney, and mucous membranes, stimulation of exocrine glands, smooth muscle relaxation in the gut wall, bronchi, and blood vessels supplying skeletal muscle, heart rate increase, glycogenolysis in liver and muscle, lipolysis in adipose tissue, thermogenesis in the brown adipose tissue, modulation of the secretion of insulin and renin (Gros et al., 1997).

The action of NA and A is mediated by adrenergic receptors (ARs), that are 7-transmembrane, G-protein coupled receptors, characterized by the presence of a ligand-binding pocket that accommodates catecholamines (Brunton et al., 2011).

Due to their location, either presynaptically or postsynaptically on neurons or effector organs such as the heart, vasculature, immune cells, adipose tissue, this class of receptors mediates a wide range of important homeostatic responses (Hayward et al., 2004).

ARs are generally classified in two principal types: α and β. As a result of new pharmacological tools and new genetic techniques, several α and β receptors are nowadays known: three α1-ARs (α1A, α1B, and α1D), three α2-ARs (α2A/D, α2B, and α2c), and three β-ARs (β1, β2, and β3). It is known that NA has major affinity for α receptors, whereas A for β receptors.

The binding of NA and A to these metabotropic receptors determines the activation of heterotrimeric G proteins and subsequently a cascade of molecular effects, which depend on the second messenger (Hayward et al., 2004). G proteins typically stimulate (via Gs protein) or inhibit (via Gi protein) the enzyme adenylyl-cyclase or activate (via Gq protein) phospholipase C (PLC; Ciccarelli et al., 2017).

In particular, the activation of α_1-AR induced the stimulation of a Gq, and consequently PLC that promote the hydrolysis of phosphatidylinositol bisphosphate producing inositol trisphosphate and diacylglycerol. The result of this succession of events is the release of ions Ca^{2+} from the endoplasmic reticulum or protein kinase C (Scanzano & Cosentino, 2015).

On the other hand, the activation of α_2-AR determines the stimulation of a Gi, that leads to the adenylate cyclase inhibition and release of cycling adenosine monophosphate. For this reason, α_2-AR is considered an inhibitory receptors, moreover, they represent the presynaptic autoreceptors that inhibit the neurotransmitter release both in the central and peripheral nervous system (Scanzano & Cosentino, 2015) in a negative feedback regulatory manner. Presynaptic receptors have an important role in the regulation of neurotransmitter release from sympathetic nerve terminals (Brunton et al., 2011).

β-AR receptors, when activated, stimulate the action of a Gs, that determines the activation of adenylate cyclase and accumulation of second messenger cAMP, in addition promote the activation of protein kinase A and phosphorylation of Ca^{2+} L-type channels with consequently entry of ions Ca^{2+}.

Generally, α_2 and β_2 receptors can be placed relatively distant from nerve endings, for example they are found on blood cells such as leukocytes and platelets. In these cases, receptors can be activated by circulating catecholamines (Brunton et a., 2011).

In contrast, α_1 and β_1 receptors, are localized mostly in the proximity of sympathetic adrenergic nerve terminals in peripheral target organs: this organization allows to activate receptors during stimulation of nerves (Brunton et al., 2011).

Moreover, a considerable variable that influences the different response of any cell or organ to sympathetic catecholamines is the density and proportion of α and β receptors. For example, bronchial smooth muscle mostly express β receptors and this determines that NA has relatively little capacity to increase bronchial airflow, while A is a potent bronchodilator (Brunton et al., 2011).

Sympathetic functions can be selectively modified by using drugs that mimic or block action of transmitters, in particular drugs are classified as sympathomimetic (agonists) and sympatholytic (antagonists) and respectively enhance and interrupt adrenergic functions.

Sympathomimetics drugs mimic the stimulation of sympathetic nervous system and can be classified as directly acting (act directly on α or β receptors), indirectly acting (act by providing more norepinephrine to act on α or β receptors), or mixed acting (act by both mechanisms). These drugs can have great or very low selectively for a specific receptors type. Obviously, also catecholamines are sympathomimetic drugs. Sympathomimetics drugs are used in clinical for treating hypotension, hypertension, heart failure, chronic obstructive pulmonary disease, nasal congestion, narcolepsy, and asthma. The α and β adrenergic antagonists block or attenuate the effects of sympathomimetic drugs (Westfall, 2009).

Here some examples of sympathomimetic drugs: isoproterenol, dobutamine and cyclosporine which are β receptors agonists, phenylephrine is an α receptors agonists, finally, ephedrine and amphetamines that are both α and β receptors agonists.

Sympatholytic drug acts as inhibitors of sympathetic system discharge and are mostly α and β adrenergic antagonists, except for some α_2 agonist that are presynaptic receptors. Clinically, sympatholytic drugs are used as antihypertensive (even if they are not election drugs due to their side effects of drowsiness, fatigue, and dry mouth) and against anxiety disturbs (Vongpatanasin et al., 2011).

Some examples of sympatholytic drugs are propranolol as inhibitor of β receptors, while guanfacine, clonidine and α-methyldopa are α receptors antagonists

1.2.3 Sympathetic Activation: Functional Aspects

The sympathetic system is essential for the preservation of homeostasis.
Typically, the sympathetic activation in response to a stress or a contingency situation, leads to a coordinated action that determines the increase of well-oxygenated, nutrient-rich blood to the working skeletal muscle. The heart can pump more blood per minute because heart rate and myocardial contractility are increased. In the gastrointestinal district sympathetic stimulation causes vasoconstriction, in order to redistribute blood away from these metabolically inactive organs (McCorry, 2007; Brunton et al., 2011). Another essential effect of sympathetic activation is the bronchodilation in the lungs, that simplifies the air exchange with external atmosphere, maximizing both an increase uptake of oxygen and elimination of carbon dioxide. From the metabolic point of view, an enhanced rate of glycogenolysis and gluconeogenesis in liver occurs, causing an increased concentration of glucose in blood in order to guarantee the essential energy source to the brain. Also, an augmented concentration of fatty acid in blood verifies, due to the increased rate of lipolysis in adipose tissue. Skeletal muscle employs fatty acid to obtain energy for contraction (McCorry, 2007; Brunton et al., 2011).
Physiologically, sympathetic system is continuously active. This allows to adjust the degree of activation in function of external components and conditions (McCorry, 2007; Brunton et al., 2011). Of course, all the effects provoked by enhanced activation of sympathetic nerves are mediated by different ARs subtypes localized in numerous organs and tissues and by their different affinity for NA and A. For example, excitatory β1 receptors are largely diffuse in heart, receptors that have equal affinity for A and NA. On smooth muscle β2 receptors are present. These receptors tend to be inhibitory and cause relaxation of the smooth muscle. Vascular smooth muscle in skeletal muscle contains both α1 and β2 receptors. In this case, NA causes strong vasoconstriction stimulating the excitatory α1 receptors. On the other hand, A, stimulating both types of receptors, causes weak vasoconstriction with the stimulation of α1 receptors and vasodilation by the stimulation of β2 receptors.
Another example of β2 receptor stimulation on smooth muscle is the bronchodilation in the lungs, caused by the stimulation of receptors by circulating A (McCorry, 2007).

1.3 SYMPATHETIC NERVOUS SYSTEM AND IMMUNE SYSTEM

1.3.1 The Immune System: General Notions

The immune system is the first line of defense of our organism. The main role of the immune system is to recognize dangerous invaders such as bacteria, viruses, but also tumor cells, and eliminate them. It is crucial that this aim is obtained avoiding responses that could damage self-tissue or eliminate beneficial microbes. For this reason, the discrimination of pathogens is one of the main features of the immune system.

The immune system is characterized by two different lines of defense: the innate and the adaptive immune response.

The innate immunity is the first defense line and can be considered composed of four types of defensive barriers: an anatomic barrier constituted by skin and mucous membrane, a physiologic barrier represented by temperature, low pH and chemical mediators, moreover, processes of endocytosis and phagocytosis function as a defensive barrier, as well as the development of inflammation. All these together represent the innate strategy actuated in defense of organism (Chaplin, 2010; Marshall et al., 2018).

Another fundamental function of innate immune system is the capability of rapidly recruiting immune cells in the site of infection, where the production of cytokines and chemokines starts. Inflammation is considered the first stage in the immune response to an invading pathogen. The development of inflammation is a necessary step to stop the spread of infection as quickly as possible. The recruitment of innate immune cells actually is aimed to brake this spread (Nathan, 2002). Numerous cells are involved in the innate immune response such as phagocytes (macrophages and neutrophils), dendritic cells, mast cells, basophils, eosinophils, natural killer (NK) cells and innate lymphoid cells (Chaplin, 2010).

The main feature of innate immune response is the ability of recognizing components of foreign pathogens referred to as pathogen-associated molecular patterns (PAMPs) and damage-associated molecular patterns (DAMPs), which are expressed by host cells during cell damage or death. The germline-encoded pattern recognition receptors (PRRs), expressed by innate immune cells, recognize PAMPs and DAMPs. Through PRRs, innate immune cells can recognize a wide range of pathogens that share same components and molecules evolutionarily

conserved, such as lipopolysaccharides (LPSs), peptidoglycans, non-methylated CpG and double-stranded RNA (Marshall et al., 2018; Vivier & Malissen, 2005). Several types of PRRs have been described: Toll-like receptors (TLRs), cytosolic nucleotide-binding, oligomerization domain containing receptors NOD-like receptors (NLRs), retinoic acid-inducible gene I (RIG)-like receptors, C-type lectins, and absent in melanoma AIM like receptors (ALRs; Akira et al., 2006; Kawai & Akira, 2010; Muñoz-Wolf & Lavelle, 2016).

The detection of PAMPs or DAMPs by PRRs leads to the activation of an inflammatory response, the first physiological reaction for the fight against pathogens (Kieser & Kagan, 2017). The repertoire of innate immune receptors is shared by individuals of a given species (Vivier & Malissen, 2005).

If on one hand the first response by the innate immune system against an invader is immediate, on the other hand, the development of an efficient response by the adaptive immune system requires some time from the contact with the antigen. The relative delay in evolving an adaptive immune response is due to the antigen-specificity that characterizes the adaptive immune response. Because of the adaptive immune cells are highly specific, usually they are not numerous but are able to proliferate when necessary. The elevated specificity of adaptive immune cells is essential to create memory cells. The memory cells are usually in a dormient state, and they activate when get in contact with pathogens previously encountered.

This precious ability is the key of the efficiency and of the advantageous contribution of adaptive immune cells against invaders (Marshall et al., 2018).

The cells of adaptive immune system are B and T lymphocytes. The T cells recognizes specific antigens with the auxilium of antigen-presenting cells APCs, while B cells differentiate in plasma cells in order to produce antibodies.

Hence, the main functions of adaptive immune system are to produce cells able to recognize specific pathogens and to create an immune memory.

The functions of innate and adaptive immune system are strictly correlated and complementary (Chaplin, 2010).

1.3.2 Toll-Like Receptors and Innate Immunity

TLRs were discovered by the 2011 Nobel Prize winners in physiology or medicine Jules Hoffmann and Bruce Beutler. Until their discovery, the innate immune system was considered as an unsophisticated part of the immune system, with unspecific role only propaedeutic to elaborate adaptive immune responses (O'Neill et al., 2013).

Initially, the Toll receptor was identified as an essential protein involved in the dorsoventral development of *Drosophila melanogaster*, and then was recognized as a fundamental mediator of the innate immune response against fungal infection in flies (Beutler, 2009). In the mid-1990s, mammalian homologous of the Toll receptor, termed TLRs, were identified and nowadays 10 members of TLRs family are known in human and 12 in mice, with TLR1-9 shared by the two species (Akira & Takeda, 2004; Kawai & Akira, 2010). TLRs have a key role in recognition of infectious pathogens in mammals (Beutler, 2004). The TLRs role in recognition of PAMPs, evidences the specificity of the innate immune response and its key role in the host defence (Kawai & Akira, 2010).

TLRs are expressed on various immune cells such as macrophages, dendritic cells, B cells, specific types of T cells, and even on non-immune cells such as neurons, fibroblasts and epithelial cells. TLRs expression is modulated by several factors like exposure to pathogens, cytokines, and environmental stressors (Akira et al., 2006).

TLRs (TLR1, TLR2, TLR4, TLR5, TLR6 and TLR11) are expressed on cells surface and are transmembrane proteins characterized by a ectodomain with leucin-rich repeats, that facilitate recognition of PAMPs, a transmembrane and an intracellular domain, the Toll/interleukin-1 (IL-1) receptors (TIR) crucial for signal transduction. These TLRs mainly recognize microbial membrane components such as lipids, lipoproteins, and proteins. Some types of TLRs are exclusively expressed in internal cellular compartments, like endoplasmic reticulum, endosomes, lysosomes, and their ligands are mainly microbial nucleic acids (Akira et al., 2006; Kawai & Akira, 2010).

The intracellular domain of TLRs is homologous with the receptor of IL-1, known as TIR. The activation of TIR leads to the recruitment of MyD88, composed of two domains: a C-terminal Toll homology domain that interacts with TIR, and a N-terminal death domain. This death domain in turn interacts with the death domain of IL-1R-associated kinase (IRAK), a serine/threonine protein kinase. This interaction determines the autophosphorylation of IRAK. At this point of cascade, IRAK links tumor necrosis factor (TNF) receptor-associated factor 6 (TRAF6), determining its oligomerization. The oligomerization of TRAF6 activates TGF-β-activated kinase (TAK-1), a mitogen-activated protein kinase (MAPK), and inhibitor of nuclear factor kappa B (IkB) kinase. The consequent of these events is the translocation of nuclear factor kappa-light-chain-enhancer of activated B cells (NF-kB) to the nucleus. The activation of IkB kinase leads also to the activation of activator protein-1 (AP-1) transcription family members Jun and c-fos. Both AP-1 and NF-kB are required for the transcription of immune

response genes, such as TNF and other pro-inflammatory cytokines genes (Akira et al., 2006; Kawai & Akira, 2010).

The first identified TLR was TLR4. Its discovery started with a genetic study which involved mice C3H/HeJ, a strain resistant to endotoxic shock provoked by lipopolysaccharide (LPS) injection, due to a mutation in the *Tlr4* gene. LPS is a component of gram-negative bacteria cell wall recognized by TLR4 (Hoshino et al., 1999). LPS is usually the most potent immunostimulant component of bacteria wall. In particular, a lipid portion of LPS termed ‘‘lipid A’’ is responsible for most of the pathogenic phenomena associated with gram-negative bacterial infection such as endotoxic shock (Akira et al., 2006).

The process of recognition of LPS by TLR4 is complex and needs accessories molecules. Firstly, LPS bounds LPS-binding protein (LBP), that is a soluble acute-phase protein synthetized by liver, intestinal cells and adipose tissue (Djuric, 2017). LBP presents LPS to a cell surface pattern recognition receptor, CD14. CD14 can be expressed on macrophages surface or secreted into serum and is a high affinity LPS receptor, hence CD-14 deficient mice show great difficulties in activate a response against LPS (Haziot et al., 1996).

In association with TLR4 ectodomain, the protein MD-2 is another accessory molecule fundamental in LPS recognition (Schromm et al., 2001; Shimazu et al., 1999).

MD-1 protein, a homologous of MD-2, bind RP105, a molecule involved in LPS recognition. This protein is localized mostly on B cell surface and is not involved in TIR domain, but has a short cytoplasmic region with a tyrosine-phosphorylation motif (Miyake et al., 1995). LPS-RP105 binding leads to the activation of proto-oncogene tyrosine-protein kinase (Syk), and the cascade of events that constitutes the innate immune response to LPS (Medzhitov, 2001).

Moreover, TLR4 is involved in the recognition of other ligands, such as respiratory syncytial virus fusion protein, heat shock protein HSP60, *Mycobacterium tuberculosis*, and *Streptococcus pneumoniae* (Kawai & Akira, 2010; Medzhitov, 2001).

While the innate immune response to gram negative bacteria is mediated by TLR4, TLR2 is responsible for that against gram positive bacteria. The component of gram-positive bacteria wall that has immunostimulatory action, analogous to LPS for TLR4, is the lipoteichoic acid (LTA). The importance of TLR2 in the host defence against gram-positive bacteria has been demonstrated using TLR2 knockout mice, which were found to be highly susceptible to challenge with *Staphylococcus aureus* or *Streptococcus pneumoniae* (Echchannaoui et al., 2002; Takeuchi et al., 2000).

TLR2s can also recognize lipoprotein and peptidoglycans. The peculiarity of TLR2 is its capability to form heterodimers with TRL1 or TLR6. These act together with coreceptors like

CD36, mostly TLR2-TLR6 dimers, and dectin-1 that binds fungus β-glucans, inducing their internalization (Kawai & Akira, 2010). A potent agonist of TLR2 is the lipopeptide S-[2,3-bis(palmitoyloxy)propyl] cysteine (Pam2Cys), which is derived from the lipid component of macrophage-activating lipopeptide2 (MALP-2) present in *Mycoplasma*. Pam2cys has the ability to bind and activate TLR2 or TLR2-TLR6 heterodimers on innate immune cells, in particular on dendritic cells, inducing the production of pro-inflammatory cytokines, specifically TNF, IFN-γ, and interleukin-12 p70 (IL-12p70; Medard et al., 2018; Zeng et al., 2010).

TLR5 detects flagellin, the major component of bacteria flagella and, specially, its D1 constant domain that is conserved among species. TLR5s are spread especially in epithelial cells of intestine and in lungs.

Bacterial DNA has a specific TLR that recognizes its presence: TLR9. Its ability is detecting CpG motif on the base of its position: TLR9s are placed in endosome, so the bacterial DNA must cross the plasma membrane to be detected. Once in the endosome, double-strands DNA start to degrade and TLR9 can recognize CpG fragments. The reason for the TLR9s position is to avoid their interaction with host DNA (Akira et al., 2006; Kawai & Akira, 2010).

Furthermore, TLR9s ae involved in the recognition of viruses' DNA, while viruses' single stranded RNA is perceived by TLR7s and TLR8s, double stranded RNA by TLR3s.

TLR3s recognize also polyinosinedeoxycytidylic acid (Poly I:C), synthetic analog of viruses' double stranded RNA. As agonist of TLR3, Poly I:C mimic a viral infection, causing the secretion of type-1 interferons (IFN-I, like IFN-alpha, beta etc,) and pro-inflammatory citokines due to the stimulation of innate immune cells (Akira et al., 2006; Waele et al., 2021). The activation of TLR3 signaling, infact, requires the involvment of an adaptor protein, TLR adaptor molecule 1 (TICAM1), whose pathway lead to the involvment of TNF receptor-associated factors TRAF3 and TRAF6 (Waele et al., 2021).

Finally, some viral-envelope proteins can be recognized by TLR4 or TLR2, resulting in pro-inflammatory cytokines production rather than specific antiviral responses.

All mentioned TLRs type's signal trasduction is mediated by MyD88, activating the MyD88-dependent pathway, with the exception of TLR3 that activates only the MyD88-indipendent pathway (Akira et al., 2006).

1.3.3 Autonomic innervation of primary and secondary lymphoid organs

The nervous and the immune system, considered the two super-systems of the body, talk to, and influence each other. In particular, the nervous influence on immunity is clear since the pionieristic studies of Felten et al, that described the sympathetic innervation of primary and secondary lymphoid organs (Felten et al., 1985), but also from the works of Besedovsky and colleagues, that introduced the concept of a neural reflex that inhibits immune function (Besedovsky et al., 1979).

The autonomic nervous system innervates lymphoid organs (which include bone marrow, thymus, spleen, lymph nodes, the mucosa, gut, and bronchus -associated lymphoid tissues, (MALT, GALT, BALT) the appendix and the Peyer's patch), and influence the immune response to immune challenges. All primary and secondary immune organs receive a substantial sympathetic innervation from sympathetic postganglionic neurons. There is no neuroanatomical evidence for a parasympathetic or vagal nerve supply to any immune organ (Nance & Sanders, 2007).

Studies focusing on the innervation of primary and secondary lymphoid organs, revealed that in bone marrow the predominant nature of nerves is sympathetic. This suggested the possible involvement of SNS in generation of immune cells, in fact, nowadays it is clear that SNS enhances motility, proliferation and release of immune cells from bone marrow (Ordovas-Montanes et al., 2015). Bone marrow express specific subclasses of α and β-ARs: the stimulation of β_2-ARs promotes haematopoiesis for all types of blood cells, while the stimulation of α-ARs, greatly suppresses granulocytes-monocyte colony-forming units and platelets production, but increases lymphopoiesis (Bellinger & Lorton, 2014).

The thymus is a primary lymphoid organ, anatomically divided in two distinct regions: the cortex and the medulla. The pivotal function of thymus is the maturation of T cells, consisting in development of specific antigen on T cells surface and eliminating self-reactive T cells.

Thymus is innervated from sympathetic fibres which derive from cervical and upper thoracic sympathetic chain, specifically from superior cervical and stellate ganglion.

Sympathetic fibres enter the thymus along blood vessels and distribute in the cortex at subcapsular plexus and corticomedullary junction (an area important for immigration of thymocytes from the thymus), spreading into medulla (Elenkov et al., 2000).

Sympathetic nerves also closely appose to macrophages, mast cells, fibroblasts, eosinophils. Probably, the functional role of these fibres is to be ascribed to regulate T cells development through the influence of different ARs (Bellinger & Lorton, 2014).

Trotter and colleagues, utilizing the transneuronal retrograde transport of pseudorabies virus (PRV), examined the thymus innervation and identified the presence of premotor sympathetic

neurons in the medulla oblongata, pons and hypothalamus, brain areas identified to be involved in responses to endotoxin or stress (Trotter et al., 2007).

The spleen receives sympathetic innervation from prevertebral sympathetic ganglia associated with the celiac-mesenteric plexus (Nance & Sanders, 2007). No evidence is found for sensory input nor for parasympathetic efferent nerves (Nance & Sanders, 2007). The peculiarity of the innervation of the spleen is that the density of sympathetic nerves in the white and red pulp can change under certain physiological and pathological conditions, for example, during the aging, sympathetic nerves are lost in white pulp (Bellinger & Lorton, 2014). Lymph nodes are secondary lymphoid organ which constantly collect, control and filter lymph. They are the principal sites for adaptive immune response. Lymph nodes are anatomically divided in cortex and medulla which connects to hilum, where the efferent vessels exit. The cortex is characterized by the presence of a superficial follicular B cells and a deep T cells area, whereas the medulla hosts macrophages. The entire lymph node is covered by a collagen-rich capsule that is penetrated by afferent lymph vessels that discharge lymph into the subcapsular sinus, a fluid-filled space that is densely lined by specialized macrophages and lymphatic endothelial cells (Huang et al., 2021).

Lymph nodes are innervated by sympathetic fibres, moreover, there is some neuroanatomical evidence that lymph nodes may receive a direct neural afferent innervation (Nance & Sanders, 2007). Sympathetic nerves enter the lymph nodes through the hilum, following the blood vessels and innervate the deeper layer of the cortex and the medulla.

There is no neuroanatomical evidence for a parasympathetic innervation of lymph nodes (Nance & Sanders, 2007; Huang et al., 2021).

Recently, a study conducted by Huang and colleagues confirm the data that state the presence of sensory fibres in lymph nodes, specifically in shallow cortex and perivascular and subcapsular space. Functionally, this may reflect the importance of sensory fibres in regulating localized inflammatory response (Huang et al., 2021).

Finally, the appendix, Peyer's patch, MALT, GALT, and BALT receive innervation from sympathetic nervous system.

1.3.4 Inflammation needs to be finely regulated

Inflammation is a complex set of interactions which takes place among soluble factors and cells. It can occur in any tissue in response to traumatic, infectious, post-ischaemic, toxic or autoimmune injury. Usually, the entire process leads to recovery from infection and to healing.

Inflammation is necessary. An impaired inflammatory response can lead to immunodeficiency, a condition that is life-threatening. As a matter of fact, people with serious genetic defects for the essential components of inflammation have a significantly increased risk of contracting serious and often fatal infections (Nathan, 2002). At the same time, inflammation comes at a cost. If exaggerated and not properly phased, it can lead to persistent tissue damage and in extreme cases it can be life-threatening. Sepsis, a clinical condition characterized by exaggerated and uncontrolled levels of systemic inflammatory cytokines, is the worldwide leading cause of death in intensive care units (Zaccone et al., 2017). Hence, it is clear that inflammation needs to be properly regulated in order to maintain the homeostasis of immune responses (Nathan, 2002).

The classical definition of inflammation comprises *rubor* (redness), *calor* (warmth), *dolor* (pain) and *tumour* (swelling), and *functio laesa* (loss of function; Netea et al., 2017).

Functionally, inflammation is defined as a protective response for the organism stimulated by invading pathogens or endogenous signals such as damaged cells, resulting in the elimination of the initial cause of injury, clearance of necrotic cells, and tissue repair (Netea et al., 2017).

The trigger of inflammation process is mostly the ligation between PAMPs and PRRs, as well as the perception of a tissue damage. The events generated by this binding are called “acute phase” response and are strictly link with the trigger of local event.

In few minutes, vasodilation and enhanced permeability of vessels due to the production of prostaglandins, determine in local infection site the infiltration of neutrophils during bacterial infection and mononuclear leukocytes during viral infection (Dempsey et al., 2003). Moreover, prostaglandins increase vascular permeability leading to the attraction in the infection site of kinin, serotonin (5-HT), and histamine, causing redness, increased blood flow and plasma exudation, hence edema. In addition, prostaglandins affect afferent C fibers producing hyperalgesia and finally, act on hypothalamic neurons involved in thermoregulation, determining the increase in Tb. Prostaglandins are synthesized by cyclooxygenase 1 and 2 enzymes (Abdulkhaleq et al., 2018).

The main actors in the acute phase response are the pro-inflammatory cytokines: TNF, interleukin-1β (IL-1β), interleukin-6 (IL-6), interleukin-8 (IL-8), and IL12p70. These have autocrine and paracrine effects leading to the local activation of macrophages and neutrophils, that exert a key role for the phagocytosis and killing of pathogens. Moreover, cytokines signal to endothelial cells to increase vascular permeability in order to induce the displacement of immune cells in the site of infection. The eventual adverse effects of this event are vasodilation and hypotension (Netea et al., 2017).

TNF is a sufficient and necessary mediator of inflammation and of endotoxic shock. The production of TNF mRNA is stimulated by NF- kB, c-Jun, AP-1 (Tracey & Cerami, 1989).

TNF exists in two forms: one is a 26 KDa transmembrane protein present on the surface of monocytes, macrophages, activated NK cells, activated T cells, endothelial cells, and fibroblasts. Transmembrane form can be cleaved by a metalloprotease, TNF-converting enzyme (TACE), producing the 17 KDa soluble TNF, the circulating form. Both transmembrane and circulating TNF share receptors TNFR1 and TNFR2, whose expression is inducible by cytokines, mostly interferons. The interaction between TNF and its receptors, enhances the translocation of NF- kB to the nucleus, implementing the production of TNF through a positive feed-back.

Furthermore, the ligation of TNF with TNFR produces the activation of 5-lipoxygenase and phospholipase A2 enzymes, that results in the production of arachidonic acid, 5-hydroxyeicosatetraenoic acid (5-HETE) and proinflammatory leukotrienes. Finally, the binding between TNF-TNFR1 induces apoptotic cell death, stimulating a signaling targeted at caspase-3, which causes cell death activating a DNase. Normally, this pathway is not induced in mammalian cells, but only in transformed cells, virus infected cells, stressed cells or biochemically imbalance cells (Chu, 2013; Holbrook et al., 2019).

Another mechanism that activates caspases contextually to inflammation process is the assemblage of inflammasome. Inflammasome is a multiprotein complex that TLRs aggregate consequently to the detection of pathogens or cells and tissues damages. The formation of inflammasome determines the activation of caspases (caspase 1 and caspase 11 in mice and caspase 4 and caspase 5 in humans), and release of pro-inflammatory cytokines, like IL-1β and IL-8 (Broz & Dixit, 2016). Moreover, it induces the pyroptosis, a lytic type of cell death, featured by cell swelling, lysis, and release of cytoplasmatic content, maybe as a consequence of pores formation in cells membrane. One other important component of inflammation is the activation of the complement system, which mediates microbial opsonisation and killing, and generates inflammatory peptides (Netea et al., 2017).

Concomitantly to the acute phase of inflammation, anti-inflammatory cytokines come in to play with the aim of starting the resolution of inflammation. The main actors implied are interleukin-10 (IL-10), released from T cells and macrophages, interleukin-37 (IL-37), Transforming growth factor beta (TGF-β) released from macrophages and platelets.

IL-10 inhibits the expression of inflammatory cytokines such as TNF, IL-6 and IL-1 by activated macrophages; whereas TGF-β suppresses cytokines production by inhibiting macrophage and Th1 cell activity; neutralizes IL-1, IL-2, IL-6, and TNF (Zhang & An, 2007).

The resolution of inflammation is the time that elapses between peak inflammatory cells influx and the clearance of these cells from inflammation site, with the return to homeostasis. Hence, the resolution is an active process during which pro-inflammatory mediators are catabolized and efferocytosis occurs (Fullerton & Gilroy, 2016).

1.3.5 Sympathetic nerves and inflammation: The Inflammatory Reflex

The CNS can influence immune function by controlling inflammation in two main ways: 1) through an endocrine pathway, activating the hypothalamus-pituitary-adrenal axis (HPA axis) to release glucocorticoids which have an anti-inflammatory function (Bellavance & Rivest, 2014); 2) via the autonomic nervous system (Pongratz & Straub, 2014).

For what concerns the reflex activation of the HPA axis, it has been shown that in response to an immune challenge, the circulating cytokines activate the PVN (Besedovsky et al., 1979). The activation of PVN implies the release of corticotropin-releasing hormone (CRH) in the portal circulation of the anterior pituitary gland. CRH, in turn, induces the release of adrenocorticotrophic hormone (ACTH) in the bloodstream by pituitary corticotropes. Finally, ACTH stimulates the production and the systemic release of glucocorticoids, by the adrenal cortex, which inhibits the inflammatory response (Bellavance & Rivest, 2014).

The brain can also influence immune function because nerves, and in particular sympathetic nerves, talk to leukocytes in lymphoid organs (see above for details, paragraph 1.3.3).

The first paper reporting a possible role for the SNS in controlling immune function dates to 1903. It described the increased redness and temperature, signs of an exaggerated inflammatory response, caused by the section of the sympathetic nerves innervating the ear in rabbits (Meltzer & Meltzer, 1903). Sympathetic nerves have the ability to inhibit or enhance the inflammatory response, depending on the immune challenge (Kenney & Ganta, 2014). Confirming this concept, different studies have shown that the sympathetic denervation of lymphoid organs influences the outcome of inflammatory processes, in some cases exacerbating it, in others decreasing it (Lorton et al., 1999; Lorton et al., 1996). It has recently been shown that the voluntary activation of the SNS, through various techniques (meditation, breathing techniques, exposure to cold), can inhibit the inflammation induced by the intravenous administration of LPS in healthy subjects (Kox et al., 2014). Immune regulation also appears to be under circadian control via structures in the CNS, such as the suprachiasmatic nucleus (SCN), which controls sympathetic and parasympathetic output to peripheral organs (Riganello et al., 2019).

Analogous to the reflex activation of the HPA axis, also sympathetic nerves are reflexly activated in response to an immune challenge (Martelli et al., 2014). Their final effect is to inhibit an excessive release of inflammatory mediators, contributing to the maintenance of the immunological homeostasis (Martelli et al., 2014). This concept was initially introduced by Besedovsky and colleagues (Besedowsky et al., 1979) and eventually revolutionized by Tracey at the beginning of the 21st century, when he introduced the concept of the inflammatory reflex (Tracey, 2002). According to the theory put forward by Tracey and colleagues, the inflammatory reflex is a vago-vagal reflex with both sensory and motor arm travelling in the vagus nerves (Tracey, 2002). The immune challenged would be sensed by vagal afferences and this information carried back to the CNS. In response to this, the efferent arm of the inflammatory reflex, that they termed the cholinergic anti-inflammatory pathway (Rosas-Ballina & Tracey, 2009), would be activated as follow: the activation of the vagal efferent fibers would induce the activation of the fibers of the splenic (sympathetic) nerve, which in turn would release NA inside the spleen. NA would bind to β_2-ARs present on a specific subpopulation of T lymphocytes, which in turn would release ACh. ACh would bind to a specific nicotinic receptor, containing the subunit α 7 (α7nAChRs), on splenic macrophages, leading to the inhibition of the translocation of the NF-kB and therefore to the inhibition of synthesis and release of TNF and other pro-inflammatory cytokines (Rosas-Ballina & Tracey, 2009).

This view of the inflammatory reflex has recently been challenged and a new model has been introduced (Martelli et al., 2014). Because, if it is true that vagal stimulation (either efferent or afferent fibers; Borovikova et al., 2000) induces a reduction of the inflammatory response, it is not equally true that this activation is physiologically, endogenously, present. In fact, it has been demonstrated that prior vagotomy, obtained by sectioning the two cervical vagi, is not associated with an increase in TNF plasma levels in response to LPS intravenous administration (Martelli et al., 2014). Furthermore, the synaptic connection between the vagus and the sympathetic splenic nerves has not been demonstrated (Martelli, et al., 2014). On the contrary, it has been shown that prior bilaterally sectioning of the greater splanchnic sympathetic nerves results in an exaggerated release of plasma TNF and other pro-inflammatory cytokines in LPS-challenged animals (Martelli, et al., 2014). These effects were not limited to TNF but also extended to IL-10, the anti-inflammatory cytokine, that was inhibited by the prior cutting of the splanchnic nerves (Marteli et al., 2014; ***Figure 2***). The administration of LPS strongly increases the efferent sympathetic activity of the splanchnic nerve and its splenic branch (Martelli et al., 2014); the splenic activity is not modified by vagotomy, while it drops dramatically when the great splanchnic nerve is cut (Martelli et al., 2014). The most likely explanation for these

observations is that the efferent arm of the inflammatory reflex is purely sympathetic and consists of the splanchnic nerve. Martelli and colleagues termed this efferent arm of the reflex the splanchnic anti-inflammatory pathway (SAIP; Martelli et al., 2016) .

In subsequent studies, the same team went to demonstrate that the target organ of the SAIP, where sympathetic nerves talk to and inhibit leukocytes, is not limited to the spleen but rather distributed across abdominal organs (Martelli et al., 2019; ***Figure 3***). Recently, a study demonstated that sheep with the SAIP compromised react to a systemic *E.Coli* infection with an exaggerated inflammatory response but, at the same time, eradicate all live bacteria in less than 90 minutes instead of days (Lankadeva et al., 2020). This result in sheep model suggests that the inflammatory reflex is a common biological response across species.

The afferent arm of the reflex is still unknown, even if the vagotomy studies suggest that this cannot travel through the vagus nerves. It could travel through different sensory spinal nerves or it could be humoral (Martelli et al., 2016).

So far, the existence of the inflammatory reflex has been demonstrated only in rats and sheep. Moreover, the importance of the SAIP in controlling inflammation has been only shown in response to immune challenges recognized by TLR4.

1.4 SYMPATHETIC NERVOUS SYSTEM AND THERMOREGULATION

1.4.1 Thermoregulation

Thermoregulation, a perfect example of homeostatic regulation, is the ability of an organism to maintain a relatively constant core Tb (Tansey & Johnson, 2015).

The maintenance of a stable Tb is pivotal to guarantee the key functions necessary for organism survival. Indeed, the temperature has a key role in biochemistry, for both reactions velocity and stability of complex molecules structures (such as proteins, DNA, RNA, lipid layers, and so on). Expanding the concept, each biological process is conditioned by the temperature and, particularly for animals, by the capability to maintain it within a narrow optimal range.

Most organisms cannot operate at a Tb below 0 °C, because water usually turns into ice, making it impossible (with few exceptions) for a cell to survive. On the other hand, life is also nearly impossible at a Tb above 45°C, as enzymes that catalyze biochemical reactions start denaturing (Romanovsky, 2018).

Based on their ability to maintain a constant Tb, animals can be divided into two main categories:

- Poikilotherms (from Greek poikilos, which means mutable);
- Homeotherms (from Greek Omoios, which means equal, same).

Poikilotherms, the vast majority of organisms belonging to the animal kingdom, are organisms whose internal temperature fluctuates as the environmental temperature varies. These animals, having a very low metabolism, absorb the heat directly from the sun. This aspect can have pros and cons: if on one hand their low metabolism forces them to be inactive during the night, on the other hand they can survive in very dry environment, with poor faunas and flora, because their food need is really reduced compared to that of mammals of the same size.

These animals have also been defined cold-blooded, because often their Tb is in the lower and middle range compatible with the life, and they cannot increase their metabolism strongly enough to prevent a drop in deep Tb.

The definition cold-blooded can induce to think that their temperature has to be always low, and they remain mandatorily passive to the environmental variations. However, this is not totally true. Cold blooded animals can show some compensatory behaviors, as thermoregulatory mechanisms. Some reptiles, in order to stay active, during the cold days look for sunny places exposing themselves to the sun and staying in contact with the soil. Other reptiles of the iguanid family and some box turtles can use the wheezing to lose heat when, exposing to the sun, the skin or the Tb increase too much. Another strategy that some poikilotherms adopt, when a warm environment is not available or when the food is scarce, is to look for a safe place and fall into lethargy. So, the better definition for these animals is "ectothermic", namely organisms that take the heat they need from the external environment.

On the contrary, homeotherms can be considered "endothermic" as they are able to generate the heat they need, even though they use around the 80 percent of the energy from their food to get that.

Homeotherms are all the animals whose internal temperature varies in a very restricted range, despite even notable thermal variations of the external environment or of their internal heat production. The homeothermy implies a fine equilibrium between heat production and loss.

These animals are warm-blooded, and they can achieve warm-bloodedness and homeothermy because they can readily generate heat due to a high basal metabolic rate, which can be increased in response to cold. Indeed, they can be defined tachymetabolic and their sustained metabolic rate is 15–50 times higher than that of bradymetabolic animals (Hammond & Diamond, 1997).

This higher metabolic rate has some consequences: it requires a more complex thermoregulation, mainly under the control of ANS, and it also requires a higher caloric intake (Cerri, 2017). Nevertheless, homeothermy is the feature that allowed mammals to spread across practically the entire planet, occupying almost every ecological niche (Grigg et al., 2004).

In mammals, normal core Tb is around 37°C, controlled within a quite narrow range (33.2–38.2°C), although there are normal fluctuations that occur throughout the day (circadian rhythm), throughout a month (menstrual cycle), and throughout a lifetime (aging; Tansey & Johnson, 2015).

It is important to note that mammal's thermoregulation system is highly asymmetric, since homeothermic animal's normal Tb is much closer to the temperature of enzymes denaturation than to that of water crystallization (Romanovsky, 2018). Hence, high Tbs are much more dangerous than low ones.

1.4.2 Central Control of Thermoregulation

Thermosensation enables mammals to maintain the homeostasis of Tb, hence to thermoregulate, and to avoid noxious temperature that may cause tissue damage.

Thermoregulation in mammals is under the control of the ANS, in particular of the sympathetic branch. The ANS regulates the thermogenesis and the heat loss to maintain an appropriate Tb through a complex reflex arc, in which an afferent and an efferent pathway can be identified (Cerri, 2017).

The afferent pathway delivers information on ambient temperature (Ta) detected by peripheral thermoreceptors localized mostly in the skin, but also in the oral cavity and upper respiratory tract. Thermoreceptors are mainly ascribable to the transient receptor potential family (TRP). They are cationic channels that act as signal transducers by altering membrane potential and intracellular calcium (Ca^{2+}) concentration. They are classified on the base of sequence homology and each TRP channel is activated within a relatively narrow temperature range. Specifically, the channels involved in cold perception are mostly TRPM8 and TRPA1, while the feeling of warming is mediated by TRPV1 and TRPV3 (Jordt et al., 2003; Samanta et al., 2018).

TRPM8 and TRPV1 are expressed in nerve terminals of dorsal root ganglia neurons and are activated below ~25 °C or above ~43 °C, respectively.

Hence, the collected temperature information from broad regions of the skin, are firstly perceived by dorsal root ganglia neurons and subsequently sent to secondary neurons located in the dorsal horn of the spinal cord (Jordt et al., 2003).

The response of the secondary neurons to skin cooling or warming, respectively, is mainly mediated by glutamatergic signals from the TRPM8 and TRPV1 channels (Ran et al., 2016). The secondary neurons project to the lateral parabrachial nucleus (LPB), in the brainstem, where there are neurons activated by either warm or cold stimuli (Nakamura & Morrison, 2010). The dorsolateral area of the LPB contains neurons that are activated by the cooling of the skin. The activation of these neurons is required for the induction of responses to cold, such as shivering and brown adipose tissue (BAT) thermogenesis (see below for details; Nakamura & Morrison, 2008).

Whereas, in the dorsomedial portion of the LPB there are neurons activated by heat exposure, and a glutamatergic activation of these neurons is essential for the induction of the autonomic responses to heat, such as the inhibition of vasoconstriction and BAT thermogenesis (Nakamura & Morrison, 2010).

The LPB neurons are a pivotal relay in processing the thermal information. Indeed, they send axonal branches to the ventrolateral thalamus, which will then relay the information to the cerebral cortex. This spinothalamic pathway provides the structural substrate for thermal sensation (Craig, 2002). This is not necessary for the autonomic responses to the detected thermal information. The anatomical substrate for the autonomic control of Tb involves the other axonal branches that the LPB neurons send to the hypothalamus, in particular to the preoptic area (POA; Nakamura & Morrison, 2010).

The POA neurons are fundamental in the integration of the thermal afferent information to control the responses to thermal stimuli, being the transition area from thermoafferent to thermoefferent pathway (Madden & Morrison, 2019). Two nuclei of the POA are involved in thermal afferent processing: the median preoptic nucleus (MnPO), and the medial preoptic area (MPA), more caudal, dorsal, and lateral respect to the MnPO (Tanaka et al., 2009). The MPA receive cutaneous thermal information, while in the MnPO are located classic warm- and cold-sensitive neurons (Cerri, 2017).

Mostly of the MnPO thermosensitive neurons are warm sensitive neurons (WSN), which increase their firing rate in response to an increase in local temperature. Moreover, most of the WSNs are γ-aminobutyric acid (GABA)-ergic neurons. Hence the main output of the POA is an inhibitory signal for thermogenesis and heat-saving processes (Madden & Morrison, 2019). The neural connections among the POA areas plays a crucial role in thermoregulation. On one

hand, the MnPo neurons, which receive the thermal information from the cold-activated dorsolateral LPB neurons, prevent the GABAergic output of the MPA neurons. On the other hand, the MnPO neurons, receiving the input from the warm-activated dorsomedial LPB neurons, activate the GABAergic output of the MPA neurons (Madden & Morrison, 2019; ***Figure 4***).

The inhibitory output from POA is involved in themoefferent pathway. The raphe pallidus area (RPa) is a pivotal area for the sympathetic control of thermoregulation. RPa is located in the lower medulla where the sympathetic premotor neurons are placed (Farmer et al., 2019). For this reason, the RPa is a key relay site that controls thermoregulatory sympathetic outflow (Cerri, 2017). The RPa is characterized by serotonergic, GABA-ergic, and glutamatergic neurons (Stornetta et al., 2005), and indirectly projects, via polysynaptic pathways, to several organs involved in thermoregulation such as BAT, heart, and skeletal muscles.

The RPa regulates three main categories of thermal efferent pathways:

- vasomotion (cutaneous vasoconstrictor sympathetic fibers);
- thermogenesis (BAT sympathetic nerves and somatic motoneurons mediating shivering);
- evaporative heat loss (cholinergic sympathetic fibers mediating sweating and efferent fibers mediating saliva secretion).

Vasomotion - The RPa contains sympathetic premotor neurons that control pre and post-ganglionic sympathetic vasoconstrictor fibers, responsible for cutaneous vasoconstriction. Hence, warm stimuli perceived by the MnPO determine GABAergic transmission to MPA, which in turn inhibits the RPa therefore promoting vasodilatation (Nakamura et al., 2002). Conversely, skin cooling excites those neurons in the MnPO, which, in turn, directly activate the RPa, consequently promoting peripheral vasoconstriction (Tanaka et al., 2011).

Therefore, the RPa neurons induce cutaneous vasoconstriction through excitatory glutamatergic and serotonergic projections to preganglionic sympathetic neurons located in the intermediolateral column of the spinal cord (Ootsuka & Blessing, 2005). The preganglionic cells project to the sympathetic ganglia, where the postganglionic neurons that directly control effector responses are placed. Additionally, a minor role can be played in this pathway also by the RVLM, considering that some RVLM neurons projecting to the spinal cord can be inhibited by POA warming (Ootsuka & Terui, 1997).

Thermogenesis - Thermogenesis is subdivided in shivering and non-shivering thermogenesis. Shivering thermogenesis is driven by the somatomotor system and is mediated by skeletal

muscles. Non-shivering thermogenesis, instead, is controlled by the SNS and occurs in brown adipose tissue (Morrison et al., 2008).

Shivering consists of a sequence of involuntary, rapid, and oscillating contractions of skeletal muscle. It starts with not coordinated and asynchronous single contractions of the muscle fibers, becoming coordinated only in a second moment. Shivering is thermogenic because the muscles contraction consumes adenosine triphosphate (ATP), isometrically, hence without develop mechanic work, so that a vast amount of energy coming from ATP hydrolysis is lost as heat production. The ATP hydrolysis also increases the muscular concentration of ADP, which stimulates the electrons' transport system and the oxygen consumption, accelerating the substrates utilization, which, in turn, allows the ADP reconversion in ATP and the concomitant heat dissipation. This physiological mechanism is also defined as "shivering thermogenesis" (Morrison et al., 2008). The sequence of neurophysiological events goes as follows: cooling stimuli activate neurons in the dorsomedial hypothalamus (DMH), which in turn stimulate the somatic muscle premotor neurons in the RPa. Finally, the input from the latter activates the gamma and alpha motoneurons in the ventral horn of the spinal cord (Tanaka et al., 2006). The activation of these neurons increases muscle tone before shivering and modulates the intensity of shivering (Schäfer & Schäfer, 1973).

On the other hand, one other effective way to produce heat, especially in chronic cold exposure is the activation of non-shivering thermogenesis, which involves the BAT. The BAT is a highly specialized type of adipose tissue, which is found in mammals and some hibernating animals. The function of this adipose reticular tissue is to generate heat. Compared to the white adipose tissue, it contains several mitochondria whose cytochromes confer it the characteristic brown color. Its anatomical distribution is strategic, and, in fact, it is found in proximity with the main blood vessels. In this way the heat generated can be rapidly transferred to the blood and distributed to all the organs. In rodents, the interscapular BAT is the largest depot, with smaller depots in the mediastinum, along the cervical and thoracic aorta, and around the kidney (Giordano et al., 2016). In human beings, BAT is less centralized than in rodents, there are significant depots in supraclavicular, neck, and paraspinal regions (Lidell et al., 2013). The thermogenic capacity of the BAT depends on the uncoupling of oxidative phosphorylation, operated by the uncoupling protein 1 (UCP1) on the internal mitochondrial membrane. The thermogenesis activity in BAT is regulated by sympathetic nerves (***Figure 5***). The NA released by the sympathetic fibers on the brown adipocytes, in consequence of the hypothalamic signal, interacts with β3-ARs. This binding causes an intracellular cascade which starts with an increased synthesis of cyclic AMP (cAMP) that activates the cAMP-dependent protein kinase

(PKA), which, in turn, activates different targets, including: i) in the cytoplasm, the Hormone-sensitive lipase, that increases the lipase (cleavage of the triglycerides present in the lipid drops into fatty acids and glycerol); ii) in the nucleus, the cAMP response element-binding protein (CREB) which stimulates the transcription of the UCP1 gene. At this point the fatty acids released from the lipid drops enter the mitochondria and if one part undergoes β-oxidation, to be oxidized and supply electrons to the respiratory chain, another part activates the UCP1. The UCP1 is a transmembrane channel protein of the inner mitochondrial membrane that, once activated, permits a passage of protons. Consequently, protons from the intramembrane space fall into the mitochondrial matrix through the UCP1 and not through ATP synthase. This mechanism is known as "uncoupling" of oxidative phosphorylation. In this way, the energy of the proton gradient is dispersed as heat, rather than be utilized to form ATP (Scotto, 2006), while the substrate utilization for the production of ATP from ADP, and the related heat-production, is maintained ongoing due to the low ATP levels (Kooijman et al., 2015).

Similarly to what happen for vasomotion, even in the case of BAT activation RPa has a key role because it contains specific premotor sympathetic neurons (Madden & Morrison, 2019).

Moreover, some studies suggest that also DMH is involved in the regulation of BAT thermogenesis. In particular, injection of muscimol, an agonist of $GABA_A$ receptors in DMH reduces BAT sympathetic nervous activity and BAT thermogenesis (Nakamura & Morrison, 2007).

Evaporative heat loss - A process for loss body heat is the evaporation of water from the skin and membrane lining the respiratory tract. In this mechanism heat is transferred to the fluid, which evaporates and leaves the body in gaseous form. Evaporation is almost the only available mechanism to lose heat.

A crucial point is how the heat produced in the core is transported in the body surface. A predominant role is played by the blood circulation, which in addition to bringing the heat from the depths of the organism to the surface, affect its distribution inside the body. This occurs mainly through the mechanisms of vasoconstriction and vasodilatation. Still the process is regulated by nervous system. In fact, the major part of arterioles are under the control of SNS (Silverthorn et al., 2007). These vessels are largely controlled by vasoconstrictor sympathetic nerves, whose firing rate is reflexively increased in response to cold and decreased in response to heat. There is also a population of sympathetic neurons to the skin whose neurotransmitters cause active vasodilatation. Hence, the thermoregulatory control via SNS can modulate the cardiovascular system in two main ways: by modifying the heart rate, and by adjusting the diameter of the vessels. It follows that the exposure to low environmental temperatures induces

vasoconstriction in cutaneous blood vessels to preserve heat; meanwhile, there is also an increase in heart rate, to amplify heat transport from thermogenic organs to the whole body. In hot environments, instead, the body has to dissipate heat, which is achieved by increasing cutaneous blood flow and by shutting down thermogenic effectors. Moreover, in these circumstances, a decrease in cardiac frequency has been detected, which is caused by a lower oxygen demand by thermogenic organs (Silverthorn et al., 2007).

Sweat is released by eccrine glands, which are distributed in huge amounts over the whole surface of the body. Thus, from the skin the evaporation of sweat permits to transfer the heat to the environment under water vapor. Sweating is mediated by the activation of sympathetic cholinergic fibers (Shibasaki et al., 2006). Moreover, it has long been recognized that POA can induce sweating (Magoun et al., 1938): the entire circuit is not yet clear, but the GABAergic WSN in the POA are connected with premotor neurons causing sweating placed in RVMM. It is possible that also periaqueductal grey area (PAG) is involved in the circuit (Farrell et al., 2013).

Unlike humans and other mammals such as cats, rodents do not sweat, but they exploit the evaporative heat loss using the salivary secretion associated with grooming in order to spread the saliva over the skin surface. The submaxillary and sublingual glands mediate saliva secretion (Stricker & Hainsworth, 1970). The parasympathetic preganglionic neurons for saliva secretion are located in the superior salivary nucleus. It has been found that salivation is reduced by lesions of the lateral hypothalamus (Stricker & Hainsworth, 1970).

Thus, even if the entire thermal salivation circuit is not yet completely understood, it is supposed that the POA stimulates the lateral hypothalamic neurons, which in turn activates the superior salivary nucleus (Hosoya et al., 1990).

1.4.3 Natural torpor

Torpor is a physiological adaptive strategy that some mammals such as squirrels, hamsters, mice, bears, bats, and others spontaneously exhibit in adverse environmental conditions, and it is characterized by an active inhibition of metabolism that causes a decrease in Tb, proportionally to the thermal gradient between the body and the ambient (Heldmaier et al., 2004; ***Figure 6***).

The reduction of Tb is regulated at some levels and mostly occurs when Ta is low. In the cold, animals must produce a great amount of heat and consume energy to compensate heat loss. However, in this situation the cost of thermoregulation may become prohibitively too high,

because thermoregulating in extreme conditions means consuming energy and this requires large quantities of food and water. This is one of the reasons why some animals, during certain times of the day or the year, enter a state of torpor. During torpor, thermoregulatory responses are still operating but the defended Tb results much lowered from the classic 37°C. Animals can rewarm themselves from the low Tb during torpor by using endogenous heat production (Geiser, 2004).

Hibernation and torpor occur at least in several species belonging to 10 mammalian orders (Geiser, 2004) and 12 avian families (McKechnie & Lovegrove, 2002). Looking at the heterogeneous diffusion of the hibernating species it can be hypothesized that this characteristic trait has been inherited by a common protomammal. Therefore, it is likely that the ability to undergo torpor was then lost in many mammals, but it was maintained in species that could take advantage of energy saving to cope with extreme cold environments and resources shortage. This means that it is plausible that the gene pool required for torpor is still present and conserved in all mammals, including humans, but the regulatory mechanisms are no longer functioning (Cerri, 2017).

There are three main states of spontaneous hypothermia in the homeotherms: hibernation, daily torpor, and estivation. These three conditions are characterized by the same physiological basis, that is, as proposed by Heldmaier (Heldmaier et al., 2004), a substantial reduction of the metabolism. If the physiological properties of hibernation, daily torpor and estivation are similar, their classification is simply represented by differences in time, duration, and the extent of physiological inhibition.

Hibernation can be defined as a physiological state, lasting days or months, in which the metabolic rate is reversibly reduced to about 5% of the basal metabolic rate but can be also less than 1% when compared to the resting metabolic rate of normothermic animals exposed to low environmental temperature. The metabolic reduction is also associated with a decrease in Tb. Hibernating species usually reduce their Tb to 10 °C or below, with a minimum of −3 °C (Geiser, 2004). However, hibernators are not in torpid state during the entire hibernation season. In fact, the hibernation period is composed by bouts of torpor, with the controlled decrease of core temperature and metabolic rate, lasting for many days or weeks, and interrupted by arousals and brief normothermic resting periods, generally lasting less than one day. The arousal from torpor is a very rapid process, but it requires a huge amount of energy. It has been calculated that during the arousal phase the metabolic rate of the animal is about six time higher than that in basal condition of euthermia, but it can bring the animal temperature from 3 to 35

°C in less than 3 hours. The role played by these arousals and euthermic periods remains still unknown (Heldelmaier et al., 2004; Geiser, 2004).

The obligate hibernators follow an endogenous circannual rhythm, which induces them to hibernate each year, usually during the cold season, from the late summer/autumn to late winter/spring, regardless of the environmental conditions. For example, it has been showed that golden-mantled ground squirrels, born in captivity and housed under constant light and Ta, continue to hibernate each year, in a period corresponding to when the winter would begin in the wild (Pengelley et al., 1976). In addition, during the summer, obligate hibernators do not undergo hibernation, even if they are exposed to winter-like light and Ta. The endogenous circannual rhythm of the obligate hibernators can also be influenced by the cycle of the food intake and body mass in animals maintained under constant laboratory conditions (Ward & Armitage, 1981). This cycle, indeed, reflects the increase in body mass, before the hibernation, of the wild hibernators, such as the artic ground squirrels, which enhance their body fat to about seven or eight-fold, with also an increase in circulating leptin (Florant et al., 2004).

In facultative hibernators, instead, the expression and the various characteristics of hibernation, like duration, Tb reached, and metabolic rate etc., can diverge significantly in the different species, and, in particular, depend on the environmental conditions. Thus, for facultative hibernators, environmental conditions, such as Ta or available resources, strongly influence the heterothermy patterns. For example, the Syrian hamster does not seem to have any endogenous hibernation rhythm and can hibernate indifferently at any time of the year if it is exposed to short photoperiod and low Ta (Hylkema & Bouma, 2011).

The daily torpor is another state of spontaneous hypothermia shown by homeotherms. This form of torpor is not as deep as hibernation, in fact, the reduction of core temperature and metabolic rate are on average less intense, besides, compared to hibernation, the daily torpor lasts just hours rather than days or weeks, and it is usually interrupted by daily feeding and foraging. In particular, during this pattern of metabolic flexibility the animals reduce their metabolic levels no more than around 25% of its basal metabolic rate (Staples, 2016). The Tb in daily heterotherms, such as small carnivorous marsupials and mice, normally decreases to near 18 °C (Staples, 2016).

Compared to hibernators, in which the seasonal rhythm seems to cause the beginning and the end of the hibernation period, in daily torpor the animals appear to follow a circadian rhythmicity, rather than a seasonal pattern (Kortner & Geiser, 2000).

Finally, the estivation is a torpid state which can be considered as an energy saving strategy in environmental conditions of dryness, high Ta and food as well as water shortage. During

estivation the duration of the torpid period can vary a lot. Although it usually lasts around 9-10 months, it can go up to two years in some species. However, in general, animals use estivation to survive to the long dry season incompatible with life.

The key elements during estivation are: the accumulation of sufficient water and food resources for the duration of the dormancy period and, at a behavioral level, the finding of a sheltered and hidden place, where animals in estivation can ensure the conservation of water in the body, minimize their exposure to atmospheric agents and hide from predators. The conservation of energy reserves to survive during the dormancy period is essential and the metabolic rate during this period drops by 10-30% compared to the animal's metabolic rate during the resting period (Storey & Storey, 1990). But one of the most important consequences of the reduced metabolism during estivation is the associated decrease in gas exchange, which lend to a reduction in evaporative water loss, probably a key selective pressure during the evolution of the estivation strategy in the hot and dry environments. In fact, defense against water loss during dormancy is crucial (Geiser, 2010).

However, it is likely that daily torpor, hibernation, and estivation all rely on similar physiological patterns and underlying mechanisms of metabolic suppression and probably they also share a similar neuronal control (Ruf & Geiser, 2015).

1.4.4 Central Control of Torpor

Torpor and hibernation are complex strategies that enable animals to survive harsh environments that are otherwise incompatible with life. These require behavioral but also physiological and biochemical adaptations to external conditions and stressful environments.

In order to regulate this process, the existence of a network able to integrate internal information (such as energy balance, core temperature, energy availability etc.) with external information (e.g. Ta, resources accessibility, possible risks etc.), and, in the end, modulate metabolism, temperature and behavioral activity is essential.

The most supported theory has been the one according to whom the main controller of torpor and hibernation state is the ANS, due to its central role in directly and indirectly regulate metabolic rate.

In particular, accordingly with the proposed theory, the onset of torpor is mediated by the parasympathetic branch of the autonomic nervous system, whereas the arousal from the hypometabolic state is driven by the sympathetic branch (Harris & Milsom, 1995).

Recently, some data have begun to point out to some neural pathways and brain areas potentially responsible for the torpor onset, highlighting in particular the role played by POA and DMH (Hrvatin et al., 2020; Takahashi et al., 2020).

It is probable that hypothalamus is involved in the regulation of torpor, due to its role in regulating thermoregulation, energetic balance, and neuroendocrine secretion. Several other hypothalamic areas could also be implicated, including the SCN. Kilduff et colleagues reported that the glucose utilization by the SCN was higher, compared to most of the other brain areas during torpor bouts (Kilduff et al., 1989). Another study showed that the expression of early gene c-Fos increases during the arousal from torpor (O'Hara et al., 1999) in the SCN. Another evidence of the pivotal role played by this area is that SCN lesions alters the circannual rhythm of hibernation and the associated circannual cycle of fats storage and reproductive behavior in ground squirrels (Ruby et al., 1998). Moreover, recent research show that, an up-regulation of the melatonin receptor Mel1a occurs during torpor in the SNC (McCarron et al., 2001). The SCN efferences project to the sub-paraventricular zone, which is involved in the regulation of the wake-sleep cycle and in thermoregulation, and to the DMH.

In the last years, a great interest has developed regarding the DMH and its role in the induction of torpor. A recent study revealed the neural pathways involved in the onset of torpor in mice (facultative heterotherms), subjected to food deprivation and exposed to cold Ta (Hitrec et al., 2019). This study was made by combining the analyses of the neural activity marker c-fos at torpor onset and of a retrograde tracer injected into the RPa, with the aim to identify all the brain areas activated during torpor and projecting to the RPa. The RPa is a key area in the thermogenic efferent pathway and is supposed to be inhibited to suppress heat production and to allow the heat loss necessary for the entrance into torpor. The main result of this study was the identification of a neural network that is active during torpor onset in mice and possibly inhibits thermogenesis. In particular, two hypothalamic areas directly projecting to the RPa showed a relevant c-fos expression. The first one is the PVN, whose activation in rats induced an inhibition of the cold-induced activation of thermogenesis (Madden & Morrison , 2019). The other one is the DMH, that can be considered an important relay of the thermoregulatory information from superior brain centers to the RPa.

A recent study by Takahashi and colleagues showed that a hypothalamic neuronal population characterized by the expression of pyroglutamylated RFamide peptide (QRFP), that has been defined Q neurons, is fundamental in mice for the entrance into torpor. These neurons are located in the anteroventral PVN and in the MPA (Takahashi et al., 2020). The authors through the chemogenetic activation of this hypothalamic population of neurons were able to induce a

long period (more than 24 hours) of hypometabolism. This condition was characterized by a reduction of the Tb, together with a reduction of the mice BAT's temperature, even if thermoregulatory mechanisms seemed still to be active. When the Ta was reduced to 12 °C, mice adopted a more conservative posture, from the heat loss point of view, and exhibited also shivering and an increase in the rate of oxygen consumption (VO2). The other characteristics of the induced torpor were the huge heart rate reduction, the decrease of the respiratory rate, the very low amplitude of the electroencephalogram (EEG), and the low levels of blood glucose, probably due to the decrement of gluconeogenesis because of the low sympathetic activity. These animals spontaneously recovered from the induced torpor and did not show any tissue damage (Takahashi et al., 2020).

Due to the double nature of the Q neurons, both GABA-ergic and glutamatergic, the authors hypothesized that the GABAergic neurotransmission by Q neurons may inhibit the excitatory circuit between DMH neurons and the RPa. While, at the same time, the glutamatergic Q neurons might excite another subset of DMH neurons to inhibit heat production.

Another candidate amongst the hypothalamic nuclei responsible to induce torpor is the POA. A recent study demonstrated that the fasting-induced torpor in mice is modulated by neurons located in the medial and lateral POA (Hrvatin et al., 2020). The researchers, through chemogenetic reactivation of these neurons, which were active during torpor onset in mice, were able to obtain a new torpor bout, with a robust decrease in central temperature, locomotor activity and metabolism, even in mice that were not food deprived. In particular, the neurons identified as regulators of torpor, expressed the vesicular glutamate transporter 2 (Vglut2) and Adenylate Cyclase Activating Polypeptide 1 (Adcyap1). Indeed, the electrophysiological activity of these neurons changed at torpor onset, and it seems that both these neurons were necessary for the drastic decrease of the brain temperature during the torpor bout. Moreover, the activity of these neurons seems to be specific for the expression of torpor, since their chemogenetic silencing had no significant effect on normal homeostatic temperature control, and on its circadian rhythmicity. The authors affirmed that the glutamatergic Adcyap1 neurons in the POA receive information about the decrease of the external temperature. In addition, they found that these neurons and the Vglut2+ neurons express leptin receptors, suggesting that the circulating leptin levels could modulate the activity of these neurons. Consequently, in response to reduced energy reserves in fasting mice and during cold exposure, these neurons might be activated and induce torpor onset (Hrvatin et al., 2020).

1.4.5 Sympathetic Nervous System Manipulation and Thermoregulation: Synthetic Torpor

In the CNS, a pivotal area involved in the thermoregulatory pathways for cold defense is the RVMM, and in particular the RPa, where sympathetic premotor neurons are located. The activation of RPa neurons triggers the non-shivering and shivering thermogenesis, cutaneous vasoconstriction, and an increase in heart rate (Blessing & Nalivaiko, 2001; Cano et al., 2003; Zaretsky et al., 2003; Morrison & Nakamura, 2011).

Anatomical studies performed on the RVMM have revealed that this area contains the vesicular glutamate transporter 3 (Vglut3), that indicates the presence of glutamatergic neurons, mostly in the rostral portion; 5-HT or tryptophan hydroxylase, a synthetic enzyme for 5-HT, mostly in the caudal portion; and glutamic acid decarboxylase-67 (GAD-67), a marker for GABAergic neurons (Morrison & Nakamura, 2011). These neurons are activated in response to cold exposure or PGE administration, confirming their involvement in thermoregulatory response (Morrison & Nakamura, 2011).

In 2003 Zaretsky and colleagues, studied in conscious freely moving rats under baseline conditions, the effects of $GABA_A$ receptors agonist and antagonist injection in RPa. What emerged from this study was that the microinjection of bicuculline methiodide, a $GABA_A$ receptors antagonist, provoked tachycardia that appeared within 1 minute and was maximal within 10 minutes but had little or no effect on blood pressure or Tb. On the other hand, microinjection in RPa of muscimol, a $GABA_A$ receptors agonist, triggered a dose-related decrease in Tb but had no effect on heart rate or blood pressure. These results indicated that sympathetic premotor neurons in RPa, whose activation has been shown previously in anesthetized rats to increase the production of heat by metabolic activation of brown fat and reduce the loss of body heat by vasoconstriction in the tail (Blessing & Nalivaiko, 2001; Morrison et al., 1999) are likely to contribute to physiological thermoregulatory activity. Specifically, thermoregulatory neurons in this region appeared to be tonically active and contributed to maintenance of Tb under baseline conditions (Zaretsky et al., 2003).

Considering the central role of RPa in thermoregulatory pathway, in 2013 Cerri and colleagues, inhibited this brain area with multiple microinjections of muscimol (6 injections, 1/h) in free behaving rats, kept at Ta 15°C, in a constant darkness, and subjected to high fat diet. The results showed an intense drop in brain temperature (with a minimum of 22 °C), heart rate (from 440 bpm to around 200 bpm) and a reduction in the total power density of the EEG. The injections resulted in a significant peripheral vasodilation while the average blood pressure did not change,

and no major cardiac arrhythmias were observed. Moreover, no behavioral abnormalities were observed in the rewarming phase and in the days following the treatment (Cerri et al., 2013). Hence, by SNS manipulation, for the first time a deep hypothermia was induced in a non-hibernating species, by inhibiting sympathetic premotor neurons involved in the efferent arm of thermoregulatory cold defense pathway. The obtained suspended animation state showed several parallels with the features of natural torpor, and for this reason it was subsequently termed "synthetic torpor" (ST; Cerri, 2017).

1.4.6 Natural Torpor and Synthetic Torpor

Torpor is used by mammals as an energy saving strategy and can last from the few hours of an episode of daily torpor to many months during hibernation. In terms of evolution, it is highly likely that torpor was a trait of the proto-mammal; therefore the gene set required to survive such state should reasonably be common among mammals (Hitrec et al., 2019; Tinganelli et al., 2019).

In the light of this, it is not surprising that natural torpor shares some peculiarities with synthetic torpor, an hypometabolic state that is artificially induced in non-hibernators by inhibiting the RPa neurons (Cerri et al., 2013).

Many organs and systems are implied in the physiological changes and adaptations that occur in natural and synthetic torpor, however herein only the ones related to the nervous system will be discussed. One of the main characteristics that brings together natural and ST is the drastic reduction of electrical activity of brain, that results in low amplitude and low frequencies waves in the EEG recorded during hypothermic and hypometabolic phase of torpor (Deboer, 1998; Cerri et al., 2013). The peculiarity of the EEG recorded during torpor is that it differs from all the known sleep stages (Vyazovskiy et al., 2017). This is in accordance with the evidence that, during torpor, the alternation between NREM sleep (non-rapid eye movement) and REM sleep (rapid eye movement) disappear from the EEG spectra (Lo Martire et al., 2020; Royo et al., 2019; for more details on sleep see 1.5). Hence, torpor should be considered as a period of sleep deprivation (Cerri et al., 2021). Moreover, as better discussed in a specific section of the introduction, several studies report that immediately after the spontaneous exit from torpor or hibernation, a long bout of high intensity NREM sleep is observed in squirrels, hamsters, lemurs, (Strijkstra & Daan, 1998; Larkin & Heller, 1999; Deboer & Tobler, 2003; Royo et al., 2019). The same happens in rats exiting from ST (Cerri et al., 2013). The NREM sleep occurring soon after torpor is extraordinarily rich in cortical slow wave activity (SWA), which

typically appears following extended periods of wakefulness. Therefore, such SWA has been proposed to reflect high levels of accumulated sleep need during the torpor bout (Larkin & Heller, 1999; see 1.5).

Another physiological change occurring at brain level and that, as better discussed later, may be associated with the peculiar EEG changes observed during torpor is the remarkable synaptic plasticity observed during the hypothermic phase. This phenomenon was described for the first time in hippocampal pyramidal neurons of hibernating ground squirrels. During the hibernation bout the dendrites were shorter, less branched and had fewer dendritic spines. During the euthermic period of arousal, dendrites completely restore their structures (Popov et al., 1992). Subsequently, the same event was described in other brain areas, such as the cortex and the thalamus (Von der Ohe et al., 2006). *In vitro* data, obtained from mouse hippocampal slices, showed that dendritic spines disappear at low temperatures, while upon rewarming, spine re-emerge in the same location from which they had disappeared. Moreover, new spines were created (Kirov et al., 2004).

The exceptionality of this phenomenon is due to the uncommon large-scale changes in nervous system of mammals after the maturity. For this reason, the rate of reorganization of dendritic microstructures and synapses that occurs during torpor and hibernation represents an exceptional event, maybe a consequence of the dramatic metabolic reduction in the whole body during hypothermic state. In fact, the preservation of cellular integrity and the maintenance of neuronal resting potential are the most energetically demanding process for the mammalian brain (Du et al., 2008), so the decrease of energy availability during hibernation is, inevitably, associated with a drastic reduction of the neuronal activity (Chatfield & Lyman, 1954). Hence, the temperature-dependent reduction of synapses should be the cause of the unusual EEG signal of torpid hibernators that show that almost no electrical cortical activity is present (Arendt & Bullmann, 2013).

1.4.7 Tau protein

A process that probably contributes to neuronal plasticity during both natural and ST is the reversible hyperphosphorylation of Tau protein (Chiocchetti et al., 2021; Hitrec et al., 2021; Luppi et al., 2019; Arendt & Bullmann, 2013).Tau is a soluble microtubule-associated protein (MAP) with a low molecular weight. Its principal function is promoting microtubule polymerization and stabilization. The regulation of Tau protein is determined by the MAPT gene (microtubule-associated protein Tau), on chromosome 17q21.31, with an alternative

splicing mechanism by which six isoforms expressed in the central nervous system, are derived. The six isoforms differ from each other by the presence of three (3R) or four (4R) repeated C-terminal sequences of 31-32 amino acids, and for the combination with the presence or absence of one or two insertions of 29 amino acids (0N, 1N, 2N), in the N-terminal part (Stieler et al., 2011).

In the mature brain, Tau is mainly expressed in neurons and it is preferentially located in axons (Kempf et al., 1996), but it has also been found in the somatodendritic compartments (Tashiro et al., 1997) and in the nucleus associated with nucleoli (Violet et al., 2014).

The functions of Tau protein in the mature brain are finely regulated by post-translational mechanisms. Among these, the phosphorylation process of a limited number of Serine (Ser) and Threonine (Thr) residues is a rapid mechanism for regulating the binding capacity of Tau to microtubules. In general, the phosphorylation induces a reduction of the binding affinity for microtubules, regulating in this way the normal physiological function of this protein in the assembly and stability of microtubules (Crespo-Biel et al., 2012).

However, if the degree of Tau protein phosphorylation becomes progressively higher it can reach a state defined of hyperphosphorylation (Crespo-Biel et al., 2012).

When hyperphosphorylated, Tau protein decreases its affinity for the microtubules, leading to the detachment of Tau protein from microtubules. Hence, Tau tends to aggregate firstly in oligomers, and then in neurofibrillary tangles (NFT), which are associated in paired helical filaments (PHF) and other intracellular aggregates that are the principal hallmark of the so-called "Tauopathies", like the Alzheimer’s disease (Goedert & Spillantini, 2011). The term Tauopathies indicates a group of about twenty neurodegenerative diseases characterized by common key features, the deposit of NFT of phosphorylated Tau protein inside neurons and/or inside glial cells (Arendt & Bullmann, 2013).

1.4.8 Tau protein, Torpor, and Hibernation

Although Tau hyperphosphorylation seems to be the basic element of neurodegenerative diseases, the increase in Tau protein phosphorylation is not always harmful. Surprisingly, the hyperphosphorylated Tau is one of the main features that characterized both natural and ST and hibernation.

The first to demonstrate the presence of aggregated PHF-Tau in hibernators were Arentd and colleagues, that demonstrated the phenomenon firstly in European ground squirrels (Arendt et al., 2003), and subsequently in Syrian hamsters, Artic ground squirrels, and Black bears (Stieler

et al., 2011; Stieler et al., 2009; Hartig et al., 2007). Another group worked on Artic ground squirrels reported the same results: during the torpor period, in the brain of hypothermic animals, tau protein is hyperphosphorylated (Su et al., 2008).

However, the presence of PHF-Tau in hibernators and torpid animals, unlike what occurs in neurodegenerative diseases, it is not associated with NFT formation, and, interestingly, this hyperphosphorylation is completely reversible, in all the species and brain areas analyzed, with the return of the animal to euthermia (Arendt & Bullmann, 2013; Stieler et al., 2011).

Moreover, Luppi and colleagues demonstrated in 2019 that the reversible Tau protein hyperphosphorylation characterized not only the natural torpor, but also the synthetic torpor. In fact, after the induction of ST in rats through the protocol setting-up by Cerri and colleagues (Cerri et al., 2013), an increased expression of hyperphosphorylated Tau was assessed in brain during the hypothermic phase, through immunohistochemistry analysis. The details of study are provided below.

Briefly, during the time course of the ST procedure, 19 brain areas were immunohistochemically analyzed, using two different antibodies: AT8 and Tau-1. AT8 recognizes phosphorylated Tau at the level of Ser202 / Thr205 residues, and it has been used as a marker of phosphorylated Tau, while Tau1 recognizes Tau when it is not phosphorylated between residues 189 and 207 and highlights the presence of dephosphorylated Tau (Luppi et al., 2019). The experimental conditions explored were: i) control, after the injection of saline; ii) N30, between the second and third injection of muscimol, when hypothalamic temperature (Thy) reached the level of 30°C; iii) N, in which animals were sacrificed 1 h after the last injection of muscimol, when Thy reached the nadir of hypothermia; iv) ER, early recovery; in which animal were sacrificed when Thy reached 35.5◦C during the rewarming after ST; v) R6, in which animals were sacrificed 6 h after ER (during this 6-h period animals sleep intensely); vi) finally, R38, in which animals were sacrificed 38 h after ER. Similarly, to what occurs in natural torpor, an increase in AT8 and a specular decrease in Tau-1 were shown upon reaching a Thy of 30°C. At the nadir of hypothermia, the peak of AT8 was reached in the majority of the brain areas analyzed and it was accompanied by the disappearance of Tau-1. In R6, AT8 was significantly reduced and in R38 it had almost completely disappeared. However, Tau-1 even at 38 hours after arousal showed values still low compared to the control condition, suggesting that Tau dephosphorylation was still only partial in spite of the absence of AT8 immunoreactivity (***Figure 7***). The data suggest that the mechanism implied in resolution of hyperphosphorylation of Tau could be actively regulated (Luppi et al., 2019) .

The meaningful similarities between the cellular process just described in natural torpor, in ST, and in part in tauopathies, support the possibility of a common mechanism in all these conditions (Luppi et al., 2019).

Especially focusing on torpor, the causes of Tau hyperphosphorylation should be found in several factors, such as hypothermia, hypometabolism, or hibernation-specific regulation of enzyme kinetics (Arendt & Bullmann, 2013).

Phosphorylation and dephosphorylation kinetic Tau is directly regulated by a complex system of kinases and phosphatases proteins. The main kinase of Tau protein is the glycogen-synthase kinase-3-β (Gsk3-β), while the main phosphatase is the protein-phosphatase-2A (PP2A). in turn, Akt can phosphorylate Gsk3-β at Ser9 residue, determining its inactivation (Xie et al., 2014). Furthermore, the temperature can influence the activity of kinases and phosphatases: hypothermia inhibits phosphatases exponentially, while the activity of kinases is inhibited only linearly (Wang & Mandelkow, 2016) , in fact in low temperature conditions the deactivation of PP2A is faster and larger than that of Gsk3-β (Su et al., 2008). Hence, one of the most important factor in reversible Tau phosphorylation during hibernation and torpor could be the temperature (Su et al., 2008).

A peculiarity observed by Su et colleagues is that in Artic ground squirrels the Tau hyperphosphorylated residues during hibernation are Ser199, Thr205, Ser214, Ser262, Ser396, and Ser404, but studying the mechanism of dephosphorylation that occurs with rewarming of animals, they report that the only sites involved are Ser199, Ser262, and Ser404. Hence the phosphorylation of Thr205, Ser214, and Ser396 residues is not reversed (Su et al., 2008). The hypothesis suggests by authors is that, considering that hyperphosphorylation might confer to Tau resistance to protease degradation (Litersky & Johnson, 1992), it is possible that phosphorylation at these sites may be useful in stabilizing or preserving Tau protein during the hypothermic process (Su et al., 2008).

Moreover, recently, a study has suggested the potential neuroprotective role of the phosphorylation of Tau in one of the just reported site, Thr205 (Ittner et al., 2016).

The explanation of all described phenomena should be given by the fact that the phosphorylation of Tau protein, caused by the alteration of enzyme activities typical of the torpid phase, induces the detachment of Tau from the microtubules, which in turn increases the instability of the microtubules, favoring their dynamic state. This cascade of related processes suggests a link between protein phosphorylation and the synaptic plasticity that appears during hibernation. In fact, the kinetic of Tau phosphorylation during the hypothermic phase of torpor and hibernation, and the subsequent dephosphorylation with the return to euthermia occur in

parallel with the regression and the following synaptic reconnection of the neurons in the brain of hibernators (Arendt et al., 2003).

1.5 SLEEP

Sleep is a behavioural state characterized by reversibility, reduced responses to external stimuli, and perceptual isolation. In different species, sleep is associated with peculiar physiological changes compared to wakefulness, but also dependent on the different sleep phases (Achermann & Borbély, 1999, Amici et al., 2014).

Sleep cyclically alternates with wakefulness on ultradian bases and, in homeotherms, sleep itself is a cyclical process characterized by the alternation of two phases which occur in a precise order: non-rapid eye movement (NREM) sleep and rapid eye movement (REM) sleep. In particular, a nightly pattern of sleep in mature humans sleeping on a regular schedule includes several reliable characteristics: Sleep begins in NREM and progresses through deeper NREM stages before the first episode of REM sleep occurs approximately 80 to 100 minutes later. Thereafter, NREM sleep and REM sleep cycle with a period of approximately 90 minutes. In the overall night, the humans sleep duration is between 7 and 8 hours and the NREM accounts for 70-80% of total sleep (Carskadon & Dement, 2011). In different species sleep duration is largely variable, but, in the majority of terrestrial mammals, the proportion between NREM sleep and REM sleep remains quite similar to that observed in humans (Siegel, 2011; Carskadon & Dement, 2011).

The two sleep phases can be distinguished based on the EEG activity and on specific somatomotor and autonomic signs (Achermann & Borbély, 1999; Carskadon & Dement, 2011). The EEG pattern in NREM sleep is defined as synchronous, and is characterized by the occurrence of slow waves. In humans, the structure of NREM sleep is further subdivided into three stages (N1-N3, American Academy of Sleep Medicine classification, AASM; Carskadon & Dement, 2011), substantially based on the progressive increase in the degree of the EEG synchronization and the occurrence in stage N2 of peculiar waveforms such as sleep spindles and K complexes. NREM sleep N1 represents a transition from wakefulness to sleep and represents the first step of the EEG synchronization with a predominance of theta activity (4.0-7.0 Hz). Stage N2 is characterized by the appearance of two EEG markers, the “K-complex” (a high voltage negative wave, followed by a slow positive wave) and the “spindle” (a 12-14 Hz oscillation with an increasing and then a decreasing amplitude, lasting around 2s). The deeper stage of NREM is the N3 one, during which the EEG is rich of high-amplitude activity in the

slow delta range (0,5-2.0 Hz). This SWA characterizes deep NREM sleep in all mammals, and it is considered to be the result of a cellular phenomenon, called “slow-oscillation”, during which cortical neurons oscillate between a hyperpolarized and silent “down-state” and a high-frequency (around 40 Hz) “upstate” (Steriade et al., 2001). NREM sleep is associated with a low muscle tonus, while brain and body metabolism and physiological variables are kept at their minimum (Parmeggiani, 2005; Amici et al., 2014).

On the other hand, REM sleep is defined by the occurrence of desynchronized, low-amplitude EEG activity that is quite similar to that observed in wakefulness (Steriade et al., 2001), and by muscle atonia (Achermann & Borbély, 1999; Carskadon & Dement, 2011). Hence, the muscle tone progressively decreases from quiet wakefulness to NREM sleep, and fully disappears during REM sleep, when muscle atonia occurs. Such atonia is interrupted by the phasic manifestation of brief twitches and jerks of limb and eye muscles (from which the term: rapid eye movement sleep). Moreover, REM sleep is characterized by a deep change in physiological regulation, with a clear instability of autonomic activity and cardiorespiratory variables, and a suppression or depression of thermoregulation (Parmeggiani , 2005; Amici et al., 2014).

Therefore, the understanding and the physiological definition of sleep cannot prescind from the study of the activity of the ANS, which regulates respiratory, cardiovascular, and metabolic parameters (Zoccoli & Amici, 2020). In fact, some differences can be found in the activity of ANS between the two phases of sleep. In particular, NREM sleep is characterized by a progressive reduction in the activity of the sympathetic nervous system and by a mild activation of the parasympathetic branch, both aimed at maintaining body homeostasis in accordance with the reduced metabolic needs of this state, preserving anyway a posture addressed to assure a thermic comfort. On the contrary, REM sleep is characterized by a variable and phasic activation of both the parasympathetic and sympathetic system. Cardiovascular and respiratory phasic events are observed, which are due to the alteration in autonomic activity. Sympathetic bursts lead to peaks in arterial blood pressure and heart rate, while phasic parasympathetic activity may even lead to asystolia (Zoccoli & Amici, 2020). Furthermore, thermoregulation is suppressed in animals and depressed in humans, and muscle atonia, that characterized this sleep phase, does not allow animals to adjust their posture according to different metabolic needs (Zoccoli & Amici, 2020).

Such a modality of physiological regulation has been defined as “poikilostatic” because it is apparently not aimed at the maintenance of body homeostasis (Parmeggiani, 2005). However, the suppression of thermoregulation may not be considered as an index of a general loss of

homeostatic control, since hypothalamic osmoregulation is apparently preserved during REM sleep (Luppi et al., 2010).

1.5.1 Sleep Homeostasis

The term homeostasis was coined by Walter Bradford Cannon, in order to describe the process of the keeping of physiological variables at nearly stable levels. Subsequently, the term was borrowed to define the tendency of sleeping animals to maintain a sort of average daily amount of sleep by increasing its duration and/or intensity (during a so-called sleep rebound) after prolonged wakefulness (sleep deprivation) or to reduce its propensity after excessive sleep (Achermann & Borbély, 2017).

During the sleep rebound which follows sleep deprivation, the time spent in NREM sleep is usually lower than the NREM sleep time lost during sleep deprivation. Moreover, the EEG spectral power in the delta band (0.5-4.0 Hz), which is an index of the degree of the SWA, has been shown to increase during the NREM sleep rebound as a function of both the duration and the intensity of prior wakefulness. Hence, it is widely established that the recovery from a NREM sleep loss requires increased NREM sleep intensity, as it is shown by the occurrence of an increased SWA both at local and global cortical level (Achermann & Borbély, 2017). Actually, SWA occurring during a NREM sleep rebound is usually larger in frontal than in parieto-occipital EEG derivations. Furthermore, the brain areas most active during wakefulness develop an increased SWA during the NREM sleep rebound. So, the amount of SWA is apparently homeostatically regulated during NREM sleep (Huber et al., 2004).

For what concerns REM sleep homeostasis, it seems that it mostly occurs in terms of its amount (Achermann & Borbély, 2017). A study by Amici and colleagues (2008) demonstrated that in rat following either total or partial REM sleep deprivation, a REM sleep rebound is observed during the recovery period, which allows the animal to fully restore the previous REM sleep loss within four days of recovery (Amici et al., 2008). The recovery is mainly linked to an increase in the frequency of REM episodes rather than their duration (Cerri et al., 2005). This evidence is not completely ascribable to humans, in which the REM sleep rebound after total sleep deprivation seems to be less intense and to be postponed after the SWA rebound in NREM sleep (Achermann & Borbély, 2017). Interestingly, allometric scaling of the dynamics of REM sleep rebound with body mass in different species suggests that small animals, such as rats, have a lower tolerance to REM sleep loss than large animals such as humans (Amici et al., 2008).

1.5.2 Sleep Homeostasis, synaptic plasticity, and the role of Tau

In 2003, Tononi and Cirelli proposed a theory according to which the mechanism underlying local and global NREM sleep homeostasis in terms of SWA is directly related to an increase in cortical synaptic strength during wakefulness which would lead to an increased neuronal synchrony during subsequent NREM sleep, leading to more frequent and large EEG slow waves. Indeed, during NREM sleep, SWA may contribute to downscale the strength of cortical synapses and would be beneficial on neuronal efficacy and function, representing a fundamental positive property of sleep on cortical performance (Tononi & Cirelli, 2003). This theory, called "synaptic homeostasis hypothesis", affirms that one major function of SWA during NREM sleep should be to avoid overloads of synaptic connections at neuronal level, by reducing the density of connections and, therefore, improving their efficiency (Tononi & Cirelli, 2003).

To date, several studies confirm this theory. For example, Vyazovskiy and colleagues (2017) showed that, in the cerebral cortex and the hippocampus of the rat, α-amino-3-hydroxy-5-methyl-4-isoxazolepropionic acid (AMPA) receptor levels are high during wakefulness and low during sleep, and changes in the phosphorylation state of these receptors are consistent with synaptic potentiation during wakefulness and depression during sleep (Vyazovskiy et al., 2017). Moreover, in vivo experiments showed that the excitatory postsynaptic field potentials are increased during wakefulness and decreased during sleep in the cerebral cortex and the hippocampus of both adult rodents and humans (Huber et al., 2013; Norimoto et al., 2018). Nevertheless, other studies reported an increase rather than a decrease of the synaptic strength during sleep (Puentes-Mestril & Aton, 2017). Additionally, other experiments found an enhancement of the functional connectivity within the hippocampal cortex neurons, during the NREM sleep which occurred following learning (Ognjanovski et al., 2014).

However, the synaptic homeostasis hypothesis does not exclude the possibility of synaptic downregulation in wake or the potentiation of some synapses during sleep, but it rather assumes that the overall balance in total synaptic strength is maintained across a 24-h time scale, with a net increase in synaptic strength in wakefulness and a net decrease across most brain circuits during the sleep (Tononi & Cirelli, 2020).

Indeed, a recent study suggests the hypothesis that a core function of sleep is to renormalize overall synaptic strength increased by wake. In this study, using a serial block-face scanning electron microscopy, 6920 synapses in the cortex of mice were reconstructed and it was found that the axon-spine interface decreases on average by 18% after 6–8 hours of sleep compared

to 6–8 hours of wake. In particular, sleep related synaptic downscaling was found in small and medium size synapses, which represent about 80% of all synapses, although not in the largest synapses (de Vivo et al., 2017).

A role in synaptic plasticity during NREM sleep may also be played by the phosphorylation of Tau protein. Indeed, a recent study showed an interesting association between Tau phosphorylation and the wake-sleep cycle. In the cortex of mice, researchers described a negative correlation between the degree of phosphorylation of Tau protein and brain temperature rhythmicity (Guisle et al., 2020). During wakefulness, when the core temperature is higher, the levels of Tau phosphorylated are low, while during the resting phase, when the central brain temperature slightly decreases, Tau results to be more phosphorylated. Indeed, heat exposure prevented the daily changes in Tau phosphorylation both in the cerebral cortex of mice exposed to a Ta of 34 °C, and also in *in vitro* experiments, where human neuroblastoma cells were incubated at a Ta of 37.4 °C, mimicking the core temperature of animals during the waking period (Guisle et al., 2020).

Another result that underlines the key role played by temperature in Tau phosphorylation during sleep is the detection of the inhibition of the PP2A, the main phosphatase of Tau, during the rest period. This is in line with studies showing that the PP2A is more active during wakefulness (Olcese, 2003), and it results to be inhibited, causing increased levels of Tau phosphorylation, by the lowering of brain temperature (Planel et al., 2004). Additionally, the authors showed that Tau phosphorylation was also prevented by acute sleep deprivation in mice. However, also in this case, the reason seemed to be the temperature, considering that the core temperature of the sleep deprived animals resulted higher than that of sleeping mice (Guisle et al., 2020).

Another recent study shows cyclical variations in the amount of extracellular Tau, precisely at the level of the cerebrospinal fluid in humans (Holth et al., 2019). In particular, Tau concentration is reduced during sleep and higher during wakefulness, also further increasing following sleep deprivation (Holth et al., 2019). However, these authors detected total-Tau levels, without distinguishing the phosphorylated forms (Guisle et al., 2020).

The physiological and molecular role played by the Tau protein in the wake-sleep cycle is still unknown, but it is assumed that Tau phosphorylation during sleep might influence the stability of the cytoskeleton and axonal transport. Consequently, this would impact on synaptic plasticity occurring during NREM sleep (Guisle et al., 2020).

1.5.3 Sleep and Arousal from Torpor

One aspect that seems apparently difficult to explain through the synaptic homeostasis hypothesis is the presence of a strong pressure to sleep soon after the arousal from a torpor bout. In fact, despite the animals exiting from a torpor bout are basically recovering from a period characterized by poor EEG activity, it has been observed that during the euthermic interbout periods, the hibernators spend most of their time sleeping (Larkin & Heller, 1999).

This phenomenon has been observed in different species and the EEG characteristics of these sleep periods are similar to those observed in mammals after a prolonged sleep deprivation, mostly characterized by an increase in the power of the delta band (Achermann & Borbély, 2017; Deboer & Tobler, 1994).

Although the significance of post-torpor NREM sleep has not yet been fully elucidated, this phenomenon has been extensively documented in several species, both seasonal hibernating, such as the arctic squirrels (Strijkstra & Daan, 1998), animals that exhibit daily torpor, like the Djungarian hamsters (Deboer & Tobler, 1994), in different species of nonhuman primates (Blanco et al., 2016; Roy & Green, 2019), and also in rats subjected to ST (Cerri et al., 2013).

The comprehension of this phenomenon could be crucial to allow the understanding of many still unclear aspects related to sleep, hibernation, torpor, and their interconnections. For example, it was the main prove against the first theory that tried to correlate torpor and sleep. Indeed, Berger (Berger, 1984) speculated that the daily torpor and hibernation evolved as an extension of NREM sleep. He developed his theory considering the common reduction in temperature and metabolic rate in both torpor and NREM sleep, and since animals seem to start their torpor bouts during a NREM sleep period. The hypothesis is confuted by the appearance of the high activity of SWA in NREM sleep immediately after the arousal from torpor bout and the predominance of sleep in most of the following euthermic period (Deboer, 1998).

Effectively, these observations suggest that the torpor period is incompatible with the sleep functions, and consequently the arousals may allow the animals to recover from a period comparable with sleep deprivation (Daan et al., 1991). During the torpid period, in fact, the alternation between NREM sleep and REM sleep disappear from the EEGs (Royo et al., 2019; Lo Martire et al., 2020).

Moreover, many data have shown that this phenomenon seems to be homeostatically regulated. In fact, SWA during NREM sleep, which occurs after the arousal from torpor, increases in proportion to the length or the previous torpor bout (Strijkstra & Daan, 1997). This is similar to the observed progressive increase in SWA, consequently to a prolongation of sleep deprivation (Tobler & Borbély, 1986). Also, during the euthermic bout a progressive decrease of SWA during NREM sleep is observed. This result seems to indicate that the sleep need

accumulated during the hibernation bout decreases during post-torpor NREM sleep (Daan et al., 1991).

Furthermore, the SWA in ground squirrels resulted also inversely correlated with the brain temperature that the animals reached during the previous torpor bout (Larkin & Heller, 1996). Another interesting observation, reported in a study by Deboer and Tobler (Deboer & Tobler, 2003), is the fact that if Djungarian hamster is sleep deprived soon after its arousal from torpor, then the power density of SWA during the recovery period will be higher compared to the SWA occurring in the first hour after arousal from torpor without sleep deprivation (Deboer & Tobler, 2003). This has also been observed to occur in the rat after ST (Squarcio, 2020).

However, other studies showed conflicting results, questioning the homeostatic regulation of the SWA occurring after torpor. In particular, in two experiments the authors deprived ground squirrels of sleep totally soon after the arousal from a torpor bout, by using two different methods: the injection of caffeine or the gentle handling of the animals. As a consequence of the sleep deprivation, the expected increase in SWA during the recovery from torpor did not occur at all (Larkin & Heller, 1999). From another study, differences emerge in the SWA occurring in post-torpor NREM sleep compared to a sleep deprivation recovery. This means that the SWAs following torpor or sleep deprivation seem to be qualitatively different (Strijkstra & Daan, 1998). These findings would indicate that the SWA after arousal from torpor, rather than indicating an homeostatic regulation of NREM sleep, may reflect some neurological processes in the recovery of neural function from a protracted period at low temperature (Larkin & Heller, 1999).

Even if the contradictory results might be the consequences of species-specific differences, for example between hibernators and daily heterotherms, or discrepancies in the methodologies used in the experiments, one hypothesis tried to address all these heterogeneous data assuming that the main role of the SWA after torpor is correlated with an intense synaptogenesis. According to this hypothesis, the loss of dendritic complexity and synapses during the hibernation period (Popov & Bocharova et al., 1992; Strijkstrat al., 2003; von der Ohe et al., 2006; von der Ohe et al., 2007) could suggest that the function of periodic arousals is restoration of synapses.

One hypothesis to justify the need for SWA even after a relatively short time of torpor is the presence of the huge autonomic and metabolic activation occurring during the rewarming period from low Tb. In fact, it has been shown that, in the rat arousing from a ST bout, the size of the Delta rebound is much lower if animals are helped to restore their normal brain temperature by being placed for one hour at Ta 37°C, a condition which favour the passive

heating of the animal (Cerri et al., 2013). Interestingly, it has been shown that the intensification of SWA in NREM sleep can occur as a consequence of stressful stimuli delivered during sleep deprivation in order to increase the activity of the SNS (Meerlo et al., 2008).

Thus, these results may suggest, in line with the sleep homeostasis hypothesis, that the increased need for NREM sleep soon after a hypothermic bout, can be generated during the brief period of rewarming, associated with a strong ANS activity and synaptogenesis, which ultimately may lead to the need for synaptic renormalization occurring through SWA synaptic downscaling (Vyazovskiy et al., 2011). Another evidence that suggests an important activation of ANS, and in particular of SNS, is the increased systemic concentration of melatonin observed in the arousal from deep hibernation (Larkin et al., 2003). In particular, from the study conducted by Larkin et colleagues, emerges that in Siberian hamsters, kept in darkness during torpor, the concentration of melatonin increases during early arousal when thermogenesis is maximal, while the concentration decreases as Tb increased during arousal, until euthermia is re-established (Larkin et al., 2003).

Melatonin, a pineal hormone, is known to convey the message of "darkness" mainly to the hypothalamic SCN, entraining its cycling functioning together with light and, therefore, regulating the circadian rhythms (Zisapel, 2018). The wake-sleep cycle represents the most overt circadian rhythm and is strongly influenced by melatonin (Zisapel, 2018). This hormone is synthesized by the pinealocytes of the pineal gland, and its synthesis is also regulated by the hypothalamic PVN. In particular, PVN projects to preganglionic sympathetic neurons of the spinal cord, and postganglionary sympathetic neurons of the superior cervical ganglia project to the pineal glands (Bittman et al., 1989). The NE, released by sympathetic nerve terminal, binds to the α and β noradrenergic receptors located on the cell membrane of the pinealocytes, activating the pathways of melatonin synthesis (Lee et al., 2019). The release of melatonin is consistent with the light/dark daily cycle, then influencing the SCN activity, but also being influenced by the main hypothalamic circadian clock regulator (Zisapel, 2018). Despite melatonin is recognized above all for its role in the control of the circadian rhythmicity, more and more evidence show that further important functions are covered by this hormone.

In fact, is well-known the role of melatonin as endogenous free radical scavenger and, extensively, as an antioxidant. *In vitro*, experiments demonstrate that the administration of melatonin determines an increased expression of antioxidant enzymes, such as superoxide dismutase and glutathione peroxidase in neuronal cell lines (Mayo et al., 2002). Interestingly, melatonin is capable of influencing microfilament and microtubule organization by acting as a cytoskeletal modulator (Benítez-King, 2006). *In vivo*, it is reported that melatonin neurogenesis

and significantly increases hippocampal synaptic density and the number of excitatory synapses, while encourages the decrement of the number of inhibitory synapses (Leung et al., 2020).

Clinically, melatonin levels are significantly reduced in Alzheimer's disease patients. However, clinical trials that implies the administration of melatonin in patients, shows prolonged total sleep time at night. However, administration of melatonin in these patients does not improve cognitive abilities (Lee et al., 2019). By considering the different effects that melatonin is able to exert within the CNS, it should be interesting reconsidering its role in all the events that characterized the arousal from torpor and hibernation period.

2. AIMS

The Sympathetic Nervous System (SNS) regulates basic bodily functions, and its action is essential for the preservation of both the homeostasis of the organism and its adaptation to environmental challenges. The primary aim of this research project has been to investigate the effects of central and peripheral SNS manipulation on immune responses and on hypothermia and sleep-related brain neural plasticity.

This research project has been subdivided in three different sub-projects: 1) Study of the sympathetic reflex control of inflammation in mice subjected to different immune challenges; 2) Study of the mechanism driving the induction and resolution of brain Tau protein phosphorylation during and after synthetic torpor; and 3) Study of the role of sleep in the dephosphorylation process of Tau during the recovery from ST.

AIM 1: Study of the sympathetic reflex control of inflammation in mice subjected to different immune challenges

The first set of experiments was aimed at studying the role of the inflammatory reflex in immune challenged mice. Recently, it has been shown, in rats, that the systemic administration of LPS produces an activation of the SAIP. Prior section of the splanchnic sympathetic nerves disinhibits the inflammatory response to intravenous LPS, causing increased circulating levels of the pro-inflammatory cytokines, TNF, IL-6 and IFN-γ, along with reduced levels of the anti-inflammatory cytokine IL-10 (Martelli et al., 2014). These observations have been recently extended to sheep, where the same authors found that the inflammatory cytokine response to systemic administration of live Escherichia coli (E. coli) was also enhanced (and that of IL-10 reduced) by prior section of the splanchnic sympathetic nerves (Lankadeva et al., 2020). Also in sheep, therefore, Martelli and colleagues found that the SAIP reflexly drives a coordinated anti-inflammatory cytokine response pattern like that established in rats.

The inflammatory reflex is activated in response to immune challenges, by mechanisms that are not fully defined. It has been characterized almost exclusively when mobilized by challenge with TLR-4 agonists. It is unknown whether other types of immune challenge also engage the SAIP. In this regard, it has been shown that NA, the main neurotransmitter released by sympathetic nerves, inhibits the release of TNF in response to TLR2, 3 and 4 ligands in vitro (Ağaç et al., 2018), so a common sympathetic anti-inflammatory action is probable. But on the other hand, Straub and colleagues found contrasting effects of chemical sympathectomy on the host response to intraperitoneal infection with Gram positive versus Gram negative bacteria: the bacterial loads of E. coli and P. aeruginosa (Gram negative, recognized by TLR4) were

decreased by peritoneal denervation while that of S. aureus (Gram positive, recognized by TLR2) was increased (Straub et al., 2005). The authors interpreted these opposite effects as a consequence of the dual, contrasting role of sympathetic nerves in influencing the innate immune reaction to gram negative and gram-positive bacteria (Straub et al., 2005).
The aim of this part of the project was, therefore, to investigate the role of the inflammatory reflex, mediated by the SAIP, on cytokine responses to different immune challenges in a new species, the mouse. Specifically, we investigated the effects of prior bilateral section of the greater sympathetic splanchnic nerves on cytokine responses to three different systemic immune challenges: (i) LPS, recognized by TLR4 (Beutler, 2004), (ii) Poly I:C, recognized by TLR3 (Beutler, 2009) and (iii) Pam2cys, recognized by TLR2 and 6 (Vorkas et al., 2021; Zou et al., 2013).

AIM 2: Study of the mechanism underlying the hypothermia-related induction and resolution of brain phosphorylated Tau protein during and after synthetic torpor

ST is a peculiar hypometabolic/hypothermic condition resembling natural torpor, which can be induced in non-hibernators. ST is followed by a period of rewarming characterized by a strong sympathetic activation, which leads to the recovery of normothermia. ST can be induced in the rat, a non-hibernating animal, by the pharmacological inhibition of the sympathetic premotor neurons in the RPa (Cerri et al., 2013). In fact, the microinjection of the $GABA_A$ agonist muscimol into the RPa has been shown to induce a reversible inhibition of thermogenesis, leading to a progressive decrease in brain temperature (down to approximately 20 °C when animals are kept at Ta 15°C), and to an inhibition of any behavioural activity, with a concomitant depression of the EEG activity (Cerri et al., 2013).
Tau is a microtubule-associated protein that, through its phosphorylation/dephosphorylation processes, plays a central role in neural plasticity (Wang & Mandelkow, 2016). The accumulation of hyperphosphorylated Tau is implied in the pathogenesis of several neurodegenerative diseases, called tauopathies (Kovacs, 2017; Crespo-Biel et al., 2012). The accumulation of the hyperphosphorylated form of Tau is also typical in the brain of animals that enter torpor and hibernate. Interestingly, this accumulation that resemble what happens in tauopathies is reversible, meaning that, when the animal recovers from torpor, Tau is dephosphorylated, returning back to normal conditions (Stieler et al., 2011; Stieler et al., 2009; Hartig et al., 2007). More recently, the same reversible phenomenon has been described also in rats entering ST (Luppi et al., 2019), but the mechanism driving this process is unknown.

This research was aimed at investigating the process of accumulation and resolution of the hyperphosphorylated form of Tau during ST and the recovery to normothermic conditions, also focusing on the possible role of the hormone melatonin. As a matter of fact, an event that characterizes the exit from natural torpor is an increased concentration of circulating melatonin (Larkin et al., 2003). It is well-known that melatonin, being involved in microtubule organization, plays a role in synaptic plasticity (Benitez-King, 2005), as well as being a sign of sympathetic activation. Therefore, in this study, the levels of the Tau protein and its degree of phosphorylation, the expression of key enzymes involved in the phosphorylation/dephosphorylation processes, and the plasma levels of melatonin and other hormones and transmitters were determined in rats subjected to and recovering from ST.

AIM 3: Study of the role of sleep in the dephosphorylation process of Tau during the recovery from synthetic torpor

The third set of experiments was aimed at investigating the effects of sleep deprivation on the levels and the kinetics of Tau phosphorylation in the parietal cortex and the hippocampus of rats, 3 and 6 hours after their exit from ST. A peculiar feature of both natural and ST is the great sleep pressure that animals exhibit soon after the arousal from torpor. In particular, at the recovery of euthermia soon after natural or synthetic torpor, animals show an intense NREM sleep bout, with a high SWA (Deboer & Tobler, 1994; Cerri et al., 2013). Since SWA in NREM sleep is considered to play a key role in neural plasticity (Tononi & Cirelli, 2003; Tononi & Cirelli, 2020), the levels of the Tau protein and its degree of phosphorylation, the expression of key enzymes involved in phosphorylation/dephosphorylation processes, and the plasma levels of melatonin and other hormones and transmitters were studied 3 and 6 hours after the exit from ST and in two groups of animals that were sleep deprived by gentle handling for either 3 or 6 hours after their exit from ST.

3. MATERIALS AND METHODS

3.1 Study of the sympathetic reflex control of inflammation in mice subjected to different immune challenges

3.1.1 Ethical approval

All animal experiments were performed in accordance with guidelines of the National Health and Medical Research Council of Australia and were approved by the Animal Experimentation Ethics Committee of the Florey Institute of Neuroscience and Mental Health.
Forty-seven C57BL6 mice (20 ± 1 g, at the day of the experiment) were housed under normal laboratory conditions: Ta set at 22 ± 1°C; 12 h:12 h light-dark cycle; food and water *ad libitum*. After their arrival in the laboratory, all animals were left undisturbed at least 7 days for a period of adaptation. All experiments were performed under general anaesthesia.

3.1.2 Experimental plan

Anaesthesia was induced and then maintained with 2% isoflurane in pure oxygen delivered by a rodent ventilator (Ugo Basile, Italy) to a face mask: the animal breathed this mixture spontaneously. All animals were positioned on an electrically heated pad to maintain the Tb at 37 ± 0.5 °C throughout the experimental procedure. Core temperature was measured continuously by a thermocouple inserted into the rectum.
In each animal, the left and right splanchnic sympathetic nerves were surgically as described (Martelli, et al., 2014). The greater splanchnic nerves were exposed retroperitoneally on each side. Once placed the mouse on heated pad, trichotomy was performed by electric shaver. The exposed skin was disinfected with ethanol (70%) to avoid bacterial contamination of the surgical field. Subsequently, surgical access to the right nerve was made through a right flank incision (1–1.5 cm) below the ribs but above the pelvis, close to the back muscles. Incision of the thin muscle sheet next to the back muscles revealed the retroperitoneal space (including the kidney, adrenal gland, and peri-renal fat), which was opened with blunt separation and retraction while keeping the peritoneum intact. The adrenal gland was pulled caudo-ventrally with a cotton bud to expose the splanchnic nerve, which was separated with fine forceps. The nerve was either cut (SplancX group) or left intact (Sham group). The left splanchnic nerve was exposed and cut or left intact by mirror image procedure through a second incision. This preparatory procedure took approximately 30 minutes for each animal.

Then, the right femoral vein was exposed and, using a 30G needle and a 0.5 cc syringe, one of the three immune challenges (see below for details) was delivered intravenously.
Ninety minutes after, the ribcage was cut open and lifted, and 0.5 ml of blood was collected by intracardiac puncture. Blood was stored in a refrigerator (~ 4 °C) overnight and the following day the serum was separated by centrifugation (4 °C at 2000 x g, 15 minutes) and immediately stored at -80 °C for subsequent cytokines measurement (***Figure 8***).

3.1.3 Experimental groups

We performed three different experiments on six different experimental groups to study the influence of the SAIP in three different systemic immune challenge.
The immune challenges delivered were the following: i) LPS, 60 µg/kg; ii) Pam2cys, 34 µg/kg and iii) Poly I:C, 1 mg/kg. Each challenge was delivered in a volume of 100 µl to two groups of mice, designated Sham and SplancX.

3.1.4 Cytokines measurements

Serum samples from all animals were assayed for TNF, IL-10, IL-6, IL12p70, interferon-γ (INF-γ), and monocyte chemoattractant protein 1 (MCP-1, also known as chemokine C-C motif ligand 2, CCL2) using a BD Cytometric Bead Array Mouse Inflammation Kit (BD BioSciences, San Diego, CA, USA) according to the manufacturer's instructions with the exception that a total of 2µl of each capture bead was used in each 50µl sample. Samples were analyzed on a Becton Dickinson FACSCanto II flow cytometer (Franklin Lakes, NJ, US) and data quantified using Becton Dickinson FCAP Array software.

3.1.5 Statistical analysis

All data are presented as means ± SEM. Statistical differences between Sham and SplancX, for each cytokine in each experiment, were determined using one-way analysis of variance (ANOVA) or Kruskal-Wallis one-way ANOVA on ranks, if normality or equal variance test failed. This was followed by Bonferroni t-test or Dunn's method to compare the two groups, Sham and SplancX. The data of TNF, measured in LPS challenged mice serum, did not pass the equal variance test and Kruskall-Wallis One Way ANOVA on Ranks followed by Dunn's Method comparison between Sham and SplancX groups was applied.

The data of IL-10, measured in Poly I:C challenged mice serum, did not pass the normality test and Kruskall-Wallis One Way ANOVA on Ranks was applied.
We also calculated the TNF:IL-10 ratio, in each experiment, as an index of the inflammatory condition of the animal following the immune challenge. These data were analyzed with Kruskal-Wallis one way ANOVA on ranks followed by Dunn's method comparison. The data of LPS and Pam2cys challenged mice did not pass the normally test, the data of Poly I:C challenged mice did not pass the equal variance test. The numbers in each experimental group were: LPS Sham n=8; LPS SplancX n=9; Pam2cys Sham n=9; Pam2cys SplancX n=9; Poly I:C Sham n=6; Poly I:C SplancX n=6.

3.2 Study of the mechanism underlying the hypothermia-related induction and resolution of brain phosphorylated Tau protein during and after synthetic torpor

3.2.1 Ethical approval

All animal experiments were conducted following the approval by the Italian National Health Authority (decree: No. 262/2020-PR), in accordance with the DL 26/2014 and the European Union Directive 2010/63/EU, and under the supervision of the Central Veterinary Service of the University of Bologna. All efforts were made to minimize the number of animals used and their pain and distress.
A total of 15 Male Sprague–Dawley rats (*250-350 gr*; Charles River) were housed in pairs in Plexiglas cages (Techniplast) under normal laboratory conditions: Ta set at 24 ± 0.5°C; 12 h:12 h light-dark (LD) cycle (L: 09:00 h–21:00 h; 100–150 lux at cage level); food and water *ad libitum.* After their arrival in the laboratory, all animals were left undisturbed at least 7 days for a period of adaptation.

3.2.2 Preoperative procedures

Thy was measured through resin insulated thermistors (B10KA303N, NTC Thermometrx, 0.3 mm diameter). The thermistors were previously inserted in a 21 G needle soldered to a 2-pin connector; insulated with electrode resin. The day before the surgery, thermistors were calibrated to evaluate their sensibility and linearity; to obtain the calibration, the end of the

thermistor was introduced in a heated bath set at a temperature of 37°C, measured with a mercury thermometer (scale 34 °C - 42 °C), and was connected to the same amplifier in direct current used during the experimental day. The impedance was then measured at three different temperatures (37.0, 38.0, 39.0°C), and the three values were interpolated.
As for the thermistors, the electrodes for the EEG were prepared in advance: two copper wires (length 2 mm, diameter 0.3) covered by an insulating layer were suitably stripped for 1 mm at the ends, and soldered to the ends of two pins connected to a connector by tin soldering. During the surgery two knots were made at the free ends of the threads, to avoid any damage to the dura mater during insertion through the cranial theca.
Cannulas for Raphe Pallidus injections were obtained from Bilaney Consultants GmbH and were disinfected with 70% alcohol solution prior to use.

3.2.3 Surgery

Before each surgical session, animals were administered with the pre-anesthetic Diazepam (Valium Roche, 5 mg/Kg intramuscular) and after sedation was obtained, they were anaesthetized with an intraperitoneal injection of Ketavet (Ketamine-HCl, Parke-Davis, 100 mg/Kg). After confirming the surgical plane of anaesthesia by the absence of blink and toe-pinch reflexes, the trichotomy of the skull was carried out using a small animal shaver. The exposed skin was disinfected with iodine solution to avoid bacterial contamination of the surgical field. The animal was then positioned on a stereotaxic frame (Kopf instruments), with the aid of a transverse support bar for the jaw (muzzle blocking bar, 4 mm) and two ear bars inserted gently in the external auditory meatus, in order to maintain the head firm; the scalp was incised in the midline from the frontal bone to the nuchal muscles with a surgical sterile blade. The periosteum was removed, and the cranium surface was cleaned, making the cranial sutures clearly visible. Using a 0.5 mm of diameter drill tip, four holes in the cranium were made, two on the left and right frontal bones (in antero-lateral position), and two on the left and right parietal bones (in postero-lateral position), to implant four stainless steel screws to ensure all the inserted probes in place. Another hole of the same dimensions was made close to bregma and above the right anterior hypothalamus to insert the calibrated thermistor to record deep brain temperature. After that, 1 hole on the parietal bone (4 mm Anterior Posterior (AP), 2 mm Lateral Latero (LL) from bregma) and 1 hole on the frontal bone (-3 mm AP, 2 mm LL from bregma) for implantation of registering and reference electrode for the EEG measurement were made. In the end, 1 hole in the occipital bone for the insertion of a guide microcannula (C315G-SPC,

Plastics One; external gauge of the guide cannula: 0.46 mm; extension of the internal cannula from the pedestal: +3.5 mm; external caliber of the internal cannula: 0.20 mm) suitable for the administration of solutions at the RPa level (from -9.7 mm to -14 mm AP; 0 mm LL; -9.5 DV from bregma). The craniotomy was made following the coordinates of "The Rat Brain in Stereotaxic Coordinates" (Paxinos & Watson, 2007; ***Figure 9***).

A functional test was performed during the surgery in order to verify the correct positioning of the guide cannula. GABA-A agonist muscimol (100nl 1mM) was injected, and the tail temperature was monitored via a thermistor positioned on the skin surface of the tail. Since the inhibition of Raphe Pallidus neurons causes massive vasodilation (Blessing & Nalivaiko, 2001), the positioning was presumed correct if a clear increase in tail surface temperature was detected within 5 minutes from muscimol injection. In absence of any physiological response, the DV and LL coordinates were adjusted and the test repeated. When the cannula was assessed to be in the right position, it was fixed with dental resin (ResPal), covering the whole surgical field, incorporating the thermistor, the EEG electrodes, and the screws.

At the end of the surgical procedure wide-spectrum antibiotics (benzathine benzylpenicillin, 12.500.000 U.I., dihydrostreptomycin sulphate 5 g/100 mL, Rubrocillina Veterinaria, Intervet—1 mL/kg) were injected to prevent any postoperative infections and 5 ml of physiological solution were administered subcutaneously for the rehydration of the animal. The post-operative pain was prevented by the administration of an analgesic (Rimadyl – Carprofen 5mg/ml, subcutaneously). After the surgery, each animal was individually housed to prevent injuries caused by other animals in the presence of surgical implants. However, during the week of post-operative recovery, the operated animals maintained visual and olfactory contact with the other rats to mitigate the effects of isolation. During the whole week after surgery, the animals were kept under close observation by an operator and the veterinary doctors of the Centralized Veterinary Service of the University of Bologna. The animal's pain, distress or suffering symptoms were constantly monitored using the Humane End Point (HEP) criteria. Animals that displayed some degree of suffering symptoms were administered, as needed, with 5mg/kg of Rimadyl (Carprofen 5mg/ml, Pfizer).

3.2.4 Experimental set-up

After recovery from surgery, three days before the experimental session, animals were placed in the recording cages, where they were connected to the instrumentation used to record physiological parameters. The experimental cages were positioned in a thermoregulated and

sound-attenuated box, which consists of a modified freezer that allows fine control of the Ta by means of a thermostat connected to the freezer compressor and to an electric stove (1500 W) positioned inside it. The thermostat activates the compressor or stove respectively whenever the temperature differs from that set by the operator. The modified freezer box was also equipped with a ventilation system, a black and white video system (Philips) for monitoring the animal's behavior, an illumination system consisting of optical fibers (100 lux) controlled by a timer, each box can contain a maximum of two recording cages, each instrumented with a rotating swivel, connected to the external amplifiers, positioned on a tilting arm above the cage, that allows the animal to move freely during the experiment.

Three days before the experiment, the EEG connector and the thermistor of the animals were connected to the swivels with copper wires, to acquire baseline of Thy and EEG activity. Data were recorded (EEG and Thy), amplified (mod. Grass 7P511L, Astro-Med Inc, West Warwick (RI), USA) and filtered with a high pass and low pass filter with the following values for each bioelectric signal: EEG 0.3 Hz / 30 Hz and Thy 0.5 Hz (for the high pass), and finally converted from analog to digital (12-bit analog-digital, CED Micro MK 1401 II) to allow the storing on a digital hard drive with a sampling rate of 500 Hz for the EEG and 50 Hz for Thy. EEG signal was subjected to a spectral analysis every second using the Fourier transform algorithm (FFT). In this way, the power density values for the Delta (0.75-4 Hz) Theta (5.5-9 Hz) and Sigma (11-16 Hz) bands were obtained. During the adaptation and the experimental period rats were exposed to a moderately below thermoneutral Ta (15°C) and constant darkness, all environmental conditions known to facilitate the occurrence of a torpor in hibernators (Cerri et al., 2013).

3.2.5 Synthetic Torpor

To induce ST, we used a consolidated protocol (Cerri et al., 2013; Luppi et al., 2019; Tinganelli et al., 2019). Briefly, a microinjecting cannula was inserted into the guide cannula placed just above the RPa. Then, 100 nl of muscimol (1 mM) was injected once an hour, six consecutive times. Following the last injection, Thy reached values of around 22°C (Cerri et al., 2013). Instead, the control group was injected with artificial cerebrospinal fluid (aCSF; EcoCyte Bioscience). During the whole experiment, EEG and Thy signals were recorded, after being opportunely amplified, filtered, and digitalized, at the aim of better monitoring animals' behavior during ST induction and in the following recovery period.

3.2.6 Experimental Plan

Animals were randomly assigned to five different experimental groups and were sacrificed at different times following the injection of either muscimol or aCSF (first injection at 8.00 a.m.). The experimental groups were the following:

- C → Control, injected with aCSF and sacrificed at around 14.00 h, exactly matching the N condition (n = 3).
- N → Nadir, sacrificed 1 h after the last injection, at 14:00 h, when Thy reached the nadir of hypothermia (n = 3).
- ER → Early Recovery; sacrificed when Thy reached approximately 35.5° C after ST, at around 16:00 h (around 2h after Ta was moved from 15 to 28° C; n = 3).
- R3 → 3h Recovery, sacrificed 3 h after ER, at around 19:00 h (n = 3).
- R6 → 6h Recovery, sacrificed 6 h after ER, at around 22:00 h (n = 3).

For each experimental group, anesthetized animals were sacrificed by decapitation in order to collect brain tissue, destined to molecular assays. Moreover, blood samples were collected from each animal for immunoenzymatic assays (***Figure 10***).

3.2.7 Protein extraction and quantification protocol

Rats (n = 15) were deeply anesthetized and, after decapitation, brains were quickly extracted and transferred to a petri dish filled with ice cold phosphate buffer saline (PBS).
Soon after the brain extraction, the organ was immersed in PBS in a petri-dish and four samples were obtained, two from the cortex and two from the hippocampus, for a maximum of 70-90mg each. The specimens collected were promptly transferred in four ice-bathed 2mL Eppendorf tubes, containing 500μL of RIPA buffer (50 mM Tris buffer, 150 mM NaCl, 10% (v/v) NP-40, containing a cocktail of protease and phosphatase inhibitors, 1 mM dithiothreitol (DTT) and 1 mM phenylmethylsulfonyl fluoride (PMSF), all obtained from Sigma-Aldrich). The tissues were then homogenized with a masher for no more than 2-3 minutes, after that they were sonicated for 20 second, briefly stirred with a vortex mixer and let stand for 30min. The whole procedure was performed in an ice bath. After that, the tubes were centrifugated at 12000xg for 30 min at 4°C and the supernatant collected. Before the storage of supernatant at -80°C, their protein content was verified by using Lowry protein quantification method (Lowry et al., 1951).

3.2.8 Western Blots

Aliquots of parietal cortex and hippocampus protein extracts were thawed on ice and processed for Western Blot (WB) analysis.

On day one of WB procedure, protein samples were denatured in a sample buffer (containing: 500mM DTT, lithium dodecyl sulfate (LDS) with Coomassie G250 and phenol red; Invitrogen™ NuPAGE) at 65°C for 10 min. Then electrophoresis was carried out for 50-60min with a 150V electric field.

The sorted protein bands in the gel were therefore transferred on a nitrocellulose membrane via wet transfer by applying a 300mA electric current for 180 min at 4°C.

Before the incubation with the primary antibody, the correct banding was assessed by staining the membranes with Ponceau S dye, which binds the amino groups and the non-covalent non-polarized protein regions thus allowing to see the protein as red bands. The nitrocellulose membranes were therefore washed with PBS-Tween 0.1% till red bands' disappearing and then incubated for 40min with the blocking solution (5% milk/PBS-Tween) to prevent antibodies non-specific binding. Finally, the membranes were stained with the primary antibody diluted in PBS-Tween at 4°C overnight.

On day 2, the membranes were rinsed three times for ten minutes with PBS-Tween prior to be incubated for 45min at room temperature with the secondary specie-specific antibodies.

Bound antibodies were detected with horseradish peroxidase-conjugated Anti-rabbit and Anti-mouse secondary antibodies. β-actin was used as a loading control. ChemiDoc™XRS+ (Image Lab™Software, Bio-Rad) was used to acquire digital images through a chemiluminescence reaction (ECL reagents, Amersham). A semi-quantitative measurement of the band intensity was performed using the same computer software and expressed as a ratio of band intensity with respect to the loading control.

3.2.9 Primary Antibodies

Membranes were stained with the following primary antibodies (See also ***Table 1***):

- Anti-Total Tau, recognizes several Tau protein isoforms between 50-70 kDa (dilution 1: 5000, Merck Millipore);
- Tau-1, binds unphosphorylated 189-207 residues (dilution 1: 5000, Merck Millipore);
- AT8, selectively marks phosphorylated Ser202 or Thr205 residues (dilution 1:1000, Thermo Fisher);

- Anti-Phospho-Tau (Thr205) (p(205)-Tau) recognizes phosphorylated Thr205 residues, part of an Aβ toxicity–inhibiting response (Ittner et al., 2016; dilution 1:1000, Thermo Fisher);
- Anti-Gsk3-β, targets the Glycogen synthase kinase 3β, the principal Tau kinase (Hernandez et al., 2013; dilution 1:3000, Cell Signaling Technology);
- Anti-Phospho-Gsk3-β (p(9)-Gsk3-β) detects phosphorylated Gsk3-β's in Ser9 residue, the inactivated form of Gsk3-β (Cross et al., 1995; dilution 1:3000, Cell Signaling Technology);
- Anti-Akt, marks diverse isoforms of Akt, Akt 1/2/3, a kinase of Gsk3-β (Cross et al., 1995; dilution 1:2000, Cell Signaling);
- Anti-Phospho-Akt (p(473)-Akt) binds phosphorylated Ser473residues of Akt's three isoforms, activated forms of Akt (Xie et al., 2014; dilution 1:2000, Cell Signaling);
- Anti-Glucose regulating protein 78 (GRP78), an enzyme implicated in the folding process of proteins (Moreno & Castiglioni, 2015; dilution 1:5000 for cortex samples, 1:3000 for hippocampus samples);
- Anti-X chromosome-linked inhibitor of apoptosis (Xiap), a protein involved in the block of apoptosis mechanism by inhibiting caspase 3/7/9 (Vudic, 2018; dilution 1:1000, Santa Cruz Biotechnology);
- Anti-Protein phosphatase 2 (PP2A), one of the most important phosphatase that takes part in cell cycling (Wlodarchak & Xing, 2016; dilution1:5000, BDT Transduction Laboratories™);
- Anti-Cleaved-caspase 3, a crucial mediator of programmed cell death cleaved at Asp175 residue (Porter & Jänicke, 1999; dilution 1:250 in cortex samples, 1:500 in hippocampus samples, Cell Signaling);
- Anti-Beta-actin, binds one of actin's isoforms, often used as loading control in western blotting (Nie et al., 2017; dilution 1:5000, Thermo Fisher).

3.2.10 Enzyme-linked immunosorbent assay

Plasma extracted from each experimental group's animals was pooled together, in order to have a sufficient amount of plasma and to reduce inter-animal variabilities, obtaining 2 samples per condition. Plasmatic concentration of Melatonin (IBL International, RE54021), Dopamine (IBL International, RE59161), Catecholamine (IBL International, RE59242), Cortisol (IBL International RE52061) and Corticosterone (Abnova, KA0468) was measured by enzyme-

linked immunosorbent assay (ELISA), in duplicate, following the manufacturer's recommendations. Optical density was read spectrophotometrically (Spark® microplate reader, Tecan).

3.2.11 Statistical analysis

The statistical analysis for the Western Blot results was carried out with the non-parametric Mann-Witney U test. For all antigens, statistical comparisons were made between the different experimental group *vs* the normothermic control animal (C).
Experimental groups: Normothermic control rats (C); Hypothermic rats at lowest temperature (Nadir, N); Rats during the arousal from ST, Thy 35,5°C (Early Recovery, ER); Normothermic rats after 3 hours from the arousal from ST (Recovery 3 hours, R3); Normothermic rats after 6 hours from the arousal from ST (Recovery 6 h, R6).
The statistical analysis for Enzyme-linked immunosorbent assay was carried out with the non-parametric Mann-Witney U test. Statistical comparisons were made between the different experimental group *vs* the normothermic control animal (C).
In all the tests, significance level was pre-set at $p<0.05$ for all comparisons. All the statistical analyses were performed using IBM SPSS Statistics 25.0 version.
All the comparisons were pre-planned, aiming at performing as few comparisons as possible. Even though apparently there are many comparisons, the non-orthogonal contrasts are only 4 and no corrections for multiple comparisons were applied (Quinn and Keough, 2002; Winer et al., 1991).

3.3 Study of the role of sleep in the dephosphorylation process of Tau during the recovery from synthetic torpor

3.3.1 Ethical approval

All animal experiments were conducted following the approval by the Italian National Health Authority (decree: No. 112/2018-PR and No. 262/2020-PR), in accordance with the DL 26/2014 and the European Union Directive 2010/63/EU, and under the supervision of the Central Veterinary Service of the University of Bologna. All efforts were made to minimize the number of animals used and their pain and distress.

A total of 6 Male Sprague–Dawley rats (*250-350 gr*; Charles River), plus 6 animals that were also part of Experiment 3.2 were housed in pairs in Plexiglas cages (Techniplast) under normal laboratory conditions: Ta set at 24 ± 0.5°C; 12 h:12 h light-dark (LD) cycle (L: 09:00 h–21:00 h; 100–150 lux at cage level); food and water *ad libitum.* After their arrival in the laboratory, all animals were left undisturbed at least 7 days for a period of adaptation.

3.3.2 Experimental Plan

Animals underwent the same surgical procedures described for Experiment 3.2 and the experimental set-up was the same used for Experiment 3.2.

Three days before the experimental session, animals were placed in the recording cages, where they were connected to the instrumentation used to record physiological parameters.

The experimental day all animals were subjected to induction of synthetic torpor, applying a consolidated protocol (Cerri et al., 2013; Luppi et al., 2019; Tinganelli et al., 2019). Briefly, a microinjecting cannula was inserted into the guide cannula placed just above the RPa. Then, 100 nl of muscimol (1 mM) was injected once an hour, for six hours. Following the last injection, Thy reached values of around 23°C (Cerri et al., 2013).

Animals were randomly assigned to four different experimental groups and were sacrificed at different end points. The animals which belongs to the 3h Recovery and 6h Recovery groups are the same animals which were also used for Experiment 3.2.

The experimental groups were the following:

- R3 → 3h Recovery, sacrificed 3 h after Thy reached 35.5 °C, at around 22:00 h (n = 3). The animals of this group normally sleep during recovery from torpor.
- R3SD → 3h Recovery during which animals were sleep deprived (SD) by gentle handling and sacrificed 3 h after the Thy reached 35.5 °C, at around 22:00 h (n = 3).
- R6→ 6h Recovery, sacrificed 6 h after Thy reached 35.5 °C, at around 22:00 h (n = 3). The animals of this group normally sleep during recovery from torpor.
- R6SD → 6h Recovery during which animals were SD by gentle handling and sacrificed 6 h after the Thy reached 35.5 °C, at around 22:00 h (n = 3).

The protocol of sleep deprivation consisted in a continuous observation of the animals in their cages during the period of recovery from ST. When the animals displayed a synchronized high-amplitude EEG pattern or assumed a sleep posture, they were aroused by tactile stimuli (Franken et al., 1991).

As in Experiment 3.2, for each experimental group, at established time points, animals were

deeply anaesthetized and sacrificed in order to collect brain tissue. Moreover, blood samples were collected from each animal for immunoenzymatic assays (***Figure 11***).

3.3.3 Protein extraction and quantification protocol

The protocol followed for extracting protein from parietal cortex and hippocampus samples of each animal was the same applied in Experiment 3.2. Subsequently, the protein content of tissue extracts were quantified by Lowry method (Lowry et al., 1951).

3.3.4 Western Blots

The protein extracts of parietal cortex and hippocampus were processed in order to perform WB analysis, utilizing the same protocol described in Experiment 3.2.
The antigens were the same investigated in samples assayed in Experiment 3.2.

3.3.5 Enzyme-linked immunosorbent assay

The animal blood samples collected at the moment of end point were processed to obtain plasma. Even in this Experiment, like in Experiment 3.2, the plasma extracted from each experimental group's animals was pooled together, in order to have a sufficient amount of plasma and to reduce inter-animal variabilities, obtaining 2 samples per condition. Plasmatic concentration of Melatonin (IBL International, RE54021), Dopamine (IBL International, RE59161), Catecholamine (IBL International, RE59242), Cortisol (IBL International RE52061) and Corticosterone (Abnova, KA0468) was measured by enzyme-linked immunosorbent assay (ELISA), in duplicate, following the manufacturer's recommendations. Optical density was read spectrophotometrically (Spark® microplate reader, Tecan).

3.3.6 Statistical analysis

The statistical analysis for the Western Blot results was carried out with Two way ANOVA test. All the WB results were analysed with the following comparisons: i) R3 *vs*. R3 SD; ii) R6 *vs*. R6 SD. In addition, to better understand the role played by the sleep pressure during ST-recovery, data from the four recovery conditions were sorted only by sleep, comparing the

normal sleep (NS; R3 and R6) groups with the SD groups (R3SD and R6SD): i.e., NS *vs*. SD. Data analysis was carried out with a linear regression model (t-test for independent samples).

The statistical analysis for Enzyme-linked immunosorbent assay was carried out with the non-parametric Mann-Witney U test. Statistical comparisons were made between R3SD *vs* R3 and R6SD *vs* R6. Also for the analysis of Enzyme-linked immunosorbent assay data from the four recovery conditions were sorted only by sleep, comparing the NS (R3 and R6) groups with the SD groups (R3SD and R6SD): i.e., NS *vs*. SD. Data analysis was carried out with a linear regression model (t-test for independent samples).

The statistical analysis for the difference in Thy in the different experimental conditions was carried out by the Student t-test for independent samples.

In all the tests, significance level was pre-set at $p<0.05$ for all comparisons. All the statistical analyses were performed using IBM SPSS Statistics 25.0 version.

All the comparisons were pre-planned, aiming at performing as few comparisons as possible. Even though apparently there are many comparisons, the non-orthogonal contrasts are only 2 and no corrections for multiple comparisons were applied (Quinn and Keough, 2002; Winer et al., 1991).

4. RESULTS

4.1 Study of the sympathetic reflex control of inflammation in mice subjected to different immune challenges

4.1.1 LPS challenge

Prior bilateral section of the greater splanchnic nerves produced a significant increase in serum TNF (Sham mice 34.6 ± 2.5 ng/ml; SplancX mice 61.1 ± 3.6 ng/ml, p<0.001; ***Figure 12*****A**), MCP-1 (Sham mice 28.8 ± 0.8 ng/ml; SplancX mice 35.5 ± 2.1 ng/ml, p=0.012; ***Figure 12*****C**), and a significant decrease in serum IL-10 (Sham mice 5.6 ± 0.5 ng/ml; SplancX mice 1.9 ± 0.4 ng/ml, p<0.001; ***Figure 12*****B**) levels and INF-γ (Sham mice 0.07 ± 0.006 ng/ml; SplancX mice 0.048 ± 0.008 ng/ml, p<0.02; ***Figure 12*****F**) levels in response to intravenous LPS. No statistical significant differences emerge in IL-6 serum concentration (Sham mice 60.82 ± 5.2 ng/ml; SplancX mice 55.42 ± 6.8 ng/ml, p=0.544; ***Figure 12*** **D**), and in IL12p70 serum concentration (Sham mice 0.12 ± 0.04 ng/ml; SplancX mice 0.025 ± 0.025 ng/ml, p=0.056; ***Figure 12*****E**).
The acute inflammatory response, calculated as TNF:IL-10 ratio, was enhanced in SplancX mice compared to Sham mice (Sham mice 6.33 ± 0.48; SplancX mice 39.73 ± 5.78, p<0.001; ***Figure 12*****G**).

4.1.2 Pam2cys challenge

Prior bilateral section of the greater splanchnic nerves induced a significant increase in TNF (Sham mice 1.3 ± 0.1 ng/ml; SplancX mice 2.0 ± 0.3 ng/ml, p=0.031; ***Figure 13*****A**) and a significant decrease in IL-10 (Sham mice 0.24 ± 0.03 ng/ml; SplancX mice 0.11 ± 0.03 ng/ml, p=0.006; ***Figure 13*****B**) serum levels in response to intravenous Pam2cys. The differences between Sham and SplancX animals in MCP-1 (Sham mice 6.3 ± 0.7 ng/ml; SplancX mice 8.1 ± 0.5 ng/ml, p=0.064; ***Figure 13*****C**), IL-6 (Sham mice 8.0 ± 0.8 ng/ml; SplancX mice 9.9 ± 1.2 ng/ml, p=0.188; ***Figure 13*****D**), IL12p70 (Sham mice 0.036 ± 0.008 ng/ml; SplancX mice 0.049 ± 0.008 ng/ml, p=0.277; ***Figure 13*****E**), and INF-γ (Sham mice 0.012 ± 0.001 ng/ml; SplancX mice 0.015 ± 0.002 ng/ml, p=0.377; ***Figure 13*****F**) serum levels were not statistically significant.
The acute inflammatory response, calculated as TNF:IL-10 ratio, was enhanced in SplancX mice compared to Sham mice (Sham mice 7.39 ± 2.47; SplancX mice 25.38 ± 12.94, p=0.01; ***Figure 13*****G**).

4.1.3 Poly I:C challenge

Prior bilateral section of the greater splanchnic nerves induced a significant increase in TNF serum levels (Sham mice 3.2 ± 0.5 ng/ml; SplancX mice 7.1 ± 1.3 ng/ml, p=0.018; ***Figure 14*A**) in response to intravenous Poly I:C. The differences between Sham and SplancX animals in serum levels of IL-10 (Sham mice 0.63 ± 0.15 ng/ml; SplancX mice 0.45 ± 0.15 ng/m, p=0.31*;* ***Figure 14*B**), MCP-1 (Sham mice 5.5 ± 0.6 ng/ml; SplancX mice 6.9 ± 0.6 ng/ml, p=0.113; ***Figure 14*C**), IL-6 (Sham mice 8.9 ± 1.3 ng/ml; SplancX mice 11.5 ± 3.4 ng/ml; p=0.492; ***Figure 14*D**), IL12p70 (Sham mice 0.019 ± 0.007 ng/ml; SplancX mice 0.025 ± 0.008 ng/ml, p=0.581; ***Figure 14*E**), and INF-γ (Sham mice 0.012 ± 0.001 ng/ml; SplancX mice 0.012 ± 0.002 ng/ml, p=0.882; ***Figure 14*F**) were not statistically significant.

The acute inflammatory response, calculated as TNF:IL-10 ratio, was enhanced in SplancX mice compared to Sham mice (Sham mice 6.15 ± 2.83; SplancX mice 23.28 ± 6.37, p=0.015; ***Figure 14*G**).

4.2 Study of the mechanism underlying the hypothermia-related induction and resolution of brain phosphorylated Tau protein during and after synthetic torpor

4.2.1 Hypothalamic temperature

During the surgery procedure, rats were implanted with a thermistor, which was placed above the right anterior hypothalamus, to record deep brain temperature (Thy). In ***Table 2***, the average Thy levels in the 1-h period which preceded animal's sacrifice are shown. The results show that Thy at the baseline was 37.98 ± 0.14 °C, while at the hypothermic Nadir Thy reached the levels of 23.26 ± 0.82 °C ($p<0.01$ *vs* C). At the Early Recovery the average Thy was 32.92 ± 0.61 ($p<0.01$ *vs* C), and Thy values increased during the following recovery period (R3: 38.59 ± 0.07, $p<0.05$ *vs* C; R6: 37.66 ± 1.54, ns *vs* C).

4.2.2 Cortical expression of Total Tau, AT8, Tau-1, and p(205)-Tau

Western blot analysis in cortex protein extracts reveals no significant differences in Total Tau (***Figure 15***) band intensity between control normothermic animals (C 1.84 ± 0.15) versus N (2.36 ± 0.59, p=0.82) or ER (2.03 ± 0.06, p=0.27) rats. Animals recovering from ST show

increased expression of Total Tau compared to normothermic control rats (C 1.84 ± 0.15 *vs* R3 4.17 ± 0.99, p<0.05; C *vs* R6 3.37 ± 0.74, p<0.05).

Regarding the evaluation of the presence of phosphorylated and dephosphorylated Tau, a statistically significant difference is measured between C rats and rats subjected to ST in both AT8 and Tau-1 expression. In particular, AT8 (***Figure 16***) levels are higher while Tau-1 (***Figure 17***) levels are lower in the N group compared to the C group (AT8: C 0.62 ± 0.083 *vs* N 4.53 ± 0.61, p<0.05; Tau-1: C 3.30 ± 0.33 *vs* N 0.78 ± 0.37, p<0.05).

No more statistically significant difference emerged in the comparison of AT8 (***Figure 16***) and Tau-1 (***Figure 17***) levels between C and other experimental groups (AT8: C 0.62 ± 0.083 *vs* ER 0.86 ± 0.48, p=0.51; C *vs* R3 0.52 ± 0.07, p=0.51; C *vs* R6 0.61 ± 0.16, p=0.82; Tau-1: C 3.30 ± 0.33 *vs* ER 3.41 ± 0.40, p=0.82; C *vs* R3 4.21 ± 1.56, p=0.51; C *vs* R6 5.21 ± 2.35, p=0.51).

Finally, we observed an increase in the levels of p(205)-Tau (***Figure 18***) during N and ER compared to the C condition (C 0.64 ± 0.26 *vs* N 8.24 ± 1.58, p<0.05; C *vs* ER 6.82 ± 1.56, p<0.05; C *vs* R3 0.42 ± 0.11, p=0.51; C *vs* R6 0.96 ± 0.27, p=0.51).

4.2.3 Hippocampal expression of Total Tau, AT8, Tau-1, and p(205)-Tau

Western blot analysis in hippocampal protein extracts reveals no significant differences in Total Tau (***Figure 15***) band intensity between control normothermic animals (C 2.23 ± 0.27 *vs* N 2.07 ± 0.25, p=0.83; C *vs* ER 1.87 ± 0.10, p=0.275; C *vs* R3 2.99 ± 0.61, p=0.513; C *vs* R6 1.92 ± 0.79, p=0.275).

Regarding the evaluation of the presence of phosphorylated and dephosphorylated Tau, a statistically significant difference is measured between C rats and rats subjected to ST in both AT8 (***Figure 16***) and Tau-1(***Figure 17)*** expression. In particular, AT8 levels are higher while Tau-1 levels are lower in the N group compared to the C group (AT8: C 0.32 ± 0.15 *vs* N 13.96 ± 5.52, p<0.05; Tau.1: C 3.89 ± 0.68 *vs* N 0.59 ± 0.09, p<0.05).

No more statistically significant difference emerged in the comparison of AT8 (***Figure 16***) levels between C and other experimental groups (C 0.32 ± 0.15 *vs* ER 2.45 ± 1.24, p=0.127; C *vs* R3 0.39 ± 0.02, p=0.513; C *vs* R6 0.32 ± 0.17, p=0.16).

Tau-1 (***Figure 17***) levels are higher in ER compared to C (C 3.89 ± 0.68 *vs* ER 2.08 ± 0.19, p<0.05). No more statistically significant difference emerged in the comparison of Tau-1 levels

between C and other experimental groups (C 3.89 ± 0.68 *vs* R3 3.61 ± 0.50, p=0.827; C *vs* R6 2.11 ± 0.97, p=0.127).
Finally, we observed an increase in the levels of p(205)-Tau (***Figure 18***) during N and ER compared to the C condition (C 0.37 ± 0.22 *vs* N 7.09 ± 0.80, p<0.05; C *vs* ER 2.96 ± 1.19, p<0.05; C *vs* R3 0.20 ± 0.05, p=0.513; C *vs* R6 0.30 ± 0.13, p=0.513).

4.2.4 Cortical expression of Gsk3-β and p(9)-Gsk3-β

Gsk3-β (***Figure 19***) is less expressed in rats subjected to ST, in particular at N and during the ER, when the Thy starts to rise, compared to control animals (C 1.27 ± 0.05 *vs* N 1.02 ± 0.031, p<0.05; C *vs* ER 0.79 ± 0.05, p<0.05). Animals belonging to the R3 and R6 experimental group show similar cortical expression of Gsk3-β, compared to control animals (C 1.27 ± 0.05 *vs* R3 1.18 ± 0.13, p=0.82; C *vs* R6 1.68 ± 0.34, p=0.51).
p(9)-Gsk3-β (***Figure 20)*** expression strongly increases during ST, at N, but then go back to normal as soon as the animal start to recover (C 0.32 ± 0.13 *vs* N 3.00 ± 1.54, p<0.05; C *vs* ER 1.14 ± 0.7, p=0.27; C *vs* R3 0.25 ± 0.08, p=0.83; C *vs* R6 0.35 ± 0.11, p=0.83).

4.2.5 Hippocampal expression of Gsk3-β and p(9)-Gsk3-β

Gsk3-β (***Figure 19***) is more expressed in ER rats, when the Thy starts to rise, compared to control animals (C 1.20 ± 0.07 *vs* ER 1.87 ± 0.15, p<0.05). Animals belonging to the N, R3 and R6 experimental group show similar cortical expression of Gsk3-β, compared to control animals (C 1.20 ± 0.07 *vs* N 1.59 ± 0.23, p=0.127; C *vs* R3 1.72 ± 0.45, p=0.275; C *vs* R6 1.43 ± 0.20, p=0.275).
p(9)-Gsk3-β (***Figure 20***) expression strongly increases during ST, at N, but then go back to normal as soon as the animal start to recover (C 0.40 ± 0.18 *vs* N 2.78 ± 0.81, p<0.05; C *vs* ER 1.96 ± 0.97, p=0.127; C *vs* R3 0.40 ± 0.06, p=0.513; C *vs* R6 0.34 ± 0.10, p=0.513).

4.2.6 Cortical expression of Akt and p(473)-Akt in cortex

A statistically significant lower levels of Akt (***Figure 21***) emerges from the comparison between C band intensity and R3 and R6 bands, during the recovery period from hypothermia (C 0.92 ± 0.02 *vs* R3 0.81 ± 0.03, p<0.05; C *vs* R6 0.76 ± 0.04, p<0.05). No further statistically

significant differences result from the comparison of Akt expression during C and N or ER (C 0.92 ± 0.02 *vs* N 0.96 ± 0.08, p=0.51; C *vs* ER 0.91 ± 0.10, p=0.51).
p(473)-Akt (***Figure 22***) cortical expression is not changed in response to ST nor during its recovery phase (C 0.32 ± 0.03 *vs* N 0.55 ± 0.47, p=0.51; C *vs* ER 0.56 ± 0.21, p=0.51; C *vs* R3 0.43 ± 0.14, p=0.51; C *vs* R6 0.50 ± 0.20, p=0.51).

4.2.7 Hippocampal expression of Akt and p(473)-Akt

No statistically significant differences result from the comparison of Akt (***Figure 21***) expression between C and other experimental groups (C 1.17 ± 0.02 *vs* N 1.11 ± 0.02, p=0.275; C *vs* ER 1.50 ± 0.30, p=0.513; C *vs* R3 1.45 ± 0.63, p=0.513; C *vs* R6 0.94 ± 0.27, p=0.513).
A statistically significant higher levels of p(473)-Akt (***Figure 22***) emerges from the comparison between C band intensity and ER. No further statistically significant differences results from the comparison of p(473)-Akt expression between C and other experimental groups (C 0.44 ± 0.04 *vs* N 0.53 ± 0.09, p=0.513; C *vs* R3 0.48 ±0.13, p=0.827; C *vs* R6 0.33 ± 0.15, p=0.513).

4.2.8 Cortical expression of GRP78

GRP78 (***Figure 23***) expression is similar in the animals belonging to N, ER and R3 experimental groups, when compared to C rats (C 0.85 ± 0.04 vs N 0.85 ± 0.03, p=0.83; C vs ER 0.77 ± 0.05, p=0.27; C vs R3 0.81 ± 0.06, p=0.82). Rats belonging to R6 group show a decrease in the levels of GRP78, compared to rats of the C group (C 0.85 ± 0.04 vs R6 0.55 ± 0.12, $p<0.05$).

4.2.9 Hippocampal expression of GRP78

Rats belonging to ER group show an increase in the expression of GRP78 (***Figure 23***) compared to rats of the C group (C 0.96 ± 0.05 vs ER 1.35 ± 0.07, $p<0.05$). No statistically significant differences result from the comparison of GRP78 expression between C and N, R3, R6 groups (C 0.96 ± 0.05 vs N 1.05 ± 0.16, p=0.827; C vs R3 0.80 ± 0.26, p=0.513; C vs R6 0.70 ± 0.29, p=0.513)

4.2.10 Cortical expression of Xiap, PP2A, and Cleaved-caspase 3 in cortex

Xiap (***Figure 24***) expression in the animals belonging to the C group is not statistically different to what observed in rats belonging to the other experimental groups (C 0.70 ± 0.09 *vs* N 0.90 ± 0.19, p=0.51; C *vs* ER 1.00 ± 0.17, p=0.13; C *vs* R3 0.63 ± 0.07, p=0.51; C *vs* R6 0.88 ± 0.32, p=0.51).

PP2A (***Figure 25***) cortical levels increase during ST, becoming statistically different from C levels only during the ER (C 0.98 ± 0.20 *vs* ER 2.02 ± 0.15, p<0.05). The rest of the experimental groups do not show a different PP2A expression compared to control rats (C group); (C 0.98 ± 0.20 *vs* N 1.38 ± 0.41, p=0.51; C *vs* R3 0.84 ± 0.05, p=0.51; C *vs* R6 0.85 ± 0.03, p=0.51).

Finally, only the animals belonging to the R3 group show decreased levels of Cleaved-caspase 3 (***Figure 26***), compared to control rats (C 0.52 ± 0.09 *vs* N 0.75 ± 0.16, p= 0.27; C *vs* ER 0.40 ± 0.12, p=0.51; C *vs* R3 0.27 ± 0.04, p<0.05; C *vs* R6 0.64 ± 0.55, p=0.51).

4.2.11 Hippocampal expression of Xiap, PP2A, and Cleaved-caspase 3

From the analysis of Xiap (***Figure 24***) band intensity emerges that the only statistically significant difference is between C and R6 group, that has lower quantity of protein (C 0.70 ±0.02 *vs* R6 0.48 ± 0.09, p<0.05). No other differences are reported (C 0.70 ±0.02 *vs* N 0.74 ± 0.14, p=0.827; ER 0.78 ± 0.07, p=0.513; R3 0.73 ± 0.09, p=0.513).

The comparison between C and other experimental groups show significant lower band intensity of PP2A (***Figure 25***) in R3 group. No difference emerges from comparing control with N, ER and R6 bands intensities (C 0.61 ± 0.02 *vs* N 0.66 ± 0.04, p=0.275; ER 0.57 ± 0.03, p=0.275; R3 0.48 ± 0.02, p<0.05; R6 0.61 ± 0.08, p=0.513).

Finally, no significant differences result comparing Cleaved-caspase 3 (***Figure 26***) levels between C and N, ER, R3 and R6 groups (C 0.12 ± 0.03 *vs* N 0.06 ± 0.03, p=0.275; ER 0.20 ± 0.07, p=0.827; R3 0.52 ± 0.35, p=0.513; R6 0.10 ± 0.04, p=0.827).

4.2.12 Enzyme-linked immunosorbent assay

Plasma concentration of melatonin, adrenaline, noradrenaline, dopamine, cortisol, and corticosterone has been assayed.

The statistical analysis shows that plasma melatonin concentration is higher in rats belonging to the experimental groups N and ER compared to control animals (C 25.39 ± 3.81 pg/ml vs N 68.38 ± 16.13 pg/ml; C vs ER 45.29 ± 6.07 pg/ml; C vs R3 30.23 ± 1.42 pg/ml; C vs R6 45.02

± 8.69 pg/ml; (***Figure 27*A**) and plasma cortisol concentration is similar in each experimental condition, compared to C, except for the ER, where we observe lower levels (C 10.08 ± 1.23 ng/ml vs N 12.03 ± 0.70 ng/ml; C vs ER 6.53 ± 0.56 ng/ml; C vs R3 8.78 ± 1.32 ng/ml; C vs R6 10.99 ± 0.60 ng/ml; (***Figure 27*F**).

Plasma levels of A, NA, Dopamine and corticosterone of hypothermic animals, belonging to the N group, and of those recovering from ST, belonging to ER, 3h, 6h are not different from the levels of normothermic rats (Dopamine: C 0.55 ± 0.20 ng/ml vs N 0.19 ± 0.02 ng/ml; C vs ER 0.25 ± 0.02 ng/ml; C vs R3 0.23 ± 0.05 ng/ml; C vs R6 0.28 ± 0.02 ng/ml; ***Figure 27*B**. Adrenaline: C 6.83 ± 2.39 ng/ml vs N 5.78 ± 1.68 ng/ml; C vs ER 7.35 ± 0.71 ng/ml; C vs R3 8.29 ± 1.9 ng/ml; C vs R6 3.05 ± 0.6 ng/ml; ***Figure 27*C**. Noradrenaline: C 2.54 ± 0.55 ng/ml vs N 2.08 ± 0.89 ng/ml; C vs ER 2.32 ± 0.66 ng/ml; C vs R3 2.01 ± 0.23 ng/ml; C vs R6 1.41 ±0.45 ng/ml; ***Figure 27*D**. Corticosterone: C 51.68 ± 9.77 ng/ml vs N 67.20 ± 9.27 ng/ml; C vs ER 66.10 ± 11.75 ng/ml; C vs R3 38.85 ± 5.12 ng/ml; C vs R6 77.83 ± 11.06 ng/ml; ***Figure 27*E**).

4.3 Study of the role of sleep in the dephosphorylation process of Tau during the recovery from synthetic torpor

4.3.1 Hypothalamic temperature

In ***Table 3***, Thy levels (average levels during the 1-h period which preceded animal's sacrifice) during the recovery period in animals which were allowed to sleep or were sleep-deprived are shown. The results show that sleep deprivation did not induce significant changes in Thy levels neither in R3SD *vs* R3 (R3: 38.59 ± 0.07 °C; R3SD: 39.04 ± 0.25 °C), nor in R6SD *vs* R6 (R6 37.66 ± 1.548 °C; R6SD 37.63 ± 0.80 °C).

4.3.2 Cortical expression of Total Tau, AT8, Tau-1, and p(205)-Tau

The Western Blot analysis shows that there are no differences in the amount of cortical Total Tau (***Figure 28***) protein expression between the groups of rats allowed to sleep and those sleep deprived during the recovery from ST (NS 3,77 ± 0.58 vs SD 4.29 ± 0.57; p=0.535; t = -0.642). The same result is reproduced analysing these data separated at 3 and 6 hours of recovery from

ST (R3 4.17 ± 0.99 vs R3SD 3.69 ± 0.22, p=0.513; R6 3.37 ± 0.74 vs R6SD 4.90 ± 1.10, p=0.513).

AT8 (***Figure 29***) cortical levels are lower in the SD animals, compared to those allowed to sleep (NS 0.56 ± 0.08 *vs* SD 0.32 ± 0.058; p=0.028; t=2.561). If we analyse in detail the recovery period from the ST, we observe that these levels are significant different only during the early phases (R3 0.52 ± 0.06 *vs* R3SD 0.23 ± 0.07, p<0.05; R6 0.61 ± 0.16 *vs* R6SD 0.41 ± 0.02, p=0.513).

Tau-1 (***Figure 30***) cortical expression during the recovery from ST is not affected by sleep deprivation (NS 4.71 ± 1.28 *vs* SD 4.73 ± 1.08; p=0.991; t= -0.01). No significant differences emerge with a more detailed analysis at different time-points (R3 4.21 ± 1.56 *vs* R3SD 3.96 ± 2.04, p=0.513; R6 5.21 ± 2.3 *vs* R6SD 5.50 ± 1.07, p=0.827).

As shown for Tau-1, also p(205)-Tau (***Figure 31***) expression is not affected by sleep deprivation (NS 0.69 ± 0.17 *vs* 1.13 ± 0.29; p=0.235; t= -1.264; R3 0.42 ± 0.10 *vs* R3SD 0.90 ± 0.37, p=0.275; R6 0.96 ± 0.26 *vs* R6SD 1.35 ± 0.50, p=0.827).

4.3.3 Hippocampal expression of Total Tau, AT8, Tau-1, and p(205)-Tau

The Western Blot analysis shows that there are no differences in the amount of cortical Total Tau (***Figure 28***) protein expression between the groups of rats allowed to sleep and those sleep deprived during the recovery from ST (NS 2.45 ± 0.5 vs SD 2.49 ± 0.6; p=0.652; t= -0.465). The same result is reproduced analysing these data separated at 3 and 6 hours of recovery from ST (R3 2.99 ± 0.61 vs R3SD 2.32 ± 0.60, p=0.513; R6 1.92 ± 0.79 vs R6SD 2.67 ± 1.21, p=0.275).

AT8 (***Figure 29***) cortical levels of SD animals are not statistically different from those of animals allowed to sleep (NS 0.51 ± 0.08 *vs* SD 0.72 ± 0.25; p=0.388; t= -0.903). In the same way, if we analyse in detail the recovery period from the ST, we observe that these levels are not different (R3 0.39 ± 0.02 *vs* R3SD 0.75 ± 0.29, p=0.513; R6 0.32 ± 0.16 *vs* R6SD 0.30 ± 0.12, p=0.827).

Tau-1 (***Figure 30***) cortical expression during the recovery from ST is not affected by sleep deprivation (NS 2.86 ± 0.6 *vs* SD 3.67 ± 0.22; p=0.228; t= -1,283). No significant differences emerge with a more detailed analysis at different time-points (R3 3.61 ± 0.50 *vs* R3SD 4.08 ± 0.20, p=0.513; R6 2.11 ± 0.97 *vs* R6SD 3.26 ± 0.19, p=0.513).

p(205)-Tau (***Figure 31***) expression during the recovery from ST is not affected by sleep deprivation (NS 0.25 ± 0.07 *vs* SD 0.96 ± 0.33; p=0.052; t= -2.201). Hippocampal p(205)-Tau expression is higher in sleep deprive animals, if we analyze in details the recovery period from ST (R3 0.20 ± 0.05 *vs* R3SD 0.47 ± 0.08, p<0.05; R6 0.30 ± 0.13 *vs* R6SD 1.45 ± 0.54 p<0.05).

4.3.4 Cortical expression of Gsk3-β and p(9)-Gsk3-β

Gsk3-β (***Figure 32***) levels of SD animals are not statistically different from those of animals allowed to sleep (NS 1.43 ± 0.19 *vs* SD 2.01 ± 0.5; p=0.302; t= -1.089). No significant differences emerge with a more detailed analysis at different time-points (R3 1.18 ± 0.13 *vs* R3SD 1.41 ± 0.076, p=0.127; R6 1.68 ± 0.34 *vs* R6SD 2.61 ± 0.93, p=0.513).
As shown for Gsk3β, p(9)-Gsk3-β (***Figure 33***) levels are not affected by sleep deprivation (R3 0.25 ± 0.08 *vs* R3SD 0.49 ± 0.15, p=0.275; R6 0.35 ± 0.11*vs* R6SD 0.59 ± 0.18, p=0.513; NS 0.3 ± 0.06 *vs* SD 0.54 ± 0.10; p=0.088; t= -1.892).

4.3.5 Hippocampal expression of Gsk3-β and p9-Gsk3-β

Gsk3-β (***Figure 32***) levels of SD animals are not statistically different from those of animals allowed to sleep (NS 1.57 ± 0.23 *vs* 1.41 ± 0.18; p=0.600; t=0.542). No significant differences emerge with a more detailed analysis at different time-points (R3 1.72 ± 0.45 *vs* R3SD 1.63 ± 0.24, p=0.827; R6 1.43 ± 0.20 *vs* R6SD 1.19 ± 0.25, p=0.827).
p(9)-Gsk3-β (***Figure 33***) levels are higher in sleep deprived animals compared to those allowed to sleep (NS 0.36 ± 0.05 *vs* SD 0.63 ± 0.10; p=0.044; t= -2.303). No significant differences emerge with a more detailed analysis at different time-points (R3 0.40 ± 0.06 *vs* R3SD 0.59 ± 0.11, p=0.127; R6 0.34 ± 0.10 *vs* R6SD 0.68 ± 0.20, p=0.127).

4.3.6 Cortical expression of Akt and p(473)-Akt

Akt (***Figure 34***) expression is not affected by sleep deprivation (R3 0.81 ± 0.03 *vs* R3SD 0.87 ± 0.08, p=0.513; R6 0.76 ± 0.04 *vs* R6SD 0.88 ± 0.18, p=0.827; NS 0.78 ± 0.02 *vs* SD 0.87 ± 0.09; p=0.350; t= -0.981).
p(473)-Akt (***Figure 35***) expression is higher in sleep deprived animals compared to those allowed to sleep (NS 0.47 ± 0.11 *vs* SD 1.09 ± 0.22; p=0.033; t= -2.476). Cortical p(473)-Akt

expression is higher in sleep deprive animals, if we analyze in details the recovery period from ST (R3 0.43 ± 0.14 *vs* R3SD 1.03 ± 0.32, p=0.275; R6 0.51 ± 0.20 *vs* R6SD 1.14 ± 0.38, p=0.127).

4.3.7 Hippocamapl expression of Akt and p(473)-Akt

Akt (***Figure 34***) levels of SD animals are not statistically different from those of animals allowed to sleep (NS 1.19 ± 0.33 *vs* SD 0.77 ± 0.08; p=0.244; t=1.239). No significant differences emerge with a more detailed analysis at different time-point (R3 1.45 ± 0.63 *vs* R3SD 0.79 ± 0.08, p=0.513; R6 0.94 ± 0.27 *vs* R6SD 0.76 ± 0.16, p=0.827).
As shown for Akt, p(473)-Akt (***Figure 35***) expression is not affected by sleep deprivation (NS 0.40 ± 0.09 *vs* SD 0.39 ± 0.05; p=0.907; t=0.120; R3 0.48 ± 0.13 *vs* R3SD 0.43 ± 0.10 p= 0.513; R6 0.33 ± 0.15 *vs* R6SD 0.36 ± 0.04, p=0.513).

4.3.8 Cortical expression of GRP78

GRP78 (***Figure 36***) cortical expression during the recovery from ST is not affected by sleep deprivation (NS 0.68 ± 0.08 *vs* SD 0.60 ± 0.09; t=0.602 p=0.560). No significant differences emerge with a more detailed analysis at different time-points (R3 0.81 ± 0.06 *vs* R3SD 0.69 ± 0.13, p=0.513; R6 0.55 ± 0.12 *vs* R6SD 0.51 ± 0.14, p=0.827).

4.3.9 Hippocampal expression of GRP78

GRP78 (***Figure 36***) hippocampal levels during the recovery from ST are not affected by sleep deprivation (NS 0.74 ± 0.17 *vs* SD 0.78 ± 0.24; p=0.905; t= -0.122). No significant differences emerge with a more detailed analysis at different time-points (R3 0.80 ± 0.26 *vs* R3SD 0.64 ± 0.19, p=0.827; R6 0.70 ± 0.29 *vs* R6SD 0.93 ± 0.49, p=0.827).

4.3.10 Cortical expression of Xiap, PP2A, and Cleaved-caspase 3

Xiap (***Figure 37)*** expression is not affected by sleep deprivation (NS 0.75 ± 0.15 *vs* SD 0.64 ± 0.09; p=0.540; t=0.634; R3 0.63 ± 0.07 *vs* R3SD 0.48 ± 0.09, p=0.275; R6 0.88 ± 0.32 *vs* R6SD 0.80 ± 0.08, p=0.827).

PP2A (***Figure 38***) cortical levels are not affected by sleep deprivation (NS 0.84 ± 0.03 *vs* SD 0.71 ± 0.06; p=0.094; t=1.853). Cortical PP2A expression is lower in sleep deprive animals at 3 hours of recovery, if we analyze in details the recovery period from ST (R3 0.84 ± 0.05 *vs* R3SD 0.70 ± 0.01, p<0.05; R6 0.85 ± 0.03 *vs* R6SD 0.73 ± 0.14, p=0.827).
Finally, Cleaved-caspase-3 (***Figure 39***) expression is not affected by sleep deprivation (NS 0.45 ± 0.26 *vs* SD 0.36 ± 0.14; p=0.764; t=0.309; R3 0.27 ± 0.04 *vs* R3SD 0.37 ± 0.17, p=0.513; R6 0.64 ±0.55 *vs* R6SD 0.36 ± 0.25, p=0.827).

4.3.11 Hippocampal expression of Xiap, PP2A, and Cleaved-caspase 3

Xiap (***Figure 37***) expression is not affected by sleep deprivation (NS 0.60 ± 0.08 *vs* SD 0.69 ± 0.1; p=0.481; t= -0.733; R3 0.73 ± 0.09 *vs* R3SD 0.63 ± 0.02, p=0.513; R6 0.48 ± 0.09 *vs* R6SD 0.77 ± 0.21, p=0.275).
PP2A (***Figure 38***) levels of SD animals are not statistically different from those of animals allowed to sleep (NS 0.54 ± 0.04 *vs* SD 0.074 ± 0.09; t=0.069; t= -2.037). Hippocampal PP2A expression is lower in normal sleep animals at 3 hours of recovery, if we analyze in details the recovery period from ST (R3 0.48 ± 0.02 *vs* R3SD 0.62 ± 0.05, p<0.05; R6 0.61 ± 0.08 *vs* R6SD 0.88 ± 0.14, p=0.275).
Finally, Cleaved-caspase-3 (***Figure 39***) expression is not affected by sleep deprivation (NS 0.30 ± 0.18 *vs* SD 0.13 ± 0.02; p=0.358; t=0.964; R3 0.52 ± 0.35 *vs* R3SD 0.12 ± 0.02, p=0.513; R6 0.10 ± 0.04 *vs* R6SD 0.14 ± 0.05, p=0.827).

4.3.12 Enzyme-linked immunosorbent assay

Plasma concentration of melatonin, adrenaline, noradrenaline, dopamine, cortisol, and corticosterone has been assayed.
The statistical analysis shows that plasma melatonin concentration is higher in sleep deprived rats compared to animals allowed to sleep (R3 30.23 ± 1.4 pg/ml; R3SD 37.46 ± 2.38 pg/ml; R6 45.02 ± 8.69 pg/ml; R6SD 51.95 ± 4.74; ***Figure 40*****A**) and plasma corticosterone concentration is statistically significant higher in R3 rats compared to R3SD animals (R3 38.85 ± 5.13 ng/ml; R3SD 56.58 ± 4.00 ng/ml; R6 77.83 ± 11.06 ng/ml; R6SD 122.0 ± 26.65 ng/ml; ***Figure 40*****E**).
Plasma levels of cortisol, A, NA and Dopamine of sleep deprived animals are not different from the levels of allowed to sleep rats (Cortisol: R3 8.78 ± 1.32 ng/ml; R3SD 11.38 ± 1.5 ng/ml; R6

10.99 ± 0.60 ng/ml; R6SD 11.35 ± 1.02 ng/ml; ***Figure 40*****F**. Dopamine R3 0.23 ± 0.05 ng/ml; R3SD 0.26 ± 0.02 ng/ml; R6 0.28 ± 0.02 ng/ml; R6SD 0.21 ± 0.02 ng/ml; ***Figure 40*****B**. Noradrenaline R3 2.01 ± 0.23 ng/ml; R3SD 2.39 ± 0.25 ng/ml; R6 1.41 ± 0.45 ng/ml; R6SD 0.79 ± 0.22 ng/ml; ***Figure 40*****D**. Adrenaline R3 8.29 ± 1.92 ng/ml; R3SD 8.28 ± 0.69 ng/ml; R6 3.05 ± 0.60 ng/ml; R6SD 4.17 ± 0.30 ng/ml; ***Figure 40*****C**).

5. DISCUSSION

The SNS is still often considered as a monolith, associated with the fight or flight response. This rather naive view, still nowadays depicted in many textbooks, has been challenged by the results of different experiments and, presently, is considered to be wrong (Janig, 2008). Each sympathetic output, consisting of the premotor, the pre-ganglionic and the post-ganglionic sympathetic neurons, has its own function and its own target, in order to fulfill a specific regulatory action. The functional specificity of sympathetic output is part of a regulated neural system. Actually, the coordination between these functionally distinct outputs proves the integration of the system and contributes to the homeostatic regulation of body functions (Janig, 2008).

This thesis tries to show that the manipulation of two different sympathetic outputs specifically influences the immune system and thermoregulation. Thus, although a generalized manipulation of the SNS can undermine the homeostatic balance, a more selective intervention can be a useful strategy to understand the physiological function of specific sympathetic nerves or to promote specific functional phenotypes, such as ST, even in species in which they do not occur spontaneously. This approach has been followed in the present study.

5.1 Study of the sympathetic reflex control of inflammation in mice subjected to different immune challenges

This study shows for the first time that the inflammatory reflex action of the SAIP is present in mice, replicating the effects observed with TLR4 challenge in rats and sheep (Martelli et al., 2014; Martelli et al., 2019; Lankadeva et al., 2020). As in those species, the anti-inflammatory action of the SAIP appears to be coordinated, in that it enhances systemic levels of the anti-inflammatory cytokine IL-10 while inhibiting those of pro-inflammatory cytokines TNF and MCP-1 (***Figure 12*** **A, B, C**; ***Figure 13*** **A, B, C**; ***Figure 14*** **A, B, C**). IL-6, IL-12, and IFN-γ (***Figure 12*** **D, E, F**; ***Figure 13*** **D, E, F**; ***Figure 14*** **D, E, F**) are more slowly responding cytokines and their serum concentrations are not affected in the considered 90 minutes.

However, previous data demonstrated that the effect of the SAIP on cytokine response is not transient and limited to TNF, MCP-1 and IL-10. Martelli and colleagues (Martelli et al., 2014), demonstrated that the section of the greater splanchnic nerves enhanced IL-6 and IFN-γ plasma levels, 4.5 and 6 hours after the injection of LPS (***Figure 2***). Hence, it is plausible that the reflex activation of the SAIP could also inhibit the release of these pro-inflammatory cytokines in mice (Martelli et al., 2014).

According to these data, Straub et colleagues (Straub et al., 2011) reported that the electrical stimulation of sympathetic nerve terminals in superfused spleen slices, taken from arthritic mice, inhibited the release of IL-6 and IFN-γ.

The second main finding is that endogenous inflammatory reflex is engaged not only in response to stimulating TLR4, but is also active against acute inflammation triggered by Pam2cys and Poly I:C (considered respectively TLR2/6 and TLR3 agonists). The reflex pattern of reciprocal effects on TNF and IL-10 levels appears to apply broadly across inflammatory ligands (***Figure 12*** **G**; ***Figure 13*** **G**; ***Figure 14*** **G**).

The anti-inflammatory effect of the SAIP is presumably induced primarily by NA, released by sympathetic terminals, acting on β2-ARs on macrophages and other immune cells. β2 agonists exert strong anti-inflammatory effects. Catecholamines, acting through β2 adrenoceptors, polarize macrophages towards the M2 anti-inflammatory phenotype (Grailer et al., 2014), inducing the release of high levels of IL-10 and arginase-1. This is associated with a reduced expression of M1 pro-inflammatory markers. The anti-inflammatory action is not limited on macrophages but extend on other leukocytes (Nijhuis et al., 2014). Furthermore, consistent with this idea, Ağaç and colleagues showed that NA inhibits TNF and enhances IL-10 production, in response to TLR2, 3 and 4-dependent immune challenges, in macrophages extracted from wild-type but not from β2-ARs-Knock Out mice (Ağaç et al., 2018).

Although the comparison is indirect, the results of the present thesis differ from those of Straub and colleagues (Straub et al., 2005; Worlicek et al., 2010). Those authors showed that the chemical ablation of peritoneal sympathetic nerves decreased *E. coli* but increased *Staphylococcus aureus* dissemination to different organs (Straub et al., 2005), suggesting an opposite role for sympathetic nerves in controlling the innate immune response to TLR4 versus TLR2 stimulation. This seems to contrast with our results that show how the acute systemic inflammatory response is still damped down, in a similar manner, by the SAIP in each of the immune challenges tested. However, the consequence of this inhibitory action for bacterial clearance was not tested here. Bacterial clearance involves many more mechanisms than only plasma cytokine secretion and experiments involving viable bacteria or viruses might give different results, as already shown by Straub and colleagues. Moreover the different methods of denervation used in the two studies have to be considered: in these experiments a selectively surgical section of the greater splanchnic nerves, efferent arm of the inflammatory reflex, has been performed, while Straub and colleagues used 6-hydroxy-dopamine treatment, a molecule that is taken up by, and destroys, sympathetic postganglionic nerve terminals (Straub et al., 2005). 6-hydroxy-dopamine specificity is not limited to sympathetic neurons but also produces

cell death of several leukocytes able to synthesize and release catecholamines, thus directly affecting the immunity of the animal treated with this toxin (Capellino et al., 2012). This may be more critical in immune responses to gram-positive rather than gram-negative immune challenges.

The results also show here, for the first time, that the SAIP dampens down the inflammatory response to systemic Poly I:C challenges. Poly I:C is a viral mimetic, structurally similar to double-stranded RNA, typical of some viruses, and is an agonist of TLR-3 (Beutler, 2009). Therefore, it could be speculated that the consequence of this action may be clinically relevant: viral stimulation of the inflammatory reflex could depress innate immune function, perhaps leading to an impaired host defence against secondary bacterial infections.

In conclusion, the inflammatory reflex, acting via the SAIP, functions in essentially the same way in all three species so far tested. It acts in a coordinated fashion to suppress levels of pro-inflammatory cytokines and enhance the levels of the anti-inflammatory cytokine, IL-10. Moreover, this reflex is engaged in similar fashion by challenge with a range of TLR ligands. All this evidence points to a fundamental biological mechanism that has been conserved by evolution, presumably because it is advantageous. Its full implications still need to be worked out, but it is already known from other studies that it is powerful: disabling the reflex can have a profound effect on the ability of innate immune mechanisms to eliminate bacteria in a systemic infection (Lankadeva et al., 2020).

5.2 Study of the mechanism underlying the hypothermia-related induction and resolution of brain phosphorylated Tau protein during and after synthetic torpor

In this study, it has been decided to pharmacologically inhibit, in a non-hibernating species, the sympathetic output that controls thermogenesis, at the level of the sympathetic premotor neurons located in the RPa. This resulted in a hypothermic/hypometabolic state called ST, similar in many aspects to natural torpor. It is known that during the period of hypothermia, that occurs during natural torpor and hibernation, the Tau protein undergoes significant hyperphosphorylation, as also happens in tauopathies (Kovacs, 2017; Crespo-Biel et al., 2012). Differently to what is observed in tauopathies, this process is reversible: the accumulation of the phosphorylated Tau protein is reversed as soon as the animal returns to a condition of normothermia (Stieler et al., 2011; Stieler et al., 2009; Hartig et al., 2007). The same phenomenon has been described in non-hibernating animals subjected to ST (Luppi et al., 2019). In the present study the phenomenon of phosphorylation and dephosphorylation of Tau, as well as the levels of enzymes involved in the process, was investigated through the WB technique. Also, since an increase in circulating melatonin is found during the exit from torpor in natural hibernating animals, the possible role of melatonin in the process was investigated.

The results of the present work confirm that the reversibility of phosphorylated Tau, that accumulates in the brain during ST, is due to an active and regulated biochemical mechanism at cellular level. But, differently from what initially hypothesized, this mechanism does not start to play a role during the recovery from ST but, on the contrary, it appears to be strongly activated soon at the nadir of hypothermia (i.e., the N condition), when Thy is closed to 21 °C (Cerri et al., 2013). Also, as hypothesized, melatonin appears to have a main role in this neuroprotective process, but no other activating factor measured in plasma samples showed some significant involvement.

Present results reflect very well, with molecular quantifications, what previously observed in these structures from our lab with Immunofluorescence (Luppi et al., 2019; ***Figure 5***). In particular, a huge accumulation of AT8 was mirrored by reduced levels of Tau-1 at N condition, both recovering normal levels at R3 (***Figure 16***; ***Figure 17***). Moreover, during the recovery period there were high levels of Total Tau, although not reaching significant differences in the hippocampus, indicating a possible stimulating effect of ST in synthetizing more Tau filaments (***Figure 15***). The consequences of higher expression of Tau are not well established, since

apparently may be considered both as a factor favoring neurotoxicity as well as a cellular neuroprotective mechanism (Esclaire et al., 1997; Lesort et al., 1997; Kovacs et al., 2017): considering the other results of the present work, the second hypothesis seems to be supported, at least here, when induced by ST. Among these results, phosphorylated p(205)-Tau form was also higher at N, also persisting at ER before returning to control levels (***Figure 18***): the phosphorylation at this specific site of Tau protein has been described as neuroprotective in respect to neurotoxicity induced by β-amyloid (Ittner et al., 2016). While the presence of p(205)-Tau at N may also results from a superimposed reaction of the relative primary antibody and AT8, that recognizes Tau phosphorylated at Ser202 and Thr205 (Malia et al., 2016), the persistence of p(205)-Tau high level at ER could be a sign of a dephosphorylation process specifically driven to favor the triggering of a neuroprotective effect.

Since the mechanism elicited by ST is totally unknown, the molecular processes that could be involved are potentially many and heterogeneous. In the present work, we decided to focus on the most representative biochemical pathways involved in Tau phospho-regulation, as well as factors involved in favoring or contrasting apoptosis, a key process driving neurodegeneration (Fricker et al., 2018). Considering the results from the molecular quantifications of Gsk3-β (***Figure 19***) and PP2A (***Figure 25***), the factors that are directly involved in the phospho-regulation of Tau, apart from some differences between the two brain structures studied (i.e. Cx and Hip), taken together they show that the mechanism elicited by ST and involving Tau is actively regulated at biochemical level. Before conducting the experiments, our hypothesis was that some regulated molecular mechanism should have been take place during the recovery period from ST, since the accumulation of phosphorylated Tau could have been explained, theoretically, by the only physicochemical characteristics of the two enzymes studied: as previously shown (Planel et al., 2004; Su et al., 2008), both enzymes are inactivated by lowering the temperature, but PP2A deactivate faster than Gsk3-β, allowing kinase activity to act more freely with a waned activity of phosphatase. This process appeared particularly effective at around 20°C (Planel et al., 2004; Su et al., 2008). Unexpectedly, present results show that as soon as during the N condition there is a massive active biochemical inhibition of Gsk3-β (i.e., by the phosphorylation of Ser9 residue; ***Figure 20***; Cross et al., 1995). This response was not expected considering that at low temperature the enzymatic activity of homeothermic mammals is generally repressed (Marshall, 1997; Aloia & Raison, 1989), apart for hibernating mammals (Aloia & Raison, 1989) due to their specifical evolution. Moreover, the inhibition of Gsk3-β in part persisted at ER, even though without reaching significant differences, but showing higher levels in respect to C and in both Cx and Hip (***Figure 20***). This process apparently appeared

important for the recovering of normal AT8 levels, together with the high level of PP2A observed only in the Cx at ER (***Figure 25)***. In order to verify that the mechanism elicited by ST is effectively neuroprotective, we also quantified some key molecular factor involved in apoptosis or stressogenic processes, in particular: i) total and active forms of Akt, also known as protein-kinase B, that has a role in neuroprotection and in contrasting apoptosis (***Figure 21***; Risso et al., 2015; Levenga et al., 2017); ii) XIAP, a key factor inhibiting apoptosis (***Figure 24***; Holcik & Korneluk, 2001); iii) Clivated-caspase 3, a commonly considered factor involved in the initiation of apoptosis (***Figure 26***; Fricker et al., 2018); iv) GRP78, a key factor regulating the "unfolded protein response", a well-recognized mechanism of cellular stress (***Figure 23***; Ibrahim et al., 2019). Overall, all these factors did not show important changes; also, when they show some, they only were transitory: as, for instance, the significantly high peaks value shown for GRP78 at ER in Hip, or the high peaks, not reaching significant levels (***Figure 23***), found for Clivated-caspase 3 at N in Cx and R3 in Hip (***Figure 26***). Anyway, it is worth noting that when significant differences in these molecular parameters were observed, very often they were toward lower values, globally indicating neuroprotective effects. The activation of caspase 3, in particular, is not always associated with apoptosis (Snigdha et al., 2012) but, in some conditions, may also be related to neuroplasticity: these conditions are represented by a mild and temporary activation of caspase 3 (Snigdha et al., 2012). In accord, our data show mild (i.e., not significant) and transient peaks of Clivated-caspase 3 in both Cx and Hip (at N and R3, respectively; ***Figure 26***). Together with the high value of p(473)-Akt (i.e., the activated and protective form; ***Figure 22***; Risso et al., 2015; Levenga et al., 2017) found at ER in Hip, these data could be reasonably considered as a molecular pattern strongly suggesting neuroprotective events, elicited by ST.

In the present work we sought to put together a molecular mechanism, going on within neurons, with a systemic physiological mechanism that could someway trigger the cellular one. Therefore, we focused on plasma melatonin (***Figure 27*****A**), due to its involvement in natural torpor arousals (Willis & Wilcox, 2014) and in neuroprotective effects (Herrera-Arozamena et al., 2016; Shukla et al., 2017), and on plasma catecholamines and corticosteroids levels that may follow a strong sympathetic hyperactivation (***Figure 27*** **B**, **C**, **D**, **F**, **G**; Saaresranta & Polo, 2003). None of those factors studied resulted significantly involved in the hypothesized mechanism but melatonin. The pineal hormone shows a dramatic increase at N, that is concomitantly with the peak of p(9)-Gsk3-β, suggesting to effectively be a main actor in the process of phosphorylation/dephosphorylation of Tau observed during and after ST. In fact, the neuroprotective effect induced by melatonin is expressed through its binding to melatonin

receptors (Liu et al., 2014; Chinchalongporn et al., 2018), that trigger the inhibition of Gsk3-β and also the activation of Akt (Liu et al., 2014). The most peculiar aspect of this molecular process, as shown by the present results, is that instead to work during the recovery period from ST, as initially supposed, it starts working hard in deep hypothermic conditions, dramatically far from the physiological temperature. Since melatonin by itself did not turn out to be effective in contrasting tauopathies (Sanchez-Barcelo et al., 2017), this may clearly suggest that at low temperature melatonin could act in a way that could not take place, normally, at physiological temperature.

5.3 Study of the role of sleep in the dephosphorylation process of Tau during the recovery from synthetic torpor

As supposed by the initial hypothesis, present results clearly show that sleep has an important role in the molecular process that leads to the dephosphorylation of phosphorylated Tau, but its role was not what hypothesized. First of all, slightly different molecular patterns were shown between Cx and Hip, but, taken together all the results, sleep deprivation apparently favor the dephosphorylation process, better helping the system to return to normal condition (***Figure 28***; ***Figure 29***; ***Figure 30***). Also, the higher values found for p(205)-Tau in Hip show that sleep deprivation, in the present conditions, is apparently neuroprotective (***Figure 31***). In support of this, both p(9)-Gsk3-β and p(473)-Akt, even without reaching significant levels, follow the very well-known antiapoptotic pattern (***Figure 35***; Risso et al., 2015; Levenga et al., 2017), further corroborated by the tendentially lower levels of Clivated-caspase 3 observed in Hip (***Figure 39***). Even though none of those factors varied significantly, their tendency follows the protective pattern (Snigdha et al., 2012). The lack of differences found for GRP78 is also indicative of the fact that sleep deprivation has not negative effect at cellular level (***Figure 36***; Ibrahim et al., 2019).

As previously discussed, also regarding the involvement of sleep for the recovery processes from ST was studied taking into consideration plasma levels of the above defined factors. In accordance with the molecular patterns found, also in this case melatonin seems to have a key role, being tendentially higher in SD animals in respect to NS (***Figure 40*A**). Moreover, the existence of a specifically different patterns of anatomical distribution of the two kinds of melatonin receptors present in the brain (i.e., MT1 and MT2; Ng et al., 2017) corroborates the

primary role melatonin apparently have, also explaining the differences in molecular patterns found between Cx and Hip (Ng et al., 2017).

The higher levels of corticosterone found in SD animals confirm that sleep deprivation, also in the present protocol, has stressful effects (***Figure 40*E**; Sanford et al., 2015); even though, at R6 the difference was not more statistically significant and anyway not accompanied by the increase of any of the plasma catecholamines determined, this suggesting that the stressful effect was probably transient.

In conclusion, taken together, these results support the fact that sleep deprivation emphasize the neuroprotective effect of the molecular mechanism triggered by ST. It is worth noting that in the present protocol sleep deprivation is short (i.e., maximum 6 hours) and acute sleep deprivation is functionally quite different from long term sleep deprivation or sleep disturbances (Amici et al., 2008). Therefore, the well-known sleep and circadian disturbances that affects taupathic patients (Saeed & Abbott, 2017) should not be considered at the same extent of what found in the present data: the apparently neuroprotective effect shown here by sleep deprivation is specific for an acute and short deprivation.

In light of the obtained results, it appears evident how the selective manipulation of a sympathetic output, involved in a specific physiological function, leads to the understanding of the function itself. This is possible because each sympathetic postganglionic terminal acts on a specific target organ (Janig, 2008).

Specifically, in the studies proposed in this thesis, sympathetic manipulation allows to investigate interesting phenomena from a physiological point of view, but also to translate them to a pathological level.

In the first study the peripheral disengagement of the SAIP leads to the understanding of its involvement in a physiological anti-inflammatory action against different immune challenges. The translation in clinical setting of this physiological function is very powerful. The direct stimulation of splanchnic nerves in chronic inflammatory disease should contribute to moderate the inflammatory levels, improving the patients' quality of life. On the other hand, blocking the reflex through the direct action on sympathetic splanchnic nerves should be a valid method to contrast the immunodeficient status that characterizes sepsis, the worldwide leading cause of death in intensive care units (Zaccone et al., 2017). Therefore, the manipulation of splanchnic sympathetic nerves, as an alternative immunotherapy, could represent an interesting perspective in the clinical setting.

In the same way, the results obtained in the other two studies, open the way to possible applications of the selective manipulation of the thermogenic sympathetic output in a clinical setting.

The complete understanding of the mechanisms by which Tau is hyperphosphorylated, at low temperature, and dephosphorylated back to normal levels, when the animal returns at euthermia, could be exploited for the treatment of human conditions, for example, in the context of tauopathies with the aim of blocking the progression of hyperphosphorylation of the Tau protein. Moreover, patients with dementia could probably recover from neuronal loss and the loss of neuronal connections, typical of their conditions.

The apparent neuroprotective action of a short sleep deprivation, described in the results, could also be readily exploited in patients under certain circumstances. It is important to keep in mind that an acute, short sleep deprivation is completely different from a long-term sleep deprivation or sleep disturbances (Amici et al., 2008).

Recently, Planel and colleagues (Planel et al., 2007) showed that in the elderly undergoing general anesthesia, cognitive disorders, confusion and delirium occur in the postoperative phase. These symptoms can persist for years in some patients and are particularly evident in patients already suffering from Alzheimer's disease. The authors showed that the hypothermia caused by general anesthesia induces a rapid increase in hyperphosphorylated Tau protein and the process is stopped when the patients return to a condition of normothermia, resembling what has been observed in rats subjected to ST. It would be interesting in these cases to observe how an acute and short sleep deprivation protocol could affect the hyperphosphorylation of the Tau protein. It could be hypothesized that an acute sleep deprivation, during the recovery to normothermia, could quickly bring back the hyperphosphorylated Tau to levels similar to those observed before the anesthesia, helping to prevent or reduce the cognitive disorders and confusion of the postoperative phase. However, it would be necessary to verify the effect that a fast dephosphorylation of the Tau protein has on microtubules. It is not certain that increasing the stability of microtubules so rapidly through an intense dephosphorylation of Tau is beneficial. As a matter of fact, physiologically, the phosphorylation and dephosphorylation of Tau are fundamental for the correct stabilization of microtubules and for their plastic modifications (Wang and Mandelwok, 2016). Therefore, it would be useful to investigate whether a modification in the kinetics of the process would cause adverse effects.

Furthermore, despite the lack of beneficial effects in response to the administration of melatonin in patients affected by tauopathies (Sanchez-Barcelo et al., 2017), it would be useful to conduct

clinical trials with more standardized methods and different doses of melatonin, to obtain further useful data and understand if this hormone can be involved in the dephosphorylation process of the Tau protein. In light of the results obtained, in concomitance with the administration of melatonin, a state of hypothermia could be induced in patients, to investigate whether melatonin acts dissimilarly at different temperatures to modulate the dephosphorylation of Tau protein.

Obviously, further studies are needed to completely understand all the investigated mechanisms and implement their applicability in the clinical setting.

6. FIGURES

Figure 1. General organization of the sympathetic system

The sympathetic preganglionic neurons (SPNs) cell bodies are located in the intermediolateral cell column of the grey matter of the spinal cord, between the first thoracic segment down to the second lumbar segment (T_1-L_2). The SPNs axons traverse the ventral horn to exit the spinal cord via the ventral roots and synapse with postganglionic neurons in peripheral sympathetic ganglia.

The sympathetic ganglia are divided in paravertebral and prevertebral ganglia.
(Modified from Benarroch, 2020)

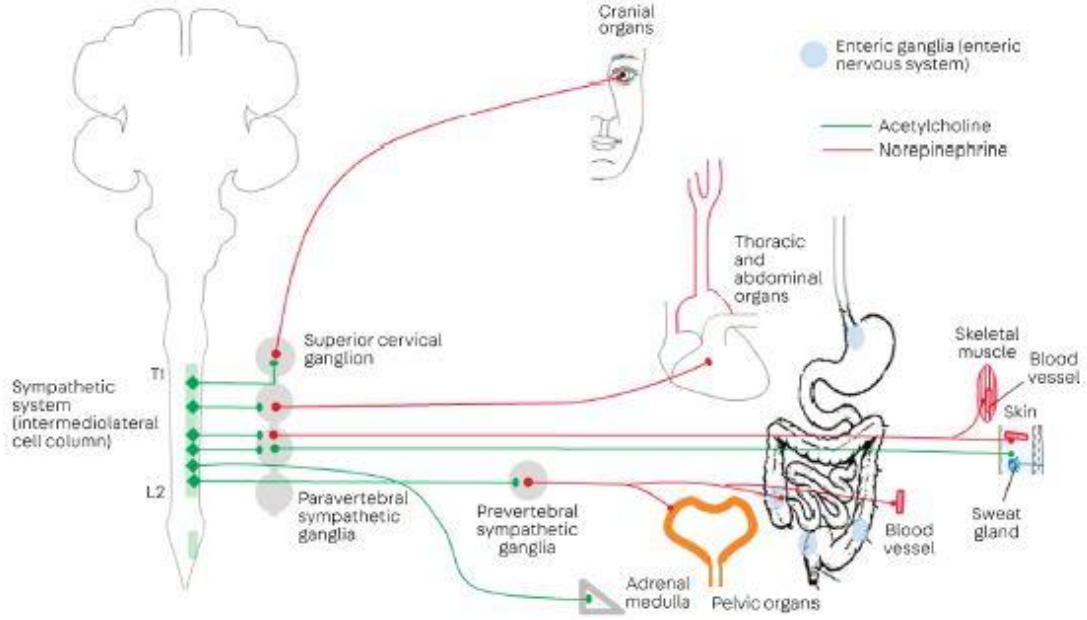
Cranial organs
Enteric ganglia (enteric nervous system)
Acetylcholine
Norepinephrine
Thoracic and abdominal organs
Skeletal muscle
Blood vessel
Skin
Superior cervical ganglion
T1
Sympathetic system (intermediolateral cell column)
L2
Paravertebral sympathetic ganglia
Prevertebral sympathetic ganglia
Blood vessel
Sweat gland
Adrenal medulla
Pelvic organs

Figure 2. Effects of splanchnic nerve section on cytokine responses to LPS in anesthetized animals

Animals were either subjected to bilateral splanchnic nerve section (SplancX, solid line) or sham-operated (Sham, dashed line). They were then injected intravenously with LPS (60 μg/kg). Arterial blood samples were collected 10 min before and every 90 min after LPS injection for cytokines measurements. The data are shown as mean ± SEM.

Fig 2 **A)** Plasma TNF level in rats challenge with LPS 60 μg/kg

Fig 2 **B**) Plasma IL-6 level in rats challenge with LPS 60 μg/kg

Fig 2 **C**) Plasma INF-γ level in rats challenge with LPS 60 μg/kg

Fig 2 **D**) Plasma IL-10 level in rats challenge with LPS 60 μg/kg

* $p<0.05$

Lipopolysaccharide (LPS); Tumor necrosis factor (TNF); Interleukin 6 (IL-6); Interferon-γ (INF-γ); Interleukin 10 (IL-10); SEM (Standard error of the mean).

(Modified from Martelli et al., 2014)

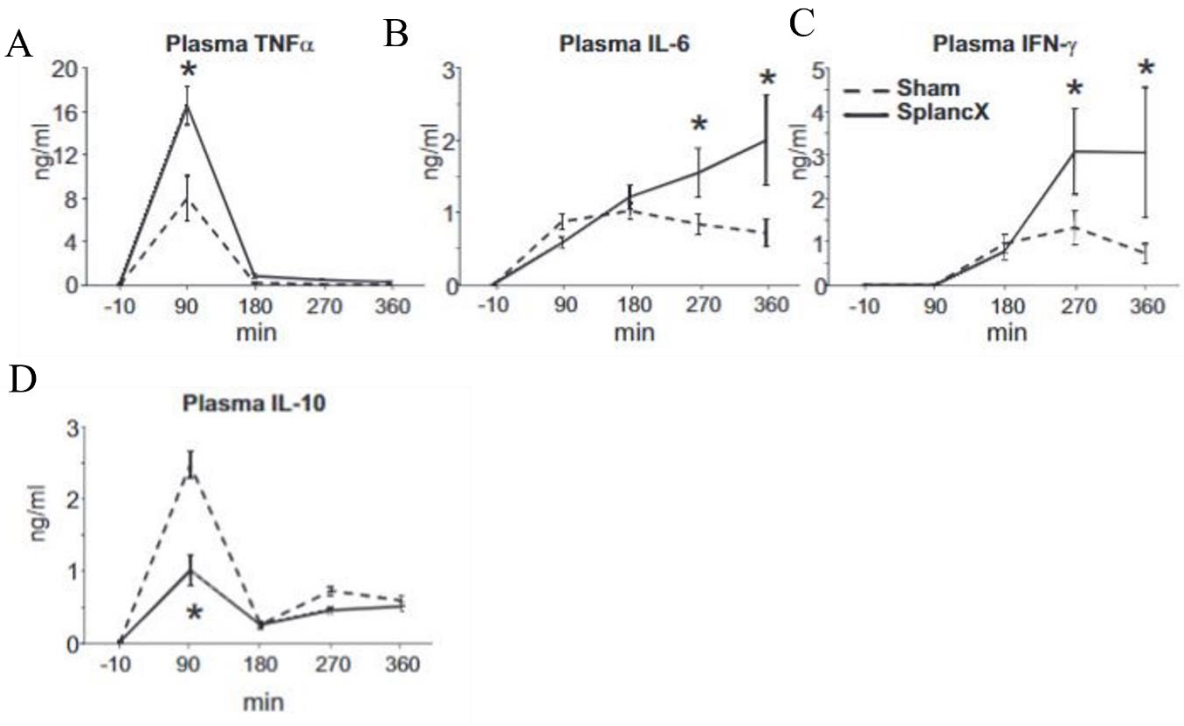
A
Plasma TNFα
ng/ml
20
16
12
8
4
0
-10
90
180
270
360
min
*
B
Plasma IL-6
ng/ml
3
2
1
0
-10
90
180
270
360
min
*
*
C
Plasma IFN-γ
Sham
SplancX
ng/ml
5
4
3
2
1
0
-10
90
180
270
360
min
*
*
D
Plasma IL-10
ng/ml
3
2
1
0
-10
90
180
270
360
min
*

Figure 3. Schema of the inflammatory reflex engaged by systemic LPS challenge

The afferent arm (in red) is proposed to be humoral, although participation of other mechanisms has not been excluded (with exception of vagal afferents). The efferent arm (in blue, to indicate its anti-inflammatory action) is the splanchnic anti-inflammatory pathway. Its anti-inflammatory action is distributed synaptically via postganglionic sympathetic neurons to a range of abdominal organs and by preganglionic fibers to the adrenal medullary chromaffin cells.

Lipopolysaccharide (LPS);

(Modified from Martelli et al., 2019)

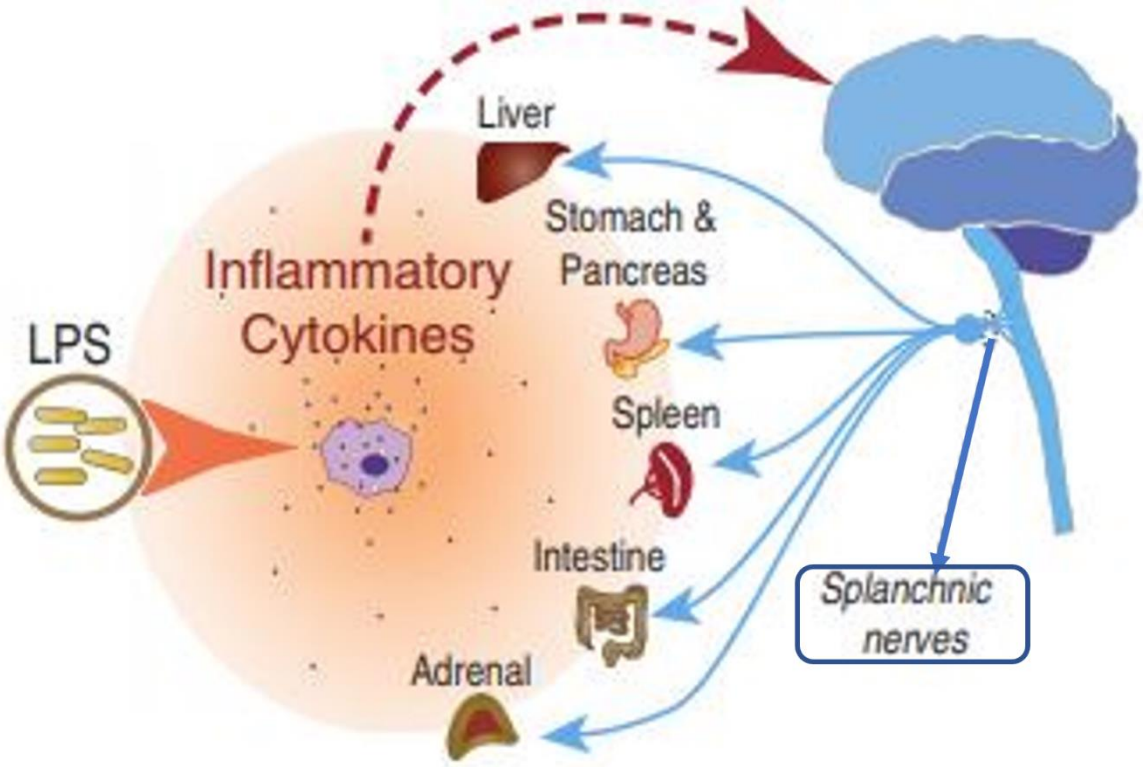
Liver
Stomach &
Pancreas
Inflammatory
Cytokines
LPS
Spleen
Intestine
Splanchnic
nerves
Adrenal

Figure 4. Model of the thermoregulatory afferent pathways

Afferent pathways from the periphery to the preoptic area. Dashed lines indicate pathways that have not been conclusively studied.

Dorsal horn (DH); Dorsal root ganglia (DRG); Dynorphin (Dyn); Glutamate (GLU); Dorsal lateral parabrachial nucleus (LPBd); External lateral parabrachial nucleus (LPBel); Median preoptic nucleus (MnPO); Medial preoptic area (MPA); Transient receptor potential subfamily M member 8 (TRPM8); Transient receptor potential vanilloid 1 (TRPV1); Nucleus tractus solitarius (NTS); Ventral portion of the lateral preoptic area (vLPO).

(Modified from Madden & Morrison, 2019).

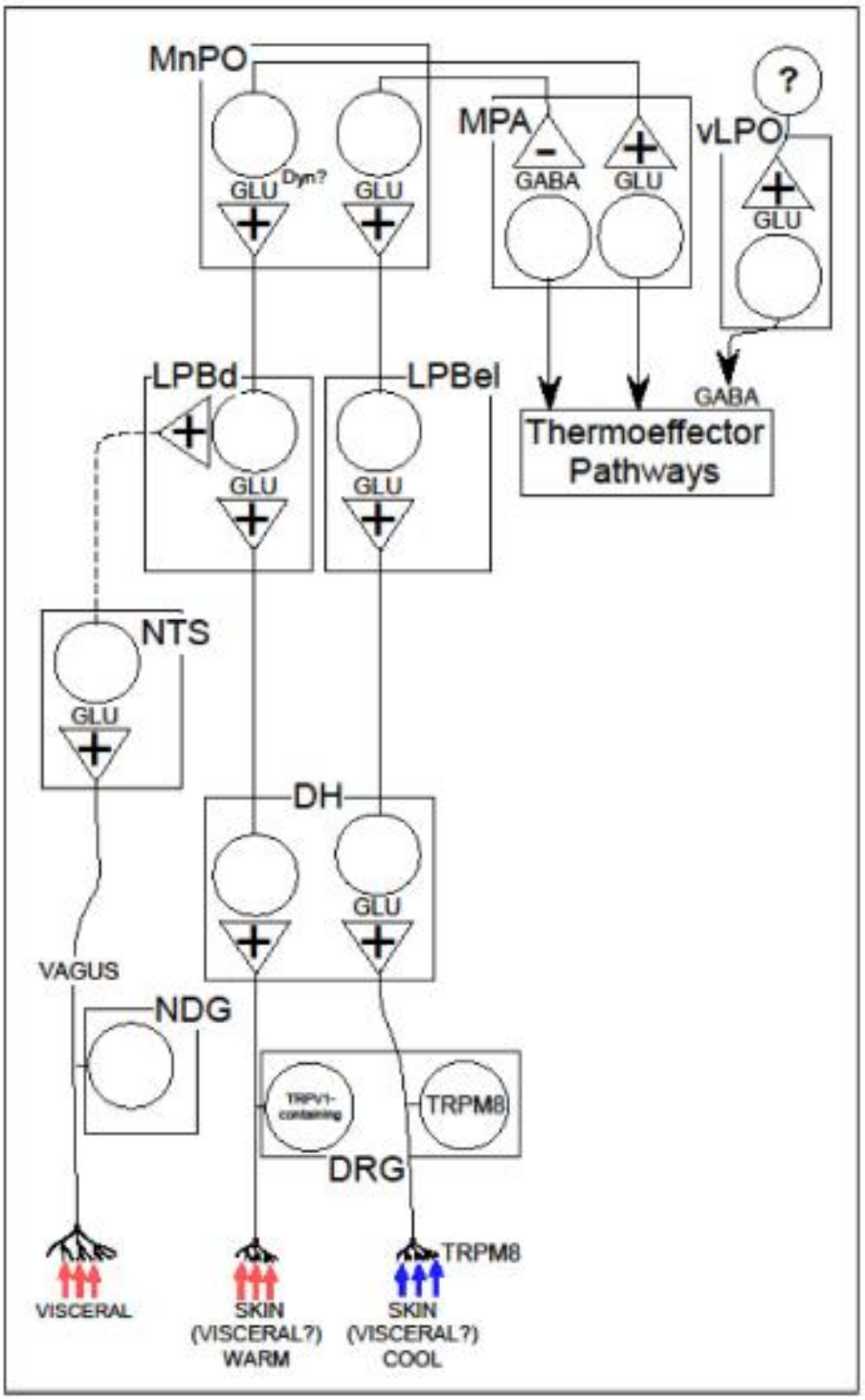
MnPO
GLU
Dyn?
GLU
MPA
GABA
GLU
vLPO
?
GLU
LPBd
LPBel
GLU
GLU
GABA
Thermoeffector
Pathways
NTS
GLU
DH
GLU
VAGUS
NDG
TRPV1-
containing
TRPM8
DRG
TRPM8
VISCERAL
SKIN
(VISCERAL?)
WARM
SKIN
(VISCERAL?)
COOL

Figure 5. Brown adipose tissue activation

The intracellular cascade starts with the β adrenergic receptors (β-AR) in brown adipocytes that are stimulated by the sympathetic nervous system (SNS) induced-release of noradrenaline (NA). These G-protein coupled receptors then activate adenylate cyclase (AC), inducing an increase in cAMP, which in turn activates protein kinase A (PKA). PKA acutely increases lipolysis by the activation of adipocyte triglyceride lipase (ATGL), hormone-sensitive lipase (HSL) and monoacylglycerol lipase (MGL), which hydrolyze the triacylglycerides to release free fatty acids (FFA) that will enter the mitochondria and will eventually be used for heat production by uncoupling protein 1 (UCP1) in the electron transport chain. The chronic effect of PKA activation increases the expression of thermogenic related genes.

(Modified from Seoane-Collazo et al., 2020).

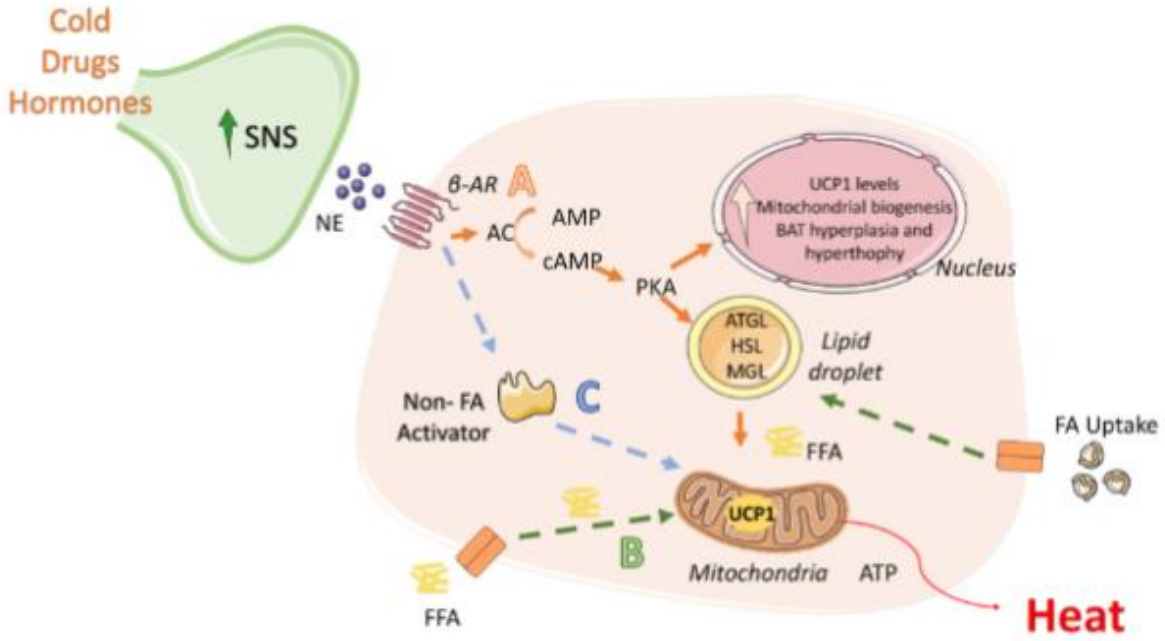
Cold
Drugs
Hormones
SNS
NE
β-AR
A
AC
AMP
cAMP
PKA
UCP1 levels
Mitochondrial biogenesis
BAT hyperplasia and
hyperthophy
Nucleus
ATGL
HSL
MGL
Lipid
droplet
Non- FA
Activator
C
FFA
FA Uptake
UCP1
B
Mitochondria
ATP
FFA
Heat

Figure 6. Environmental influence on the induction of torpor in mammals

Torpor is a physiological adaptive strategy that some mammals spontaneously exhibit in adverse environmental conditions which directly affect the quantity and quality of available food, and it is characterized by an active inhibition of metabolism that causes a decrease in body temperature, heart rate, and physical activity.

(Modified from Melvin & Andrews, 2009)

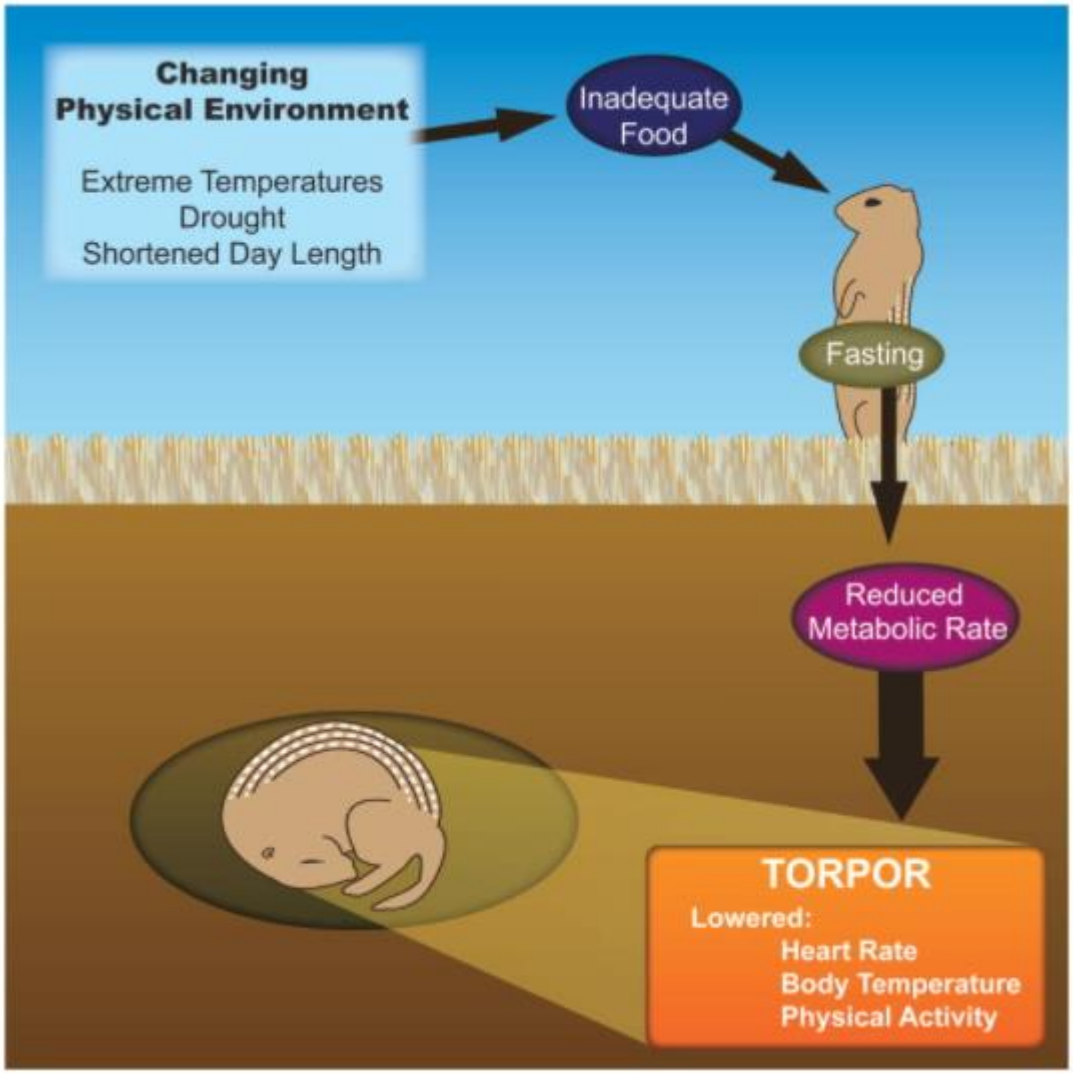
Changing
Physical Environment
Extreme Temperatures
Drought
Shortened Day Length
Inadequate
Food
Fasting
Reduced
Metabolic Rate
TORPOR
Lowered:
Heart Rate
Body Temperature
Physical Activity

Figure 7. Representative pictures of NeuN, AT8 and Tau-1 staining

Fig.7 **A**) CA3 field of the hippocampus. Left column represents NeuN staining (neuronal maker). Right column represents the same corresponding field depicted in the left column, but stained for AT8 (phosphorylated Tau). C, control; N, nadir; ER, early recovery during the arousal from ST, Thy 35,5°C; R38, recovery 38 h after the 35,5°C Thy was reached. (calibration bar: 100 μm).

Fig.7 **B**) The paraventricular nucleus of the hypothalamus (PVH). Left column represents NeuN staining (neuronal maker). Right column represents the same corresponding field depicted in the left column but stained for Tau-1 (non-phosphorylated Tau). C, control; N, nadir of hypothermia; R38, samples taken 38 h after 35.5°C Thy was reached. 3V, third ventricle. (calibration bar: 100 μm).

Synthetic Torpor (ST); paraventricular nucleus of the hypothalamus (PVN); Third ventricles (3V); Hypothalamic temperature (Thy).

(Modified from Luppi et al., 2019).

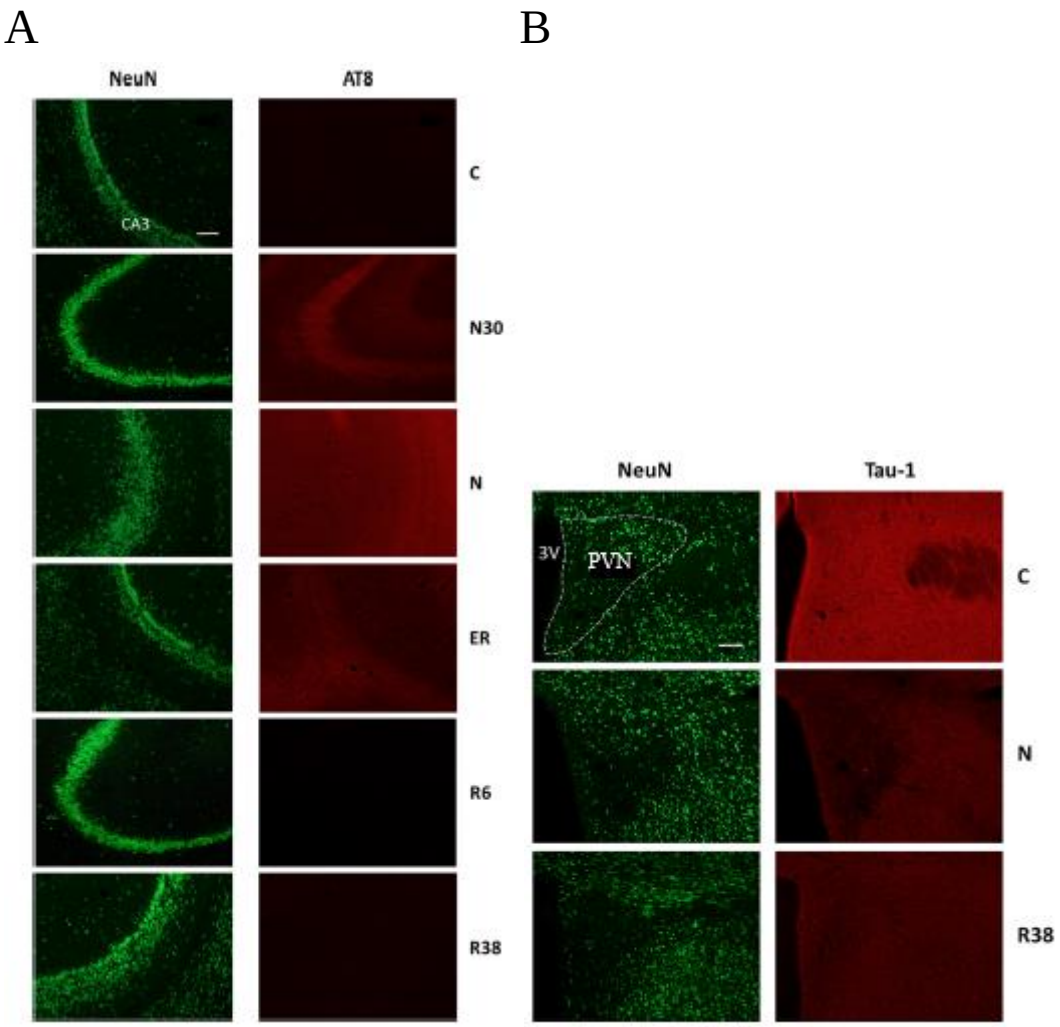
A
B
NeuN
AT8
CA3
C
N30
N
ER
R6
R38
NeuN
Tau-1
3V
PVN
C
N
R38

Figure 8. Study of the sympathetic reflex control of inflammation in mice subjected to different immune challenges: Experimental plan

Anaestetized mice (n=47) were subjected to surgery: the splanchnic nerves were exposed through a retroperitoneal approach and bilaterally cut (SplancX group) or left intact (Sham group). After the surgery mice were injected with one of the following immune challenges: i) LPS, 60 μg/kg; ii) Pam2cys, 34 μg/kg and iii) Poly I:C, 1 mg/kg. Each challenge was delivered in a volume of 100 μl to two groups of mice, designated Sham and SplancX.

The experimental groups were the following:

- Sham mice injected with LPS 60 μg/kg (n=8);
- SplancX mice injected with LPS 60 μg/kg (n=9);
- Sham mice injected with Pam2cys 34 μg/kg (n=9);
- SplancX mice injected with Pam2cys 34 μg/kg (n=9);
- Sham mice injected with Poly I:C 1 mg/Kg (n=6);
- SplancX mice injected with Poly I:C 1mg/Kg (n=6).

Ninety minutes after, the ribcage was cut open and lifted, and 0.5 ml of blood was collected by intracardiac puncture. Blood was stored in a refrigerator (~ 4 °C) overnight and the following day the serum was separated by centrifugation (4 °C at 2000 x g, 15 minutes) and immediately stored at -80 °C for subsequent cytokines measurement.

SplancX (mice with bilateral section of splanchnic nerves); Sham (mice Sham operated, with intact splanchnic nerves); Lipopolysaccharide (LPS); S-[2,3-bis(palmitoyloxy)propyl] cysteine (Pam2cys);Polyinosinedeoxycytidylic acid (Poly I:C).

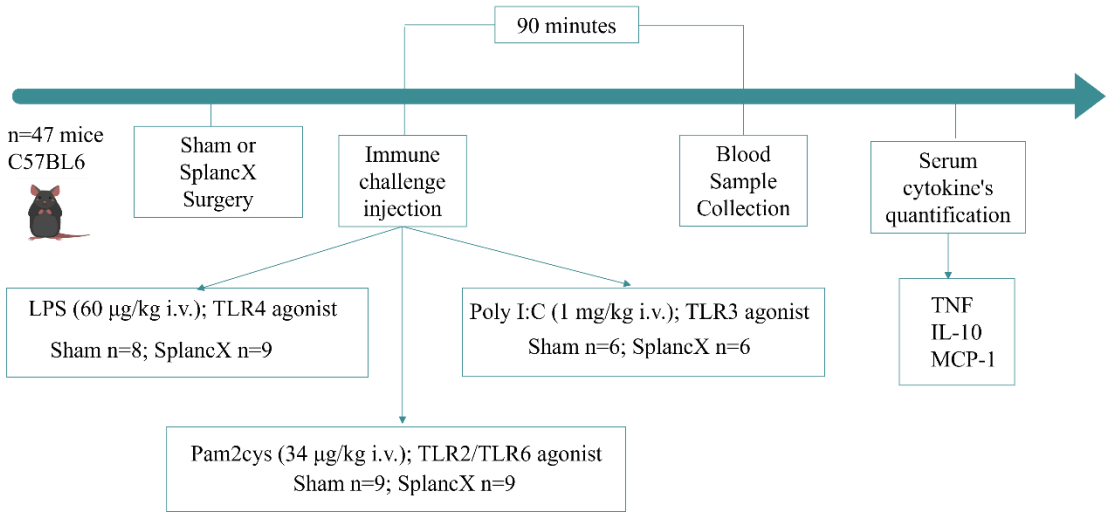
90 minutes
n=47 mice
C57BL6
Sham or
SplancX
Surgery
Immune
challenge
injection
Blood
Sample
Collection
Serum
cytokine's
quantification
LPS (60 µg/kg i.v.); TLR4 agonist
Sham n=8; SplancX n=9
Poly I:C (1 mg/kg i.v.); TLR3 agonist
Sham n=6; SplancX n=6
TNF
IL-10
MCP-1
Pam2cys (34 µg/kg i.v.); TLR2/TLR6 agonist
Sham n=9; SplancX n=9

Figure 9. Study of the mechanism underlying the hypothermia-related induction and resolution of brain phosphorylated Tau protein during and after synthetic torpor: surgical procedures

The upper figure is a representation of a rat skull: the blue symbol on the occipital bone is the superficial spot where the guide cannula was inserted during the surgery through a craniotomy. The four grey dots represent the sites of placement of the screws to hold the implant, the green dot indicates the placement of the hypothalamic thermistor, and the red squares the placement of the EEG electrodes. The coronal section below shows the target (raphe pallidus) of the microcannula.

Synthetic torpor (ST); Electroencephalogram (EEG).

(Modified from Paxinos & Watson, 2007)

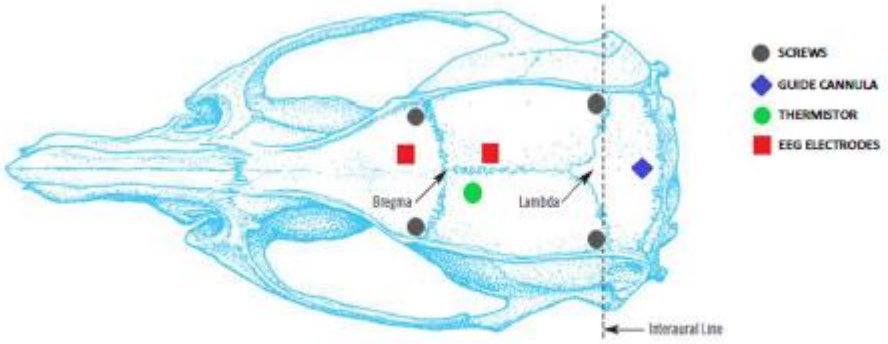
SCREWS
GUIDE CANNULA
THERMISTOR
EEG ELECTRODES
Bregma
Lambda
Interaural Line

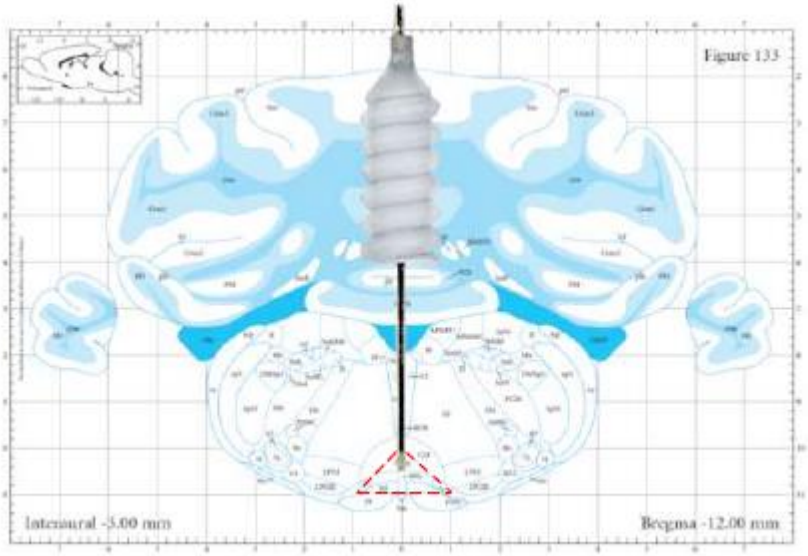
Figure 133
Interaural -3.00 mm
Bregma -12.00 mm

Figure 10. Study of the mechanism underlying the hypothermia-related induction and resolution of brain phosphorylated Tau protein during and after synthetic torpor: experimental plan

Animals were randomly assigned to five different experimental groups and were sacrificed at different times following the injection of either muscimol or aCSF (first injection at 8.00 a.m.). The experimental groups were the following:

- C → Control, injected with aCSF and sacrificed at around 14.00 h, exactly matching the N condition (n = 3).
- N → Nadir, sacrificed 1 h after the last injection, at 14:00 h, when Thy reached the nadir of hypothermia (Thy= 23.2 ± 0.8° C mean ± SEM; n = 3).
- ER → Early Recovery; sacrificed when Thyreached 35.5° C after ST, at around 16:00 h (2 h after Ta was moved from 15 to 28° C; n = 3).
- R3 → 3h Recovery, sacrificed 3 h after ER, at around 19:00 h (n = 3).
- R6 → 6h Recovery, sacrificed 6 h after ER, at around 22:00 h (n = 3).

For each experimental group, at established time points, animals were deeply anaesthetized and sacrificed in order to collect brain tissue. Moreover, blood samples were collected from each animal for immunoenzymatic assays.

Artificial cerebrospinal fluid(aCSF); SEM (Standard error of the mean).

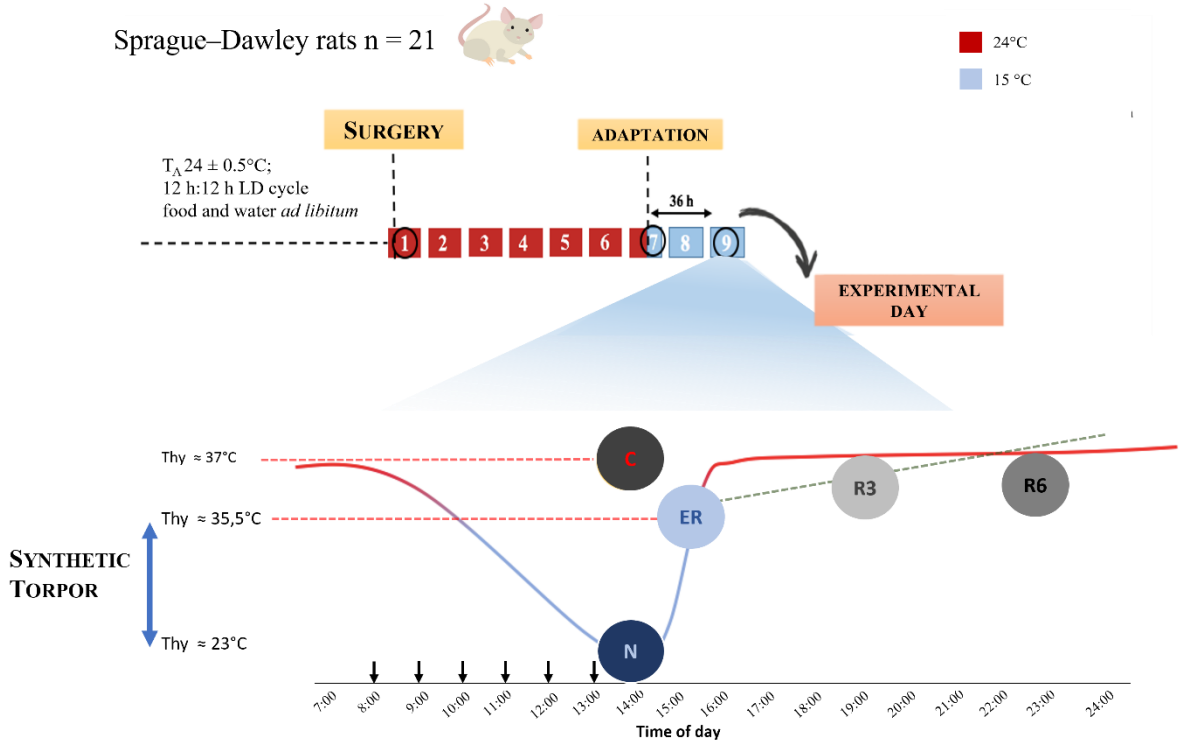
Sprague–Dawley rats n = 21
24°C
15 °C
SURGERY
ADAPTATION
T_A 24 ± 0.5°C;
12 h:12 h LD cycle
food and water *ad libitum*
36 h
1
2
3
4
5
6
7
8
9
EXPERIMENTAL DAY
Thy ≈ 37°C
Thy ≈ 35,5°C
Thy ≈ 23°C
SYNTHETIC TORPOR
C
ER
N
R3
R6
7:00
8:00
9:00
10:00
11:00
12:00
13:00
14:00
15:00
16:00
17:00
18:00
19:00
20:00
21:00
22:00
23:00
24:00
Time of day

Table 1. Primary antibodies employed in this study

Primary antibodies used in WB analysis.

Monoclonal (Mono-); Polyclonal (Poly-); Mouse (M); Rabbit (R); Phosphorylated (p-); Western Blot (WB); Cortex (Cx); Hippocampus (Hip).

Antibody	Type	Species	Specificity	MW (kDa)	Source and dilution
Anti-Total Tau	Mono-	M	Several Tau protein isoforms between 50-70 kDa	50-70	Merck Millipore; WB 1:5000
Tau-1	Mono-	M	No phosphorylated 189-207 residues	52-68	Merck Millipore; WB 1:5000
AT8	Mono-	M	PHF-Tau (Ser 202/Thr205)	68-70	Thermo Fisher; WB 1:1000
Anti-Phospho-Tau (Thr205)	Poly-	R	Phospho-Tau (Thr205)	68-70	Thermo Fisher; WB 1:1000
Anti-Gsk3-β	Mono-	R	Gsk-3β	46	Cell Signaling Technology; WB 1:3000
Anti-Phospho-Gsk3-β	Mono-	R	p- Gsk3β(pSer9)	46	Cell Signaling Technology; WB 1:3000
Anti-Akt	Poly-	R-	Total Akt1, Akt2, Akt3	56-60	Cell Signaling; WB 1:2000
Anti-Phospho-Akt	Poly-	R	p-Akt1 (pSer473), p-Akt2 (pSer473). P-Akt3 (pSer473)	56-60	Cell Signaling; WB 1:2000
Anti-GRP78	Mono-	R	GRP78	78	Cell Signaling; WB Cx 1:5000; WB Hip 1:3000
Anti-Xiap	Mono-	M	Xiap	54	Santa Cruz Biotechnology; WB 1:1000
Anti-PP2A Catalytic α	Mono-	M	PP2A	36	BDT Transduction Laboratories™; WB 1:5000
Anti-Cleaved-caspase 3	Poly-	R	Cleaved Caspase 3 (Asp175)	17-19	Cell Signaling; WB Cx 1:250; WB Hip 1:500
Anti-β-actin	Mono-	M	β-actin	42	Thermo Fisher; WB 1:5000

Figure 11. Study of the role of sleep in the dephosphorylation process of Tau during the recovery from synthetic torpor: Experimental plan

Animals were randomly assigned to four different experimental groups and were sacrificed at different times following the injection of muscimol (first injection at 8.00 a.m.) and the subsequent ST. The animals belonged to 3h Recovery and 6h Recovery groups were the same animals of Experiment 3.2. The experimental groups were the following:

- R3NS → 3h Recovery, sacrificed 3 h after Thy reached 35.5 °C, at around 22:00 h (*n*=3). The animals of this group normally sleep during recovery from torpor.
- R3SD → 3h Recovery during which animals were sleep deprived by gentle handling and sacrificed 3 h after the Thy reached 35.5 °C, at around 22:00 h (*n*=3).
- R6NS → 6h Recovery, sacrificed 6 h after Thy reached 35.5 °C, at around 22:00 h (*n*=3). The animals of this group normally sleep during recovery from torpor.
- R6SD → 6h Recovery during which animals were sleep deprived by gentle handling and sacrificed 6 h after the Thy reached 35.5 °C, at around 22:00 h (*n*=3).

For each experimental group, at established time points, animals were deeply anaesthetized and sacrificed in order to collect brain tissue. Moreover, blood samples were collected from each animal for immunoenzymatic assays.

Synthetic torpor (ST); Normal sleep (NS); Sleep deprivation (SD); SEM (Standard error of the mean).

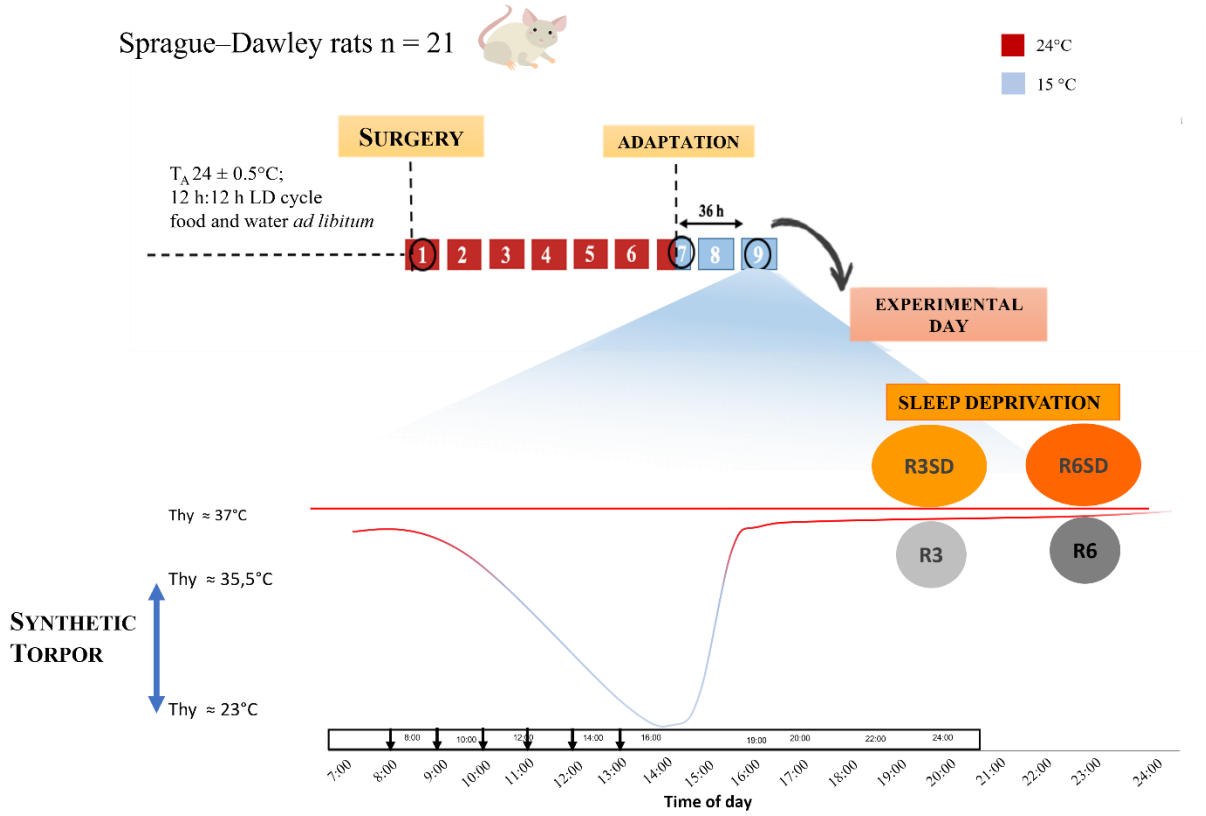
Sprague–Dawley rats n = 21
24°C
15 °C
SURGERY
ADAPTATION
T_A 24 ± 0.5°C;
12 h:12 h LD cycle
food and water *ad libitum*
36 h
1
2
3
4
5
6
7
8
9
EXPERIMENTAL DAY
SLEEP DEPRIVATION
R3SD
R6SD
R3
R6
Thy ≈ 37°C
Thy ≈ 35,5°C
Thy ≈ 23°C
SYNTHETIC TORPOR
8:00
10:00
12:00
14:00
16:00
19:00
20:00
22:00
24:00
7:00
8:00
9:00
10:00
11:00
12:00
13:00
14:00
15:00
16:00
17:00
18:00
19:00
20:00
21:00
22:00
23:00
24:00
Time of day

Figure 12. Effects of splanchnic nerves section on serum cytokines to LPS challenge

The panels show, respectively, serum **A**) TNF, **B**) IL-10, **C**) MCP-1, **D**) IL-6, **E**) IL12p70, **F**) INF-γ levels in mice with splanchnic nerves cut (SplancX, n=9) or sham-cut (Sham, n=8), measured 90 minutes after i.v. injection of LPS (60 µg/kg).

Fig.12 **G**) serum TNF:IL10 ratio, calculated as index of the inflammatory status.

Experimental groups: Mice with bilateral splanchnic nerves cut (SplancX, n=9); mice with intact splanchnic nerves (Sham, n=8).

Bars represent mean ± SEM. *** $p<0.001$; ** $p<0.01$; * $p<0.05$.

Lipopolysaccharide (LPS); Tumor necrosis factor (TNF); Interleukin 10 (IL-10); Monocyte chemoattractant protein-1 (MCP-1); Interleukin 6 (IL-6); Interleukin 12 p70 (IL12p70); Interferon-γ (INF-γ); SEM (Standard error of the mean).

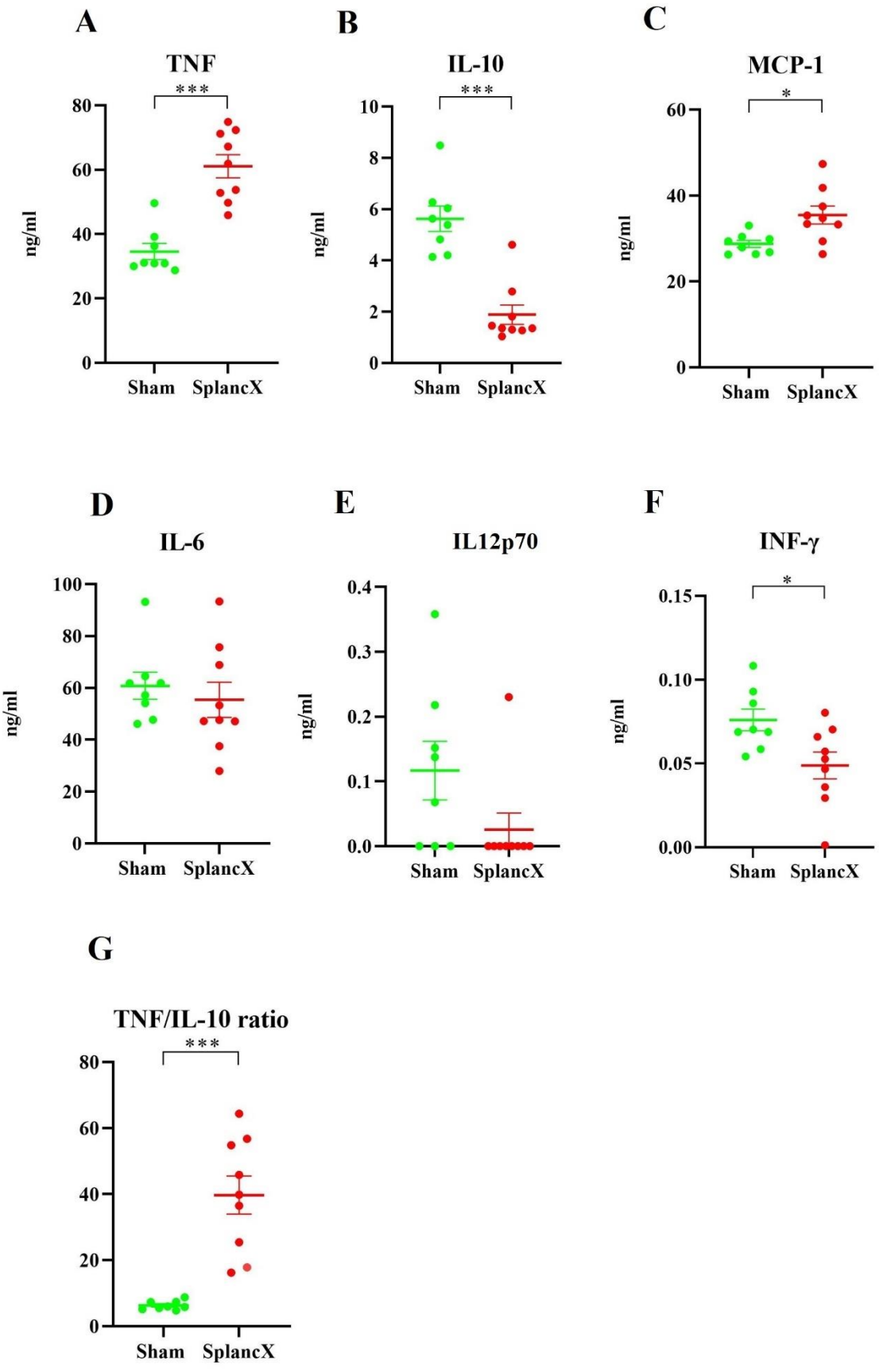
A
TNF
***
ng/ml
80
60
40
20
0
Sham
SplancX
B
IL-10
***
ng/ml
10
8
6
4
2
0
Sham
SplancX
C
MCP-1
*
ng/ml
60
40
20
0
Sham
SplancX
D
IL-6
ng/ml
100
80
60
40
20
0
Sham
SplancX
E
IL12p70
ng/ml
0.4
0.3
0.2
0.1
0.0
Sham
SplancX
F
INF-γ
*
ng/ml
0.15
0.10
0.05
0.00
Sham
SplancX
G
TNF/IL-10 ratio
***
80
60
40
20
0
Sham
SplancX

Figure 13. Effects of splanchnic nerves section on serum cytokines to Pam2cys challenge

The panels show, respectively, serum **A**) TNF, **B**) IL-10, **C**) MCP-1, **D**) IL-6, **E**) IL12p70, **F**) INF-γ levels in mice with splanchnic nerves cut (SplancX, n=8) or sham-cut (Sham, n=8), measured 90 minutes after i.v. injection of Pam2cys (34 µg/kg).

Fig.13 **G**) serum TNF:IL10 ratio, calculated as index of the inflammatory status.

Experimental groups: Mice with bilateral splanchnic nerves cut (SplancX); mice with intact splanchnic nerves (Sham).

Bars represent mean ± SEM. *** $p<0.001$; ** $p<0.01$; * $p<0.05$.

S-[2,3-bis(palmitoyloxy)propyl] cysteine (Pam2cys); Tumor necrosis factor (TNF); Interleukin 10 (IL-10); Monocyte chemoattractant protein-1 (MCP-1); Interleukin 6 (IL-6); Interleukin 12 p70 (IL12p70); Interferon-γ (INF-γ); SEM (Standard error of the mean).

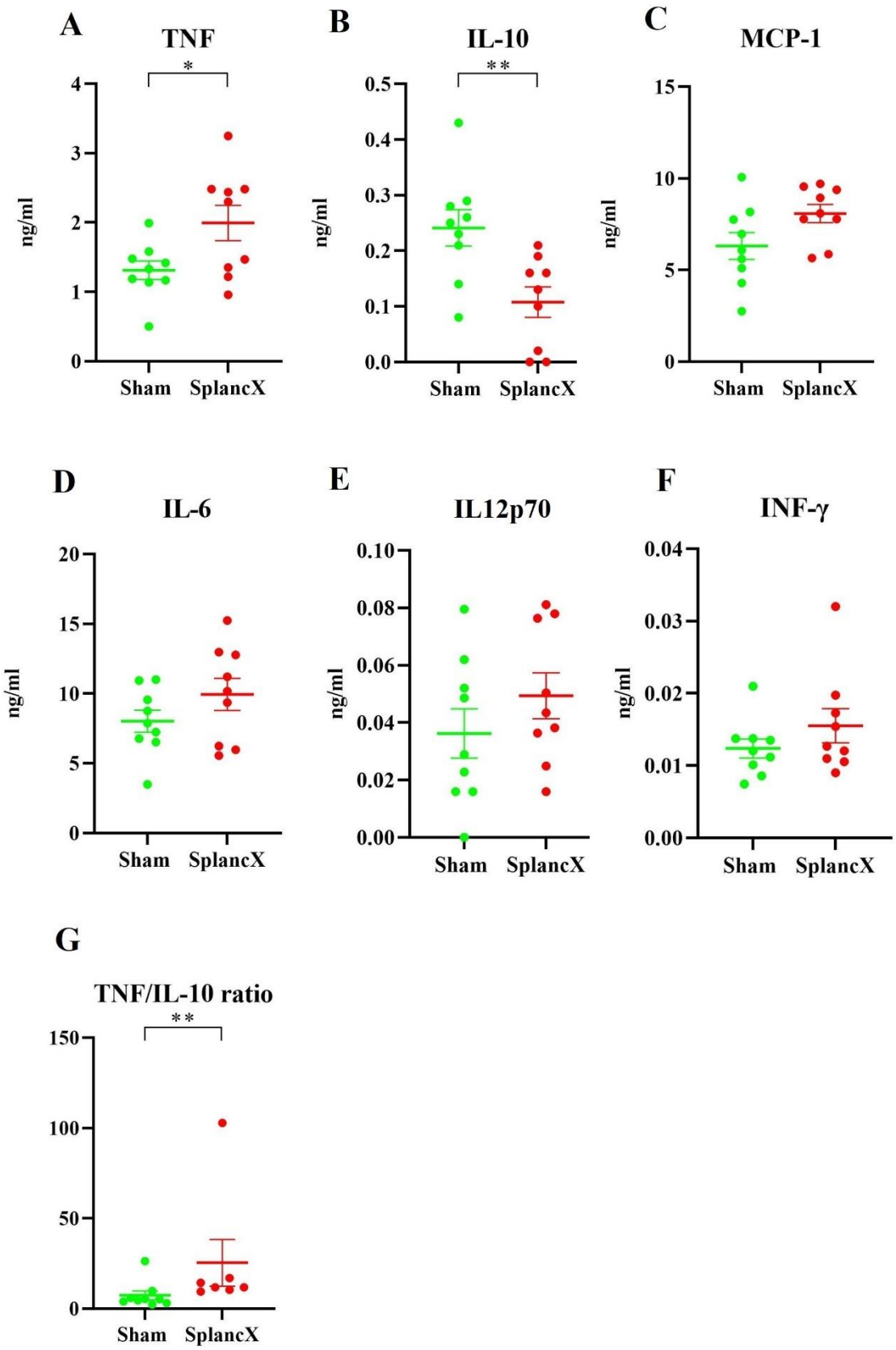
A
TNF
*
ng/ml
4
3
2
1
0
Sham
SplancX
B
IL-10
**
ng/ml
0.5
0.4
0.3
0.2
0.1
0.0
Sham
SplancX
C
MCP-1
ng/ml
15
10
5
0
Sham
SplancX
D
IL-6
ng/ml
20
15
10
5
0
Sham
SplancX
E
IL12p70
ng/ml
0.10
0.08
0.06
0.04
0.02
0.00
Sham
SplancX
F
INF-γ
ng/ml
0.04
0.03
0.02
0.01
0.00
Sham
SplancX
G
TNF/IL-10 ratio
**
150
100
50
0
Sham
SplancX

Figure 14. Effects of splanchnic nerves section on serum cytokines to Poly I:C challenge

The panels show, respectively, serum **A**) TNF, **B**) IL-10, **C**) MCP-1, **D**) IL-6, **E**) IL12p70, **F**) INF-γ levels in mice with splanchnic nerves cut (SplancX, n=6) or sham-cut (Sham, n=6), measured 90 minutes after i.v. injection of Poly I:C (1 mg/kg).

Fig.14 **G**) serum TNF:IL10 ratio, calculated as index of the inflammatory status.

Bars represent mean ± SEM. *** $p<0.001$; ** $p<0.01$; * $p<0.05$.

Sham Polyinosinedeoxycytidylic acid (Poly I:C); Tumor necrosis factor (TNF); Interleukin 10 (IL-10); Monocyte chemoattractant protein-1 (MCP-1); Interleukin 6 (IL-6); Interleukin 12 p70 (IL12p70); Interferon-γ (INF-γ); SEM (Standard error of the mean).

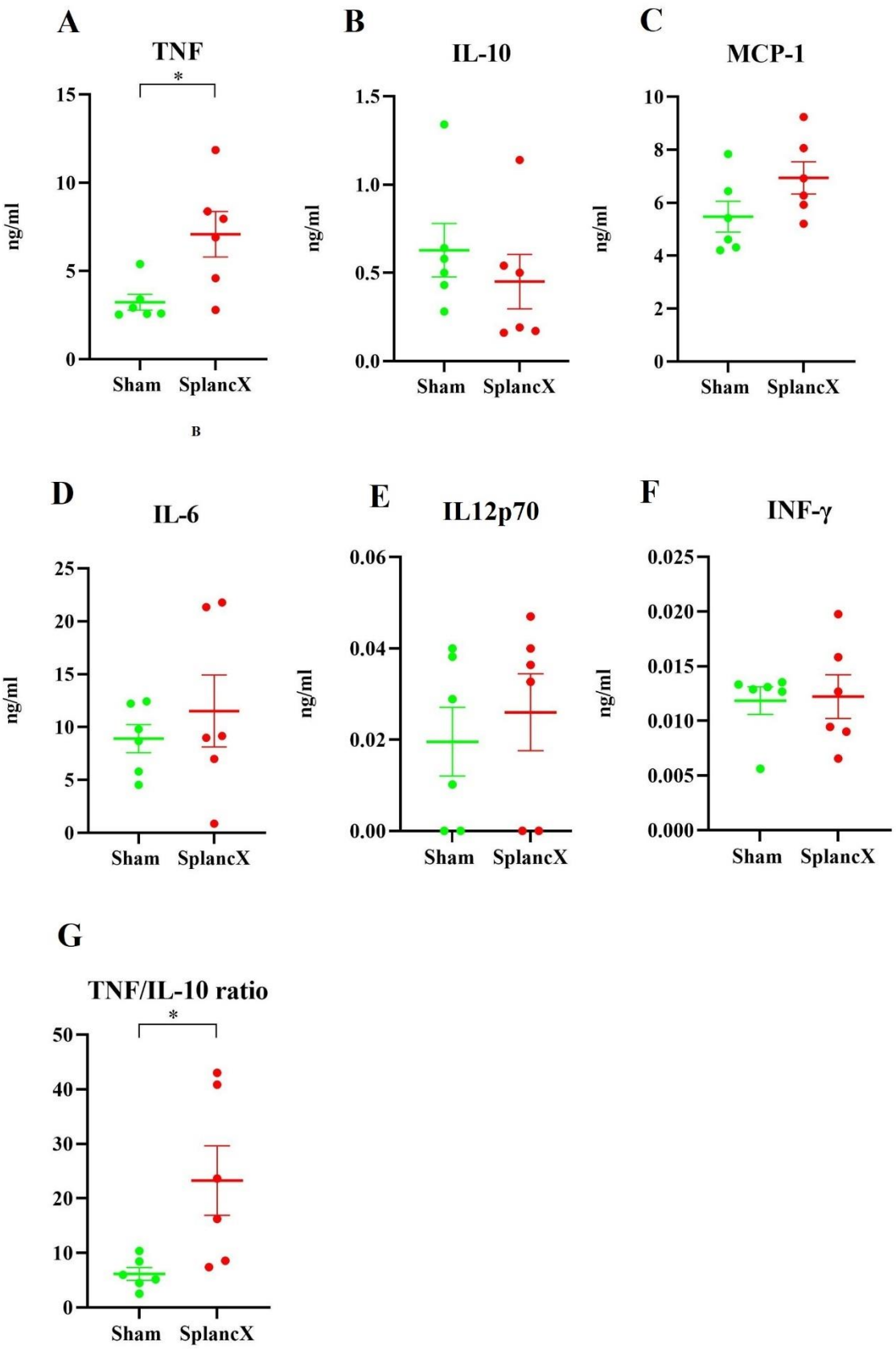
A
TNF
*
ng/ml
15
10
5
0
Sham
SplancX
B
B
IL-10
ng/ml
1.5
1.0
0.5
0.0
Sham
SplancX
C
MCP-1
ng/ml
10
8
6
4
2
0
Sham
SplancX
D
IL-6
ng/ml
25
20
15
10
5
0
Sham
SplancX
E
IL12p70
ng/ml
0.06
0.04
0.02
0.00
Sham
SplancX
F
INF-γ
ng/ml
0.025
0.020
0.015
0.010
0.005
0.000
Sham
SplancX
G
TNF/IL-10 ratio
*
50
40
30
20
10
0
Sham
SplancX

Table 2. Study of the mechanism underlying the hypothermia-related induction and resolution of brain phosphorylated Tau protein during and after synthetic torpor: hypothalamic temperature

Average Thy levels (°C, mean ± SEM) in the 1-h period which preceded the sacrifice of the animals are shown. Experimental groups: Normothermic control rats (C); Hypothermic rats at their lowest temperature (Nadir, N); Rats during the arousal from ST, Thy35,5°C (Early Recovery, ER); Normothermic rats after 3 hours after the arousal from ST (Recovery after 3 hours, R3); Normothermic rats after 6 hours after the arousal from ST (Recovery after 6 h, R6). For all groups, n=3, except in C, n=2 due to a thermistor's damage in one rat.

* $p<0.05$ *vs* C

** $p<0.01$ *vs* C

Hypothalamic temperature (Thy); SEM (Standard error of the mean); Synthetic torpor (ST).

	MEAN	SEM
C	37.98	0.14
N	23.26	0.82 **
ER	32.92	0.61 *
R3	38.59	0.06 *
R6	37.66	1.54

Figure 15. Total Tau in brain extracts of cortex and hippocampus

Using the specific antibody Anti-Total Tau, the levels of several isoforms of Tau protein between 50-70 KDa were analyzed by WB in brain extracts of cortex (Cx, n=3) and hippocampus (Hip, n=3).

Fig.15 **A**) WB analysis of one representative sample for each experimental group.

Fig.15 **B**) Mean values ± SEM of normalized Total Tau expression calculated as the ratio between band intensities of Total Tau with the corresponding β-actin band in each experimental condition.

Experimental groups: Normothermic control rats (C); Hypothermic rats at lowest temperature (Nadir, N); Rats during the arousal from ST, Thy35,5°C (Early Recovery, ER); Normothermic rats after 3 hours after the arousal from ST (Recovery after 3 hours, R3); Normothermic rats after 6 hours after the arousal from ST (Recovery after 6 h, R6).

*: significant comparisons ($p<0.05$).

Western Blot (WB); Hippocampus (Hip); Cortex (Cx); SEM (Standard error of the mean); Synthetic torpor (ST); Hypothalamic temperature (Thy).

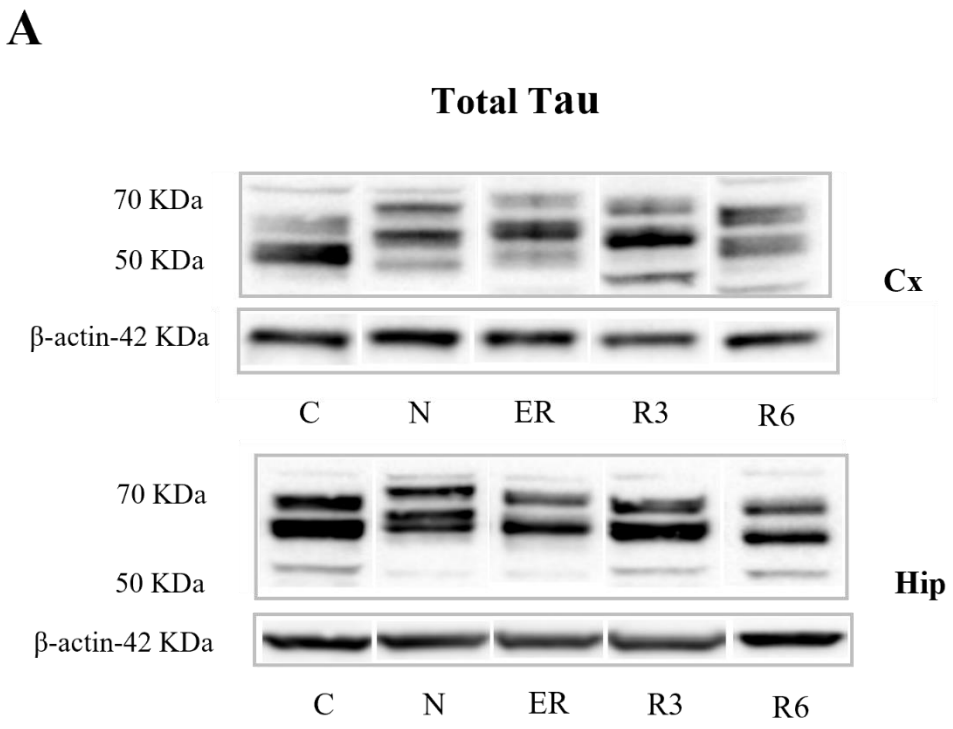
A
Total Tau
70 KDa
50 KDa
β-actin-42 KDa
Cx
C
N
ER
R3
R6
70 KDa
50 KDa
β-actin-42 KDa
Hip
C
N
ER
R3
R6

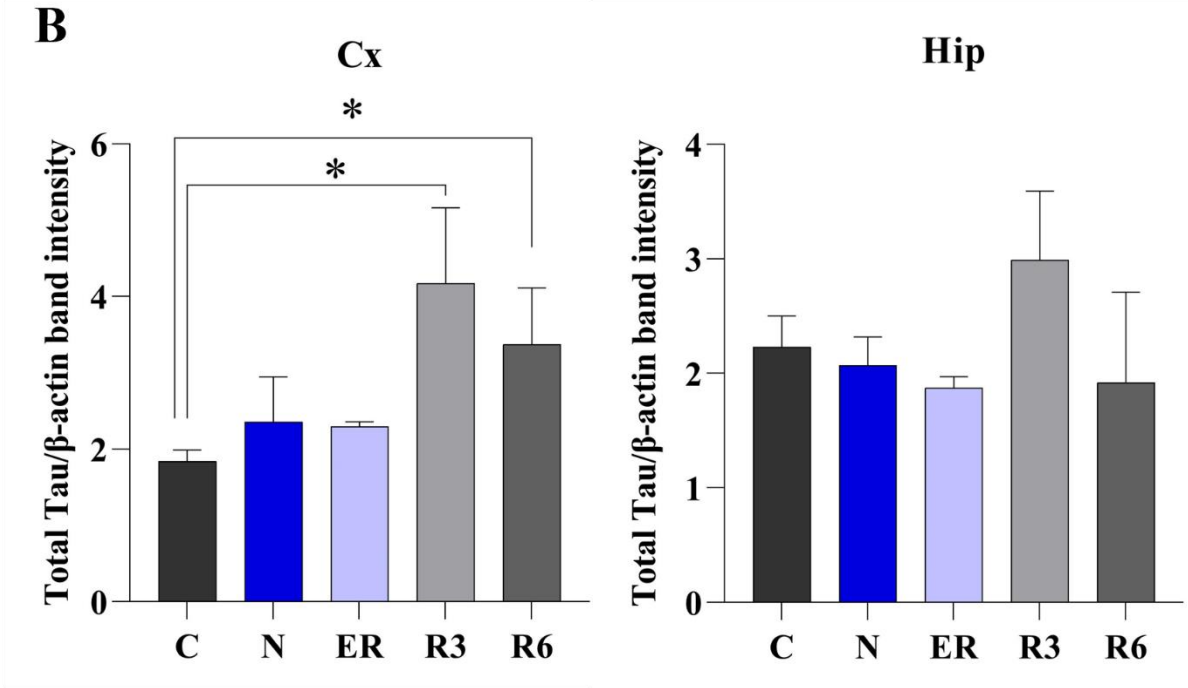
B
Cx
*
*
Total Tau/β-actin band intensity
0
2
4
6
C
N
ER
R3
R6
Hip
Total Tau/β-actin band intensity
0
1
2
3
4
C
N
ER
R3
R6

Figure 16. AT8 in brain extracts of cortex and hippocampus

Using the specific antibody AT8, the levels of phosphorylated tau protein on residues Ser202 or Thr205 were analyzed by WB in brain extracts of cortex (Cx, n=3) and hippocampus (Hip, n=3).

Fig.16 **A**) WB analysis of one representative sample for each experimental group.

Fig.16 **B**) Mean values ± SEM of normalized AT8 expression calculated as the ratio between band intensities of AT8 with the corresponding β-actin band in each experimental condition.

Experimental groups: Normothermic control rats (C); Hypothermic rats at lowest temperature (Nadir, N); Rats during the arousal from ST, Thy35,5°C (Early Recovery, ER); Normothermic rats after 3 hours after the arousal from ST (Recovery after 3 hours, R3); Normothermic rats after 6 hours after the arousal from ST (Recovery after 6 h, R6).

*: significant comparisons ($p<0.05$).

Western Blot (WB); Cortex (Cx); Hippocampus (Hip); SEM (Standard error of the mean); Synthetic torpor (ST); Hypothalamic temperature (Thy).

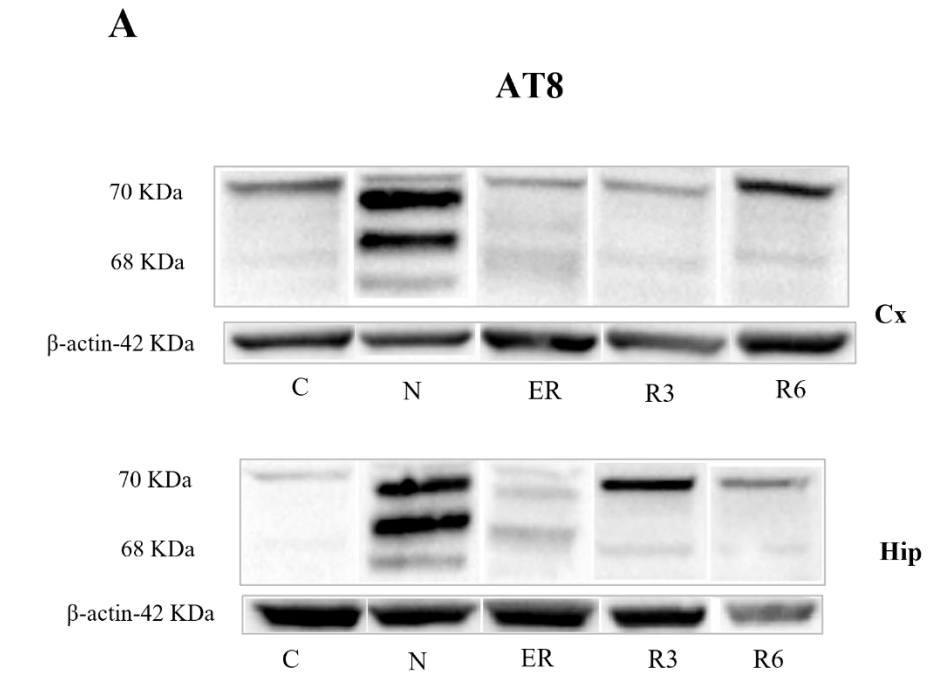
A
AT8
70 KDa
68 KDa
β-actin-42 KDa
Cx
C
N
ER
R3
R6
70 KDa
68 KDa
β-actin-42 KDa
Hip
C
N
ER
R3
R6

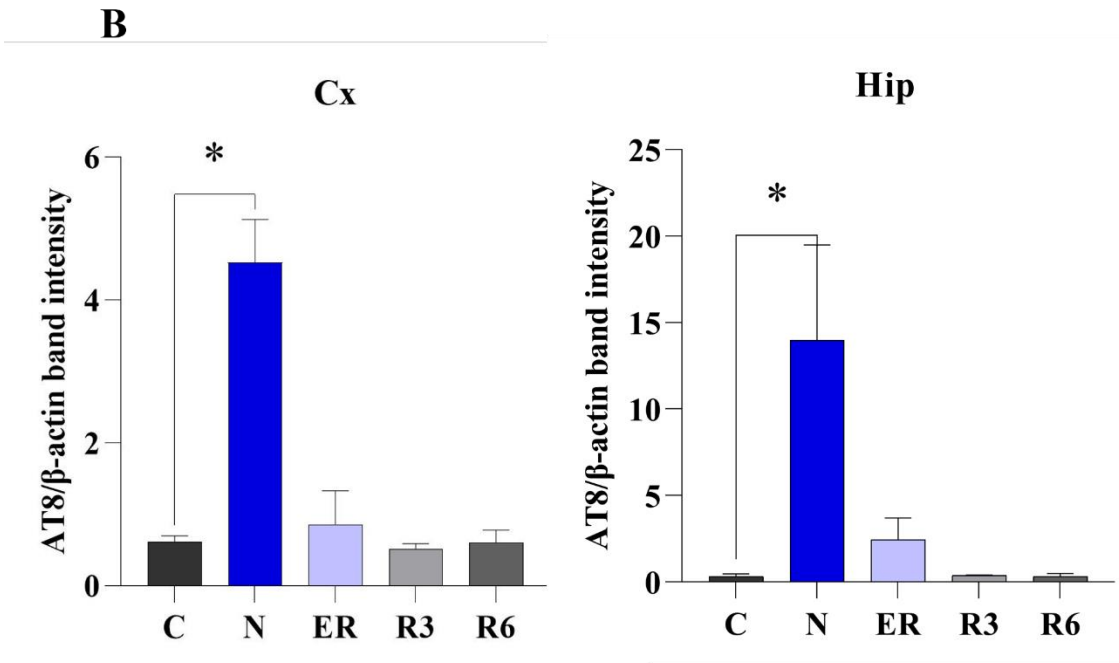
B
Cx
AT8/β-actin band intensity
6
4
2
0
*
C
N
ER
R3
R6
Hip
AT8/β-actin band intensity
25
20
15
10
5
0
*
C
N
ER
R3
R6

Figure 17. Tau-1 in brain extracts of cortex and hippocampus

Using the specific antibody Tau-1, the levels of dephosphorylated tau protein on residues 189-207 were analyzed by WB in brain extracts of cortex (Cx, n=3) and hippocampus (Hip, n=3).

Fig.17 **A**) WB analysis of one representative sample for each experimental group.

Fig.17 **B**) Mean values ± SEM of normalized Tau-1 expression calculated as the ratio between band intensities of Tau-1 with the corresponding β-actin band in each experimental condition.

Experimental groups: Normothermic control rats (C); Hypothermic rats at lowest temperature (Nadir, N); Rats during the arousal from ST, Thy35,5°C (Early Recovery, ER); Normothermic rats after 3 hours after the arousal from ST (Recovery after 3 hours, R3); Normothermic rats after 6 hours after the arousal from ST (Recovery after 6 h, R6).

*: significant comparisons ($p<0.05$).

Western Blot (WB); Cortex (Cx); Hippocampus (Hip); SEM (Standard error of the mean); Synthetic torpor (ST); Hypothalamic temperature (Thy).

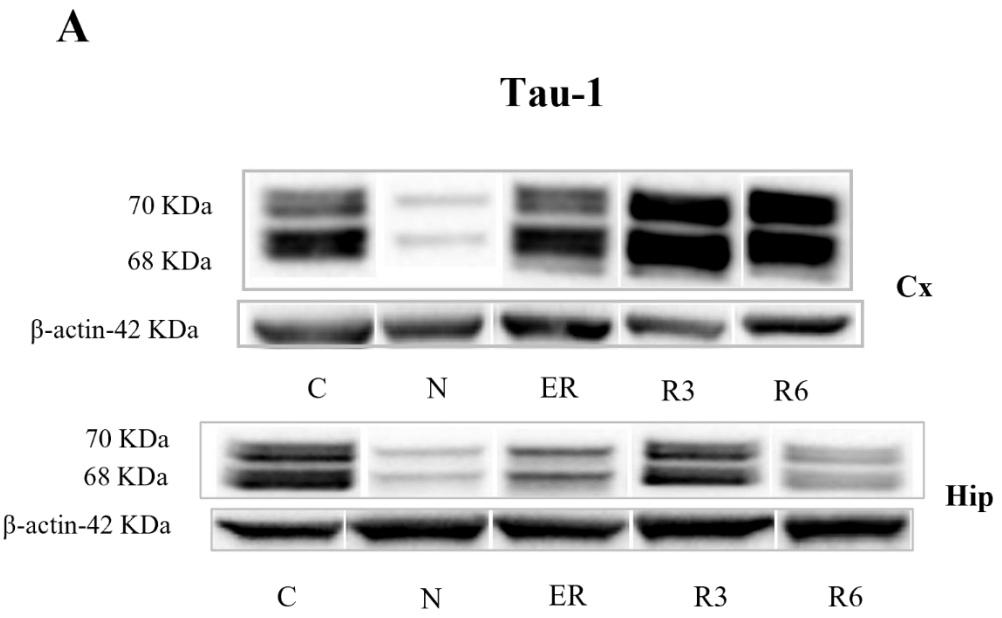
A
Tau-1
70 KDa
68 KDa
β-actin-42 KDa
Cx
C
N
ER
R3
R6
70 KDa
68 KDa
β-actin-42 KDa
Hip
C
N
ER
R3
R6

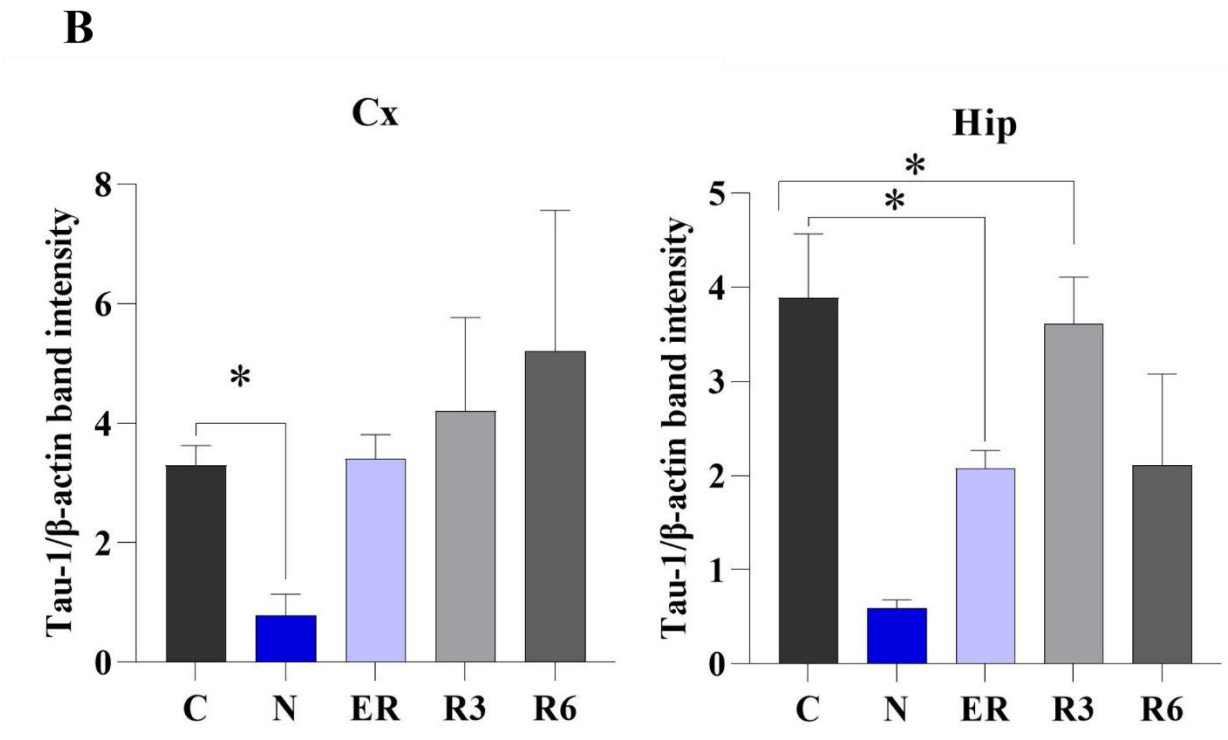
B
Cx
Tau-1/β-actin band intensity
0
2
4
6
8
*
C
N
ER
R3
R6
Hip
Tau-1/β-actin band intensity
0
1
2
3
4
5
*
*
C
N
ER
R3
R6

Figure 18. p(205)-Tau in brain extracts of cortex and hippocampus

Using the specific antibody Anti-Phospho-Tau (Thr205), the levels of phosphorylated tau protein on Thr205 residues was analyzed by WB in brain extracts of cortex (Cx, n=3) and hippocampus (Hip, n=3).

Fig.18 **A**) WB analysis of one representative sample for each experimental group.

Fig.18 **B**) Mean values ± SEM of normalized p(205)-Tau expression calculated as the ratio between band intensities of p(205)-Tau with the corresponding β-actin band in each experimental condition.

Experimental groups: Normothermic control rats (C); Hypothermic rats at lowest temperature (Nadir, N); Rats during the arousal from ST, Thy35,5°C (Early Recovery, ER); Normothermic rats after 3 hours after the arousal from ST (Recovery after 3 hours, R3); Normothermic rats after 6 hours after the arousal from ST (Recovery after 6 h, R6).

*: significant comparisons ($p<0.05$).

Western Blot (WB); Cortex (Cx); Hippocampus (Hip); SEM (Standard error of the mean); Synthetic torpor (ST); Hypothalamic temperature (Thy).

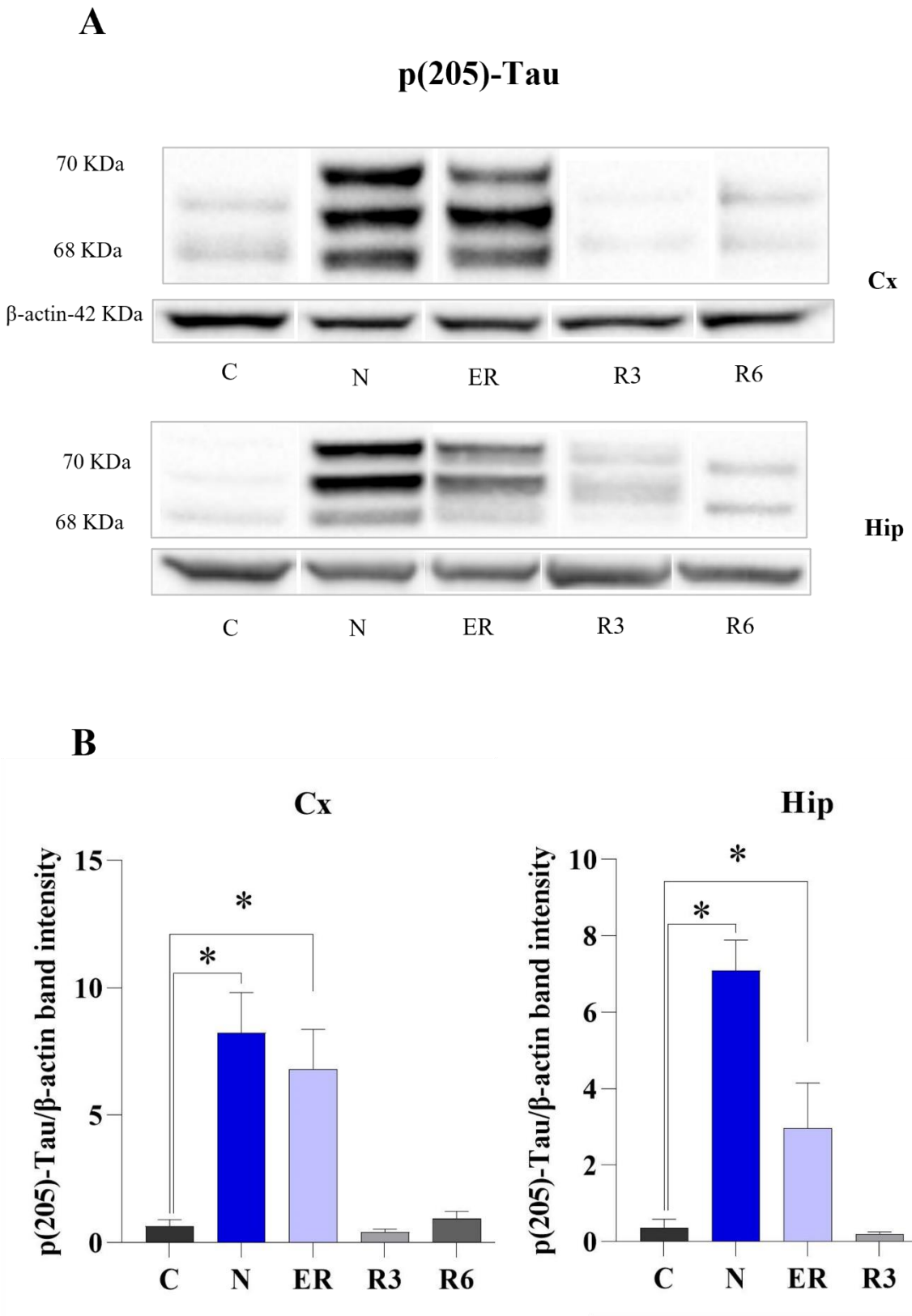
A
p(205)-Tau
70 KDa
68 KDa
β-actin-42 KDa
Cx
C
N
ER
R3
R6
70 KDa
68 KDa
Hip
C
N
ER
R3
R6
B
Cx
p(205)-Tau/β-actin band intensity
15
10
5
0
*
*
C
N
ER
R3
R6
Hip
p(205)-Tau/β-actin band intensity
10
8
6
4
2
0
*
*
C
N
ER
R3
R6

Figure 19. Gsk3-β in brain extracts of cortex and hippocampus

Using the specific antibody Anti-Gsk3-β, the levels of Gsk3-β was analyzed by WB in brain extracts of cortex (Cx, n=3) and hippocampus (Hip, n=3).

Fig.19 **A**) WB analysis of one representative sample for each experimental group.

Fig.19 **B**) Mean values ± SEM of normalized Gsk3-β expression calculated as the ratio between band intensities of Gsk3-β with the corresponding β-actin band in each experimental condition.

Experimental groups: Normothermic control rats (C); Hypothermic rats at lowest temperature (Nadir, N); Rats during the arousal from ST, Thy35,5°C (Early Recovery, ER); Normothermic rats after 3 hours after the arousal from ST (Recovery after 3 hours, R3); Normothermic rats after 6 hours after the arousal from ST (Recovery after 6 h, R6).

*: significant comparisons ($p<0.05$).

Western Blot (WB); Cortex (Cx); Hippocampus (Hip); SEM (Standard error of the mean); Synthetic torpor (ST); Hypothalamic temperature (Thy).

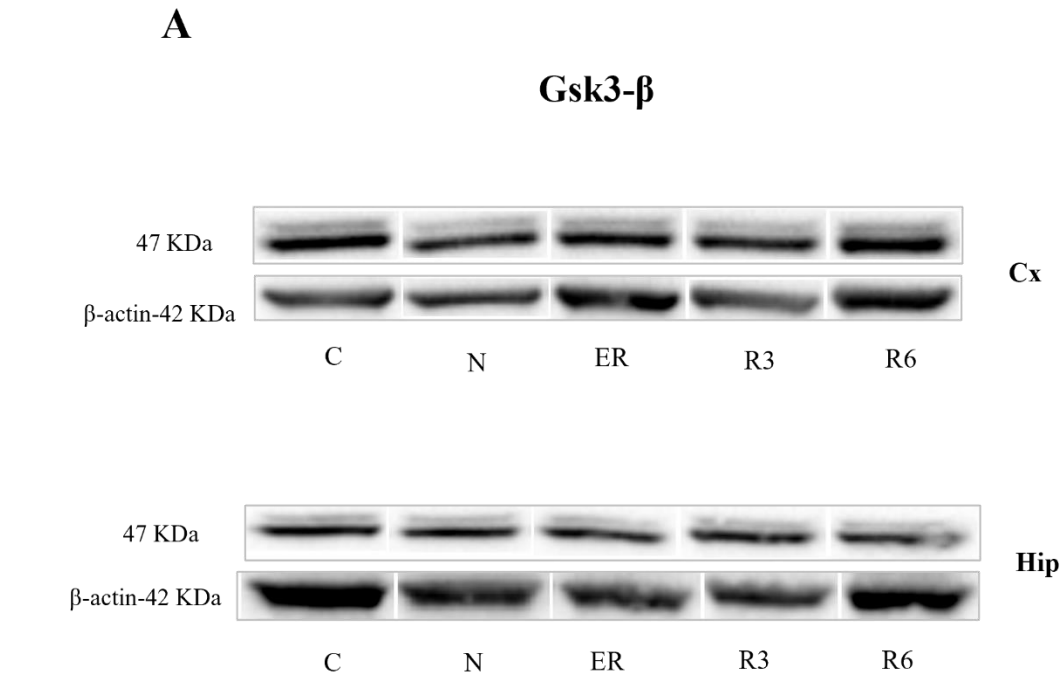
A
Gsk3-β
47 KDa
β-actin-42 KDa
Cx
C
N
ER
R3
R6
47 KDa
β-actin-42 KDa
Hip
C
N
ER
R3
R6

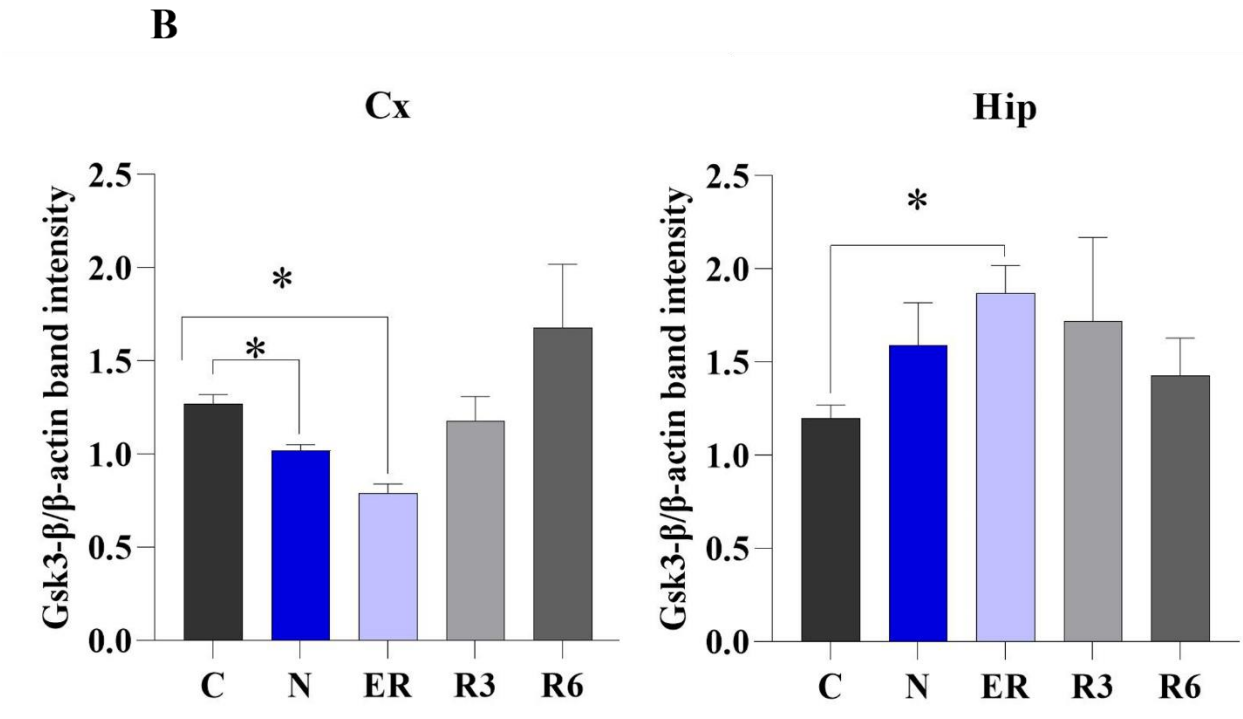
B
Cx
Hip
Gsk3-β/β-actin band intensity
2.5
2.0
1.5
1.0
0.5
0.0
*
*
C
N
ER
R3
R6

Figure 20. p(9)-Gsk3-β in brain extracts of cortex and hippocampus

Using the specific antibody Anti-Phospho-Gsk3-β, the levels of Gsk3-β phosphorylated on Ser9 residue was analyzed by WB in brain extracts of cortex (Cx, n=3) and hippocampus (Hip, n=3).

Fig.20 **A**) WB analysis of one representative sample for each experimental group.

Fig.20 **B**) Mean values ± SEM of normalized p(9)-Gsk3-β expression calculated as the ratio between band intensities of p(9)-Gsk3-β with the corresponding β-actin band in each experimental condition.

Experimental groups: Normothermic control rats (C); Hypothermic rats at lowest temperature (Nadir, N); Rats during the arousal from ST, Thy35,5°C (Early Recovery, ER); Normothermic rats after 3 hours after the arousal from ST (Recovery after 3 hours, R3); Normothermic rats after 6 hours after the arousal from ST (Recovery after 6 h, R6).

*: significant comparisons ($p<0.05$).

Western Blot (WB); Cortex (Cx); Hippocampus (Hip); SEM (Standard error of the mean); Synthetic torpor (ST); Hypothalamic temperature (Thy).

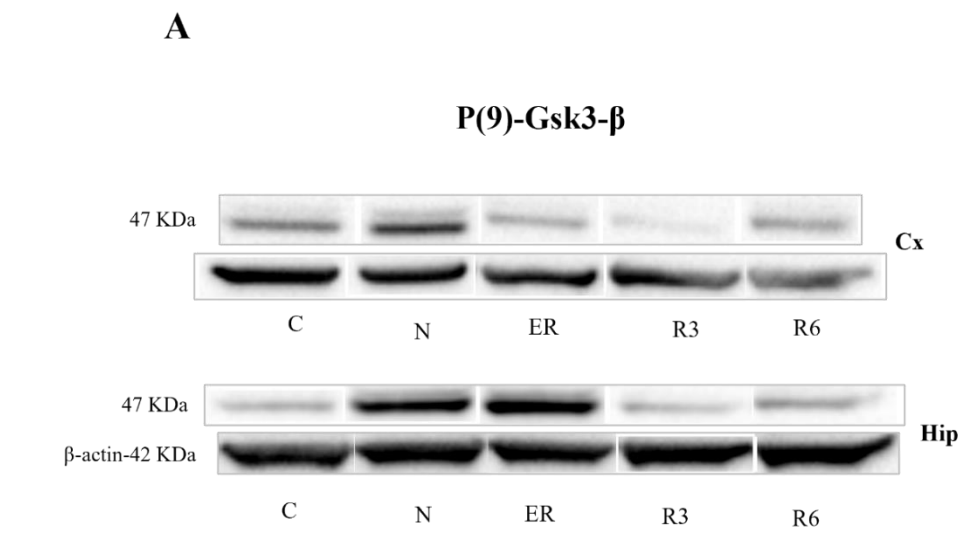
A
P(9)-Gsk3-β
47 KDa
Cx
C
N
ER
R3
R6
47 KDa
β-actin-42 KDa
Hip
C
N
ER
R3
R6

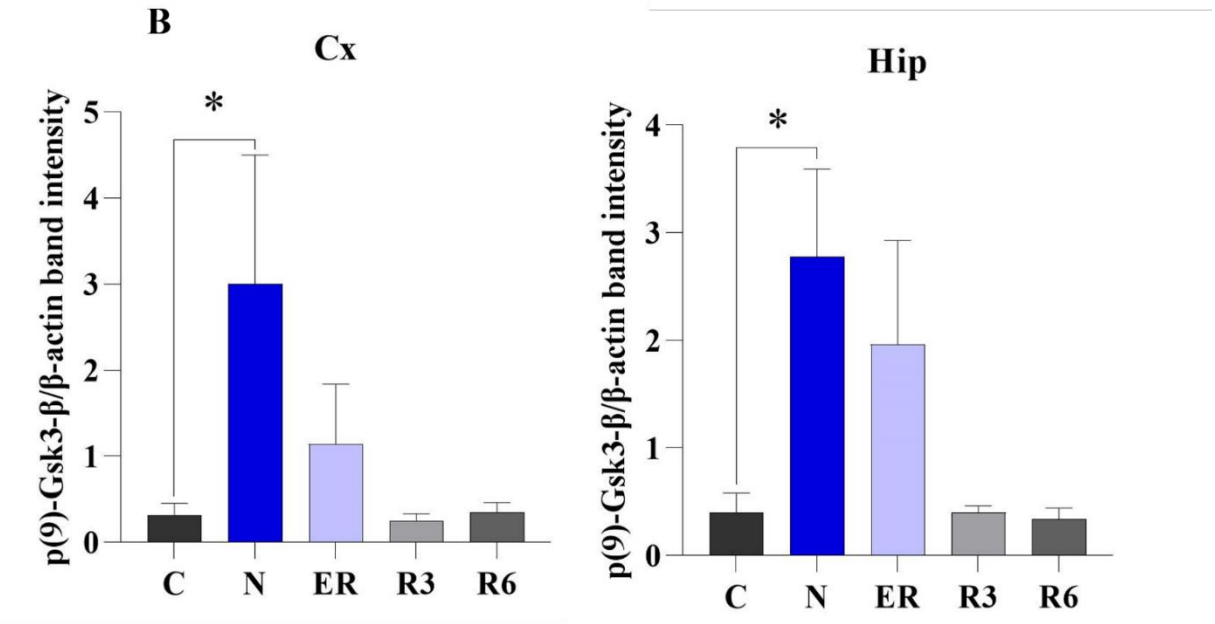
B
Cx
p(9)-Gsk3-β/β-actin band intensity
*
0
1
2
3
4
5
C
N
ER
R3
R6
Hip
p(9)-Gsk3-β/β-actin band intensity
*
0
1
2
3
4
C
N
ER
R3
R6

Figure 21. Akt in brain extracts of cortex and hippocampus

Using the specific antibody Anti-Akt, the levels of the diverse isoforms Akt 1/2/3 was analyzed by WB in brain extracts of cortex (Cx, n=3) and hippocampus (Hip, n=3).

Fig.21 **A**) WB analysis of one representative sample for each experimental group.

Fig.21 **B**) Mean values ± SEM of normalized Akt expression calculated as the ratio between band intensities of Akt with the corresponding β-actin band in each experimental condition.

Experimental groups: Normothermic control rats (C); Hypothermic rats at lowest temperature (Nadir, N); Rats during the arousal from ST, Tb 35,5°C (Early Recovery, ER); Normothermic rats after 3 hours after the arousal from ST (Recovery after 3 hours, R3); Normothermic rats after 6 hours after the arousal from ST (Recovery after 6 h, R6).

*: significant comparisons ($p<0.05$).

Western Blot (WB); Cortex (Cx); Hippocampus (Hip); SEM (Standard error of the mean); Synthetic torpor (ST); Hypothalamic temperature (Thy).

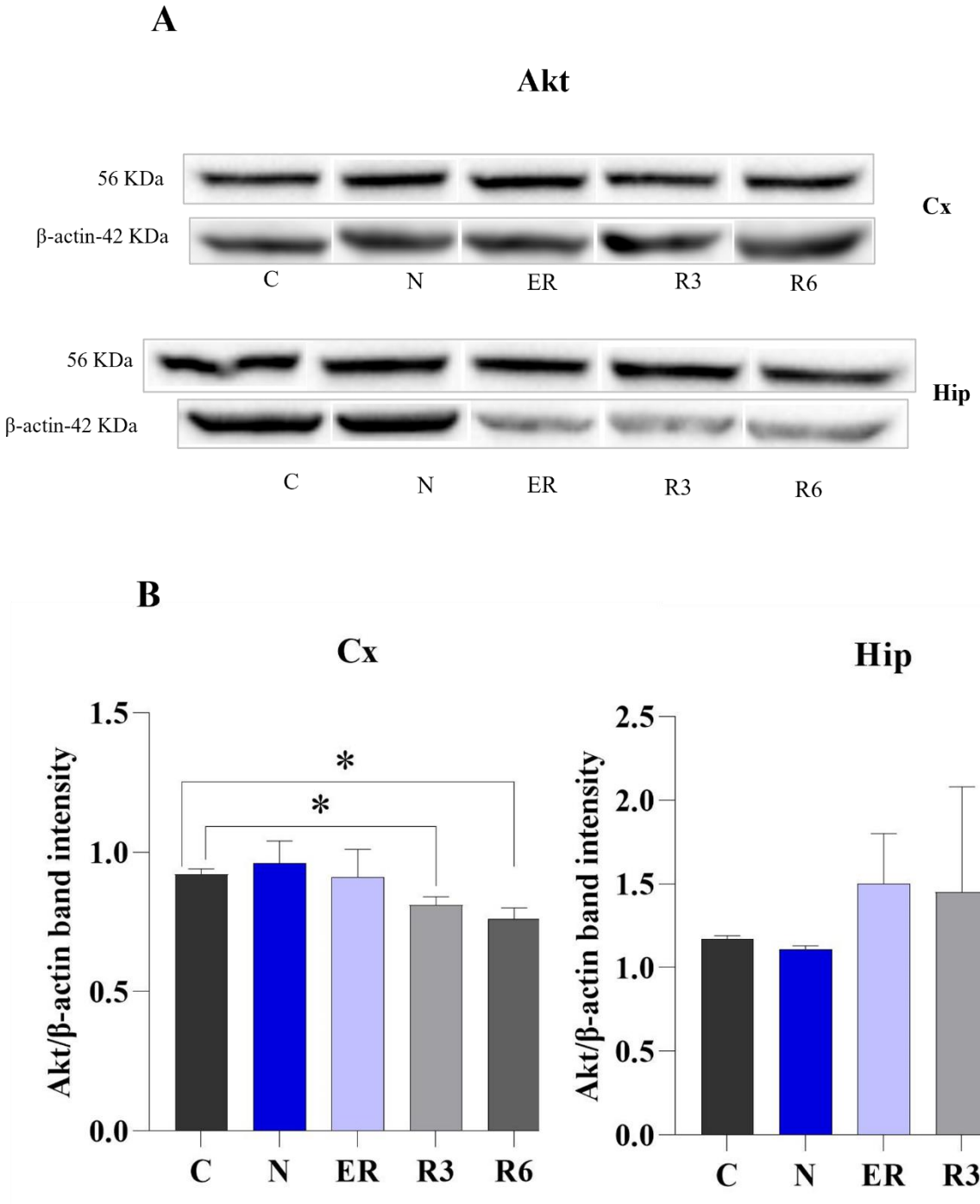
A
Akt
56 KDa
β-actin-42 KDa
Cx
C
N
ER
R3
R6
56 KDa
β-actin-42 KDa
Hip
C
N
ER
R3
R6
B
Cx
Akt/β-actin band intensity
1.5
1.0
0.5
0.0
*
*
C
N
ER
R3
R6
Hip
Akt/β-actin band intensity
2.5
2.0
1.5
1.0
0.5
0.0
C
N
ER
R3
R6

Figure 22. p(473)-Akt in brain extracts of cortex and hippocampus

Using the specific antibody Anti-Phospho-Akt, the levels of the diverse isoforms Akt 1/2/3 phosphorylated on Ser473 residues was analyzed by WB in brain extracts of cortex (Cx, n=3) and hippocampus (Hip, n=3).

Fig.22 **A**) WB analysis of one representative sample for each experimental group.

Fig.22 **B**) Mean values ± SEM of normalized p(473)-Akt expression calculated as the ratio between band intensities of p(473)-Akt with the corresponding β-actin band in each experimental condition

Experimental groups: Normothermic control rats (C); Hypothermic rats at lowest temperature (Nadir, N); Rats during the arousal from ST, Thy35,5°C (Early Recovery, ER); Normothermic rats after 3 hours after the arousal from ST (Recovery after 3 hours, R3); Normothermic rats after 6 hours after the arousal from ST (Recovery after 6 h, R6).

*: significant comparisons ($p<0.05$).

Western Blot (WB); Cortex (Cx); Hippocampus (Hip); SEM (Standard error of the mean); Synthetic torpor (ST); Hypothalamic temperature (Thy).

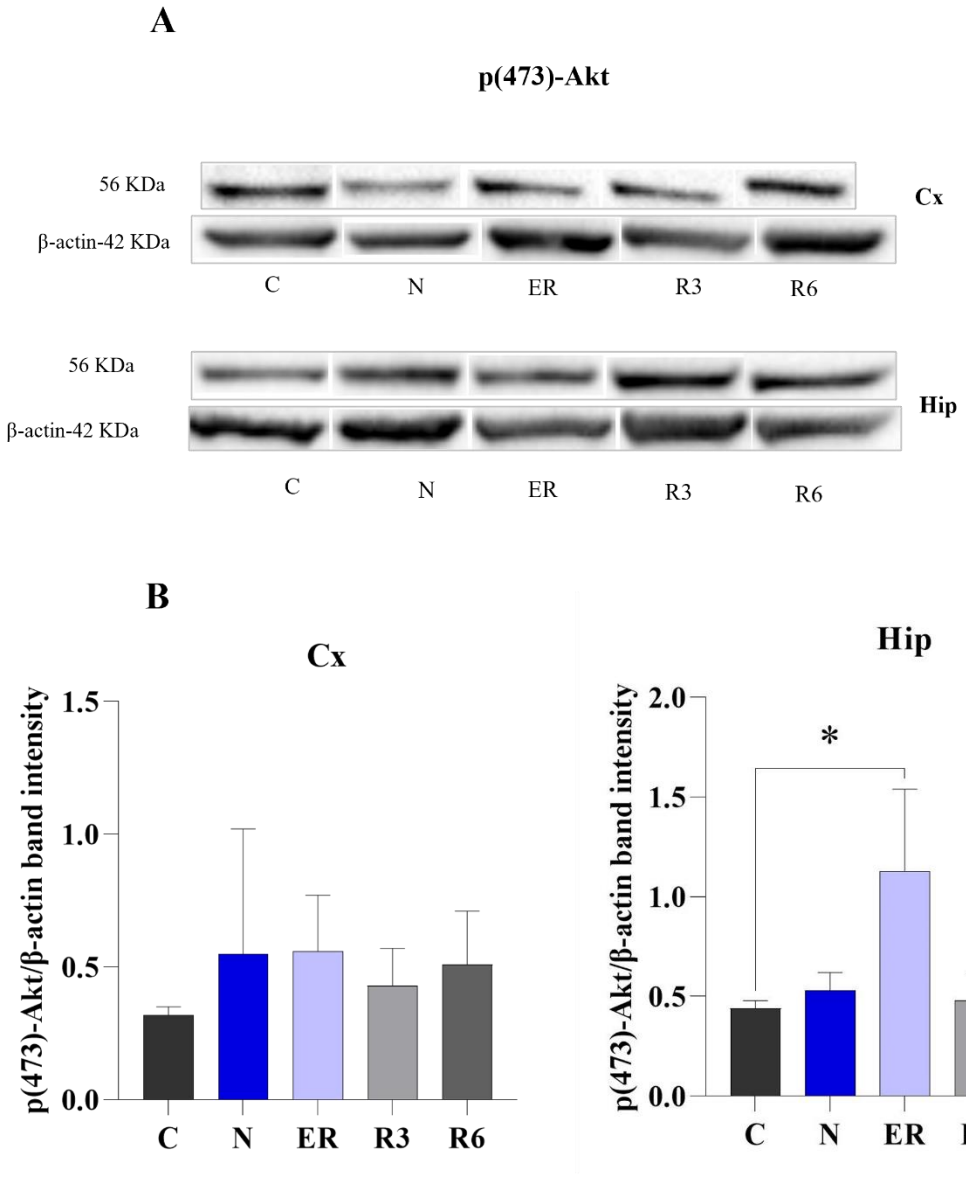
A
p(473)-Akt
56 KDa
β-actin-42 KDa
Cx
C
N
ER
R3
R6
56 KDa
β-actin-42 KDa
Hip
C
N
ER
R3
R6
B
Cx
p(473)-Akt/β-actin band intensity
1.5
1.0
0.5
0.0
C
N
ER
R3
R6
Hip
p(473)-Akt/β-actin band intensity
2.0
1.5
1.0
0.5
0.0
*
C
N
ER
R3
R6

Figure 23. GRP78 in brain extracts of cortex and hippocampus

Using the specific antibody Anti-Glucose regulating protein 78, the levels of GRP78 was analyzed by WB in brain extracts of cortex (Cx, n=3) and hippocampus (Hip, n=3).

Fig.23 **A**) WB analysis of one representative sample for each experimental group.

Fig.23 **B**) Mean values ± SEM of normalized GRP78 expression calculated as the ratio between band intensities of GRP78 with the corresponding β-actin band in each experimental condition. Experimental groups: Normothermic control rats (C); Hypothermic rats at lowest temperature (Nadir, N); Rats during the arousal from ST, Thy35,5°C (Early Recovery, ER); Normothermic rats after 3 hours after the arousal from ST (Recovery after 3 hours, R3); Normothermic rats after 6 hours after the arousal from ST (Recovery after 6 h, R6).

*: significant comparisons ($p<0.05$).

Western Blot (WB); Cortex (Cx); Hippocampus (Hip); SEM (Standard error of the mean); Synthetic torpor (ST); Hypothalamic temperature (Thy).

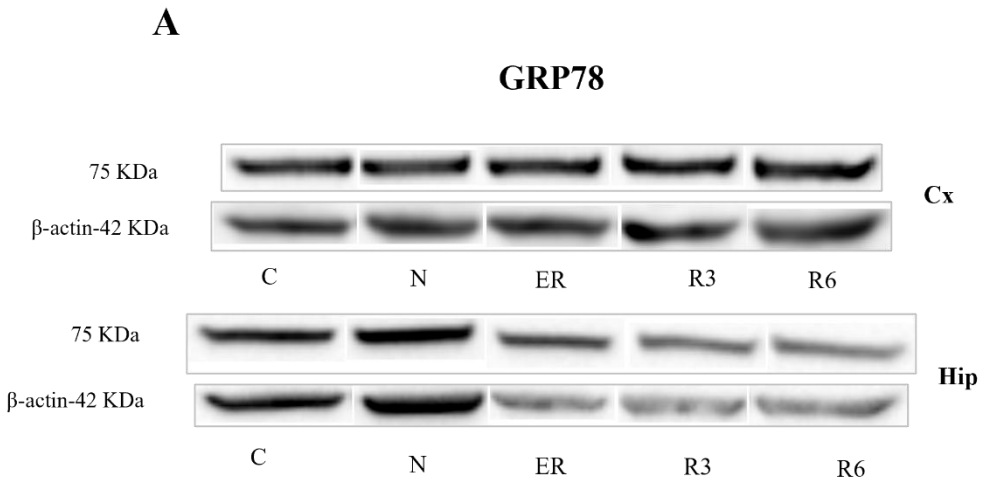
A
GRP78
75 KDa
β-actin-42 KDa
Cx
C
N
ER
R3
R6
75 KDa
β-actin-42 KDa
Hip
C
N
ER
R3
R6

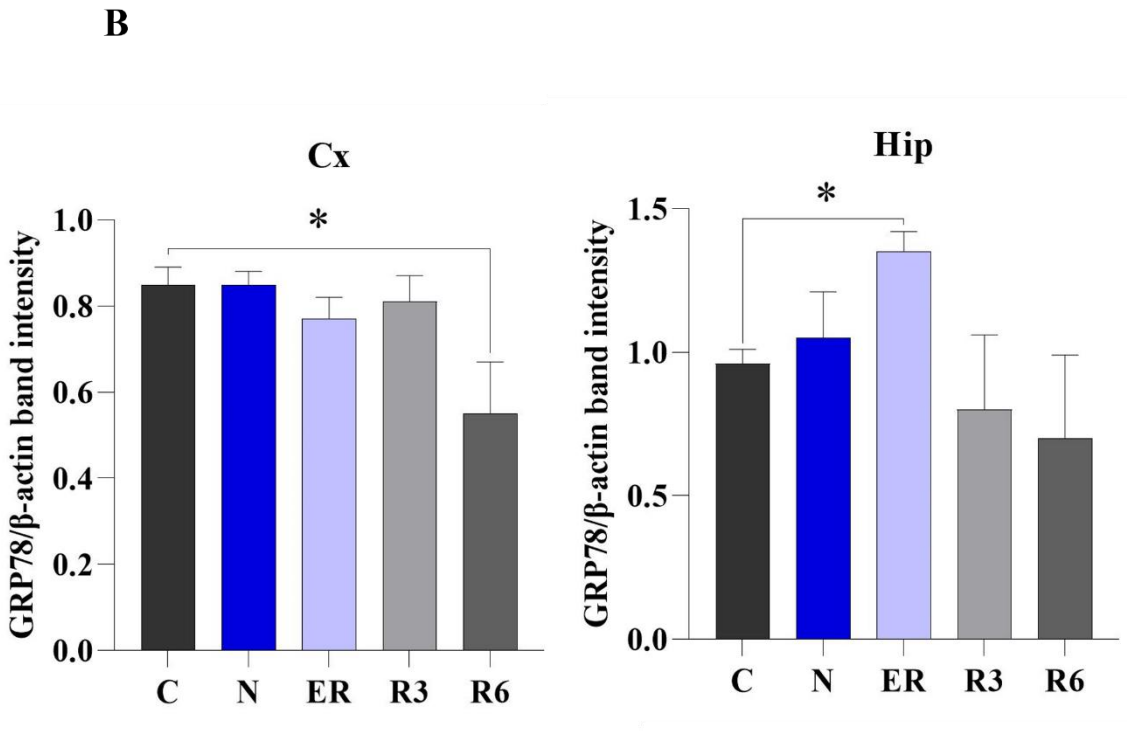
B
Cx
GRP78/β-actin band intensity
1.0
0.8
0.6
0.4
0.2
0.0
*
C
N
ER
R3
R6
Hip
GRP78/β-actin band intensity
1.5
1.0
0.5
0.0
*
C
N
ER
R3
R6

Figure 24. Xiap in brain extracts of cortex and hippocampus

Using the specific antibody Anti-X chromosome-linked inhibitor of apoptosis, the levels of Xiap was analyzed by WB in brain extracts of cortex (Cx, n=3) and hippocampus (Hip, n=3). ***Fig.24*** **A**) WB analysis of one representative sample for each experimental group.

Fig.24 **B**) Mean values ± SEM of normalized Xiap expression calculated as the ratio between band intensities of Xiap with the corresponding β-actin band in each experimental condition.

Experimental groups: Normothermic control rats (C); Hypothermic rats at lowest temperature (Nadir, N); Rats during the arousal from ST, Thy35,5°C (Early Recovery, ER); Normothermic rats after 3 hours after the arousal from ST (Recovery after 3 hours, R3); Normothermic rats after 6 hours after the arousal from ST (Recovery after 6 h, R6).

*: significant comparisons ($p<0.05$).

Western Blot (WB); Cortex (Cx); Hippocampus (Hip); SEM (Standard error of the mean); Synthetic torpor (ST); Hypothalamic temperature (Thy).

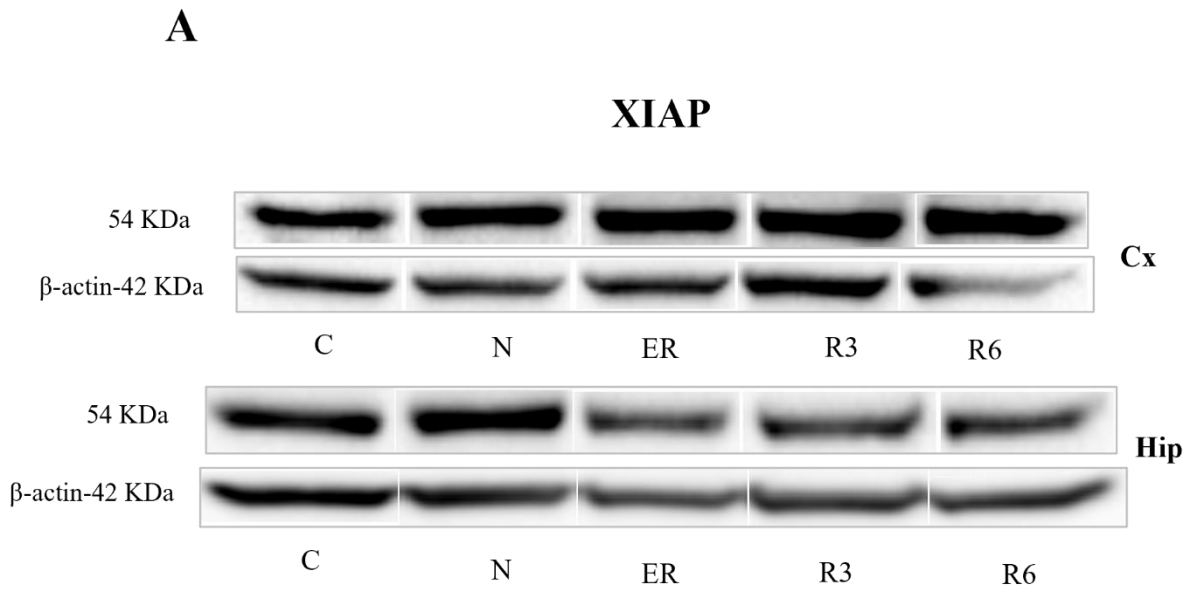
A
XIAP
54 KDa
β-actin-42 KDa
Cx
C
N
ER
R3
R6
54 KDa
β-actin-42 KDa
Hip
C
N
ER
R3
R6

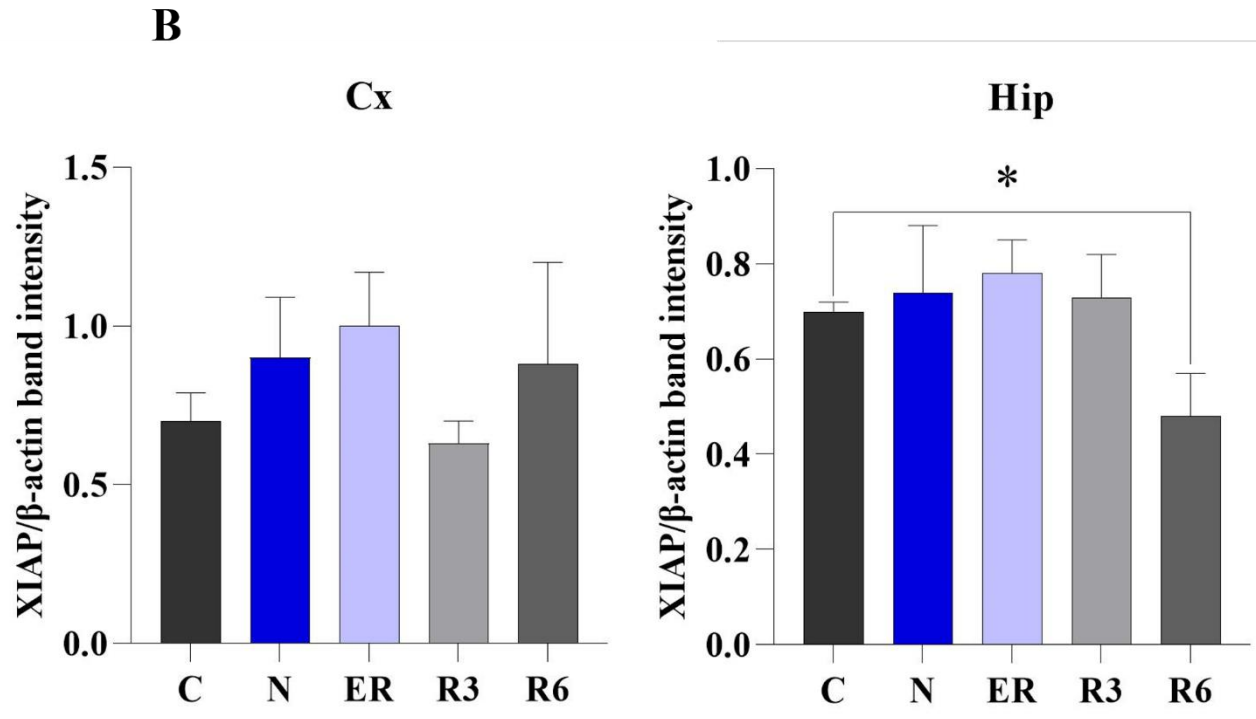
B
Cx
XIAP/β-actin band intensity
1.5
1.0
0.5
0.0
C
N
ER
R3
R6
Hip
XIAP/β-actin band intensity
*
1.0
0.8
0.6
0.4
0.2
0.0
C
N
ER
R3
R6

Figure 25. PP2A in brain extracts of cortex and hippocampus

Using the specific antibody Anti-Protein phosphatase 2, the levels of PP2A was analyzed by WB in brain extracts of cortex (Cx, n=3) and hippocampus (Hip, n=3).

***Fig.25* A**) WB analysis of one representative sample for each experimental group.

***Fig.25* B**) Mean values ± SEM of normalized PP2A expression calculated as the ratio between band intensities of PP2A with the corresponding β-actin band in each experimental condition.

Experimental groups: Normothermic control rats (C); Hypothermic rats at lowest temperature (Nadir, N); Rats during the arousal from ST, Thy35,5°C (Early Recovery, ER); Normothermic rats after 3 hours after the arousal from ST (Recovery after 3 hours, R3); Normothermic rats after 6 hours after the arousal from ST (Recovery after 6 h, R6).

*: significant comparisons ($p<0.05$).

Western Blot (WB); Cortex (Cx); Hippocampus (Hip); SEM (Standard error of the mean); Synthetic torpor (ST); Hypothalamic temperature (Thy).

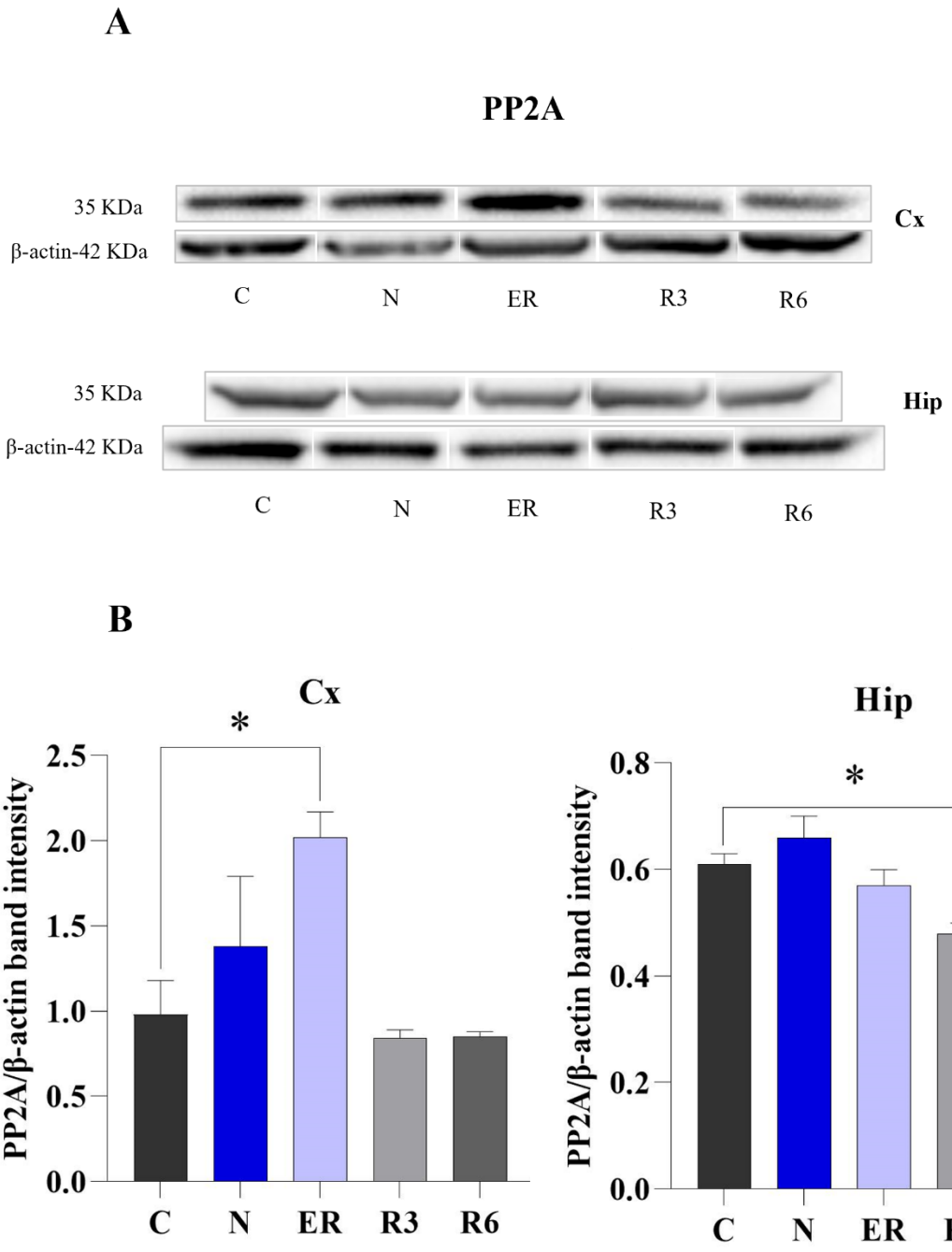
A
PP2A
35 KDa
β-actin-42 KDa
Cx
C
N
ER
R3
R6
35 KDa
β-actin-42 KDa
Hip
C
N
ER
R3
R6
B
Cx
*
PP2A/β-actin band intensity
2.5
2.0
1.5
1.0
0.5
0.0
C
N
ER
R3
R6
Hip
*
PP2A/β-actin band intensity
0.8
0.6
0.4
0.2
0.0
C
N
ER
R3
R6

Figure 26. Cleaved-caspase 3 in brain extracts of cortex and hippocampus

Using the specific antibody Anti-Cleaved-Caspase 3, the levels of caspase 3 cleaved on Asp175 residue was analyzed by WB in brain extracts of cortex (Cx, n=3) and hippocampus (Hip, n=3).

Fig.26 **A**) WB analysis of one representative sample for each experimental group.

Fig.26 **B**) Mean values ± SEM of normalized Cleaved-caspase 3 expression calculated as the ratio between band intensities of Cleaved-caspase 3 with the corresponding β-actin band in each experimental condition.

Experimental groups: Normothermic control rats (C); Hypothermic rats at lowest temperature (Nadir, N); Rats during the arousal from ST, Thy35,5°C (Early Recovery, ER); Normothermic rats after 3 hours after the arousal from ST (Recovery after 3 hours, R3); Normothermic rats after 6 hours after the arousal from ST (Recovery after 6 h, R6).

*: significant comparisons ($p<0.05$).

Western Blot (WB); Cortex (Cx); Hippocampus (Hip); SEM (Standard error of the mean); Synthetic torpor (ST); Hypothalamic temperature (Thy).

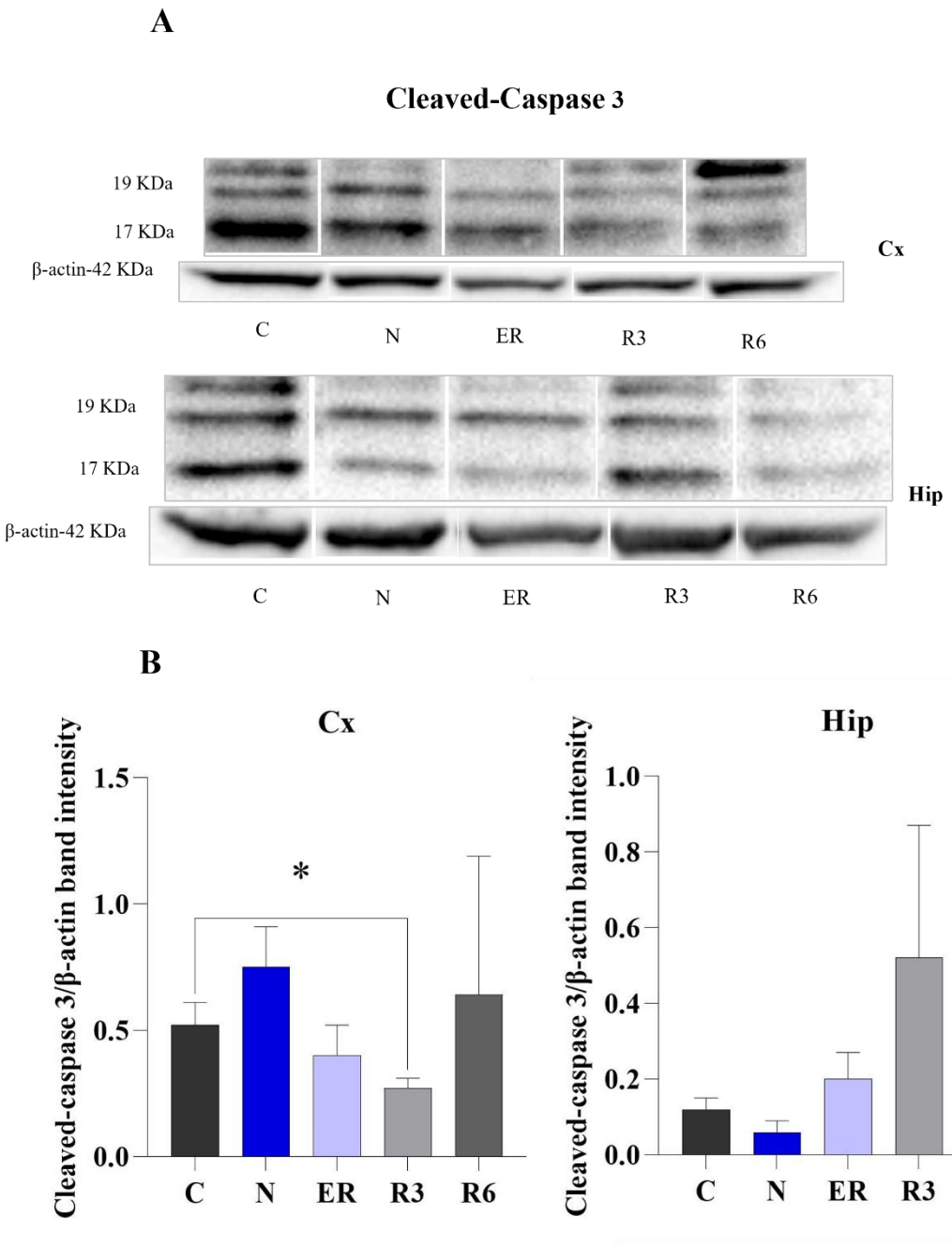
A
Cleaved-Caspase 3
19 KDa
17 KDa
β-actin-42 KDa
Cx
C
N
ER
R3
R6
19 KDa
17 KDa
β-actin-42 KDa
Hip
C
N
ER
R3
R6
B
Cx
Cleaved-caspase 3/β-actin band intensity
1.5
1.0
0.5
0.0
*
C
N
ER
R3
R6
Hip
Cleaved-caspase 3/β-actin band intensity
1.0
0.8
0.6
0.4
0.2
0.0
C
N
ER
R3
R6

Figure 27. Plasma concentration of melatonin, dopamine, adrenaline, noradrenaline, corticosterone, cortisol

***Fig.27* A**) Mean values ± SEM of melatonin plasma concentration in each experimental group.

***Fig.27* B**) Mean values ± SEM of dopamine plasma concentration in each experimental group.

***Fig.27* C**) Mean values ± SEM of adrenaline plasma concentration in each experimental group.

***Fig.27* D**) Mean values ± SEM of noradrenaline plasma concentration in each experimental group.

***Fig.27* E**) Mean values ± SEM of corticosterone plasma concentration in each experimental group.

***Fig.27* F**) Mean values ± SEM of cortisol plasma concentration in each experimental group.

Experimental groups: Normothermic control rats (C); Hypothermic rats at lowest temperature (Nadir, N); Rats during the arousal from ST, Thy35,5°C (Early Recovery, ER); Normothermic rats after 3 hours after the arousal from ST (Recovery after 3 hours, R3); Normothermic rats after 6 hours after the arousal from ST (Recovery after 6 h, R6).

*: significant comparisons ($p<0.05$).

SEM (Standard error of the mean); Synthetic torpor (ST); Hypothalamic temperature (Thy).

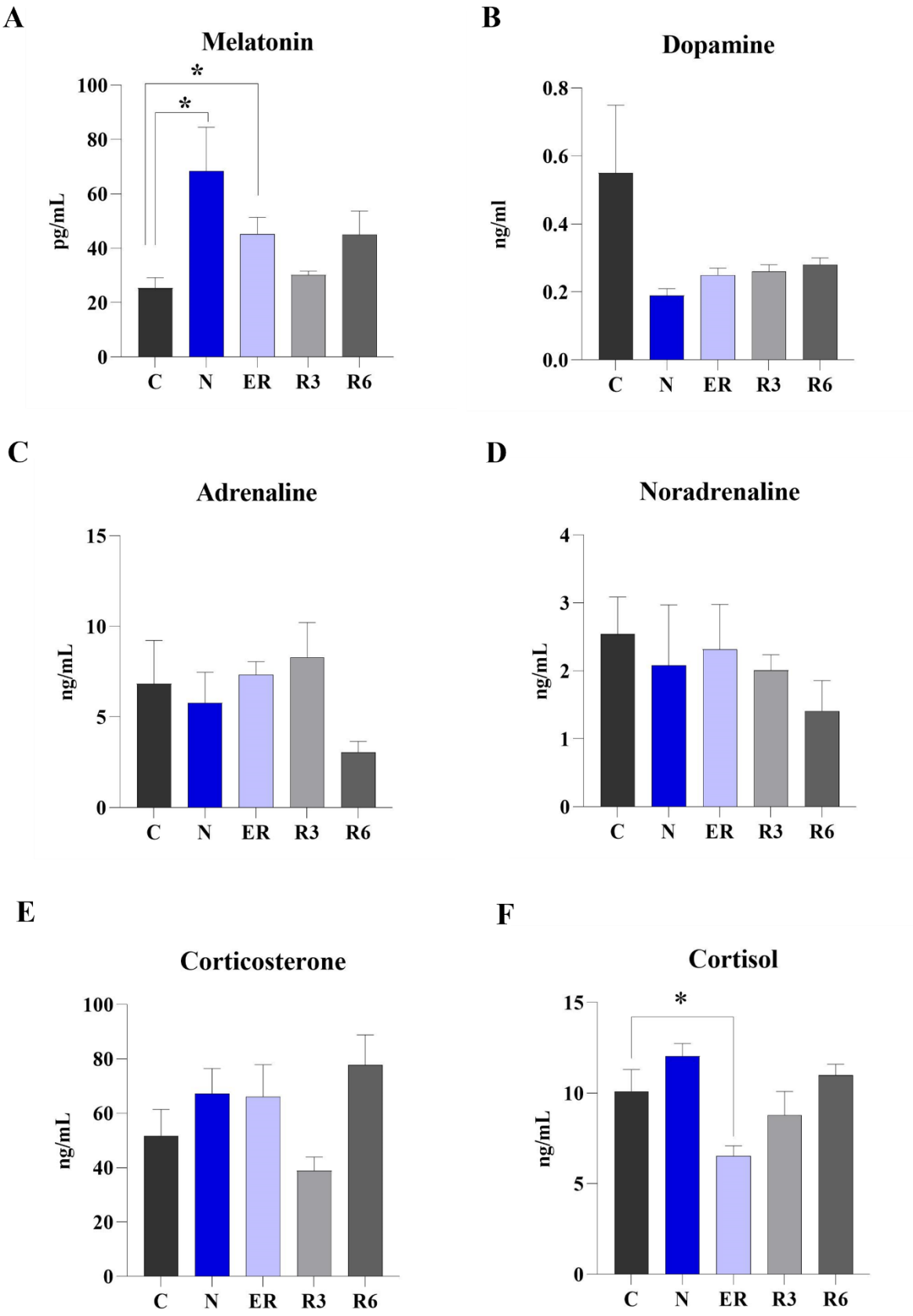
A
Melatonin
pg/mL
100
80
60
40
20
0
*
*
C
N
ER
R3
R6
B
Dopamine
ng/ml
0.8
0.6
0.4
0.2
0.0
C
N
ER
R3
R6
C
Adrenaline
ng/mL
15
10
5
0
C
N
ER
R3
R6
D
Noradrenaline
ng/mL
4
3
2
1
0
C
N
ER
R3
R6
E
Corticosterone
ng/mL
100
80
60
40
20
0
C
N
ER
R3
R6
F
Cortisol
ng/mL
15
10
5
0
*
C
N
ER
R3
R6

Table 3. Study of the role of sleep in the dephosphorylation process of Tau during the recovery from synthetic torpor: hypothalamic temperature

Average Thy levels (°C, mean ± SEM) in the 1-h period which preceded the sacrifice of the animals are shown. Experimental groups: Normothermic rats after 3 hours after the arousal from ST, rats allowed to sleep (Recovery after 3 hours, R3); Normothermic rats after 3 hours after the arousal from ST, sleep deprived rats (Recovery after 3 hours, R3SD); Normothermic rats after 6 hours after the arousal from ST, rats allowed to sleep (Recovery after 6 h, R6); Normothermic rats after 6 hours after the arousal from ST, sleep deprived rats (Recovery after 6 h, R6SD). For all groups, n=3, except for R6, n=2 due to a thermistor's damage in one rat.

Hypothalamic temperature (Thy); Synthetic torpor (ST); Normal sleep (NS); Sleep deprivation (SD); SEM (Standard error of the mean).

	MEAN	SEM
R3	38.59	0.06
R3SD	39.04	0.26
R6	37.66	1.54
R6SD	37.63	0.80

Figure 28. Total Tau in brain extracts of cortex and hippocampus

Using the specific antibody Anti-Total Tau, the levels of several isoforms of tau protein between 50-70 KDa were analyzed by WB in brain extracts of cortex (Cx, n=3) and hippocampus (Hip, n=3).

Fig.28 **A**) WB analysis of one representative sample for each experimental group.

Fig.28 **B**) Mean values ± SEM of normalized Total Tau expression calculated as the ratio between band intensities of Total tau with the corresponding β-actin band in NS and SD experimental group (n=6 per group).

Fig.28 **C**) Mean values ± SEM of normalized Total Tau expression calculated as the ratio between band intensities of Total Tau with the corresponding β-actin band in each experimental group.

Experimental groups: Normothermic rats allowed to sleep during 3 hours after the arousal from ST, (Recovery after 3 hours, R3); Normothermic rats sleep deprive during 3 hours after the arousal from ST (R3SD); Normothermic rats after 6 hours from the arousal from ST (Recovery after 6 h, R6); Normothermic rats sleep deprive during 6 hours after the arousal from ST (R6SD).

*: significant comparisons ($p<0.05$).

Western Blot (WB); Cortex (Cx); Hippocampus (Hip); SEM (Standard error of the mean); Normal sleep (NS); Sleep deprived (SD); Synthetic torpor (ST).

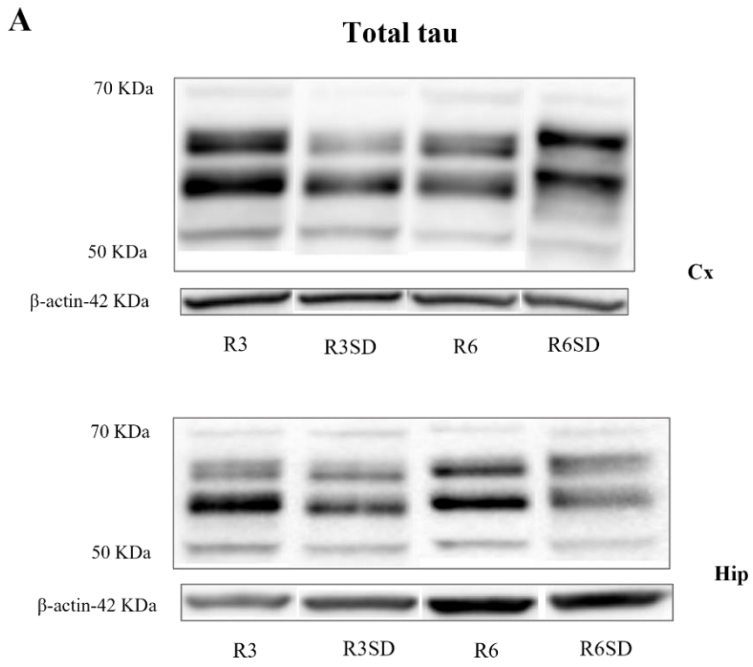
A
Total tau
70 KDa
50 KDa
β-actin-42 KDa
Cx
R3
R3SD
R6
R6SD
70 KDa
50 KDa
β-actin-42 KDa
Hip
R3
R3SD
R6
R6SD

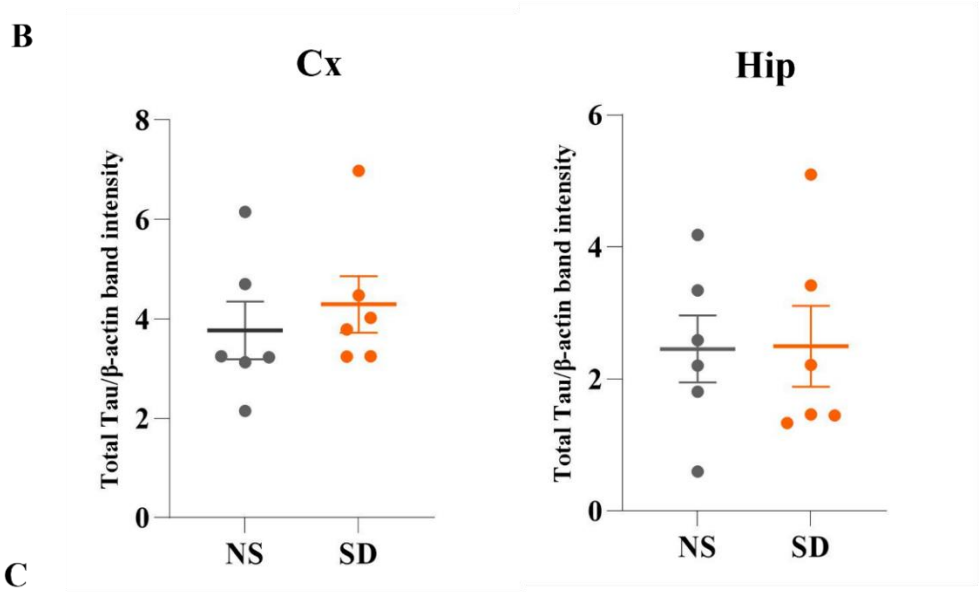
B
Cx
Total Tau/β-actin band intensity
0
2
4
6
8
NS
SD
Hip
Total Tau/β-actin band intensity
0
2
4
6
NS
SD

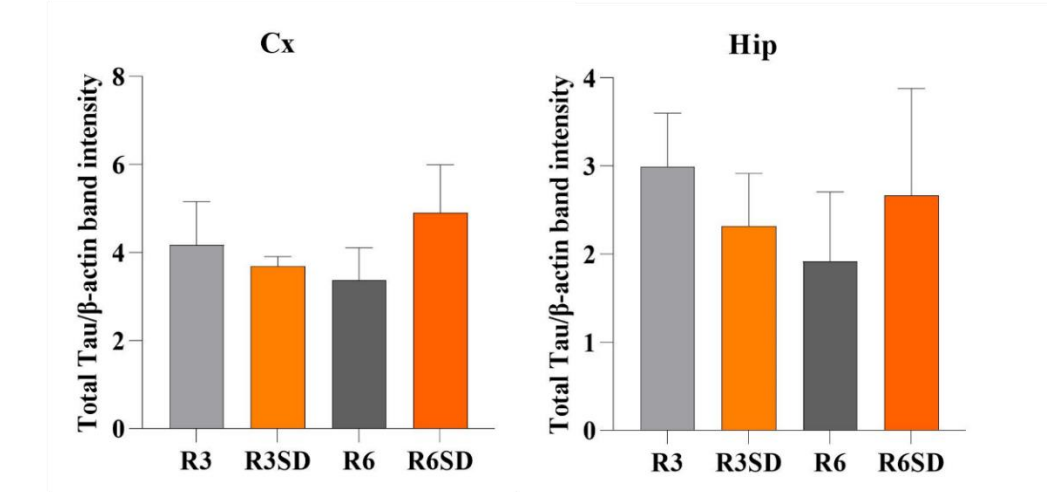
C
Cx
Total Tau/β-actin band intensity
0
2
4
6
8
R3
R3SD
R6
R6SD
Hip
Total Tau/β-actin band intensity
0
1
2
3
4
R3
R3SD
R6
R6SD

Figure 29. AT8 in brain extracts of cortex and hippocampus

Using the specific antibody AT8, the levels of phosphorylated tau protein on Ser202 or Thr205 residues was analyzed by WB in brain extracts of cortex (Cx, n=3) and hippocampus (Hip, n=3).

Fig.29 **A**) WB analysis of one representative sample for each experimental group.

Fig.29 **B**) Mean values ± SEM of normalized AT8 expression calculated as the ratio between band intensities of AT8 with the corresponding β-actin band in NS and SD experimental group (n=6 per group).

Fig.29 **C**) Mean values ± SEM of normalized AT8 expression calculated as the ratio between band intensities of AT8 with the corresponding β-actin band in each experimental group.

Experimental groups: Normothermic rats allowed to sleep during 3 hours after the arousal from ST, (Recovery after 3 hours, R3); Normothermic rats sleep deprive during 3 hours after the arousal from ST (R3SD); Normothermic rats after 6 hours from the arousal from ST (Recovery after 6 h, R6); Normothermic rats sleep deprive during 6 hours after the arousal from ST (R6SD).

*: significant comparisons ($p<0.05$).

Western Blot (WB); Cortex (Cx); Hippocampus (Hip); SEM (Standard error of the mean); Normal sleep (NS); Sleep deprived (SD); Synthetic torpor (ST).

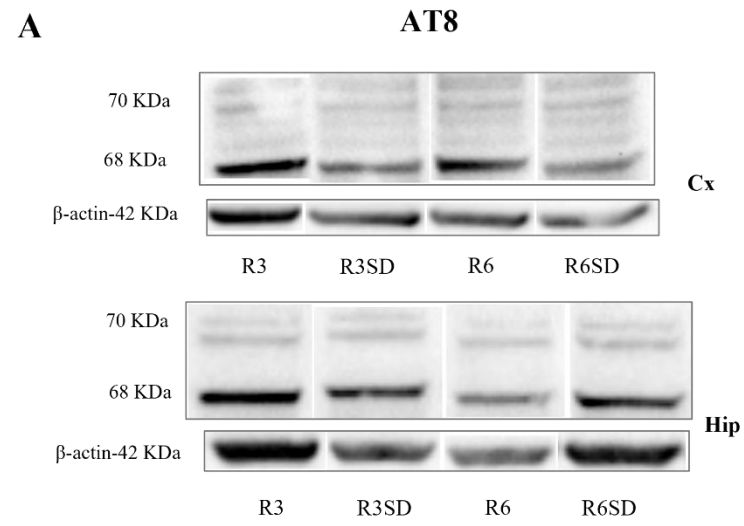
A
AT8
70 KDa
68 KDa
β-actin-42 KDa
Cx
R3
R3SD
R6
R6SD
70 KDa
68 KDa
β-actin-42 KDa
Hip
R3
R3SD
R6
R6SD

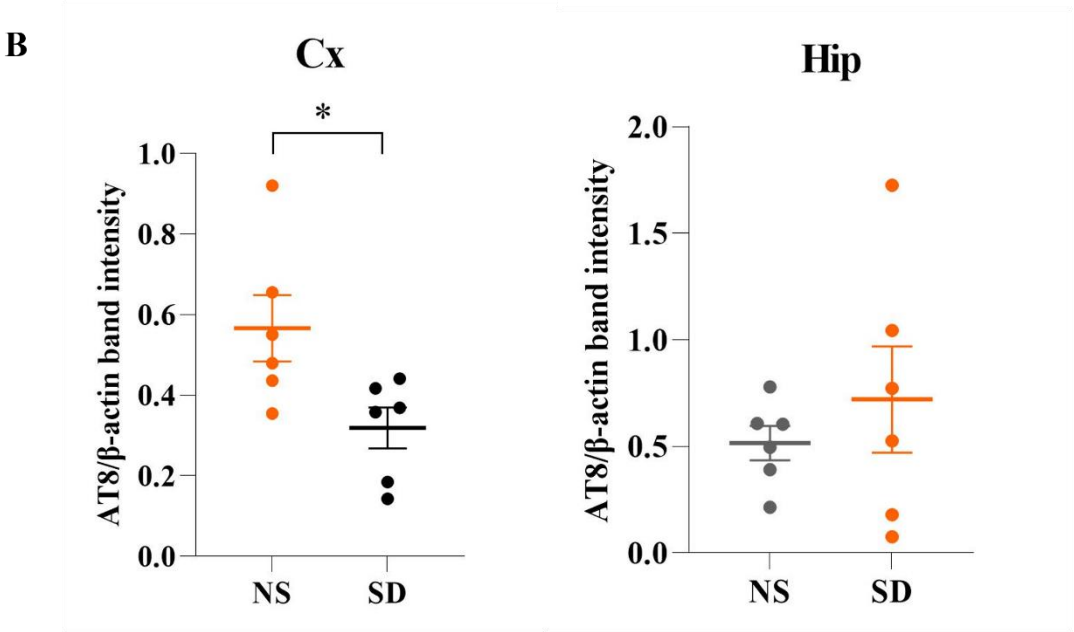
B
Cx
*
AT8/β-actin band intensity
1.0
0.8
0.6
0.4
0.2
0.0
NS
SD
Hip
2.0
1.5
1.0
0.5
0.0
NS
SD

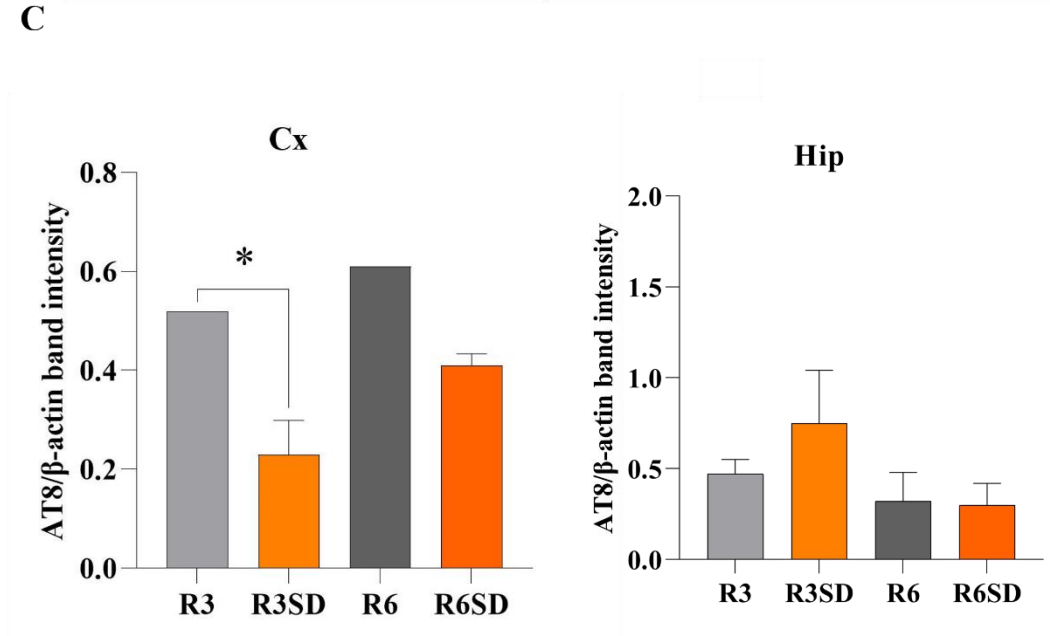
C
Cx
*
AT8/β-actin band intensity
0.8
0.6
0.4
0.2
0.0
R3
R3SD
R6
R6SD
Hip
2.0
1.5
1.0
0.5
0.0
R3
R3SD
R6
R6SD

Figure 30. Tau-1 in brain extracts of cortex and hippocampus

Using the specific antibody Anti-Tau-1, the levels of dephosphorylated tau protein on 189-207 residues was analyzed by WB in brain extracts of cortex (Cx, n=3) and hippocampus (Hip, n=3).

Fig.30 **A**) WB analysis of one representative sample for each experimental group.

Fig.30 **B**) Mean values ± SEM of normalized Tau-1 expression calculated as the ratio between band intensities of Tau-1 with the corresponding β-actin band in NS and SD experimental group (n=6 per group).

Fig.30 **C**) Mean values ± SEM of normalized Tau-1 expression calculated as the ratio between band intensities of Tau-1 with the corresponding β-actin band in each experimental group.

Experimental groups: Normothermic rats allowed to sleep during 3 hours after the arousal from ST, (Recovery after 3 hours, R3); Normothermic rats sleep deprive during 3 hours after the arousal from ST (R3SD); Normothermic rats after 6 hours from the arousal from ST (Recovery after 6 h, R6); Normothermic rats sleep deprive during 6 hours after the arousal from ST (R6SD).

*: significant comparisons ($p<0.05$).

Western Blot (WB); Cortex (Cx); Hippocampus (Hip); SEM (Standard error of the mean); Normal sleep (NS); Sleep deprived (SD); Synthetic torpor (ST).

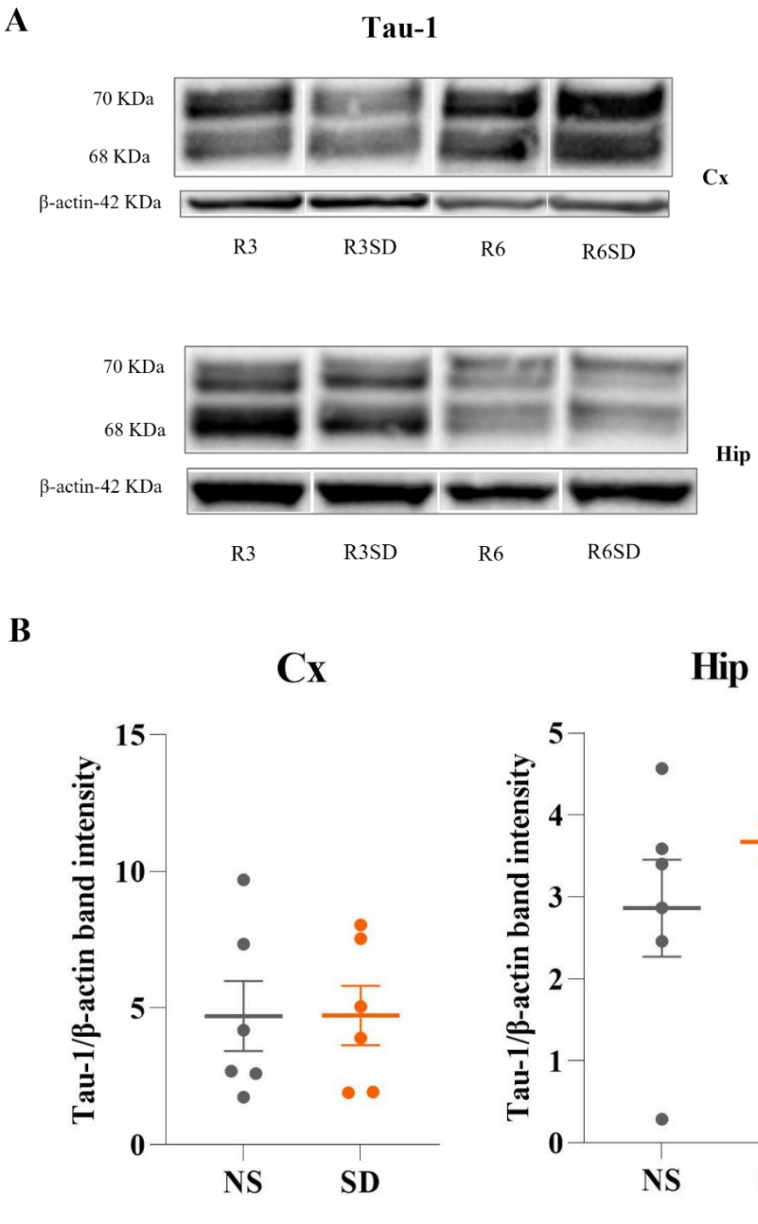
A
Tau-1
70 KDa
68 KDa
β-actin-42 KDa
Cx
R3
R3SD
R6
R6SD
70 KDa
68 KDa
β-actin-42 KDa
Hip
R3
R3SD
R6
R6SD
B
Cx
Hip
Tau-1/β-actin band intensity
15
10
5
0
NS
SD
Tau-1/β-actin band intensity
5
4
3
2
1
0
NS
SD
C
Cx
Hip
Tau-1/β-actin band intensity
8
6
4
2
0
R3
R3SD
R6
R6SD
Tau-1/β-actin band intensity
5
4
3
2
1
0
R3
R3SD
R6
R6SD

Figure 31. p(205)-Tau in brain extracts of cortex and hippocampus

Using the specific antibody Anti-Phospho-Tau (Thr205), the levels of phosphorylated tau protein on Thr205 residues was analyzed by Western Blot (WB) in brain extracts of cortex (Cx, n=3) and hippocampus (Hip, n=3).

Fig.31 **A**) WB analysis of one representative sample for each experimental group.

Fig.31 **B**) Mean values ± SEM of normalized p(205)-Tau expression calculated as the ratio between band intensities of p(205)-Tau with the corresponding β-actin band in NS and SD experimental group (n=6 per group).

Fig.31 **C**) Mean values ± SEM of normalized p(205)-Tau expression calculated as the ratio between band intensities of p(205)-Tau with the corresponding β-actin band in each experimental group.

Experimental groups: Normothermic rats allowed to sleep during 3 hours after the arousal from ST, (Recovery after 3 hours, R3); Normothermic rats sleep deprive during 3 hours after the arousal from ST (R3SD); Normothermic rats after 6 hours from the arousal from ST (Recovery after 6 h, R6); Normothermic rats sleep deprive during 6 hours after the arousal from ST (R6SD).

*: significant comparisons ($p<0.05$).

Western Blot (WB); Cortex (Cx); Hippocampus (Hip); SEM (Standard error of the mean); Normal sleep (NS); Sleep deprived (SD); Synthetic torpor (ST).

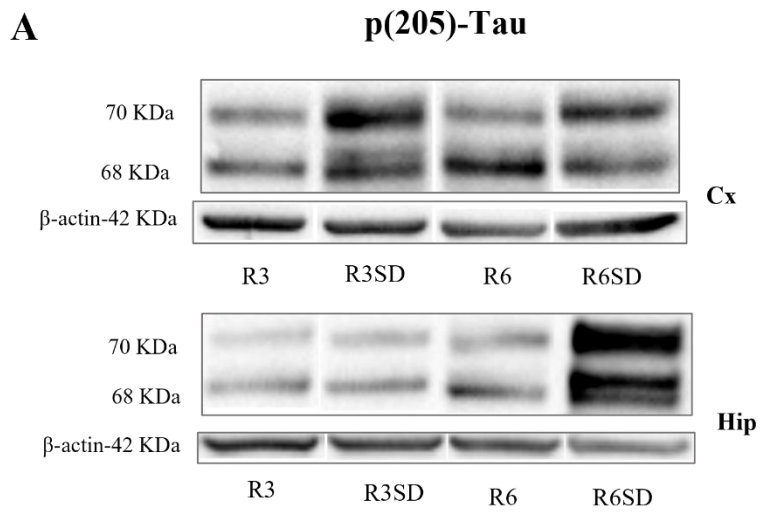
A
p(205)-Tau
70 KDa
68 KDa
β-actin-42 KDa
Cx
R3
R3SD
R6
R6SD
70 KDa
68 KDa
β-actin-42 KDa
Hip
R3
R3SD
R6
R6SD

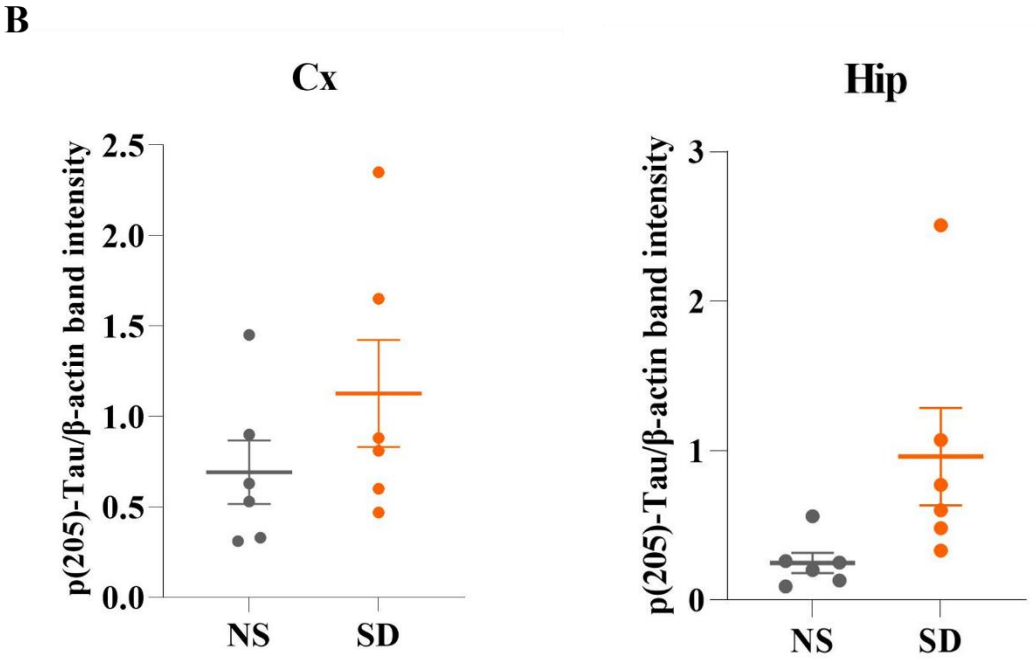
B
Cx
p(205)-Tau/β-actin band intensity
2.5
2.0
1.5
1.0
0.5
0.0
NS
SD
Hip
p(205)-Tau/β-actin band intensity
3
2
1
0
NS
SD

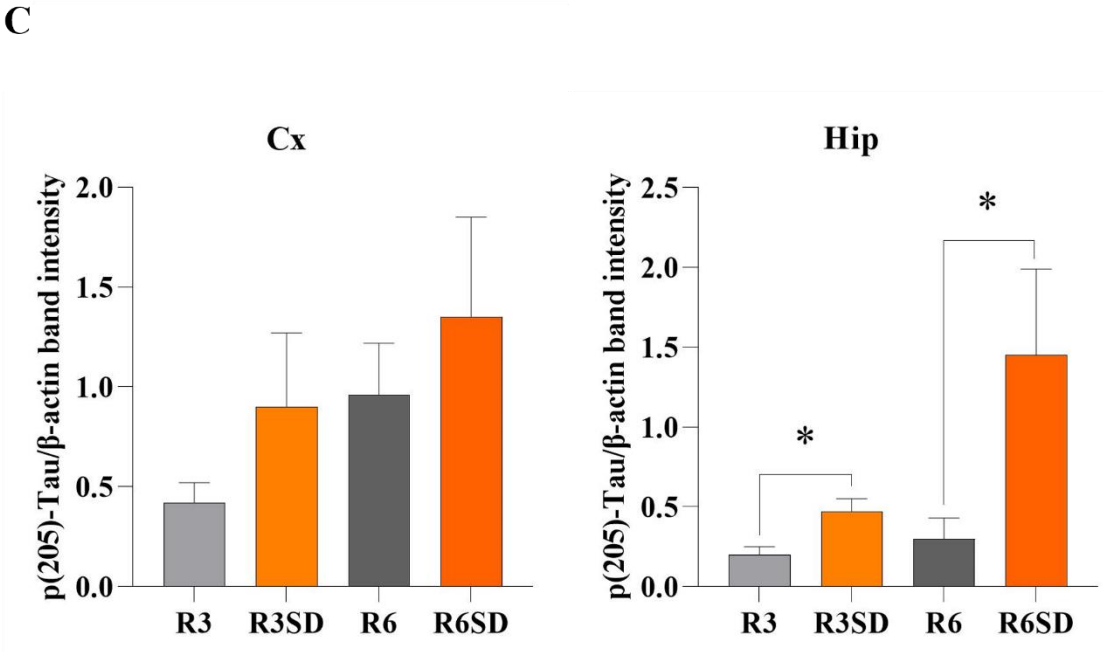
C
Cx
p(205)-Tau/β-actin band intensity
2.0
1.5
1.0
0.5
0.0
R3
R3SD
R6
R6SD
Hip
p(205)-Tau/β-actin band intensity
2.5
2.0
1.5
1.0
0.5
0.0
*
*
R3
R3SD
R6
R6SD

Figure 32. Gsk3-β in brain extracts of cortex and hippocampus

Using the specific antibody Anti-Gsk3-β, the levels of Gsk3-β was analyzed by WB in brain extracts of cortex (Cx, n=3) and hippocampus (Hip, n=3).

Fig.32 **A**) WB analysis of one representative sample for each experimental group.

Fig.32 **B**) Mean values ± SEM of normalized Gsk3-β expression calculated as the ratio between band intensities of Gsk3-β with the corresponding β-actin band in NS and SD experimental group (n=6 per group).

Fig.32 **C**) Mean values ± SEM of normalized Gsk3-β expression calculated as the ratio between band intensities of Gsk3-β with the corresponding β-actin band in each experimental group.

Experimental groups: Normothermic rats allowed to sleep during 3 hours after the arousal from ST, (Recovery after 3 hours, R3); Normothermic rats sleep deprive during 3 hours after the arousal from ST (R3SD); Normothermic rats after 6 hours from the arousal from ST (Recovery after 6 h, R6); Normothermic rats sleep deprive during 6 hours after the arousal from ST (R6SD).

*: significant comparisons ($p<0.05$).

Western Blot (WB); Cortex (Cx); Hippocampus (Hip); SEM (Standard error of the mean); Normal sleep (NS); Sleep deprived (SD); Synthetic torpor (ST).

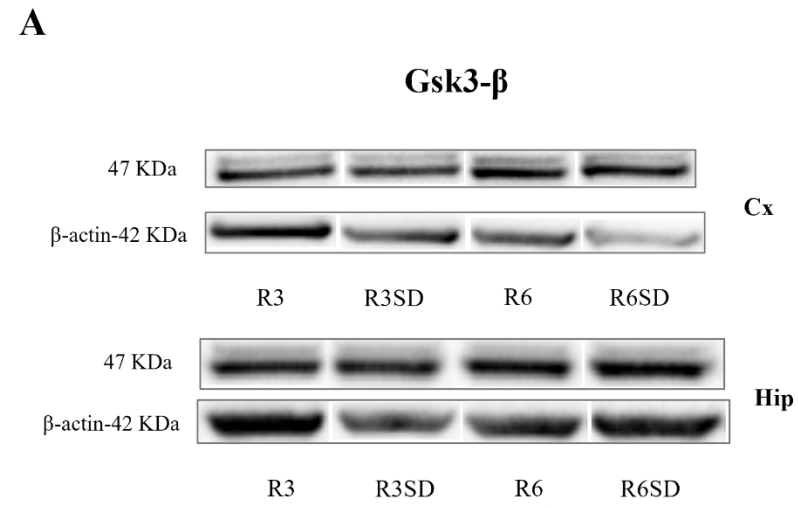
A
Gsk3-β
47 KDa
β-actin-42 KDa
Cx
R3
R3SD
R6
R6SD
47 KDa
β-actin-42 KDa
Hip
R3
R3SD
R6
R6SD

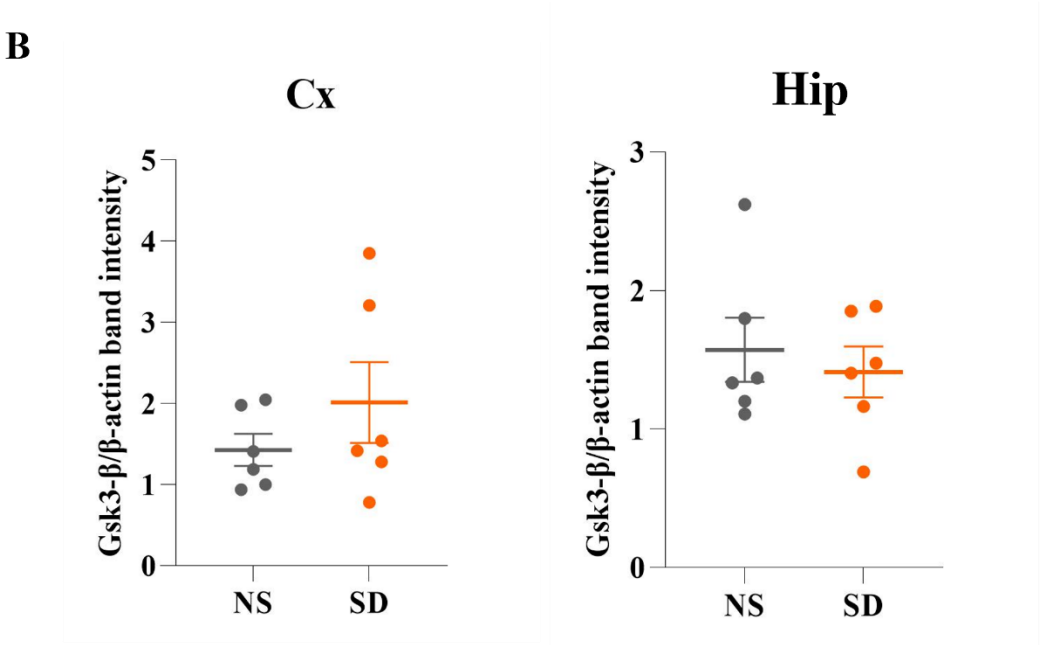
B
Cx
Gsk3-β/β-actin band intensity
0
1
2
3
4
5
NS
SD
Hip
Gsk3-β/β-actin band intensity
0
1
2
3
NS
SD

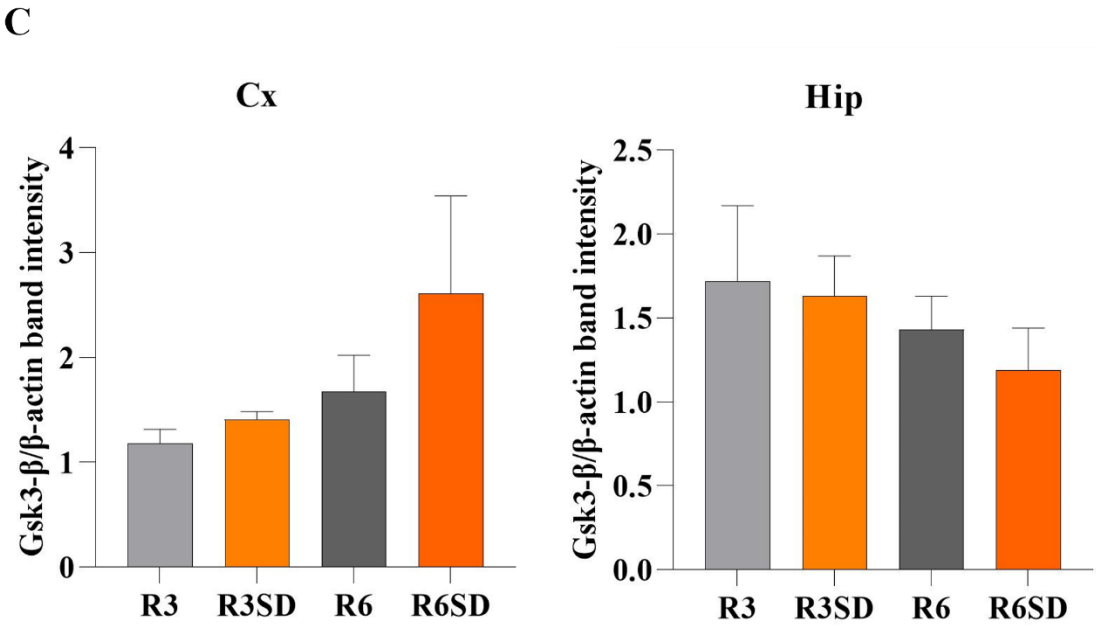
C
Cx
Gsk3-β/β-actin band intensity
0
1
2
3
4
R3
R3SD
R6
R6SD
Hip
Gsk3-β/β-actin band intensity
0.0
0.5
1.0
1.5
2.0
2.5
R3
R3SD
R6
R6SD

Figure 33. p(9)-Gsk3-β in brain extracts of cortex and hippocampus

Using the specific antibody Anti-Phospho-Gsk3-β, the levels of Gsk3-β phosphorylated on Ser9 residue was analyzed by WB in brain extracts of cortex (Cx, n=3) and hippocampus (Hip, n=3).

Fig.33 **A**) WB analysis of one representative sample for each experimental group.

Fig.33 **B**) Mean values ± SEM of normalized p(9)-Gsk3-β expression calculated as the ratio between band intensities of p(9)-Gsk3-β with the corresponding β-actin band in NS and SD experimental group (n=6 per group).

Fig.33 **C**) Mean values ± SEM of normalized p(9)-Gsk3-β expression calculated as the ratio between band intensities of p(9)-Gsk3-β with the corresponding β-actin band in each experimental group.

Experimental groups: Normothermic rats allowed to sleep during 3 hours after the arousal from ST, (Recovery after 3 hours, R3); Normothermic rats sleep deprive during 3 hours after the arousal from ST (R3SD); Normothermic rats after 6 hours from the arousal from ST (Recovery after 6 h, R6); Normothermic rats sleep deprive during 6 hours after the arousal from ST (R6SD).

*: significant comparisons ($p<0.05$).

Western Blot (WB); Cortex (Cx); Hippocampus (Hip); SEM (Standard error of the mean); Normal sleep (NS); Sleep deprived (SD); Synthetic torpor (ST).

A

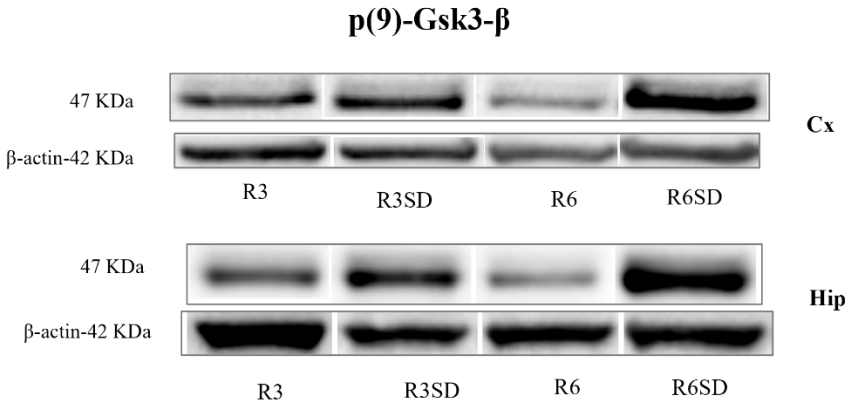
p(9)-Gsk3-β
47 KDa
β-actin-42 KDa
Cx
R3
R3SD
R6
R6SD
47 KDa
β-actin-42 KDa
Hip
R3
R3SD
R6
R6SD

B

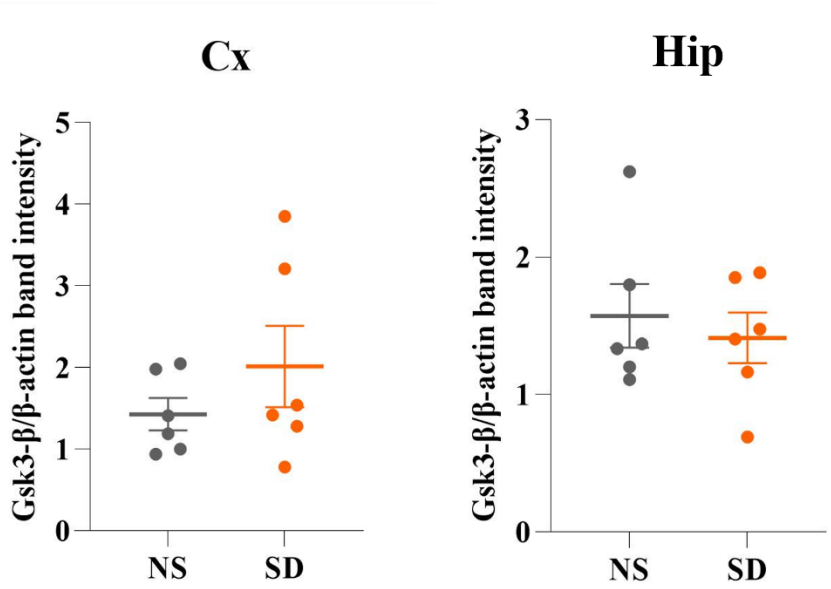
Cx
Hip
Gsk3-β/β-actin band intensity
0
1
2
3
4
5
NS
SD

C

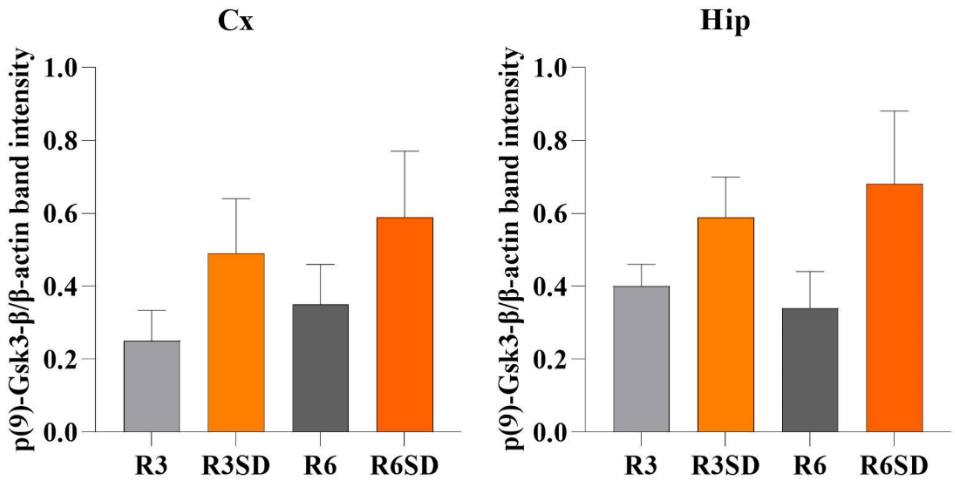
Cx
Hip
p(9)-Gsk3-β/β-actin band intensity
0.0
0.2
0.4
0.6
0.8
1.0
R3
R3SD
R6
R6SD

Figure 34. Akt in brain extracts of cortex and hippocampus

Using the specific antibody Anti-Akt, the levels of the diverse isoforms Akt 1/2/3 was analyzed by WB in brain extracts of cortex (Cx, n=3) and hippocampus (Hip, n=3).

Fig.34 **A**) WB analysis of one representative sample for each experimental group.

Fig.34 **B**) Mean values ± SEM of normalized Akt expression calculated as the ratio between band intensities of Akt with the corresponding β-actin band in NS and SD experimental group (n=6 per group).

Fig.34 **C**) Mean values ± SEM of normalized Akt expression calculated as the ratio between band intensities of Akt with the corresponding β-actin band in each experimental group.

Experimental groups: Normothermic rats allowed to sleep during 3 hours after the arousal from ST, (Recovery after 3 hours, R3); Normothermic rats sleep deprive during 3 hours after the arousal from ST (R3SD); Normothermic rats after 6 hours from the arousal from ST (Recovery after 6 h, R6); Normothermic rats sleep deprive during 6 hours after the arousal from ST (R6SD).

*: significant comparisons ($p<0.05$).

Western Blot (WB); Cortex (Cx); Hippocampus (Hip); SEM (Standard error of the mean); Normal sleep (NS); Sleep deprived (SD); Synthetic torpor (ST).

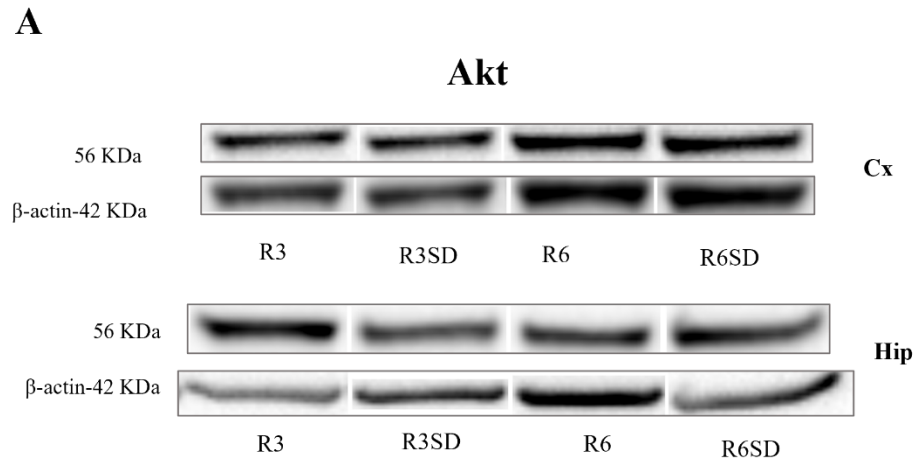
A
Akt
56 KDa
β-actin-42 KDa
Cx
R3
R3SD
R6
R6SD
56 KDa
β-actin-42 KDa
Hip
R3
R3SD
R6
R6SD

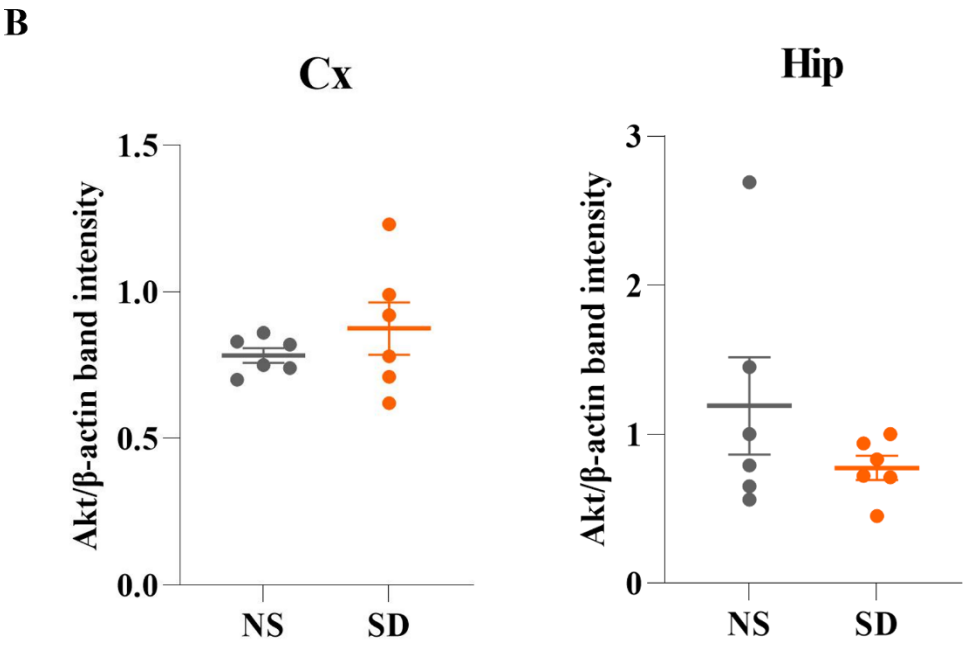
B
Cx
Akt/β-actin band intensity
1.5
1.0
0.5
0.0
NS
SD
Hip
Akt/β-actin band intensity
3
2
1
0
NS
SD

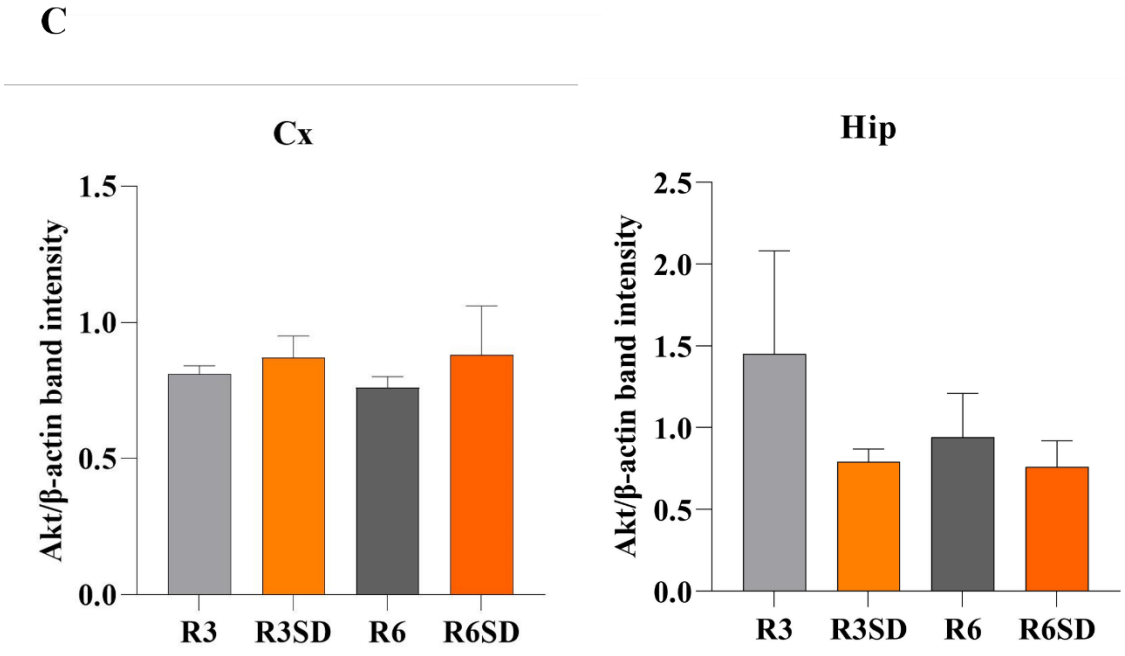
C
Cx
Akt/β-actin band intensity
1.5
1.0
0.5
0.0
R3
R3SD
R6
R6SD
Hip
Akt/β-actin band intensity
2.5
2.0
1.5
1.0
0.5
0.0
R3
R3SD
R6
R6SD

Figure 35. p(473)-Akt in brain extracts of cortex and hippocampus

Using the specific antibody Anti-Phospho-Akt, the levels of the diverse isoforms Akt 1/2/3 phosphorylated on Ser273 residues was analyzed by WB in brain extracts of cortex (Cx, n=3) and hippocampus (Hip, n=3).

***Fig.35* A**) WB analysis of one representative sample for each experimental group.

***Fig.35* B**) Mean values ± SEM of normalized p(473)-Akt expression calculated as the ratio between band intensities of p(473)-Akt with the corresponding β-actin band in NS and SD experimental group (n=6 per group).

***Fig.35* C**) Mean values ± SEM of normalized p(473)-Akt expression calculated as the ratio between band intensities of p(473)-Akt with the corresponding β-actin band in each experimental group.

Experimental groups: Normothermic rats allowed to sleep during 3 hours after the arousal from ST, (Recovery after 3 hours, R3); Normothermic rats sleep deprive during 3 hours after the arousal from ST (R3SD); Normothermic rats after 6 hours from the arousal from ST (Recovery after 6 h, R6); Normothermic rats sleep deprive during 6 hours after the arousal from ST (R6SD).

*: significant comparisons ($p<0.05$).

Western Blot (WB); Cortex (Cx); Hippocampus (Hip); SEM (Standard error of the mean); Normal sleep (NS); Sleep deprived (SD); Synthetic torpor (ST).

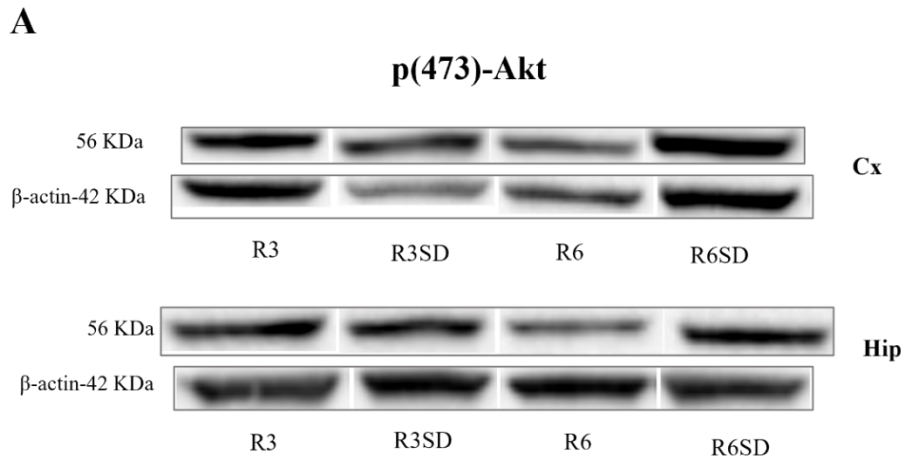
A
p(473)-Akt
56 KDa
β-actin-42 KDa
Cx
R3
R3SD
R6
R6SD
56 KDa
β-actin-42 KDa
Hip
R3
R3SD
R6
R6SD

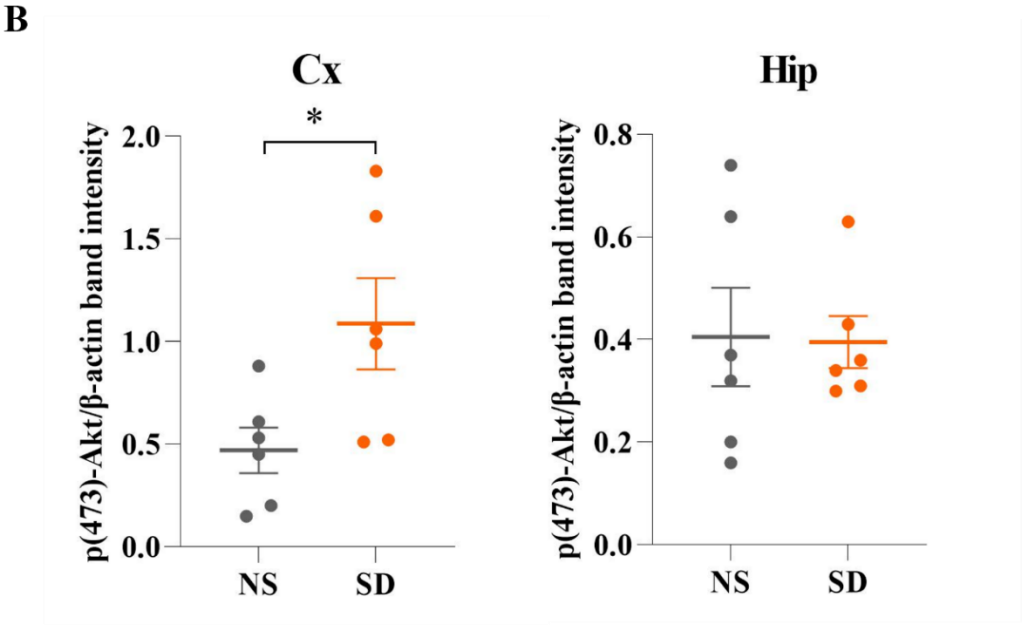
B
Cx
Hip
p(473)-Akt/β-actin band intensity
2.0
1.5
1.0
0.5
0.0
*
NS
SD
0.8
0.6
0.4
0.2
0.0

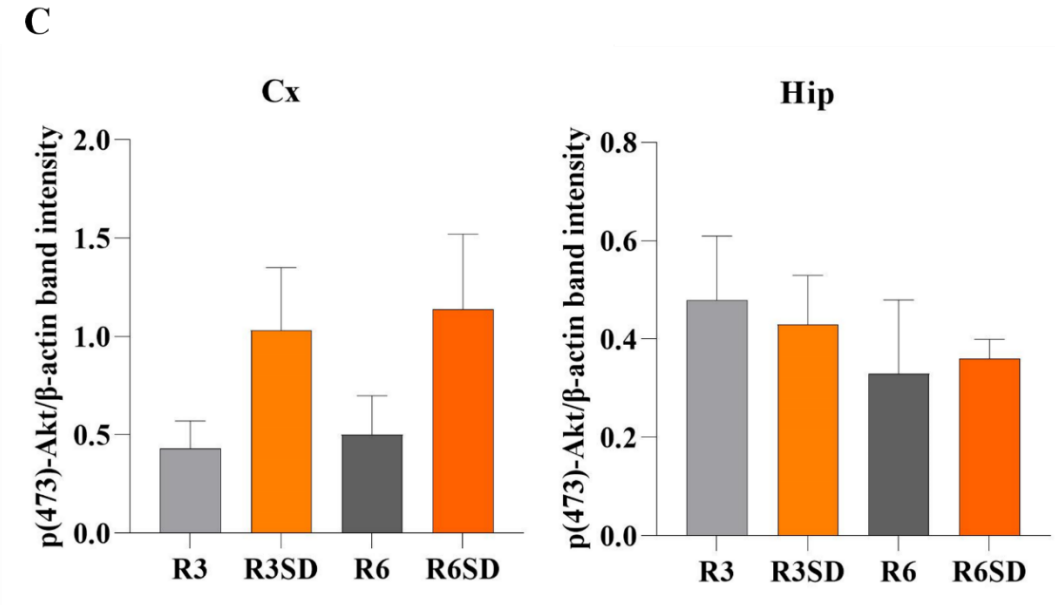
C
Cx
Hip
p(473)-Akt/β-actin band intensity
2.0
1.5
1.0
0.5
0.0
R3
R3SD
R6
R6SD
0.8
0.6
0.4
0.2
0.0

Figure 36. GRP78 in brain extracts of cortex and hippocampus

Using the specific antibody Anti-Glucose regulating protein 78, the levels of GRP78 was analyzed by WB in brain extracts of cortex (Cx, n=3) and hippocampus (Hip, n=3).

Fig.36 **A**) WB analysis of one representative sample for each experimental group.

Fig.36 **B**) Mean values ± SEM of normalized GRP78 expression calculated as the ratio between band intensities of GRP78 with the corresponding β-actin band in NS and SD experimental group (n=6 per group).

Fig.36 **C**) Mean values ± SEM of normalized GRP78 expression calculated as the ratio between band intensities of GRP78 with the corresponding β-actin band in each experimental group.

Experimental groups: Normothermic rats allowed to sleep during 3 hours after the arousal from ST, (Recovery after 3 hours, R3); Normothermic rats sleep deprive during 3 hours after the arousal from ST (R3SD); Normothermic rats after 6 hours from the arousal from ST (Recovery after 6 h, R6); Normothermic rats sleep deprive during 6 hours after the arousal from ST (R6SD).

*: significant comparisons ($p<0.05$).

Western Blot (WB); Cortex (Cx); Hippocampus (Hip); SEM (Standard error of the mean); Normal sleep (NS); Sleep deprived (SD); Synthetic torpor (ST).

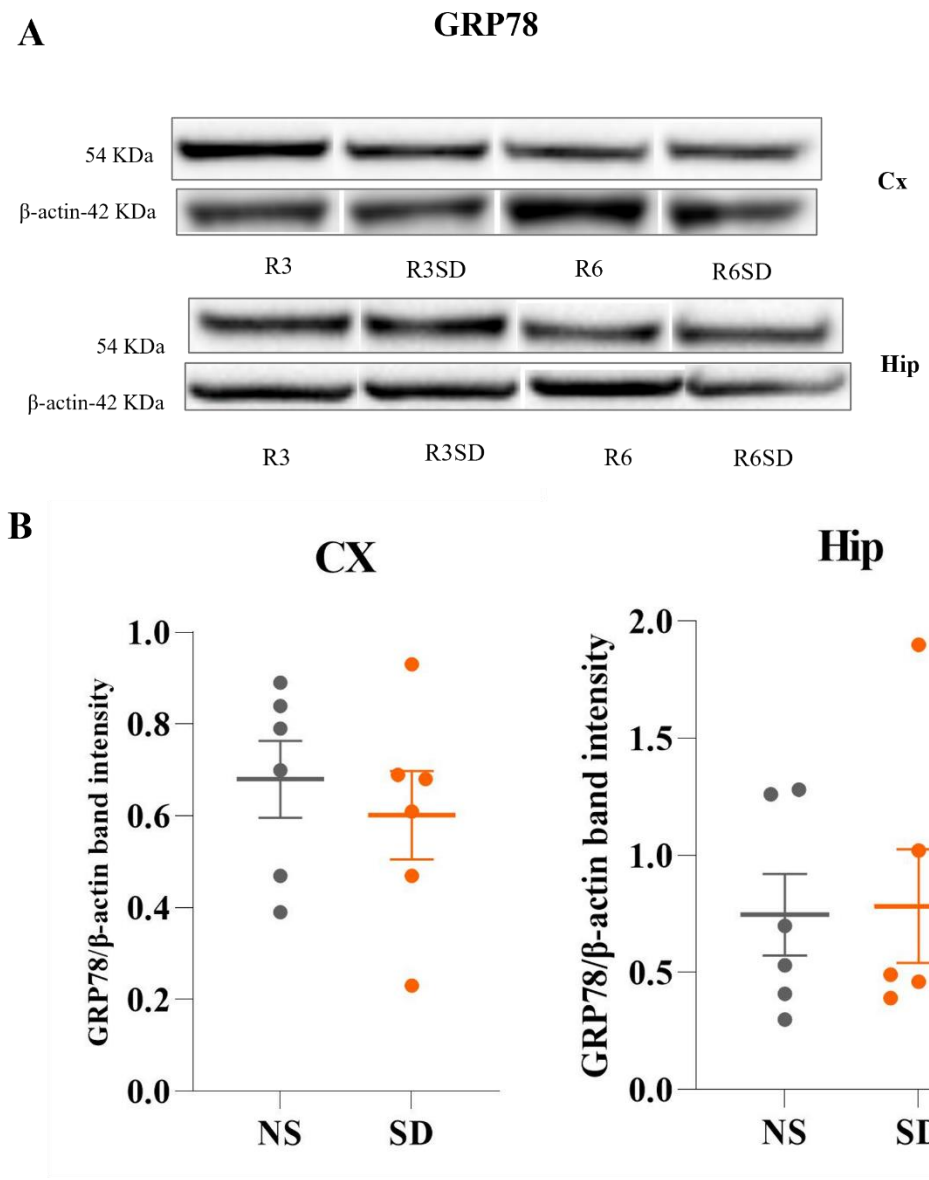
A
GRP78
54 KDa
β-actin-42 KDa
Cx
R3
R3SD
R6
R6SD
54 KDa
β-actin-42 KDa
Hip
R3
R3SD
R6
R6SD
B
CX
GRP78/β-actin band intensity
1.0
0.8
0.6
0.4
0.2
0.0
NS
SD
Hip
GRP78/β-actin band intensity
2.0
1.5
1.0
0.5
0.0
NS
SD
C
Cx
GRP78/β-actin band intensity
1.0
0.8
0.6
0.4
0.2
0.0
R3
R3SD
R6
R6SD
Hip
GRP78/β-actin band intensity
1.5
1.0
0.5
0.0
R3
R3SD
R6
R6SD

Figure 37. Xiap in brain extracts of cortex and hippocampus

Using the specific antibody Anti-X chromosome-linked inhibitor of apoptosis, the levels of Xiap was analyzed by WB in brain extracts of cortex (Cx, n=3) and hippocampus (Hip, n=3).

Fig.37 **A**) WB analysis of one representative sample for each experimental group.

Fig.37 **B**) Mean values ± SEM of normalized Xiap expression calculated as the ratio between band intensities of Xiap with the corresponding β-actin band in NS and SD experimental group (n=6 per group).

Fig.37 **C**) Mean values ± SEM of normalized Xiap expression calculated as the ratio between band intensities of Xiap with the corresponding β-actin band in each experimental group.

Experimental groups: Normothermic rats allowed to sleep during 3 hours after the arousal from ST, (Recovery after 3 hours, R3); Normothermic rats sleep deprive during 3 hours after the arousal from ST (R3SD); Normothermic rats after 6 hours from the arousal from ST (Recovery after 6 h, R6); Normothermic rats sleep deprive during 6 hours after the arousal from ST (R6SD).

*: significant comparisons ($p<0.05$).

Western Blot (WB); Cortex (Cx); Hippocampus (Hip); SEM (Standard error of the mean); Normal sleep (NS); Sleep deprived (SD); Synthetic torpor (ST).

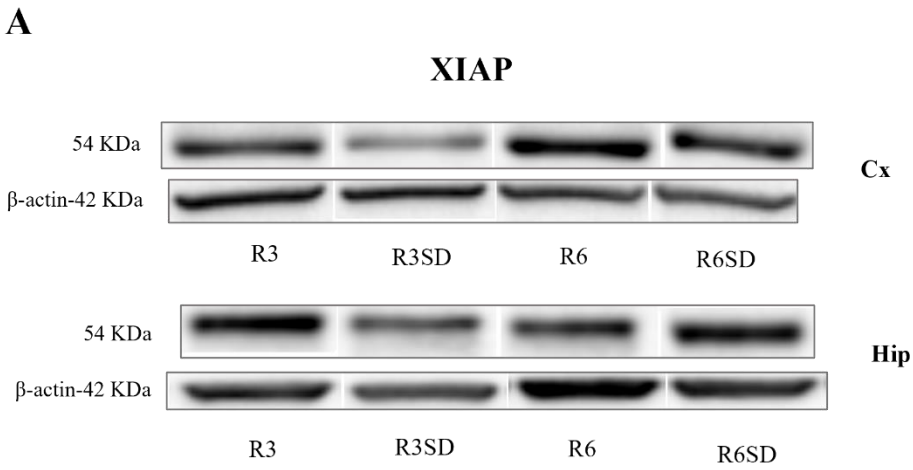
A
XIAP
54 KDa
β-actin-42 KDa
Cx
R3
R3SD
R6
R6SD
54 KDa
β-actin-42 KDa
Hip
R3
R3SD
R6
R6SD

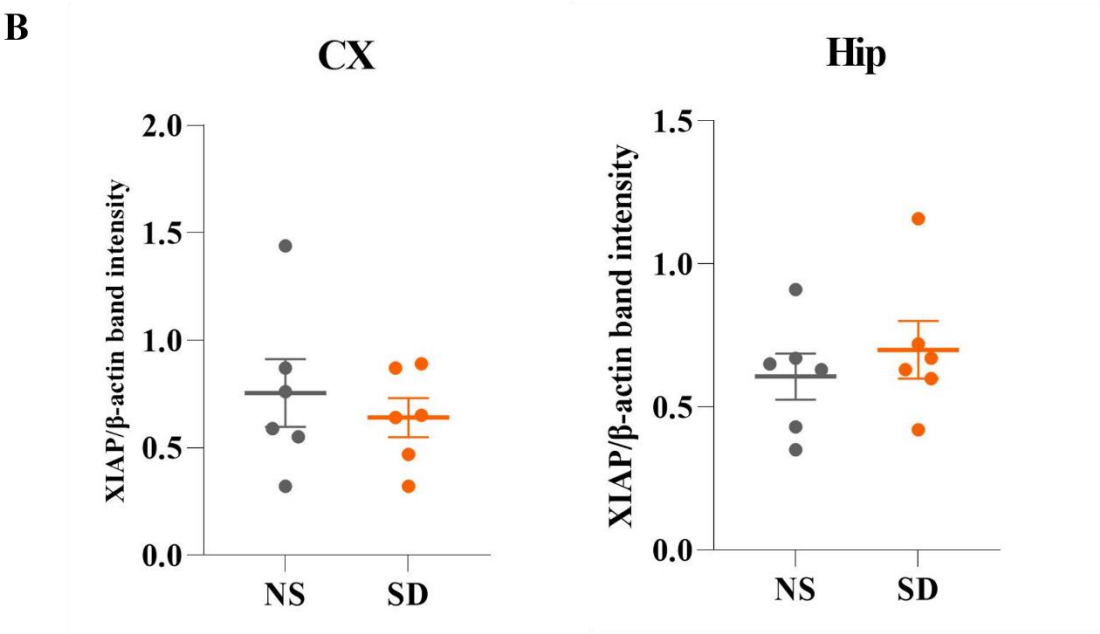
B
CX
XIAP/β-actin band intensity
2.0
1.5
1.0
0.5
0.0
NS
SD
Hip
XIAP/β-actin band intensity
1.5
1.0
0.5
0.0
NS
SD

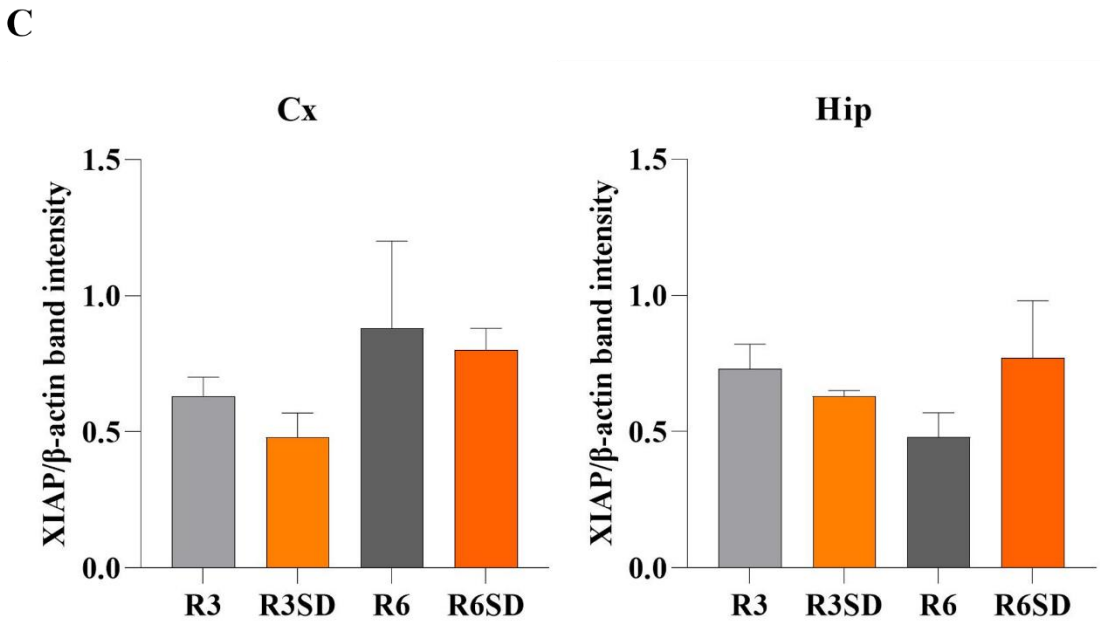
C
Cx
XIAP/β-actin band intensity
1.5
1.0
0.5
0.0
R3
R3SD
R6
R6SD
Hip
XIAP/β-actin band intensity
1.5
1.0
0.5
0.0
R3
R3SD
R6
R6SD

Figure 38. PP2A in brain extracts of cortex and hippocampus

Using the specific antibody Anti-Protein phosphatase 2, the levels of PP2A was analyzed by WB in brain extracts of cortex (Cx, n=3) and hippocampus (Hip, n=3).

***Fig.38* A**) WB analysis of one representative sample for each experimental group.

***Fig.38* B**) Mean values ± SEM of normalized PP2A expression calculated as the ratio between band intensities of PP2A with the corresponding β-actin band in NS and SD experimental group (n=6 per group).

***Fig.38* C**) Mean values ± SEM of normalized PP2A expression calculated as the ratio between band intensities of PP2A with the corresponding β-actin band in each experimental group.

Experimental groups: Normothermic rats allowed to sleep during 3 hours after the arousal from ST, (Recovery after 3 hours, R3); Normothermic rats sleep deprive during 3 hours after the arousal from ST (R3SD); Normothermic rats after 6 hours from the arousal from ST (Recovery after 6 h, R6); Normothermic rats sleep deprive during 6 hours after the arousal from ST (R6SD).

*: significant comparisons ($p<0.05$).

Western Blot (WB); Cortex (Cx); Hippocampus (Hip); SEM (Standard error of the mean); Normal sleep (NS); Sleep deprived (SD); Synthetic torpor (ST).

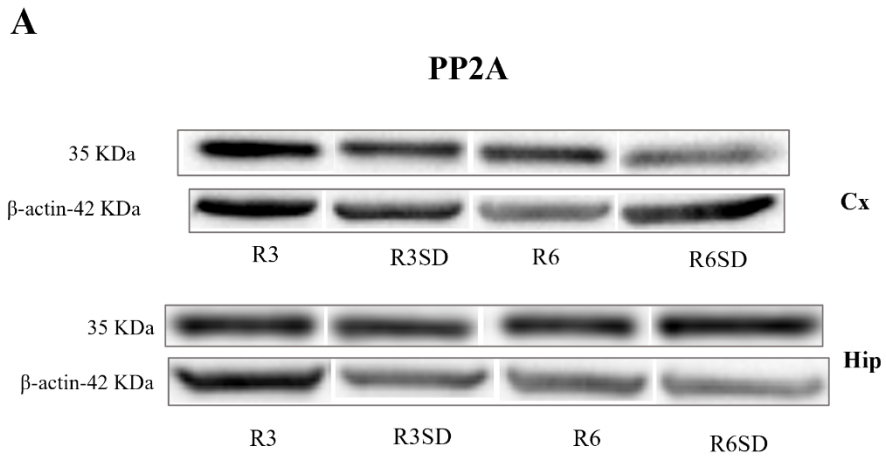
A
PP2A
35 KDa
β-actin-42 KDa
Cx
R3
R3SD
R6
R6SD
35 KDa
β-actin-42 KDa
Hip
R3
R3SD
R6
R6SD

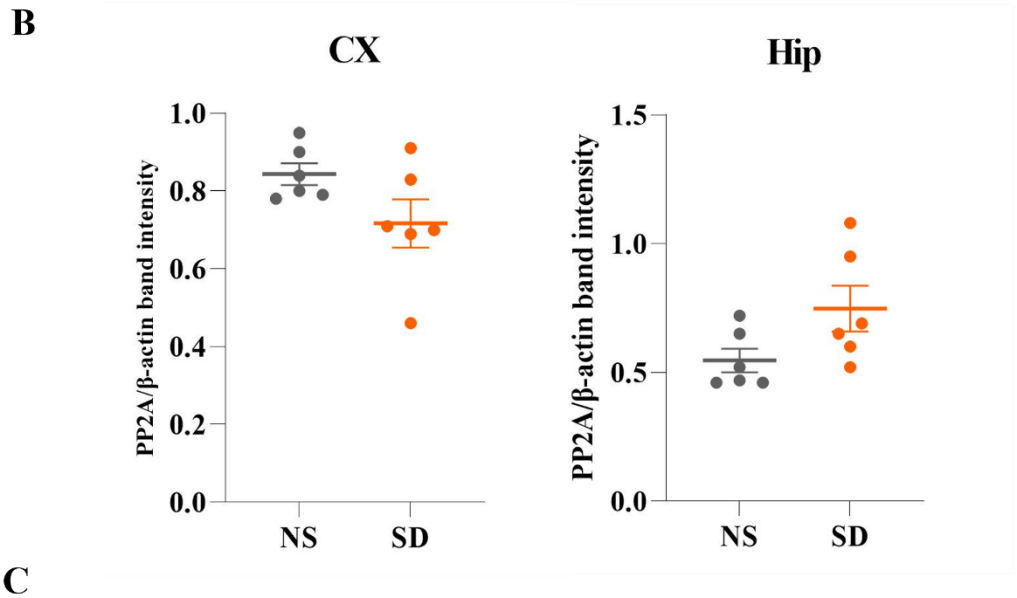
B
CX
Hip
PP2A/β-actin band intensity
1.0
0.8
0.6
0.4
0.2
0.0
1.5
1.0
0.5
0.0
NS
SD

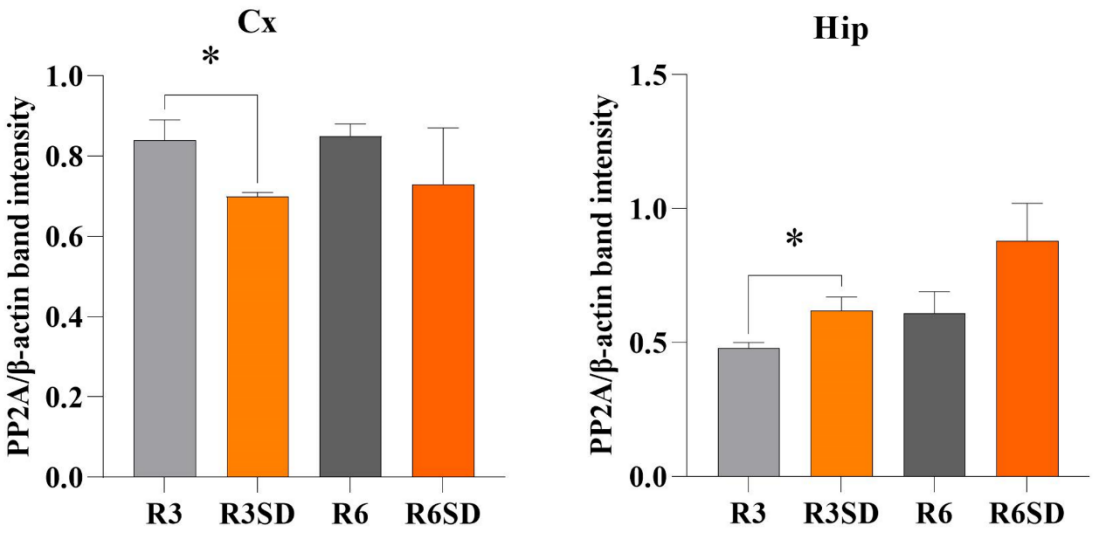
C
Cx
Hip
*
PP2A/β-actin band intensity
1.0
0.8
0.6
0.4
0.2
0.0
1.5
1.0
0.5
0.0
R3
R3SD
R6
R6SD

Figure 39. Cleaved-caspase 3 in brain extracts of cortex and hippocampus

Using the specific antibody Anti-Cleaved-Caspase 3, the levels of caspase 3 cleaved on Asp175 residue was analyzed by WB in brain extracts of cortex (Cx, n=3) and hippocampus (Hip, n=3).

Fig.39 **A**) WB analysis of one representative sample for each experimental group.

Fig.39 **B**) Mean values ± SEM of normalized Cleaved-caspase 3 expression calculated as the ratio between band intensities of Cleaved-caspase 3 with the corresponding β-actin band in NS and SD experimental group (n=6 per group).

Fig.39 **C**) Mean values ± SEM of normalized Cleaved-caspase 3 expression calculated as the ratio between band intensities of Cleaved-caspase 3 with the corresponding β-actin band in each experimental group.

Experimental groups: Normothermic rats allowed to sleep during 3 hours after the arousal from ST, (Recovery after 3 hours, R3); Normothermic rats sleep deprive during 3 hours after the arousal from ST (R3SD); Normothermic rats after 6 hours from the arousal from ST (Recovery after 6 h, R6); Normothermic rats sleep deprive during 6 hours after the arousal from ST (R6SD).

*: significant comparisons ($p<0.05$).

Western Blot (WB); Cortex (Cx); Hippocampus (Hip); SEM (Standard error of the mean); Normal sleep (NS); Sleep deprived (SD); Synthetic torpor (ST).

A

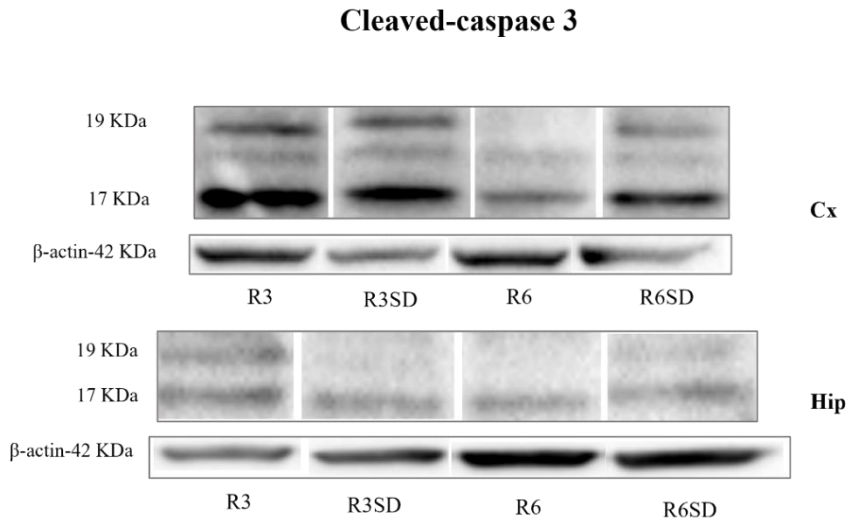
Cleaved-caspase 3
19 KDa
17 KDa
β-actin-42 KDa
Cx
R3
R3SD
R6
R6SD
19 KDa
17 KDa
β-actin-42 KDa
Hip
R3
R3SD
R6
R6SD

B

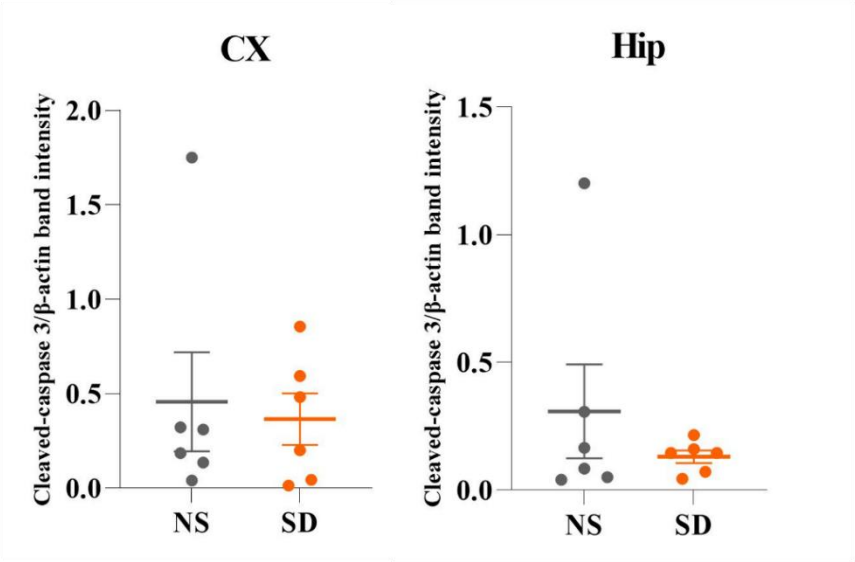
CX
Hip
Cleaved-caspase 3/β-actin band intensity
2.0
1.5
1.0
0.5
0.0
NS
SD
Cleaved-caspase 3/β-actin band intensity
1.5
1.0
0.5
0.0
NS
SD

C

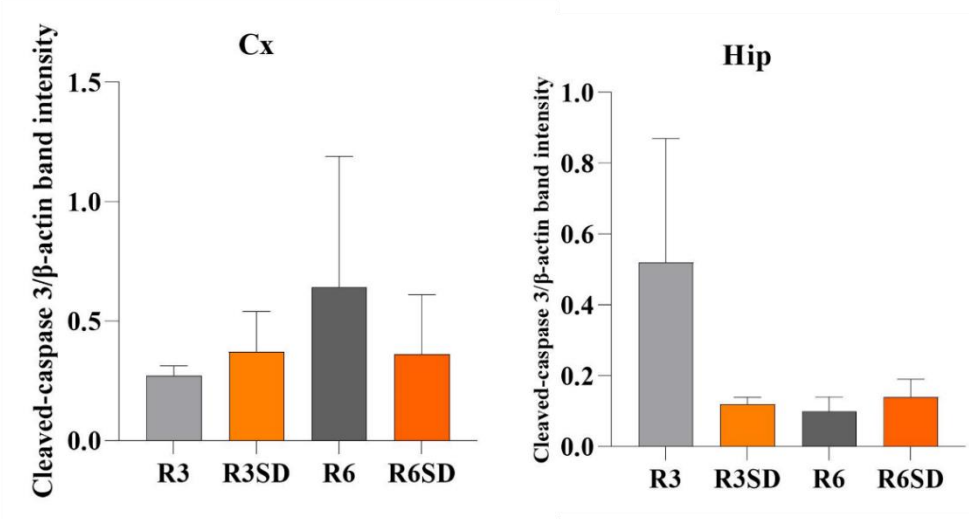
Cx
Cleaved-caspase 3/β-actin band intensity
1.5
1.0
0.5
0.0
R3
R3SD
R6
R6SD
Hip
Cleaved-caspase 3/β-actin band intensity
1.0
0.8
0.6
0.4
0.2
0.0
R3
R3SD
R6
R6SD

Figure 40. Plasma concentration of melatonine, dopamine, adrenaline, noradrenaline, corticosterone, cortisol

Fig.40 **A**) Mean values ± SEM of melatonin plasma concentration in each experimental group.

Fig.40 **B**) Mean values ± SEM of dopamine plasma concentration in each experimental group.

Fig.40 **C**) Mean values ± SEM of adrenaline plasma concentration in each experimental group.

Fig.40 **D**) Mean values ± SEM of noradrenaline plasma concentration in each experimental group.

Fig.40 **E**) Mean values ± SEM of corticosterone plasma concentration in each experimental group.

Fig.40 **F**) Mean values ± SEM of cortisol plasma concentration in each experimental group.

Experimental groups: Normothermic rats allowed to sleep during 3 hours after the arousal from ST, (Recovery after 3 hours, R3); Normothermic rats sleep deprive during 3 hours after the arousal from ST (R3SD); Normothermic rats after 6 hours from the arousal from ST (Recovery after 6 h, R6); Normothermic rats sleep deprive during 6 hours after the arousal from ST (R6SD).

*: significant comparisons ($p<0.05$).

SEM (Standard error of the mean); Sleep deprived (SD); Synthetic torpor (ST).

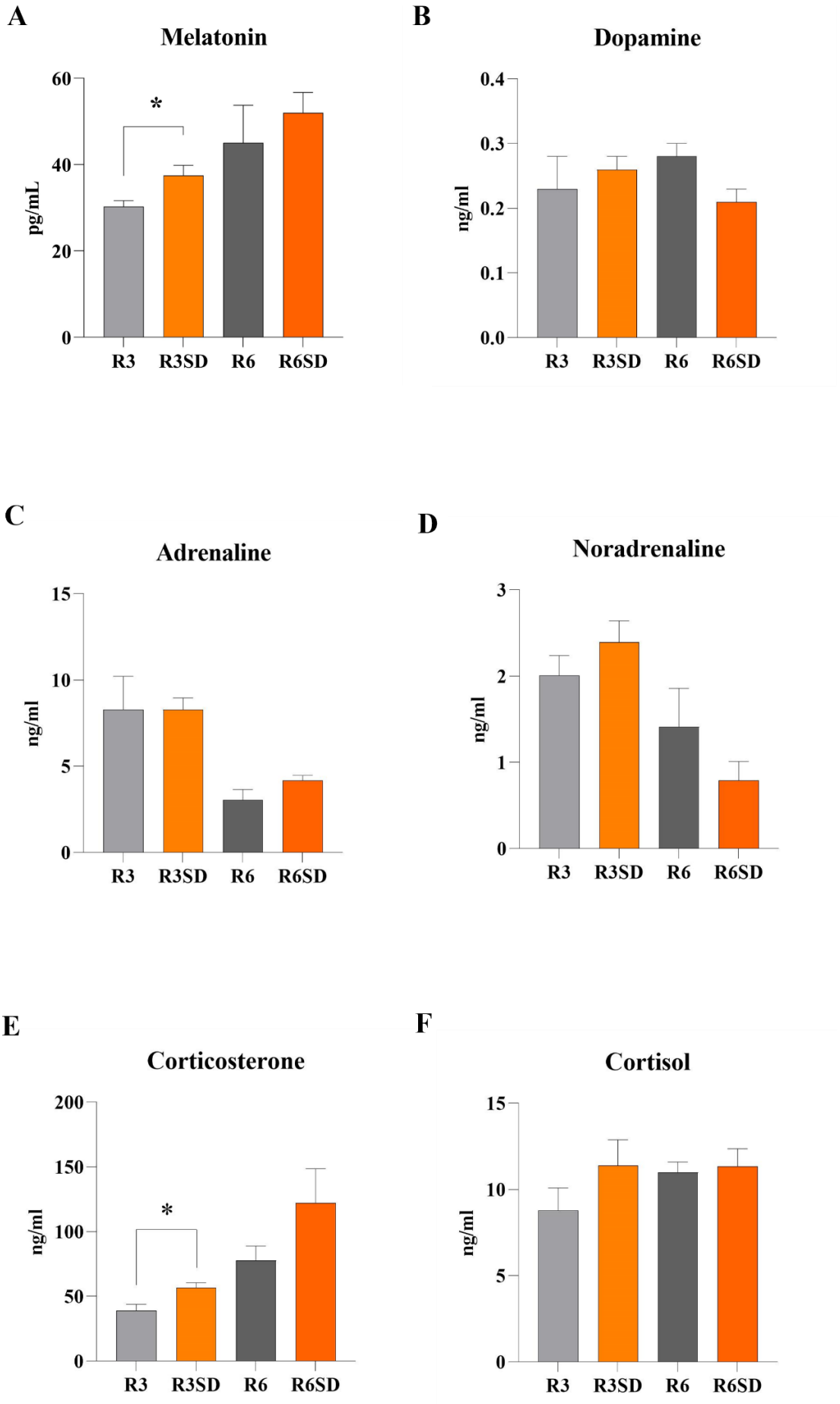
A
Melatonin
pg/mL
60
40
20
0
*
R3
R3SD
R6
R6SD
B
Dopamine
ng/ml
0.4
0.3
0.2
0.1
0.0
R3
R3SD
R6
R6SD
C
Adrenaline
ng/ml
15
10
5
0
R3
R3SD
R6
R6SD
D
Noradrenaline
ng/ml
3
2
1
0
R3
R3SD
R6
R6SD
E
Corticosterone
ng/ml
200
150
100
50
0
*
R3
R3SD
R6
R6SD
F
Cortisol
ng/ml
15
10
5
0
R3
R3SD
R6
R6SD

7. REFERENCES

Abdulkhaleq, L. A., Assi, M. A., Abdullah, R., Zamri-Saad, M., Taufiq-Yap, Y. H., & Hezmee, M. N. M. (2018). The crucial roles of inflammatory mediators in inflammation: A review. In *Veterinary World* (Vol. 11, Issue 5, pp. 627–635). Veterinary World. https://doi.org/10.14202/vetworld.2018.627-635

Achermann, P.;, & Borbély, A. A. (2017). *Sleep homeostasis and models of sleep regulation*. https://doi.org/10.5167/uzh-124066

Ağaç, D., Estrada, L. D., Maples, R., Hooper, L. V., & Farrar, J. D. (2018). The β2-adrenergic receptor controls inflammation by driving rapid IL-10 secretion. *Brain, Behavior, and Immunity*, *74*, 176–185. https://doi.org/10.1016/J.BBI.2018.09.004

Akira, S., & Takeda, K. (2004). Toll-like receptor signalling. In *Nature Reviews Immunology* (Vol. 4, Issue 7, pp. 499–511). Nature Publishing Group. https://doi.org/10.1038/nri1391

Akira, S., Uematsu, S., & Takeuchi, O. (2006). Pathogen recognition and innate immunity. In *Cell* (Vol. 124, Issue 4, pp. 783–801). Cell Press. https://doi.org/10.1016/j.cell.2006.02.015

Aloia, R. C., & Raison, J. K. (1989). Membrane function in mammalian hibernation. *BBA - Reviews on Biomembranes*, *988*(1), 123–146. https://doi.org/10.1016/0304-4157(89)90007-5

Amici, R., Bastianini, S., Berteotti, C., Cerri, M., Del Vecchio, F., Lo Martire, V., Luppi, M., Perez, E., Silvani, A., Zamboni, G., & Zoccoli, G. (2014). Sleep and bodily functions: The physiological interplay between body homeostasis and sleep homeostasis. *Archives Italiennes de Biologie*, *152*(2–3), 66–78. https://doi.org/10.12871/000298292014232

Amici, R., Cerri, M., Ocampo-Garcés, A., Baracchi, F., Dentico, D., Jones, C. A., Luppi, M., Perez, E., Parmeggiani, P. L., & Zamboni, G. (2008). Cold exposure and sleep in the rat: REM sleep homeostasis and body size. *Sleep*, *31*(5), 708–715. https://doi.org/10.1093/sleep/31.5.708

Arendt, T., & Bullmann, T. (2013). Neuronal plasticity in hibernation and the proposed role of the microtubule-associated protein tau as a “master switch” regulating synaptic gain in neuronal networks. *Https://Doi.Org/10.1152/Ajpregu.00117.2013*, *305*(5), 478–489. https://doi.org/10.1152/AJPREGU.00117.2013

Arendt, T., Stieler, J., Strijkstra, A. M., Hut, R. A., Rüdiger, J., Van der Zee, E. A., Harkany, T., Holzer, M., & Härtig, W. (2003). Reversible paired helical filament-like phosphorylation of tau is an adaptive process associated with neuronal plasticity in hibernating animals. *Journal of Neuroscience*, *23*(18), 6972–6981. https://doi.org/10.1523/jneurosci.23-18-06972.2003

Bankenahally, R., & Krovvidi, H. (2016). Autonomic nervous system: anatomy, physiology, and relevance in anaesthesia and critical care medicine. *BJA Education*, *16*(11), 381–387. https://doi.org/10.1093/bjaed/mkw011

Basnayake, S. D., Green, A. L., & Paterson, D. J. (2012). Mapping the central neurocircuitry that integrates the cardiovascular response to exercise in humans. *Experimental Physiology*, *97*(1), 29–38. https://doi.org/10.1113/expphysiol.2011.060848

Bellavance, M. A., & Rivest, S. (2014). The HPA - immune axis and the immunomodulatory actions of glucocorticoids in the brain. *Frontiers in Immunology*, *5*(MAR). https://doi.org/10.3389/fimmu.2014.00136

Bellinger, D. L., & Lorton, D. (2014). Autonomic regulation of cellular immune function. *Autonomic Neuroscience: Basic and Clinical*, *182*, 15–41. https://doi.org/10.1016/j.autneu.2014.01.006

Benarroch, E. E. (2020). Physiology and Pathophysiology of the Autonomic Nervous System. In *CONTINUUM Lifelong Learning in Neurology* (Vol. 26, Issue 1, pp. 12–24). Lippincott Williams and Wilkins. https://doi.org/10.1212/CON.0000000000000817

Benarroch, E. E. (1993). The Central Autonomic Network: Functional Organization, Dysfunction, and Perspective. *Mayo Clinic Proceedings*, *68*(10), 988–1001. https://doi.org/10.1016/S0025-6196(12)62272-1

Benedict, C.., Blennow, K., Zetterberg, H., Cedernaes, J. (2020). Effects of acute sleep loss on diurnal plasma dynamics of CNS health biomarkers in young men. *Neurology*, 94(11), 1-10. https://doi.org/10.1212/WNL.0000000000008866

Benítez-King, G. (2006). Melatonin as a cytoskeletal modulator: implications for cell physiology and disease. *Journal of Pineal Research*, *40*(1), 1–9. https://doi.org/10.1111/J.1600-079X.2005.00282.X

Berger, R. J. (1984). Slow wave sleep, shallow torpor and hibernation: Homologous states of diminished metabolism and body temperature. *Biological Psychology*, *19*(3–4), 305–326. https://doi.org/10.1016/0301-0511(84)90045-0

Besedovsky, H. O., Rey, A. del, Sorkin, E., Da Prada, M., & Keller, H. H. (1979). Immunoregulation mediated by the sympathetic nervous system. *Cellular Immunology*, *48*(2), 346–355. https://doi.org/10.1016/0008-8749(79)90129-1

Beutler, B. (2004). Inferences, questions and possibilities in Toll-like receptor signalling. *Nature 2004 430:6996*, *430*(6996), 257–263. https://doi.org/10.1038/nature02761

Beutler, B. A. (2009a). TLRs and innate immunity. In *Blood* (Vol. 113, Issue 7, pp. 1399–1407). Blood. https://doi.org/10.1182/blood-2008-07-019307

Beutler, B. A. (2009b). TLRs and innate immunity. In *Blood* (Vol. 113, Issue 7, pp. 1399–1407). Blood. https://doi.org/10.1182/blood-2008-07-019307

Bittman, E. L., Crandell, R. G., & Lehman, M. N. (1989). Influences of the paraventricular and suprachiasmatic nuclei and olfactory bulbs on melatonin responses in the golden hamster. *Biology of Reproduction*, *40*(1), 118–126. https://doi.org/10.1095/biolreprod40.1.118

Blanco, M. B., Dausmann, K. H., Faherty, S. L., Klopfer, P., Krystal, A. D., Schopler, R., & Yoder, A. D. (2016). Hibernation in a primate: does sleep occur? *Royal Society Open Science*, *3*(8). https://doi.org/10.1098/RSOS.160282

Blessing, W. W., & Nalivaiko, E. (2001). Raphe magnus/pallidus neurons regulate tail but not mesenteric arterial blood flow in rats. *Neuroscience*, *105*(4), 923–929. https://doi.org/10.1016/S0306-4522(01)00251-2

Borovikova, L. V., Ivanova, S., Zhang, M., Yang, H., Botchkina, G. I., Watkins, L. R., Wang, H., Abumrad, N., Eaton, J. W., & Tracey, K. J. (2000). Vagus nerve stimulation attenuates the systemic inflammatory response to endotoxin. *Nature*, *405*(6785), 458–462. https://doi.org/10.1038/35013070

Broz, P., & Dixit, V. M. (2016). Inflammasomes: mechanism of assembly, regulation and signalling. *Nature Reviews Immunology 2016 16:7*, *16*(7), 407–420. https://doi.org/10.1038/NRI.2016.58

Brunton, (2011). Adrenergic Agonists and Antagonists. The Pharmacological Basis of Therapeutics. 14Th Edition.

Cano, G., Passerin, A. M., Schiltz, J. C., Card, J. P., Morrison, S. F., & Sved, A. F. (2003). Anatomical substrates for the central control of sympathetic outflow to interscapular adipose tissue during cold exposure. *Journal of Comparative Neurology*, *460*(3), 303–326. https://doi.org/10.1002/CNE.10643

Capellino, S., Weber, K., Gelder, M., Härle, P., & Straub, R. H. (2012). First appearance and location of catecholaminergic cells during experimental arthritis and elimination by chemical sympathectomy. *Arthritis and Rheumatism*, *64*(4), 1110–1118. https://doi.org/10.1002/art.33431

Carskadon, M. A., & Dement, W. C. (n.d.). *Chapter 2-Normal Human Sleep : An Overview*.

Cerri, M. (2017). The Central Control of Energy Expenditure: Exploiting Torpor for Medical Applications. *Annual Review of Physiology*, *79*, 167–186. https://doi.org/10.1146/annurev-physiol-022516-034133

Cerri, M., Hitrec, T., Luppi, M., & Amici, R. (2021). Be cool to be far: Exploiting hibernation for space exploration. *Neuroscience & Biobehavioral Reviews*, *128*, 218–232. https://doi.org/10.1016/J.NEUBIOREV.2021.03.037

Cerri, M., Mastrotto, M., Tupone, D., Martelli, D., Luppi, M., Perez, E., Zamboni, G., & Amici, R. (2013). The inhibition of neurons in the central nervous pathways for thermoregulatory cold defense induces a suspended animation state in the rat. *Journal of Neuroscience*, *33*(7), 2984–2993. https://doi.org/10.1523/JNEUROSCI.3596-12.2013

Cerri, M., Ocampo-Garces, A., Amici, R., Baracchi, F., Capitani, P., Jones, C. A., Luppi, M., Perez, E., Parmeggiani, P. L., & Zamboni, G. (2005). Cold Exposure and Sleep in the Rat: Effects on Sleep Architecture and the Electroencephalogram. *Sleep*, *28*(6), 694–705. https://doi.org/10.1093/SLEEP/28.6.694

Chaplin, D. D. (2010). Overview of the immune response. *Journal of Allergy and Clinical Immunology*, *125*(2 SUPPL. 2). https://doi.org/10.1016/j.jaci.2009.12.980

Chatfield, P.O., Lyman, C.P. (1954). Subcortical electrical activity in the golden hamster during arousal from hibernation. *Electroencephalography and Clinical Neurophysiology*, 6, 403-408. https://doi.org/10.1016/0013-4694(54)90054-1.

Chinchalongporn, V., Shukla, M., & Govitrapong, P. (2018). Melatonin ameliorates Aβ42-induced alteration of βAPP-processing secretases via the melatonin receptor through the Pin1/GSK3β/NF-κB pathway in SH-SY5Y cells. *Journal of Pineal Research*, *64*(4).

https://doi.org/10.1111/jpi.12470

Chiocchetti, R., Hitrec, T., Giancola, F., Sadeghinezhad, J., Squarcio, F., Galiazzo, G., Piscitiello, E., Silva, M. De, Cerri, M., Amici, R., & Luppi, M. (2021). Phosphorylated Tau protein in the myenteric plexus of the ileum and colon of normothermic rats and during synthetic torpor. *Cell and Tissue Research 2021 384:2*, *384*(2), 287–299. https://doi.org/10.1007/S00441-020-03328-0

Chu, W. M. (2013). Tumor necrosis factor. In *Cancer Letters* (Vol. 328, Issue 2, pp. 222–225). Elsevier Ireland Ltd. https://doi.org/10.1016/j.canlet.2012.10.014

Ciccarelli, M., Sorriento, D., Coscioni, E., Iaccarino, G., & Santulli, G. (2017). Adrenergic Receptors. In *Endocrinology of the Heart in Health and Disease: Integrated, Cellular, and Molecular Endocrinology of the Heart* (pp. 285–315). Elsevier Inc. https://doi.org/10.1016/B978-0-12-803111-7.00011-7

Coote, J. H., & Spyer, K. M. (2018). Central control of autonomic function. *Brain and Neuroscience Advances*, *2*, 2398212818812012. https://doi.org/10.1177/2398212818812012

Craig, A. D. (2002). How do you feel? Interoception: the sense of the physiological condition of the body. *Nature Reviews Neuroscience 2002 3:8*, *3*(8), 655–666. https://doi.org/10.1038/nrn894

Crespo-Biel, N., Theunis, C., & Van Leuven, F. (2012). Protein Tau: Prime cause of synaptic and neuronal degeneration in alzheimer's disease. *International Journal of Alzheimer's Disease*. https://doi.org/10.1155/2012/251426

Cross, D. A. E., Alessi, D. R., Cohen, P., Andjelkovich, M., & Hemmings, B. A. (1995a). Inhibition of glycogen synthase kinase-3 by insulin mediated by protein kinase B. *Nature*, *378*(6559), 785–789. https://doi.org/10.1038/378785a0

Cross, D. A. E., Alessi, D. R., Cohen, P., Andjelkovich, M., & Hemmings, B. A. (1995b). Inhibition of glycogen synthase kinase-3 by insulin mediated by protein kinase B. *Nature*, *378*(6559), 785–789. https://doi.org/10.1038/378785a0

Daan, S., Barnes, B. M., & Strijkstra, A. M. (1991). Warming up for sleep? — Ground squirrels sleep during arousals from hibernation. *Neuroscience Letters*, *128*(2), 265–268. https://doi.org/10.1016/0304-3940(91)90276-Y

De Diego, A. M. G., Gandía, L., & García, A. G. (2008). A physiological view of the central and peripheral mechanisms that regulate the release of catecholamines at the adrenal medulla. *Acta Physiologica*, *192*(2), 287–301. https://doi.org/10.1111/j.1748-1716.2007.01807.x

De Vivo, L., Bellesi, M., Marshall, W., Bushong, E. A., Ellisman, M. H., Tononi, G., & Cirelli, C. (2017). Ultrastructural evidence for synaptic scaling across the wake/sleep cycle. *Science*, *355*(6324), 507–510. https://doi.org/10.1126/science.aah5982

Deboer, T. (1998). Brain temperature dependent changes in the electroencephalogram power spectrum of humans and animals. *Journal of Sleep Research*, *7*(4), 254–262. https://doi.org/10.1046/j.1365-2869.1998.00125.x

Deboer, T., & Tobler, I. (1994). Sleep EEG after daily torpor in the Djungarian hamster: similarity to the effects of sleep deprivation. *Neuroscience Letters*, *166*(1), 35–38. https://doi.org/10.1016/0304-3940(94)90834-6

Deboer, T., & Tobler, I. (2003). Sleep Regulation in the Djungarian Hamster: Comparison of the Dynamics Leading to the Slow-Wave Activity Increase After Sleep Deprivation and Daily Torpor. *Sleep*, *26*(5), 567–572. https://doi.org/10.1093/SLEEP/26.5.567

Dempsey, P. W., Vaidya, S. A., & Cheng, G. (2003). The Art of War: Innate and adaptive immune responses. In *Cellular and Molecular Life Sciences* (Vol. 60, Issue 12, pp. 2604–2621). Springer. https://doi.org/10.1007/s00018-003-3180-y

Djuric, Z. (2017). Obesity-associated cancer risk: the role of intestinal microbiota in the etiology of the host proinflammatory state. In *Translational Research* (Vol. 179, pp. 155–167). Mosby Inc. https://doi.org/10.1016/j.trsl.2016.07.017

Donald, D. E., & Shepherd, J. T. (1979). Cardiac receptors: Normal and disturbed function. *The American Journal of Cardiology*, *44*(5), 873–878. https://doi.org/10.1016/0002-9149(79)90216-9

Du, F., Zhu, X. H., Zhang, Y., Friedman, M., Zhang, N., Uğurbil, K., & Chen, W. (2008). Tightly coupled brain activity and cerebral ATP metabolic rate. *Proceedings of the National Academy of Sciences of the United States of America*, *105*(17), 6409–6414. https://doi.org/10.1073/pnas.0710766105

Echchannaoui, H., Frei, K., Schnell, C., Leib, S. L., Zimmerli, W., & Landmann, R. (2002). Toll-like receptor 2-deficient mice are highly susceptible to Streptococcus pneumoniae meningitis because of reduced bacterial clearing and enhanced inflammation. *Journal of Infectious Diseases*, *186*(6), 798–806. https://doi.org/10.1086/342845

Elenkov, I.J., Wilder, R.L., Chrousos, G.P:, Vizi, E.S. (2000). The sympathetic nerve--an integrative interface between two supersystems: the brain and the immune system.Pharmacological reviews, 52(4), 595-638. https://pubmed.ncbi.nlm.nih.gov/11121511/.

Ernest, M., Hunja, C., Arakura, Y., Haraga, Y., Abkallo, H. M., Zeng, W., Jackson, D. C., Chua, B., & Culleton, R. (2018). The Toll-Like Receptor 2 agonist PEG-Pam2Cys as an immunochemoprophylactic and immunochemotherapeutic against the liver and transmission stages of malaria parasites. *International Journal for Parasitology: Drugs and Drug Resistance*, *8*(3), 451–458. https://doi.org/10.1016/j.ijpddr.2018.10.006

Esclaire, F., Lesort, M., Blanchard, C., & Hugon, J. (1997). Glutamate Toxicity Enhances Tau Gene Expression in Neuronal Cultures. *J. Neurosci. Res*, *49*, 309–318. https://doi.org/10.1002/(SICI)1097-4547(19970801)49:3

Farmer, D. G. S., Pracejus, N., Dempsey, B., Turner, A., Bokiniec, P., Paton, J. F. R., Pickering, A. E., Burguet, J., Andrey, P., Goodchild, A. K., McAllen, R. M., & McMullan, S. (2019). On the presence and functional significance of sympathetic premotor neurons with collateralized spinal axons in the rat. *Journal of Physiology*, *597*(13), 3407–3423. https://doi.org/10.1113/JP277661

Farrell, M. J., Trevaks, D., Taylor, N. A. S., & McAllen, R. M. (2013). Brain stem

representation of thermal and psychogenic sweating in humans. *Https://Doi.Org/10.1152/Ajpregu.00041.2013*, *304*(10), 810–817. https://doi.org/10.1152/AJPREGU.00041.2013

Felten, D.L., Felten, D.Y., Carlson, S.L., Olschowka, L.A. & Livnat, S. (1985). Noradrenergic and peptidergic innervation of lymphoid tissue. Journal of Immunology 135; 755-765.

Florant, G. L., Porst, H., Peiffer, A., Hudachek, S. F., Pittman, C., A.Summers, S., Rajala, M. W., & Scherer, P. E. (2004). Fat-cell mass, serum leptin and adiponectin changes during weight gain and loss in yellow-bellied marmots (Marmota flaviventris). *Journal of Comparative Physiology B 2004 174:8*, *174*(8), 633–639. https://doi.org/10.1007/S00360-004-0454-0

Franken, P., Dijk, D. J., Tobler, I., & Borbely, A. A. (1991). Sleep deprivation in rats: Effects on EEG power spectra, vigilance states, and cortical temperature. *American Journal of Physiology - Regulatory Integrative and Comparative Physiology*, *261*(1 30-1). https://doi.org/10.1152/ajpregu.1991.261.1.r198

Fricker, M., Tolkovsky, A. M., Borutaite, V., Coleman, M., & Brown, G. C. (2018). Neuronal cell death. *Physiological Reviews*, *98*(2), 813–880. https://doi.org/10.1152/physrev.00011.2017

Fullerton, J. N., & Gilroy, D. W. (2016). Resolution of inflammation: A new therapeutic frontier. In *Nature Reviews Drug Discovery* (Vol. 15, Issue 8, pp. 551–567). Nature Publishing Group. https://doi.org/10.1038/nrd.2016.39

Furness, J.B. (2006). The organisation of the autonomic nervous system: peripheral connections. Autonomic Neuroscience 130 (1-2).

Geiser, F. (2004). Metabolic Rate and Body Temperature Reduction During Hibernation and Daily Torpor. *Http://Dx.Doi.Org/10.1146/Annurev.Physiol.66.032102.115105*, *66*, 239–274. https://doi.org/10.1146/ANNUREV.PHYSIOL.66.032102.115105

Geiser, F. (2010). Aestivation in mammals and birds. *Progress in Molecular and Subcellular Biology*, *49*, 95–111. https://doi.org/10.1007/978-3-642-02421-4_5

Giordano, A., Frontini, A., Castellucci, M., & Cinti, S. (2016). Presence and Distribution of Cholinergic Nerves in Rat Mediastinal Brown Adipose Tissue: *Http://Dx.Doi.Org/10.1369/Jhc.3A6246.2004*, *52*(7), 923–930. https://doi.org/10.1369/JHC.3A6246.2004

Goedert, M., & Spillantini, M. G. (2011). Pathogenesis of the tauopathies. *Journal of Molecular Neuroscience*, *45*(3), 425–431. https://doi.org/10.1007/s12031-011-9593-4

Goodwin, G. M., McCloskey, D. I., & Mitchell, J. H. (1972). Cardiovascular and respiratory responses to changes in central command during isometric exercise at constant muscle tension. *The Journal of Physiology*, *226*(1), 173. https://doi.org/10.1113/JPHYSIOL.1972.SP009979

Grailer, J. J., Haggadone, M. D., Sarma, J. V., Zetoune, F. S., & Ward, P. A. (2014). Induction of M2 regulatory macrophages through the β2- Adrenergic receptor with protection during endotoxemia and acute lung injury. *Journal of Innate Immunity*, *6*(5), 607–618.

https://doi.org/10.1159/000358524

Grigg, G. C., Beard, L. A., & Augee, M. L. (2004). The evolution of endothermy and its diversity in mammals and birds. *Physiological and Biochemical Zoology*, *77*(6), 982–997. https://doi.org/10.1086/425188

Gros, R., Benovic, J. L., Tan, C. M., & Feldman, R. D. (1997). G-protein-coupled receptor kinase activity is increased in hypertension. *Journal of Clinical Investigation*, *99*(9), 2087–2093. https://doi.org/10.1172/JCI119381

Guisle, I., Gratuze, M., Petry, S., Morin, F., Keraudren, R., Whittington, R. A., Hébert, S. S., Mongrain, V., & Planel, E. (2020). Circadian and sleep/wake-dependent variations in tau phosphorylation are driven by temperature. *Sleep*, *43*(4). https://doi.org/10.1093/sleep/zsz266

Hammond, K. A., & Diamond, J. (1997). Maximal sustained energy budgets in humans and animals. *Nature 1997 386:6624*, *386*(6624), 457–462. https://doi.org/10.1038/386457a0

Harding, E.C., Franks, N.P., Wisden, W. Sleep and thermoregulation. *Current Opinion in Physiology*, 15, 7-13. 10.1016/j.cophys.2019.11.008

Harris, M. B., & Milsom, W. K. (1995). Parasympathetic influence on heart rate in euthermic and hibernating ground squirrels. *Journal of Experimental Biology*, *198*(4), 931–937. https://doi.org/10.1242/JEB.198.4.931

Härtig, W., Stieler, J., Boerema, A. S., Wolf, J., Schmidt, U., Weißfuß, J., Bullmann, T., Strijkstra, A. M., & Arendt, T. (2007). Hibernation model of tau phosphorylation in hamsters: Selective vulnerability of cholinergic basal forebrain neurons - Implications for Alzheimer's disease. *European Journal of Neuroscience*, *25*(1), 69–80. https://doi.org/10.1111/j.1460-9568.2006.05250.x

Hayward, L. F., Mueller, P. J., & Hasser, E. M. (2004). Adrenergic Receptors. In *Encyclopedia of Endocrine Diseases* (pp. 112–115). Elsevier. https://doi.org/10.1016/B0-12-475570-4/00039-1

Haziot, A., Ferrero, E., Köntgen, F., Hijiya, N., Yamamoto, S., Silver, J., Stewart, C. L., & Goyert, S. M. (1996). Resistance to endotoxin shock and reduced dissemination of gram-negative bacteria in CD14-deficient mice. *Immunity*, *4*(4), 407–414. https://doi.org/10.1016/S1074-7613(00)80254-X

Heldmaier, G., Ortmann, S., & Elvert, R. (2004). Natural hypometabolism during hibernation and daily torpor in mammals. *Respiratory Physiology and Neurobiology*, *141*(3), 317–329. https://doi.org/10.1016/j.resp.2004.03.014

Hernandez, F., Lucas, J. J., & Avila, J. (2013). GSK3 and tau: Two convergence points in Alzheimer's disease. *Journal of Alzheimer's Disease*, *33*(SUPPL. 1). https://doi.org/10.3233/JAD-2012-129025

Herrera-Arozamena, C., Martí-Marí, O., Estrada, M., Revenga, M. de la F., & Rodríguez-Franco, M. I. (2016). Recent Advances in Neurogenic Small Molecules as Innovative Treatments for Neurodegenerative Diseases. *Molecules*, *21*(9). https://doi.org/10.3390/MOLECULES21091165

Hitrec, T., Luppi, M., Bastianini, S., Squarcio, F., Berteotti, C., Martire, V. Lo, Martelli, D., Occhinegro, A., Tupone, D., Zoccoli, G., Amici, R., & Cerri, M. (2019). Neural control of fasting-induced torpor in mice. *Scientific Reports 2019 9:1*, *9*(1), 1–12. https://doi.org/10.1038/s41598-019-51841-2

Hitrec, T., Squarcio, F., Cerri, M., Martelli, D., Occhinegro, A., Piscitiello, E., Tupone, D., Amici, R., & Luppi, M. (2021). Reversible Tau Phosphorylation Induced by Synthetic Torpor in the Spinal Cord of the Rat. *Frontiers in Neuroanatomy*, *0*, 3. https://doi.org/10.3389/FNANA.2021.592288

Holbrook, J., Lara-Reyna, S., Jarosz-Griffiths, H., & McDermott, M. (2019). Tumour necrosis factor signalling in health and disease [version 1; referees: 2 approved]. In *F1000Research* (Vol. 8). F1000 Research Ltd. https://doi.org/10.12688/f1000research.17023.1

Holcik, M., & Korneluk, R. G. (2001). XIAP, the guardian angel. *Nature Reviews Molecular Cell Biology*, *2*(7), 550–556. https://doi.org/10.1038/35080103

Holth, J. K., Fritschi, S. K., Wang, C., Pedersen, N. P., Cirrito, J. R., Mahan, T. E., Finn, M. B., Manis, M., Geerling, J. C., Fuller, P. M., Lucey, B. P., & Holtzman, D. M. (2019). The sleep-wake cycle regulates brain interstitial fluid tau in mice and CSF tau in humans. *Science*, *363*(6429), 880–884. https://doi.org/10.1126/SCIENCE.AAV2546

Hoshino, K., Takeuchi, O., Kawai, T., Sanjo, H., Ogawa, T., Takeda, Y., Takeda, K., & Akira, S. (1999). Cutting Edge: Toll-Like Receptor 4 (TLR4)-Deficient Mice Are Hyporesponsive to Lipopolysaccharide: Evidence for TLR4 as the Lps Gene Product. *The Journal of Immunology*, *162*(7).

Hosoya, Y., Sugiura, Y., Ito, R., & Kohno, K. (1990). Descending projections from the hypothalamic paraventricular nucleus to the A5 area, including the superior salivatory nucleus, in the rat. *Experimental Brain Research 1990 82:3*, *82*(3), 513–518. https://doi.org/10.1007/BF00228793

Hrvatin, S., Sun, S., Wilcox, O. F., Yao, H., Lavin-Peter, A. J., Cicconet, M., Assad, E. G., Palmer, M. E., Aronson, S., Banks, A. S., Griffith, E. C., & Greenberg, M. E. (2020). Neurons that regulate mouse torpor. *Nature 2020 583:7814*, *583*(7814), 115–121. https://doi.org/10.1038/s41586-020-2387-5

Huang, S., Ziegler, C. G. K., Austin, J., Mannoun, N., Vukovic, M., Ordovas-Montanes, J., Shalek, A. K., & von Andrian, U. H. (2021). Lymph nodes are innervated by a unique population of sensory neurons with immunomodulatory potential. *Cell*, *184*(2), 441-459.e25. https://doi.org/10.1016/j.cell.2020.11.028

Huber, R., Ghilardi, M. F., Massimini, M., & Tononi, G. (2004). Local sleep and learning. *Nature*, *430*(6995), 78–81. https://doi.org/10.1038/nature02663

Huber, R., Mäki, H., Rosanova, M., Casarotto, S., Canali, P., Casali, A. G., Tononi, G., & Massimini, M. (2013). Human cortical excitability increases with time awake. *Cerebral Cortex*, *23*(2), 332–338. https://doi.org/10.1093/cercor/bhs014

Hylkema, M. N., & Bouma, H. R. (2011). Reversible remodeling of lung tissue during hibernation in the Syrian hamster Mimicking hibernation to prevent mitochondrial injury in sepsis View project Hibernation View project. *Article in Journal of Experimental*

Biology. https://doi.org/10.1242/jeb.052704

Ibrahim, I. M., Abdelmalek, D. H., & Elfiky, A. A. (2019). GRP78: A cell's response to stress. *Life Sciences*, *226*, 156–163. https://doi.org/10.1016/j.lfs.2019.04.022

Ittner, A., Chua, S. W., Bertz, J., Volkerling, A., Van Der Hoven, J., Gladbach, A., Przybyla, M., Bi, M., Van Hummel, A., Stevens, C. H., Ippati, S., Suh, L. S., Macmillan, A., Sutherland, G., Kril, J. J., Silva, A. P. G., Mackay, J., Poljak, A., Delerue, F., … Ittner, L. M. (2016). Site-specific phosphorylation of tau inhibits amyloid-β toxicity in Alzheimer's mice. *Science*, *354*(6314), 904–908. https://doi.org/10.1126/science.aah6205

Janig, W. (2008) Integrative Action of the Autonomic Nervous System: Neurobiology of Homeostasis. *Cambridge University Press*

Jordt, S.E., McKemy, D.D., Julius, D. (2003). Lessons from peppers and peppermint: themolecular logic of thermosensation. *Current Opinion in Neurobiology*, 13, 487–49. https://doi.org/10.1016/S0959-4388(03)00101-6

Josephs, K. A., Murray, M. E., Tosakulwong, N., Whitwell, J. L., Knopman, D. S., Machulda, M. M., Weigand, S. D., Boeve, B. F., Kantarci, K., Petrucelli, L., Lowe, V. J., Jack, C. R., Petersen, R. C., Parisi, J. E., & Dickson, D. W. (2017). Tau aggregation influences cognition and hippocampal atrophy in the absence of beta-amyloid: a clinico-imaging-pathological study of primary age-related tauopathy (PART). *Acta Neuropathologica*, *133*(5), 705–715. https://doi.org/10.1007/s00401-017-1681-2

Katzung, B. (2018). *Basic & Clinical Pharmacology Fourteenth Edition a LANGE medical book Want more papers like this?*

Kawai, T., & Akira, S. (2010). The role of pattern-recognition receptors in innate immunity: Update on toll-like receptors. In *Nature Immunology* (Vol. 11, Issue 5, pp. 373–384). Nature Publishing Group. https://doi.org/10.1038/ni.1863

Kempf, M., Clement, A., Faissner, A., Lee, G., & Brandt, R. (1996). Tau binds to the distal axon early in development of polarity in a microtubule- and microfilament-dependent manner. *Journal of Neuroscience*, *16*(18), 5583–5592. https://doi.org/10.1523/jneurosci.16-18-05583.1996

Kenney, M., & Ganta, C. (2014). Autonomic Nervous System and Immune System Interactions. *Comprehensive Physiology*, *4*(3), 1177. https://doi.org/10.1002/CPHY.C130051

Kieser, K. J., & Kagan, J. C. (2017). Multi-receptor detection of individual bacterial products by the innate immune system. In *Nature Reviews Immunology* (Vol. 17, Issue 6, pp. 376–390). Nature Publishing Group. https://doi.org/10.1038/nri.2017.25

Kilduff, T. S., Radeke, C. M., Randall, T. L., Sharp, F. R., & Heller, H. C. (1989). Suprachiasmatic nucleus: Phase-dependent activation during the hibernation cycle. *American Journal of Physiology - Regulatory Integrative and Comparative Physiology*, *257*(3). https://doi.org/10.1152/ajpregu.1989.257.3.r605

Kirov, S. A., Petrak, L. J., Fiala, J. C., & Harris, K. M. (2004). Dendritic spines disappear with chilling but proliferate excessively upon rewarming of mature hippocampus. *Neuroscience*, *127*(1), 69–80. https://doi.org/10.1016/j.neuroscience.2004.04.053

Kooijman, S., van den Heuvel, J. K., & Rensen, P. C. N. (2015). Neuronal Control of Brown Fat Activity. *Trends in Endocrinology and Metabolism*, *26*(11), 657–668. https://doi.org/10.1016/j.tem.2015.09.008

Körtner, G., & Geiser, F. (2000). The temporal organization of daily torpor and hibernation: Circadian and circannual rhythms. *Chronobiology International*, *17*(2), 103–128. https://doi.org/10.1081/CBI-100101036

Kovacs, G. G. (2018). Tauopathies. *Handbook of Clinical Neurology*, *145*, 355–368. https://doi.org/10.1016/B978-0-12-802395-2.00025-0

Kox, M., Eijk, L. T. van, Zwaag, J., Wildenberg, J. van den, Sweep, F. C. G. J., Hoeven, J. G. van der, & Pickkers, P. (2014). Voluntary activation of the sympathetic nervous system and attenuation of the innate immune response in humans. *Proceedings of the National Academy of Sciences of the United States of America*, *111*(20), 7379. https://doi.org/10.1073/PNAS.1322174111

Lankadeva, Y. R., May, C. N., McKinley, M. J., Neeland, M. R., Ma, S., Hocking, D. M., Robins-Browne, R., Bedoui, S., Farmer, D. G. S., Bailey, S. R., Martelli, D., & McAllen, R. M. (2020a). Sympathetic nerves control bacterial clearance. *Scientific Reports*, *10*(1). https://doi.org/10.1038/s41598-020-72008-4

Lankadeva, Y. R., May, C. N., McKinley, M. J., Neeland, M. R., Ma, S., Hocking, D. M., Robins-Browne, R., Bedoui, S., Farmer, D. G. S., Bailey, S. R., Martelli, D., & McAllen, R. M. (2020b). Sympathetic nerves control bacterial clearance. *Scientific Reports*, *10*(1). https://doi.org/10.1038/s41598-020-72008-4

Larkin, J. E., & Heller, H. C. (1996). Temperature sensitivity of sleep homeostasis during hibernation in the golden-mantled ground squirrel. *American Journal of Physiology - Regulatory Integrative and Comparative Physiology*, *270*(4 39-4). https://doi.org/10.1152/ajpregu.1996.270.4.r777

Larkin, Jennie E., & Heller, H. C. (1999). Sleep after arousal from hibernation is not homeostatically regulated. *Https://Doi.Org/10.1152/Ajpregu.1999.276.2.R522*, *276*(2 45-2), 522–529. https://doi.org/10.1152/AJPREGU.1999.276.2.R522

Larkin, Jennie E., Yellon, S. M., & Zucker, I. (2003). Melatonin Production Accompanies Arousal from Daily Torpor in Siberian Hamsters. *Physiological and Biochemical Zoology*, *76*(4), 577–585. https://doi.org/10.1086/375436

Lee, J. G., Woo, Y. S., Park, S. W., Seog, D.-H., Seo, M. K., & Bahk, W.-M. (2019). The Neuroprotective Effects of Melatonin: Possible Role in the Pathophysiology of Neuropsychiatric Disease. *Brain Sciences*, *9*(10). https://doi.org/10.3390/BRAINSCI9100285

Lesort, M., Blanchard, C., Yardin, C., Esclaire, F., & Hugon, J. (1997). Cultured neurons expressing phosphorylated tau are more resistant to apoptosis induced by NMDA or serum deprivation. *Molecular Brain Research*, *45*(1), 127–132. https://doi.org/10.1016/S0169-328X(96)00284-7

Leung, J. W. H., Cheung, K. K., Ngai, S. P. C., Tsang, H. W. H., & Lau, B. W. M. (2020). Protective effects of melatonin on neurogenesis impairment in neurological disorders and

its relevant molecular mechanisms. *International Journal of Molecular Sciences*, *21*(16), 1–30. https://doi.org/10.3390/ijms21165645

Levenga, J., Wong, H., Milstead, R. A., Keller, B. N., Laplante, L. E., & Hoeffer, C. A. (2017). AKT isoforms have distinct hippocampal expression and roles in synaptic plasticity. *ELife*, *6*. https://doi.org/10.7554/ELIFE.30640

Lidell, M. E., Betz, M. J., Leinhard, O. D., Heglind, M., Elander, L., Slawik, M., Mussack, T., Nilsson, D., Romu, T., Nuutila, P., Virtanen, K. A., Beuschlein, F., Persson, A., Borga, M., & Enerbäck, S. (2013). Evidence for two types of brown adipose tissue in humans. *Nature Medicine*, *19*(5), 631–634. https://doi.org/10.1038/nm.3017

Litersky, J. M., & Johnson, G. V. W. (1992). Phosphorylation by cAMP-dependent protein kinase inhibits the degradation of tau by calpain. *Journal of Biological Chemistry*, *267*(3), 1563–1568. https://doi.org/10.1016/S0021-9258(18)45982-0

Liu, D., Wei, N., Man, H.-Y., Lu, Y., Zhu, L.-Q., & Wang, J.-Z. (2014). The MT2 receptor stimulates axonogenesis and enhances synaptic transmission by activating Akt signaling. *Cell Death & Differentiation 2015 22:4*, *22*(4), 583–596. https://doi.org/10.1038/CDD.2014.195

Lo Martire, V., Berteotti, C., Bastianini, S., Alvente, S., Valli, A., Cerri, M., Amici, R., Silvani, A., Swoap, S. J., & Zoccoli, G. (2020). The physiological signature of daily torpor is not orexin dependent. *Journal of Comparative Physiology B: Biochemical, Systemic, and Environmental Physiology*, *190*(4), 493–507. https://doi.org/10.1007/s00360-020-01281-6

Lorton, D., Bellinger, D., Duclos, M., Felten, S. Y., & Felten, D. L. (1996). Application of 6-hydroxydopamine into the fatpads surrounding the draining lymph nodes exacerbates adjuvant-induced arthritis. *Journal of Neuroimmunology*, *64*(2), 103–113. https://doi.org/10.1016/0165-5728(95)00150-6

Lorton, D., Lubahn, C., Klein, N., Schaller, J., & Bellinger, D. L. (1999). Dual role for noradrenergic innervation of lymphoid tissue and arthritic joints in adjuvant-induced arthritis. *Brain, Behavior, and Immunity*, *13*(4), 315–334. https://doi.org/10.1006/brbi.1999.0564

Lowry, O. H., Rosebrough, N. J., Farr, A. L., & Randall, R. J. (1951). Protein measurement with the Folin phenol reagent. *The Journal of Biological Chemistry*, *193*(1), 265–275. https://doi.org/10.1016/s0021-9258(19)52451-6

Luppi, M., Hitrec, T., Di Cristoforo, A., Squarcio, F., Stanzani, A., Occhinegro, A., Chiavetta, P., Tupone, D., Zamboni, G., Amici, R., & Cerri, M. (2019a). Phosphorylation and dephosphorylation of tau protein during synthetic torpor. *Frontiers in Neuroanatomy*, *13*. https://doi.org/10.3389/fnana.2019.00057

Luppi, M., Hitrec, T., Di Cristoforo, A., Squarcio, F., Stanzani, A., Occhinegro, A., Chiavetta, P., Tupone, D., Zamboni, G., Amici, R., & Cerri, M. (2019b). Phosphorylation and dephosphorylation of tau protein during synthetic torpor. *Frontiers in Neuroanatomy*, *13*, 57. https://doi.org/10.3389/fnana.2019.00057

Luppi, M., Martelli, D., Amici, R., Baracchi, F., Cerri, M., Dentico, D., Perez, E., & Zamboni,

G. (2010). Hypothalamic osmoregulation is maintained across the wake–sleep cycle in the rat. *Journal of Sleep Research*, *19*(3), 394–399. https://doi.org/10.1111/J.1365-2869.2009.00810.X

Madden, C. J., & Morrison, S. F. (2019). Central nervous system circuits that control body temperature. *Neuroscience Letters*, *696*, 225–232. https://doi.org/10.1016/j.neulet.2018.11.027

Magoun, H. W., Harrison, F., Brobeck, J. R., & Ranson, S. W. (1938). Activation Of Heat Loss Mechanisms By Local Heating Of The Brain. *Https://Doi.Org/10.1152/Jn.1938.1.2.101*, *1*(2), 101–114. https://doi.org/10.1152/JN.1938.1.2.101

Malia, T. J., Teplyakov, A., Ernst, R., Wu, S. J., Lacy, E. R., Liu, X., Vandermeeren, M., Mercken, M., Luo, J., Sweet, R. W., & Gilliland, G. L. (2016). Epitope mapping and structural basis for the recognition of phosphorylated tau by the anti-tau antibody AT8. *Proteins: Structure, Function and Bioinformatics*, *84*(4), 427–434. https://doi.org/10.1002/prot.24988

Marshall, C. J. (1997). Cold-adapted enzymes. *Trends in Biotechnology*, *15*(9), 359–364. https://doi.org/10.1016/S0167-7799(97)01086-X

Marshall, J. S., Warrington, R., Watson, W., & Kim, H. L. (2018). An introduction to immunology and immunopathology. In *Allergy, Asthma and Clinical Immunology* (Vol. 14, Issue Suppl 2). BioMed Central Ltd. https://doi.org/10.1186/s13223-018-0278-1

Martelli, D., Farmer, D. G. S., & Yao, S. T. (2016). The splanchnic anti-inflammatory pathway: could it be the efferent arm of the inflammatory reflex? *Experimental Physiology*, *101*(10), 1245–1252. https://doi.org/10.1113/EP085559

Martelli, D., McKinley, M. J., & McAllen, R. M. (2014). The cholinergic anti-inflammatory pathway: A critical review. *Autonomic Neuroscience: Basic and Clinical*, *182*, 65–69. https://doi.org/10.1016/j.autneu.2013.12.007

Martelli, D., Yao, S. T., Mckinley, M. J., & Mcallen, R. M. (2014). Reflex control of inflammation by sympathetic nerves, not the vagus. *Journal of Physiology*, *592*(7), 1677–1686. https://doi.org/10.1113/jphysiol.2013.268573

Martelli, D., Farmer, D. G. S., McKinley, M. J., Yao, S. T., & McAllen, R. M. (2019a). Anti-inflammatory reflex action of splanchnic sympathetic nerves is distributed across abdominal organs. *American Journal of Physiology - Regulatory Integrative and Comparative Physiology*, *316*(3), R235–R242. https://doi.org/10.1152/ajpregu.00298.2018

Martelli, D., Farmer, D. G. S., McKinley, M. J., Yao, S. T., & McAllen, R. M. (2019b). Anti-inflammatory reflex action of splanchnic sympathetic nerves is distributed across abdominal organs. *American Journal of Physiology - Regulatory Integrative and Comparative Physiology*, *316*(3), R235–R242. https://doi.org/10.1152/ajpregu.00298.2018

Martelli, D., Yao, S. T., Mancera, J., McKinley, M. J., & McAllen, R. M. (2014). Reflex control of inflammation by the splanchnic anti-inflammatory pathway is sustained and independent of anesthesia. *American Journal of Physiology - Regulatory Integrative and*

Comparative Physiology, *307*(9), R1085–R1091. https://doi.org/10.1152/ajpregu.00259.2014

Mayo, J. C., Sainz, R. M., Antolín, I., Herrera, F., Martin, V., & Rodriguez, C. (2002). Melatonin regulation of antioxidant enzyme gene expression. *Cellular and Molecular Life Sciences*, *59*(10), 1706–1713. https://doi.org/10.1007/PL00012498

McCarron, R. M., Sieckmann, D. G., Yu, E. Z., Frerichs, K., & Hallenbeck, J. M. (2001). *Hibernation, a State of Natural Tolerance to Profound Reduction in Organ Blood Flow and Oxygen Delivery Capacity*. https://apps.dtic.mil/sti/citations/ADA405751

McCorry, L. K. (2007). Physiology of the autonomic nervous system. *American Journal of Pharmaceutical Education*, *71*(4). https://doi.org/10.5688/aj710478

McDougall, S. J., Münzberg, H., Derbenev, A. V., & Zsombok, A. (2014). Central control of autonomic functions in health and disease. *Frontiers in Neuroscience*, *8*(JAN). https://doi.org/10.3389/FNINS.2014.00440

McKechnie, A. E., & Lovegrove, B. G. (2002). Avian Facultative Hypothermic Responses: A Review. *The Condor*, *104*(4), 705–724. https://doi.org/10.1093/CONDOR/104.4.705

Medzhitov, R. (2001). Toll-like receptors and innate immunity. In *Nature Reviews Immunology* (Vol. 1, Issue 2, pp. 135–145). European Association for Cardio-Thoracic Surgery. https://doi.org/10.1038/35100529

Meerlo, P., Sgoifo, A., & Suchecki, D. (2008). Restricted and disrupted sleep: Effects on autonomic function, neuroendocrine stress systems and stress responsivity. *ARTICLE IN PRESS Sleep Medicine Reviews*, *12*, 197–210. https://doi.org/10.1016/j.smrv.2007.07.007

Meltzer, S. J., & Meltzer, C. (1903). On a Difference in the Influence upon Inflammation between the Section of the Sympathetic Nerve and the Removal of the sympathetic Ganglion. *The Journal of Medical Research*, *10*(1), 135. https://www.ncbi.nlm.nih.gov/pmc/articles/PMC2105951/

Melvin, R. G., & Andrews, M. T. (2009). Torpor induction in mammals: Recent discoveries fueling new ideas. *Trends in Endocrinology and Metabolism: TEM*, *20*(10), 490. https://doi.org/10.1016/J.TEM.2009.09.005

Miyake, K., Yamashita, Y., Ogata, M., Sudo, T., & Kimoto, M. (1995). RP105, a novel B cell surface molecule implicated in B cell activation, is a member of the leucine-rich repeat protein family. *The Journal of Immunology*, *154*(7).

Moreno, J. A., & Tiffany-Castiglioni, E. (2015). The Chaperone Grp78 in Protein Folding Disorders of the Nervous System. *Neurochemical Research*, *40*(2), 329–335. https://doi.org/10.1007/s11064-014-1405-0

Morrison, S. F., & Nakamura, K. (2011a). Central neural pathways for thermoregulation. *Frontiers in Bioscience : A Journal and Virtual Library*, *16*(1), 74. /pmc/articles/PMC3051412/

Morrison, S. F., & Nakamura, K. (2011b). Central neural pathways for thermoregulation. *Frontiers in Bioscience : A Journal and Virtual Library*, *16*(1), 74.

/pmc/articles/PMC3051412/

Morrison, S. F., Nakamura, K., & Madden, C. J. (2008). Central control of thermogenesis in mammals. *Experimental Physiology*, *93*(7), 773–797. https://doi.org/10.1113/expphysiol.2007.041848

Morrison, S. F., Sved, A. F., & Passerin, A. M. (1999). GABA-mediated inhibition of raphe pallidus neurons regulates sympathetic outflow to brown adipose tissue. *American Journal of Physiology - Regulatory Integrative and Comparative Physiology*, *276*(2 45-2). https://doi.org/10.1152/ajpregu.1999.276.2.r290

Muñoz-Wolf, N., & Lavelle, E. C. (2016). Innate immune receptors. In *Methods in Molecular Biology* (Vol. 1417, pp. 1–43). Humana Press Inc. https://doi.org/10.1007/978-1-4939-3566-6_1

Nakamura, K., Matsumura, K., Kaneko, T., Kobayashi, S., Katoh, H., & Negishi, M. (2002). The Rostral Raphe Pallidus Nucleus Mediates Pyrogenic Transmission from the Preoptic Area. *Journal of Neuroscience*, *22*(11), 4600–4610. https://doi.org/10.1523/JNEUROSCI.22-11-04600.2002

Nakamura, K., Matsumura, K., Kobayashi, S., & Kaneko, T. (2005). Sympathetic premotor neurons mediating thermoregulatory functions. *Neuroscience Research*, *51*(1), 1–8. https://doi.org/10.1016/j.neures.2004.09.007

Nakamura, K., & Morrison, S. F. (2007). Central efferent pathways mediating skin cooling-evoked sympathetic thermogenesis in brown adipose tissue. *American Journal of Physiology - Regulatory Integrative and Comparative Physiology*, *292*(1). https://doi.org/10.1152/ajpregu.00427.2006

Nakamura, K., & Morrison, S. F. (2008). A thermosensory pathway that controls body temperature. *Nature Neuroscience*, *11*(1), 62–71. https://doi.org/10.1038/nn2027

Nakamura, K., & Morrison, S. F. (2010). A thermosensory pathway mediating heat-defense responses. *Proceedings of the National Academy of Sciences*, *107*(19), 8848–8853. https://doi.org/10.1073/PNAS.0913358107

Nance, D. M., & Sanders, V. M. (2007). Autonomic innervation and regulation of the immune system (1987-2007). *Brain, Behavior, and Immunity*, *21*(6), 736–745. https://doi.org/10.1016/j.bbi.2007.03.008

Nathan, C. (2002). Points of control in inflammation. *Nature*, *420*(6917), 846–852. https://doi.org/10.1038/nature01320

Netea, M. G., Balkwill, F., Chonchol, M., Cominelli, F., Donath, M. Y., Giamarellos-Bourboulis, E. J., Golenbock, D., Gresnigt, M. S., Heneka, M. T., Hoffman, H. M., Hotchkiss, R., Joosten, L. A. B., Kastner, D. L., Korte, M., Latz, E., Libby, P., Mandrup-Poulsen, T., Mantovani, A., Mills, K. H. G., … Dinarello, C. A. (2017). A guiding map for inflammation. In *Nature Immunology* (Vol. 18, Issue 8, pp. 826–831). Nature Publishing Group. https://doi.org/10.1038/ni.3790

Ng, K. Y., Leong, M. K., Liang, H., & Paxinos, G. (2017). Melatonin receptors: distribution in mammalian brain and their respective putative functions. *Brain Structure and Function*,

222(7), 2921–2939. https://doi.org/10.1007/s00429-017-1439-6

Nie, X., Li, C., Hu, S., Xue, F., Kang, Y. J., & Zhang, W. (2017). An appropriate loading control for western blot analysis in animal models of myocardial ischemic infarction. *Biochemistry and Biophysics Reports*, *12*, 108. https://doi.org/10.1016/J.BBREP.2017.09.001

Nijhuis, L. E., Olivier, B. J., Dhawan, S., Hilbers, F. W., Boon, L., Wolkers, M. C., Samsom, J. N., & Jonge, W. J. de. (2014). Adrenergic β2 Receptor Activation Stimulates Anti-Inflammatory Properties of Dendritic Cells In Vitro. *PLOS ONE*, *9*(1), e85086. https://doi.org/10.1371/JOURNAL.PONE.0085086

Norimoto, H., Makino, K., Gao, M., Shikano, Y., Okamoto, K., Ishikawa, T., Sasaki, T., Hioki, H., Fujisawa, S., & Ikegaya, Y. (2018). Hippocampal ripples down-regulate synapses. *Science*, *359*(6383), 1524–1527. https://doi.org/10.1126/SCIENCE.AAO0702

O'Hara, B. F., Watson, F. L., Srere, H. K., Kumar, H., Wiler, S. W., Welch, S. K., Bitting, L., Heller, H. C., & Kilduff, T. S. (1999). Gene Expression in the Brain across the Hibernation Cycle. *Journal of Neuroscience*, *19*(10), 3781–3790. https://doi.org/10.1523/JNEUROSCI.19-10-03781.1999

O'Neill, L. A. J., Golenbock, D., & Bowie, A. G. (2013). The history of Toll-like receptors-redefining innate immunity. In *Nature Reviews Immunology* (Vol. 13, Issue 6, pp. 453–460). Nat Rev Immunol. https://doi.org/10.1038/nri3446

Ognjanovski, N., Maruyama, D., Lashner, N., Zochowski, M., & Aton, S. J. (2014). CA1 hippocampal network activity changes during sleep-dependent memory consolidation. *Frontiers in Systems Neuroscience*, *0*(1 APR), 61. https://doi.org/10.3389/FNSYS.2014.00061

Ohe, C. G. von der, Darian-Smith, C., Garner, C. C., & Heller, H. C. (2006). Ubiquitous and Temperature-Dependent Neural Plasticity in Hibernators. *Journal of Neuroscience*, *26*(41), 10590–10598. https://doi.org/10.1523/JNEUROSCI.2874-06.2006

Olcese, J. (2003). Circadian signaling in the chick pineal organ. *Chronobiology International*, *20*(4), 617–636. https://doi.org/10.1081/CBI-120022409

Ondicova, K., & Mravec, B. (2010). Multilevel interactions between the sympathetic and parasympathetic nervous systems: A minireview. *Endocrine Regulations*, *44*(2), 69–75. https://doi.org/10.4149/endo_2010_02_69

Ootsuka, Y., & Blessing, W. W. (2005). Activation of slowly conducting medullary raphé-spinal neurons, including serotonergic neurons, increases cutaneous sympathetic vasomotor discharge in rabbit. *American Journal of Physiology - Regulatory Integrative and Comparative Physiology*, *288*(4 57-4). https://doi.org/10.1152/AJPREGU.00564.2004

Ootsuka, Y., & Terui, N. (1997). Functionally different neurons are organized topographically in the rostral ventrolateral medulla of rabbits. *Journal of the Autonomic Nervous System*, *67*(1–2), 67–78. https://doi.org/10.1016/S0165-1838(97)00094-5

Ordovas-Montanes, J., Rakoff-Nahoum, S., Huang, S., Riol-Blanco, L., Barreiro, O., & von

Andrian, U. H. (2015). The Regulation of Immunological Processes by Peripheral Neurons in Homeostasis and Disease. *Trends in Immunology*, *36*(10), 578–604. https://doi.org/10.1016/j.it.2015.08.007

Parmeggiani, P. L. (2005). Physiologic regulation in sleep. In Principles and Practice of Sleep Medicine, 5th Edition. https://doi.org/10.1016/C2009-0-59875-3

Paxinos, G., & Watson, C. (2007). *The rat brain in stereotaxic coordinates*.

Pengelley, E. T., Asmundson, S. J., Barnes, B., & Aloia, R. C. (1976). Relationship of light intensity and photoperiod to circannual rhythmicity in the hibernating ground squirrel, Citellus lateralis. *Comparative Biochemistry and Physiology Part A: Physiology*, *53*(3), 273–277. https://doi.org/10.1016/S0300-9629(76)80035-7

Planel, E., Miyasaka, T., Launey, T., Chui, D. H., Tanemura, K., Sato, S., Murayama, O., Ishiguro, K., Tatebayashi, Y., & Takashima, A. (2004). Alterations in Glucose Metabolism Induce Hypothermia Leading to Tau Hyperphosphorylation through Differential Inhibition of Kinase and Phosphatase Activities: Implications for Alzheimer's Disease. *Journal of Neuroscience*, *24*(10), 2401–2411. https://doi.org/10.1523/JNEUROSCI.5561-03.2004

Planel, E., Richter, K.E.G., Nolan, C.E., Finley, J.E., Liu, L., Wen,Y., Krishnamurthy, P., Herman, M., Wang, L., Schachter, J.B., Nelson, R.B., Lau, L.F., & Duff, K.E. (2007). Anesthesia Leads to Tau Hyperphosphorylation through Inhibition of Phosphatase Activity by Hypothermia. Journal of Neuroscience, 27 (12), 3090-3097. DOI: https://doi.org/10.1523/JNEUROSCI.4854-06.2007

Pongratz, G., & Straub, R. H. (2014). The sympathetic nervous response in inflammation. *Arthritis Research & Therapy*, *16*(1). https://doi.org/10.1186/S13075-014-0504-2

Popov, V. I., Bocharova, L. S., & Bragin, A. G. (1992). Repeated changes of dendritic morphology in the hippocampus of ground squirrels in the course of hibernation. *Neuroscience*, *48*(1), 45–51. https://doi.org/10.1016/0306-4522(92)90336-Z

Porter, A. G., & Jänicke, R. U. (1999). Emerging roles of caspase-3 in apoptosis. *Cell Death and Differentiation*, *6*(2), 99–104. https://doi.org/10.1038/sj.cdd.4400476

Puentes-Mestril, C., & Aton, S. J. (2017). Linking network activity to synaptic plasticity during sleep: Hypotheses and recent data. *Frontiers in Neural Circuits*, *11*. https://doi.org/10.3389/fncir.2017.00061

Purves, D., Augustine, G. J., Fitzpatrick, D., Katz, L. C., LaMantia, A.-S., McNamara, J. O., & Williams, S. M. (2001). *The Biogenic Amines*. https://www.ncbi.nlm.nih.gov/books/NBK11035/

Quinn, G.P., & Keough, M.J. (2002). Experimental Design and Data Analysis for Biologists. Cambridge University Press.

Ran, C., Hoon, M. A., & Chen, X. (2016). The Coding of Cutaneous Temperature in the Spinal Cord. *Nature Neuroscience*, *19*(9), 1201. https://doi.org/10.1038/NN.4350

Riganello, F., Prada, V., Soddu, A., Perri, C. di, & Sannita, W. G. (2019). Circadian Rhythms

and Measures of CNS/Autonomic Interaction. *International Journal of Environmental Research and Public Health*, *16*(13). https://doi.org/10.3390/IJERPH16132336

Risso, G., Blaustein, M., Pozzi, B., Mammi, P., & Srebrow, A. (2015). Akt/PKB: One kinase, many modifications. *Biochemical Journal*, *468*(2), 203–214. https://doi.org/10.1042/BJ20150041

Romanovsky, A. A. (2018). The thermoregulation system and how it works. *Handbook of Clinical Neurology*, *156*, 3–43. https://doi.org/10.1016/B978-0-444-63912-7.00001-1

Rosas-Ballina, M., & Tracey, K. J. (2009). Cholinergic control of inflammation. *Journal of Internal Medicine*, *265*(6), 663–679. https://doi.org/10.1111/J.1365-2796.2009.02098.X

Roy, H. A., & Green, A. L. (2019). The central autonomic network and regulation of bladder function. In *Frontiers in Neuroscience* (Vol. 13, Issue JUN, p. 535). Frontiers Media S.A. https://doi.org/10.3389/fnins.2019.00535

Royo, J., Aujard, F., & Pifferi, F. (2019). Daily Torpor and Sleep in a Non-human Primate, the Gray Mouse Lemur (Microcebus murinus). *Frontiers in Neuroanatomy*, *0*, 87. https://doi.org/10.3389/FNANA.2019.00087

Ruby, N. F., Dark, J., Heller, H. C., & Zucker, I. (1998). Suprachiasmatic nucleus: Role in circannual body mass and hibernation rhythms of ground squirrels. *Brain Research*, *782*(1–2), 63–72. https://doi.org/10.1016/S0006-8993(97)01263-8

Ruf, T., & Geiser, F. (2015). Daily torpor and hibernation in birds and mammals. *Biological Reviews*, *90*(3), 891–926. https://doi.org/10.1111/BRV.12137

Saaresranta, T., & Polo, O. (2003). Sleep-disordered breathing and hormones. *European Respiratory Journal*, *22*(1), 161–172. https://doi.org/10.1183/09031936.03.00062403

Saeed, Y., & Abbott, S. M. (2017). Circadian Disruption Associated with Alzheimer's Disease. *Current Neurology and Neuroscience Reports*, *17*(4). https://doi.org/10.1007/s11910-017-0745-y

Samanta, A., Hughes, T. E. T., & Moiseenkova-Bell, V. Y. (2018). Transient Receptor Potential (TRP) Channels. *Sub-Cellular Biochemistry*, *87*, 141. https://doi.org/10.1007/978-981-10-7757-9_6

Sanchez-Barcelo, E. J., Revilla, N., Mediavilla, M. D., Martinez-Cue, C., & Reiter, R. J. (2017). Clinical Uses of Melatonin in Neurological Diseases and Mental and Behavioural Disorders. *Current Medicinal Chemistry*, *24*(35). https://doi.org/10.2174/0929867324666170718105557

Sanford, L. D., Suchecki, D., & Meerlo, P. (2015). Stress, arousal, and sleep. *Current Topics in Behavioral Neurosciences*, *25*, 379–410. https://doi.org/10.1007/7854_2014_314

Scanzano, A., & Cosentino, M. (2015). Adrenergic regulation of innate immunity: A review. In *Frontiers in Pharmacology* (Vol. 6, Issue Aug). Frontiers Media S.A. https://doi.org/10.3389/fphar.2015.00171

Schäfer, S. S., & Schäfer, S. (1973). The role of the primary afference in the generation of a cold shivering tremor. *Experimental Brain Research*, *17*(4), 381–393.

https://doi.org/10.1007/BF00234101

Schromm, A. B., Lien, E., Henneke, P., Chow, J. C., Yoshimura, A., Heine, H., Latz, E., Monks, B. G., Schwartz, D. A., Miyake, K., & Golenbock, D. T. (2001). Molecular genetic analysis of an endotoxin nonresponder mutant cell line: A point mutation in a conserved region of MD-2 abolishes endotoxin-induced signaling. *Journal of Experimental Medicine*, *194*(1), 79–88. https://doi.org/10.1084/jem.194.1.79

Schultz, H. D., Li, Y. L., & Ding, Y. (2007). Arterial Chemoreceptors and Sympathetic Nerve Activity. *Hypertension*, *50*(1), 6–13. https://doi.org/10.1161/HYPERTENSIONAHA.106.076083

Scotto, P. (2006). Fisiologia - Pietro Scotto - Paolo Mondola - Libro - Poletto - | IBS.Retrieved June 8, 2020, from https://www.ibs.it/fisiologia-libro-vari/e/9788895033501

Seoane-Collazo, P., Martínez-Sánchez, N., Milbank, E., & Contreras, C. (2020). Incendiary leptin. In Nutrients (Vol. 12, Issue 2). MDPI AG. https://doi.org/10.3390/nu12020472

Shibasaki, M., Wilson, T. E., & Crandall, C. G. (2006). Neural control and mechanisms of eccrine sweating during heat stress and exercise. *Journal of Applied Physiology*, *100*(5), 1692–1701. https://doi.org/10.1152/japplphysiol.01124.2005

Shimazu, R., Akashi, S., Ogata, H., Nagai, Y., Fukudome, K., Miyake, K., & Kimoto, M. (1999). MD-2, a molecule that confers lipopolysaccharide responsiveness on toll- like receptor 4. *Journal of Experimental Medicine*, *189*(11), 1777–1782. https://doi.org/10.1084/jem.189.11.1777

Shukla, M., Govitrapong, P., Boontem, P., Reiter, R. J., & Satayavivad, J. (2017). Mechanisms of Melatonin in Alleviating Alzheimer's Disease. *Current Neuropharmacology*, *15*(7), 1010. https://doi.org/10.2174/1570159X15666170313123454

Siegel, J. M. (2011). REM sleep: A biological and psychological paradox. *Sleep Medicine Reviews*, *15*(3), 139. https://doi.org/10.1016/J.SMRV.2011.01.001

Silverthorn, D. U., Ober, W. C., Garrison, C. W., Silverthorn, A. C., & Agnati, L. (2007). *Fisiologia : un approccio integrato*.

Snigdha, S., Smith, E. D., Prieto, G. A., & Cotman, C. W. (2012). Caspase-3 activation as a bifurcation point between plasticity and cell death. *Neuroscience Bulletin*, *28*(1), 14–24. https://doi.org/10.1007/s12264-012-1057-5

Squarcio, F. (2020). Neurophysiological, Molecular And Pathophysiological Aspects Of Synthetic Torpor. PhD Theshis, University of Bologna.

Staples, J. F. (2016). Metabolic flexibility: Hibernation, torpor, and estivation. *Comprehensive Physiology*, *6*(2), 737–771. https://doi.org/10.1002/cphy.c140064

Steriade, M., Timofeev, I., & Grenier, F. (2001). Natural waking and sleep states: A view from inside neocortical neurons. *Journal of Neurophysiology*, *85*(5), 1969–1985. https://doi.org/10.1152/jn.2001.85.5.1969

Stieler, J. T., Bullmann, T., Kohl, F., Tøien, O., Brückner, M. K., Härtig, W., Barnes, B. M., & Arendt, T. (2011). The physiological link between metabolic rate depression and tau

phosphorylation in mammalian hibernation. *PLoS ONE*, *6*(1). https://doi.org/10.1371/journal.pone.0014530

Storey, K. B., & Storey, J. M. (1990). Metabolic rate depression and biochemical adaptation in anaerobiosis, hibernation and estivation. *Quarterly Review of Biology*, *65*(2), 145–174. https://doi.org/10.1086/416717

Stornetta, R. L., Rosin, D. L., Simmons, J. R., McQuiston, T. J., Vujovic, N., Weston, M. C., & Guyenet, P. G. (2005). Coexpression of vesicular glutamate transporter-3 and γ-aminobutyric acidergic markers in rat rostral medullary raphe and intermediolateral cell column. *Journal of Comparative Neurology*, *492*(4), 477–494. https://doi.org/10.1002/cne.20742

Straub, R. H., Pongratz, G., Weidler, C., Linde, H. J., Kirschning, C. J., Glück, T., Schölmerich, J., & Falk, W. (2005). Ablation of the sympathetic nervous system decreases gram-negative and increases gram-positive bacterial dissemination: Key roles for tumor necrosis factor/phagocytes and interleukin-4/lymphocytes. *Journal of Infectious Diseases*, *192*(4), 560–572. https://doi.org/10.1086/432134

Straub, R. H., Rauch, L., Rauh, L., & Pongratz, G. (2011). Sympathetic inhibition of IL-6, IFN-γ, and KC/CXCL1 and sympathetic stimulation of TGF-β in spleen of early arthritic mice. *Brain, Behavior, and Immunity*, *25*(8), 1708–1715. https://doi.org/10.1016/j.bbi.2011.07.001

Stricker, E. M., & Hainsworth, F. R. (1970). Evaporative cooling in the rat: effects of hypothalamic lesions and chorda tympani damage. *Canadian Journal of Physiology and Pharmacology*, *48*(1), 11–17. https://doi.org/10.1139/y70-002

Stieler, J. T., Bullmann, T., Kohl, F., Tøien, O., Brückner, M. K., Härtig, W., Barnes, B. M., & Arendt, T. (2011). The physiological link between metabolic rate depression and tau phosphorylation in mammalian hibernation. PLoS ONE, 6(1), e14530. https://doi.org/10.1371/journal.pone.0014530

Strijkstra, A. M., & Daan, S. (1997). Ambient temperature during torpor affects NREM sleep EEG during arousal episodes in hibernating European ground squirrels. *Neuroscience Letters*, *221*(2–3), 177–180. https://doi.org/10.1016/S0304-3940(96)13321-8

Strijkstra, A. M., & Daan, S. (1998). Dissimilarity of slow-wave activity enhancement by torpor and sleep deprivation in a hibernator. *Https://Doi.Org/10.1152/Ajpregu.1998.275.4.R1110*, *275*(4 44-4). https://doi.org/10.1152/AJPREGU.1998.275.4.R1110

Strijkstra, A. M., Hut, R. A., De Wilde, M. C., Stieler, J., & Van Der Zee, E. A. (2003). Hippocampal synaptophysin immunoreactivity is reduced during natural hypothermia in ground squirrels. *Neuroscience Letters*, *344*(1), 29–32. https://doi.org/10.1016/S0304-3940(03)00399-9

Su, B., Wang, X., Drew, K. L., Perry, G., Smith, M. A., & Zhu, X. (2008). Physiological regulation of tau phosphorylation during hibernation. *Journal of Neurochemistry*, *105*(6), 2098–2108. https://doi.org/10.1111/j.1471-4159.2008.05294.x

Takahashi, T. M., Sunagawa, G. A., Soya, S., Abe, M., Sakurai, K., Ishikawa, K., Yanagisawa,

M., Hama, H., Hasegawa, E., Miyawaki, A., Sakimura, K., Takahashi, M., & Sakurai, T. (2020). A discrete neuronal circuit induces a hibernation-like state in rodents. *Nature 2020 583:7814*, *583*(7814), 109–114. https://doi.org/10.1038/s41586-020-2163-6

Takeuchi, O., Hoshino, K., & Akira, S. (2000). Cutting Edge: TLR2-Deficient and MyD88-Deficient Mice Are Highly Susceptible to Staphylococcus aureus Infection . *The Journal of Immunology*, *165*(10), 5392–5396. https://doi.org/10.4049/jimmunol.165.10.5392

Tanaka, M., McKinley, M. J., & McAllen, R. M. (2011). Preoptic–Raphé Connections for Thermoregulatory Vasomotor Control. *The Journal of Neuroscience*, *31*(13), 5078. https://doi.org/10.1523/JNEUROSCI.6433-10.2011

Tanaka, M., Owens, N. C., Nagashima, K., Kanosue, K., & McAllen, R. M. (2006). Reflex activation of rat fusimotor neurons by body surface cooling, and its dependence on the medullary raphé. *The Journal of Physiology*, *572*(2), 569–583. https://doi.org/10.1113/JPHYSIOL.2005.102400

Tansey, E. A., & Johnson, C. D. (2015). Recent advances in thermoregulation. *Advances in Physiology Education*, *39*(1), 139–148. https://doi.org/10.1152/advan.00126.2014

Tashiro, K., Hasegawa, M., Ihara, Y., & Iwatsubo, T. (1997). Somatodendritic localization of phosphorylated tau in neonatal and adult rat cerebral cortex. *NeuroReport*, *8*(12), 2797–2801. https://doi.org/10.1097/00001756-199708180-00029

Tinganelli, W., Hitrec, T., Romani, F., Simoniello, P., Squarcio, F., Stanzani, A., Piscitiello, E., Marchesano, V., Luppi, M., Sioli, M., Helm, A., Compagnone, G., Morganti, A. G., Amici, R., Negrini, M., Zoccoli, A., Durante, M., & Cerri, M. (2019). Hibernation and radioprotection: Gene expression in the liver and testicle of rats irradiated under synthetic torpor. *International Journal of Molecular Sciences*, *20*(2). https://doi.org/10.3390/ijms20020352

Tobler, I., & Borbély, A. A. (1986). Sleep EEG in the rat as a function of prior waking. *Electroencephalography and Clinical Neurophysiology*, *64*(1), 74–76. https://doi.org/10.1016/0013-4694(86)90044-1

Tononi, G., & Cirelli, C. (2003). Sleep and synaptic homeostasis: a hypothesis. *Brain Research Bulletin*, *62*(2), 143–150. https://doi.org/10.1016/J.BRAINRESBULL.2003.09.004

Tononi, G., & Cirelli, C. (2020). Sleep and synaptic down-selection. *European Journal of Neuroscience*, *51*(1), 413–421. https://doi.org/10.1111/ejn.14335

Tracey, K. J. (2002). The inflammatory reflex. *Nature*, *420*(6917), 853–859. https://doi.org/10.1038/nature01321

Tracey, K. J., & Cerami, A. (1989). Studies of Cachexia in Parasitic Infection. *Annals of the New York Academy of Sciences*, *569*(1), 211–218. https://doi.org/10.1111/J.1749-6632.1989.TB27371.X

Trotter, R. N., Stornetta, R. L., Guyenet, P. G., & Roberts, M. R. (2007). Transneuronal mapping of the CNS network controlling sympathetic outflow to the rat thymus. *Autonomic Neuroscience: Basic and Clinical*, *131*(1–2), 9–20. https://doi.org/10.1016/j.autneu.2006.06.001

Violet, M., Delattre, L., Tardivel, M., Sultan, A., Chauderlier, A., Caillierez, R., Talahari, S., Nesslany, F., Lefebvre, B., Bonnefoy, E., Buée, L., & Galas, M. C. (2014). A major role for Tau in neuronal DNA and RNA protection in vivo under physiological and hyperthermic conditions. *Frontiers in Cellular Neuroscience*, *8*(MAR). https://doi.org/10.3389/fncel.2014.00084

Vivier, E., & Malissen, B. (2005). Innate and adaptive immunity: Specificities and signaling hierarchies revisited. In *Nature Immunology* (Vol. 6, Issue 1, pp. 17–21). Nat Immunol. https://doi.org/10.1038/ni1153

Von Der Ohe, C. G., Garner, C. C., Darian-Smith, C., & Heller, H. C. (2007). Synaptic protein dynamics in hibernation. *Journal of Neuroscience*, *27*(1), 84–92. https://doi.org/10.1523/JNEUROSCI.4385-06.2007

Vongpatanasin, W., Kario, K., Atlas, S. A., & Victor, R. G. (2011). Central sympatholytic drugs. In *Journal of Clinical Hypertension* (Vol. 13, Issue 9, pp. 658–661). https://doi.org/10.1111/j.1751-7176.2011.00509.x

Vorkas, C. K., Levy, O., Skular, M., Li, K., Aubé, J., & Glickman, M. S. (2021). Efficient 5-OP-RU-induced enrichment of mucosa-associated invariant t cells in the murine lung does not enhance control of aerosol mycobacterium tuberculosis infection. *Infection and Immunity*, *89*(1). https://doi.org/10.1128/IAI.00524-20

Vucic, D. (2018). XIAP at the crossroads of cell death and inflammation. *Oncotarget*, *9*(44), 27319–27320. https://doi.org/10.18632/oncotarget.25363

Vyazovskiy, V. V., Palchykova, S., Achermann, P., Tobler, I., & Deboer, T. (2017). Different Effects of Sleep Deprivation and Torpor on EEG Slow-Wave Characteristics in Djungarian Hamsters. *Cerebral Cortex*, *27*(2), 950–961. https://doi.org/10.1093/CERCOR/BHX020

Vyazovskiy, Vladyslav V., Cirelli, C., & Tononi, G. (2011). Electrophysiological correlates of sleep homeostasis in freely behaving rats. *Progress in Brain Research*, *193*, 17. https://doi.org/10.1016/B978-0-444-53839-0.00002-8

Waele, J. De, Verhezen, T., Heijden, S. van der, Berneman, Z. N., Peeters, M., Lardon, F., Wouters, A., & Smits, E. L. J. M. (2021). A systematic review on poly(I:C) and poly-ICLC in glioblastoma: adjuvants coordinating the unlocking of immunotherapy. *Journal of Experimental & Clinical Cancer Research 2021 40:1*, *40*(1), 1–20. https://doi.org/10.1186/S13046-021-02017-2

Wang, Y., & Mandelkow, E. (2016). Tau in physiology and pathology. *Nature Reviews Neuroscience*, *17*(1), 5–21. https://doi.org/10.1038/nrn.2015.1

Ward, J. M., & Armitage, K. B. (1981). Circannual rhythms of food consumption, body mass, and metabolism in yellow-bellied marmots. *Comparative Biochemistry and Physiology Part A: Physiology*, *69*(4), 621–626. https://doi.org/10.1016/0300-9629(81)90146-8

Westfall, T. C. (2009). Sympathomimetic Drugs and Adrenergic Receptor Antagonists. In *Encyclopedia of Neuroscience* (pp. 685–695). Elsevier Ltd. https://doi.org/10.1016/B978-008045046-9.01156-6

Willis, C. K. R., & Wilcox, A. (2014). Hormones and hibernation: possible links between hormone systems, winter energy balance and white-nose syndrome in bats. *Hormones and Behavior*, *66*(1), 66–73. https://doi.org/10.1016/J.YHBEH.2014.04.009

Winer, B.J., Brown, D.R., & Michelis, K.M. (1991). Statistical Principles in Experimental Design. McGraw-Hill.

Wlodarchak, N., & Xing, Y. (2016). PP2A as a master regulator of the cell cycle. *Critical Reviews in Biochemistry and Molecular Biology*, *51*(3), 162. https://doi.org/10.3109/10409238.2016.1143913

Worlicek, M., Knebel, K., Linde, H. J., Moleda, L., Schölmerich, J., Straub, R. H., & Wiest, R. (2010). Splanchnic sympathectomy prevents translocation and spreading of E coli but not S aureus in liver cirrhosis. *Gut*, *59*(8), 1127–1134. https://doi.org/10.1136/gut.2009.185413

Xie, M., Shi, R., Pan, Y., Zeng, T., Chen, Q., Wang, S., & Liao, X. (2014). Proteasome Inhibition-Induced Downregulation of Akt/GSK-3β Pathway Contributes to Abnormality of Tau in Hippocampal Slice. *Molecular Neurobiology*, *50*(3), 888–895. https://doi.org/10.1007/s12035-014-8702-0

Yaffe, D., Forrest, L. R., & Schuldiner, S. (2018). The ins and outs of vesicular monoamine transporters. *Journal of General Physiology*, *150*(5), 671–682. https://doi.org/10.1085/jgp.201711980

Zaccone, V., Tosoni, A., Passaro, G., Vallone, C.V., Impagnatiello, M., Li Puma, D., De Cosmo, S., Landolfi, R., Mirijello, A., Internal Medicine Sepsis Study Group. (2017). Sepsis in Internal Medicine wards: current knowledge, uncertainties and new approaches for management optimization. *Annals of Medicine*, 49 (7); 582-592. doi: 10.1080/07853890.2017.1332776.

Zaretsky, D. V., Zaretskaia, M. V., & DiMicco, J. A. (2003). Stimulation and blockade of GABAA receptors in the raphe pallidus: Effects on body temperature, heart rate, and blood pressure in conscious rats. *American Journal of Physiology - Regulatory Integrative and Comparative Physiology*, *285*(1 54-1). https://doi.org/10.1152/ajpregu.00016.2003

Zeng, W., Eriksson, E., Chua, B., Grollo, L., & Jackson, D. C. (2010). Structural requirement for the agonist activity of the TLR2 ligand Pam2Cys. *Amino Acids*, *39*(2), 471–480. https://doi.org/10.1007/s00726-009-0463-0

Zhang, J.-M., & An, J. (2007). Cytokines, Inflammation and Pain. *International Anesthesiology Clinics*, *45*(2), 27. https://doi.org/10.1097/AIA.0B013E318034194E

Zhou, J., Zhang, J., Lam, S.P., Tang, X., Wing, Y.K. (2015). Clinical Biomarkers of Neurodegeneration in REM Sleep Behavior Disorder. *Journal of sleep medicine,* 12(2), 27-33. https://doi.org/10.13078/jsm.15006

Zigmond, R. E., Schwarzschild, M. A., & Rittenhouse, A. R. (1989). Acute regulation of tyrosine hydroxylase by nerve activity and by neurotransmitters via phosphorylation. In *Annual Review of Neuroscience* (Vol. 12, pp. 415–461). Annual Reviews 4139 El Camino Way, P.O. Box 10139, Palo Alto, CA 94303-0139, USA . https://doi.org/10.1146/annurev.ne.12.030189.002215

Zisapel, N. (2018). New perspectives on the role of melatonin in human sleep, circadian rhythms and their regulation. *British Journal of Pharmacology*, *175*(16), 3190–3199. https://doi.org/10.1111/BPH.14116

Zoccoli, G., & Amici, R. (2020). Sleep and autonomic nervous system. *Current Opinion in Physiology*, *15*, 128–133. https://doi.org/10.1016/J.COPHYS.2020.01.002

Zoccoli, Giovanna, & Amici, R. (2020). Sleep and autonomic nervous system. In *Current Opinion in Physiology* (Vol. 15, pp. 128–133). Elsevier Ltd. https://doi.org/10.1016/j.cophys.2020.01.002

Zou, J., Kawai, T., Tsuchida, T., Kozaki, T., Tanaka, H., Shin, K. S., Kumar, H., & Akira, S. (2013). Poly ic triggers a cathepsin d- and ips-1-dependent pathway to enhance cytokine production and mediate dendritic cell necroptosis. *Immunity*, *38*(4), 717–728. https://doi.org/10.1016/j.immuni.2012.12.007